

**Self-organization Approach for Conducting
Polypyrrole and Their Copolymer
Nanomaterials**

THESIS SUBMITTED TO

THE UNIVERSITY OF KERALA

FOR THE AWARD OF THE DEGREE OF THE

DOCTOR OF PHILOSOPHY

IN CHEMISTRY

UNDER THE FACULTY OF SCIENCE

BY

JINISH ANTONY. M

CHEMICAL SCIENCES & TECHNOLOGY DIVISION
NATIONAL INSTITUTE FOR INTERDISCIPLINARY
SCIENCE & TECHNOLOGY (CSIR)
THIRUVANANTHAPURAM- 695 019
KERALA, INDIA.

2010

Dedicated to.....

My Beloved Parents

DECLARATION

I hereby declare that the Ph.D thesis entitled “**Self-organization Approach for Conducting Polypyrrole and Their Copolymer Nanomaterials**” is an independent work carried out by me at the Chemical Sciences and Technology Division, National Institute for Interdisciplinary Science and Technology (CSIR), Thiruvananthapuram, under the supervision of Dr. M. Jayakannan, it has not been submitted any where else for any other degree, diploma or title.

Jinish Antony. M

Thiruvananthapuram

December 2010

राष्ट्रीय अंतर्विषयी विज्ञान तथा प्रौद्योगिकी संस्थान

(वैज्ञानिक एवं प्रौद्योगिकी अनुसंधान परिषद्)
(पहले क्षेत्रीय अनुसंधान प्रयोगशाला)

NATIONAL INSTITUTE FOR INTERDISCIPLINARY SCIENCE AND TECHNOLOGY

(Council of Scientific & Industrial Research)

(formerly Regional Research laboratory)


इन्डस्ट्रियल इस्टेट डाक घर, तिरुवनन्तपुरम 695 019, भारत
Industrial Estate P.O., Thiruvananthapuram 695 019, India



CERTIFICATE

This is to certify that the work embodied in the thesis entitled “Self-organization Approach for Conducting Polypyrrole and Their Copolymer Nanomaterials” has been carried out by **Mr. Jinish Antony. M** under my supervision at the Chemical Sciences and Technology Division of National Institute for Interdisciplinary Science and Technology (*Formerly Regional Research Laboratory*), Thiruvananthapuram

Thiruvananthapuram


Dr. M. Jayakannan
(Thesis Supervisor)

ACKNOWLEDGMENTS

I wish to express my deepest gratitude to my thesis supervisor, **Prof. M. Jayakannan** for suggesting an interesting problem, intellectual support, encouragement and enthusiasm expressed throughout the course of this research work.

I am highly thankful to Dr. Suresh Das, Director; Prof. T. K. Chandrashekar and Dr. B. C. Pai, former Directors, NIIST, Trivandrum for providing all the research facilities for Ph. D work.

I am thankful to Prof. K. N. Ganesh, Director, IISER, Pune, for providing research facilities and accommodation at IISER Pune.

I owe a special note of gratitude to Dr. M. L. P. Reddy for generous help and suggestions.

I also express my sincere thanks to Dr. S.K. Asha for her suggestions, advices and help. I also thank Dr. K. Krishnamurthy, NCL, Pune for his suggestions.

I am very thankful to Academic programme committee (APC) Chairman, Mr. Harikrishna Batt for his official helps.

I am very thankful to Dr. C. Pavithran, Dr. J. D. Sudha, Dr. V. S. Prasad, Dr. A. R. R. Menon and Mr. M. Brahmakumar, Polymer lab, NIIST, for their various helps.

I would like to thank scientists in Chemical science and technology division, NIIST, especially photo-sciences and photonic section, Prof. M. V. George, Dr. A. Ajayaghosh, Dr. George Thomas, Dr. D. Ramaiah, Dr. K. R. Gopidas, Dr. V. G. Anand (IISER Pune) and Dr. A. Srinivasan (NIISER Bhubaneswar).

I would like to thank my NIIST lab mates Deepa, Amrutha, **Anil**, Bala, Anish, Smitha, Deepak, Jancy, Rekha, Shinto, Raman, Prasanth, Bindu, Reena, Sasikala, Biju, Ambili Raj, Vishnu, Sivakala, Chameswary, Biju Francis, Binu, Ramakrishnan, Tony, Shanthil, Deepak, Dhanesh, Aravind and others.

I would like to thank my friends at IISER Pune, Mahima, Shekhar, Smita, Sachin, Anupam, Sandeep, Ananthraj, Pramod, Anurag, Abighyan, Rahul, Biplav,

Shiva, Suresh Prajapat and others. I also thank my friends at NCL, Pune, Nagesh, Koushal, Ganashyam, Chinmay, Senthil, Nisha and others.

I am very much thankful to Dr. Peter Koshy, Mr. M. R. Chandran, Mr. Narendraraj, Mr. Robert Philip, Dr. U. Syamaprasad, Mr. P. Gurusamy, Mrs. Soumini, Mr. Adarsh and Mrs. Viji of NIIST for their help in SEM, TEM, WXR, NMR, CHN and Mass analysis. I also thank Dr. C.P. Sharma and Dr. Willi Paul, SCTIMST, Thiruvananthapuram for DLS.

I fall in short of words in expressing my gratitude to my parents for their love and motivation throughout my education. I thank my brother, Aniesh Antony for his help and suggestions.

Finally, financial assistance from University Grants Commission (UGC), New Delhi is gratefully acknowledged.

Jinish

CONTENTS

	Pages
Declaration	iii
Certificate	iv
Acknowledgment	v
List of tables	xi
List of figures	xii
Abbreviations	xvi
Preface	xvii
<i>Chapter 1: Introduction</i>	1-33
1.1. Introduction to nanomaterials	2
1.2. Self-assembly approach for nanomaterials	4
1.3. Amphiphilic surfactants in self assembly	9
1.4. Self assembly in polymeric systems	13
1.5. Origin of conducting polymers	15
1.6. Polypyrrole	19
1.6.1 General methods of polypyrrole synthesis	20
1.7. Polypyrrole nanomaterials	22
1.7.1. Soft template method	22
1.7.2 Template free method	24
1.7.3. Hard template method	24
1.7.4 Electrochemical synthesis	25
1.7.5 Dispersion route	26
1.7.6 Other routes	27
1.8. Application of polypyrrole nanomaterials	28
1.8.1. Sensors	28
1.8.2. Electrochromic devices	29

1.8.3. Actuator	30
1.9. Aim of thesis	31
<i>Chapter 2: Renewable Anionic Amphiphilic Surfactant for Polypyrrole Nanomaterials.</i>	34-71
2.1. Introduction	35
2.2. Experimental methods	41
2.2.1 Materials	41
2.2.2 General procedures	41
2.2.3 Synthesis surfactant-I	42
2.2.4 Synthesis of polypyrrole nanomaterials	43
2.3. Results and Discussions	45
2.3.1 Synthesis of new azobenzene surfactant	45
2.3.2 Micellar behaviour of surfactant	47
2.3.3 Polypyrrole nanospheres via emulsion route	50
2.3.4 Morphology of polypyrrole nanomaterials	52
2.3.5 Polypyrrole nanospheres via dilution route	57
2.3.6 Morphology of nanomaterials via dilution Route	58
2.3.7 Mechanism of nanomaterial Formation	60
2.3.8 Properties of polypyrrole nanomaterials	65
2.4. Conclusions	71
<i>Chapter 3: Micellar Template Approach for Polypyrrole-Co-Polyaniline Nanomaterials</i>	72-107
3.1. Introduction	73
3.2. Experimental procedures	76
3.2.1 Materials	77
3.2.2 General procedure	76
3.3. Results and discussions	82
3.3.1. Synthesis of copolymer nanomaterials	82
3.3.2. Structural characterization of copolymers	83
3.3.3. Morphology of nanomaterials	86

3.3.4. Mechanism of nanostructure transformation	87
3.3.5. Role of anionic structure on copolymer morphology	92
3.3.6. Morphology of copolymers synthesized using surfactant-2	97
3.3.7. Properties of copolymer nanomaterials	99
3.4. Conclusions	107

Chapter 4: Evolution of Multiple Nano Structures from Identical Copolymer Composition *108-132*

4.1. Introduction	109
4.2. Experimental methods	111
4.2.1. Materials	111
4.2.2. General procedures	111
4.3. Results and discussion	113
4.3.1. Synthesis of copolymers via dilution route	113
4.3.2. Structural characterization of copolymers	115
4.3.3. Morphology of nanomaterials	116
4.3.4. Mechanism of nanomaterial formation	119
4.3.5. Properties of nanomaterials	123
4.4. Conclusions	132

Chapter 5: Polyaniline Nano-scaffold for Colorimetric Sensing of Biomolecules *133-162*

5.1 Introduction	134
5.2 Experimental methods	138
5.2.1 Materials	138
5.2.2 General procedures	138
5.3 Results and discussions	140
5.3.1 Synthesis and characterisation of PSPA	140
5.3.2 Solid State properties of the self doped polymer	144
5.3.3 Absorption properties and colorimetric sensing	147
5.3.4 Mechanism of color sensing	154
5.3.5 DLS and zeta potential Measurements	157

5.4 Conclusions	161
<i>Chapter 6: Summary and Conclusions</i>	163-166
List of Publications	167-168
Bibliography and references	169-189

List of Tables

Table 1.1.	4
Table 1.2.	11
Table 1.3.	16
Table 2.1.	51
Table 2.2.	58
Table 2.3.	67
Table 2.4.	70
Table 3.1.	73
Table 3.2.	82
Table 3.3.	95
Table 3.4.	102
Table 4.1.	114
Table 4.2.	118
Table 4.3.	130
Table 5.1.	135

List of Figures

Figure 1.1.	2
Figure 1.2.	3
Figure 1.3.	6
Figure 1.4.	6
Figure 1.5.	7
Figure 1.6.	9
Figure 1.7.	10
Figure 1.8.	12
Figure 1.9.	13
Figure 1.10.	14
Figure 1.11.	16
Figure 1.12.	17
Figure 1.13.	18
Figure 1.14.	19
Figure 1.15.	20
Figure 1.16.	21
Figure 1.17.	23
Figure 1.18.	24
Figure 1.19.	25
Figure 1.20.	26
Figure 1.21.	29
Figure 1.22.	30
Figure 1.23.	31
Figure 2.1.	36
Figure 2.2.	38
Figure 2.3.	38
Figure 2.4.	39
Figure 2.5.	39
Figure 2.6.	41
Figure 2.7.	45
Figure 2.8.	46

Figure 2.9.	47
Figure 2.10.	48
Figure 2.11.	48
Figure 2.12.	49
Figure 2.13.	50
Figure 2.14.	52
Figure 2.15.	53
Figure 2.16.	54
Figure 2.17.	55
Figure 2.18.	56
Figure 2.19.	57
Figure 2.20.	59
Figure 2.21.	59
Figure 2.22.	60
Figure 2.23.	61
Figure 2.24.	62
Figure 2.25.	63
Figure 2.26.	64
Figure 2.27.	65
Figure 2.28.	65
Figure 2.29.	66
Figure 2.30.	69
Figure 2.31.	69
Figure 3.1.	74
Figure 3.2.	75
Figure 3.3.	83
Figure 3.4.	84
Figure 3.5.	85
Figure 3.6.	86
Figure 3.7.	87
Figure 3.8.	88
Figure 3.9.	89
Figure 3.10.	90

Figure 3.11.	91
Figure 3.12.	91
Figure 3.13.	93
Figure 3.14.	94
Figure 3.15.	96
Figure 3.16.	97
Figure 3.17.	98
Figure 3.18.	98
Figure 3.19.	99
Figure 3.20.	99
Figure 3.21.	100
Figure 3.22.	101
Figure 3.23.	104
Figure 3.24.	105
Figure 3.25.	106
Figure 4.1.	110
Figure 4.2.	114
Figure 4.3.	115
Figure 4.4.	116
Figure 4.5.	117
Figure 4.6.	118
Figure 4.7.	119
Figure 4.8.	120
Figure 4.9.	122
Figure 4.10.	123
Figure 4.11.	124
Figure 4.12.	125
Figure 4.13.	125
Figure 4.14.	126
Figure 4.15.	127
Figure 4.16.	128
Figure 4.17.	129
Figure 4.18.	131

Figure 5.1.	134
Figure 5.2.	136
Figure 5.3.	137
Figure 5.4.	141
Figure 5.5.	142
Figure 5.6.	142
Figure 5.7.	143
Figure 5.8.	144
Figure 5.9.	144
Figure 5.10.	145
Figure 5.11.	146
Figure 5.12.	146
Figure 5.13.	147
Figure 5.14.	148
Figure 5.15.	149
Figure 5.16.	150
Figure 5.17.	150
Figure 5.18.	151
Figure 5.19.	152
Figure 5.20.	153
Figure 5.21.	154
Figure 5.22.	155
Figure 5.23.	157
Figure 5.24.	158
Figure 5.25.	159
Figure 5.26.	160

ABBREVIATIONS

nm	Nanometer
DNA	Deoxyribonucleic acid
RNA	Ribonucleic acid
<i>ca</i>	Around
CMC	Critical micellar concentration
P	Packing parameter
CTAB	Cetyltrimethylammonium bromide
DTAB	Dodecyltrimethylammonium bromide
SAM's	Self-assembled monolayers
PPy	Polypyrrole
PANI	Polyaniline
V ₂ O ₅	Vanadium pentoxide
AAO	Anodic aluminium oxide
PC	Polycarbonate
β-NSA	Beta-naphthylene sulfonic acid
PEDOT	Poly-(3,4-ethylenedioxy thiophene)
CNSL	Cashew nut shell liquid
DLS	Dynamic light scattering
APS	Ammonium persulfate
WXRd	Wide angle X-ray Diffraction
SEM	Scanning electron microscopy
TEM	Transmission electron microscopy
ppm	Parts per million
TMS	Tetramethylsilane
ET	Electron transfer
NMR	Nuclear magnetic resonance

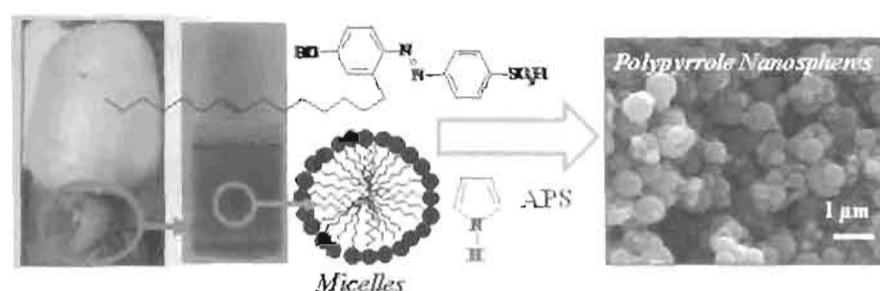
PREFACE

Conducting polypyrrole nanomaterials are widely studied due to their potential applications in electronic devices and chemical/bio-sensors. Development of molecular self-organization template approach for synthesizing polypyrrole and their copolymer nanomaterials is an emerging important area of research. In this thesis, renewable resource based amphiphilic anionic surfactants were designed and utilized as templates for producing polypyrrole and their copolymer nanomaterials like nanospheres, nano-fibers, nano-rods and nano-tubes, etc. Effort has been put to understand the mechanistic aspects of the nanomaterial formation and also their structure-property relationships. Further, colorimetric sensing of biomolecules like vitamin-C and cysteine were also achieved based on a custom designed self-doped polyaniline nano-aggregates. The research work is compiled into the following parts:

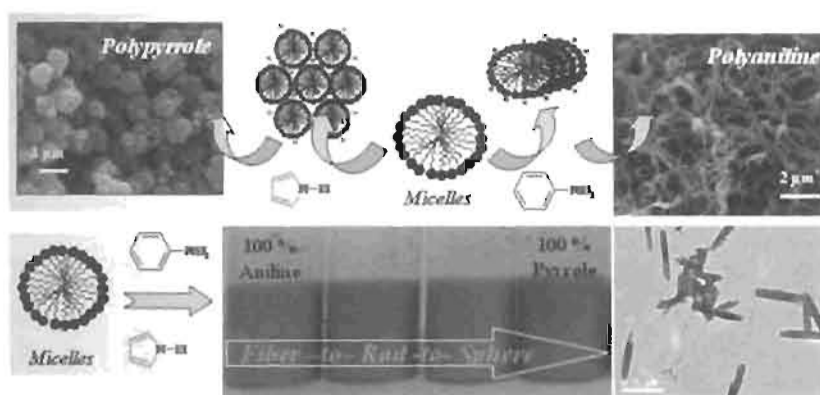
- (i) Development of amphiphilic anionic template based on renewable resource cardanol for polypyrrole nanomaterials.
- (ii) Development of polypyrrole-co-polyaniline random copolymer nanomaterials and their structure-property relationships.
- (iii) Morphology evolution in copolymer nanomaterials from identical chemical constituents
- (iv) Polyaniline nano-aggregates for colorimetric sensing of biomolecules like vitamin-C and cysteine.

The thesis has been divided into six chapters. First chapter gives a brief introduction to polypyrrole and copolymer nanostructures, different synthetic methodologies, properties and their applications. The second chapter describes the development of unique amphiphilic anionic surfactant 4-[4-hydroxy-2 ((Z)-pentadec-8-enyl) phenylazo]-benzene sulfonic acid, from cardanol and its utilization as molecular template for polypyrrole nanomaterials. Dynamic light scattering (DLS) are employed as tools to trace the factors which control the mechanism of polypyrrole nanomaterials formation. DLS studies confirmed that the surfactant existed in the form of spherical micelles of 4.8 nm diameter in water. The micellar behaviour of the reaction medium was precisely controlled by varying the composition of [pyrrole]/[surfactant] ratio ranging from 3 to 100. Polypyrrole nanospheres of 150-800 nm were successfully prepared via oxidative polymerization route. Electron

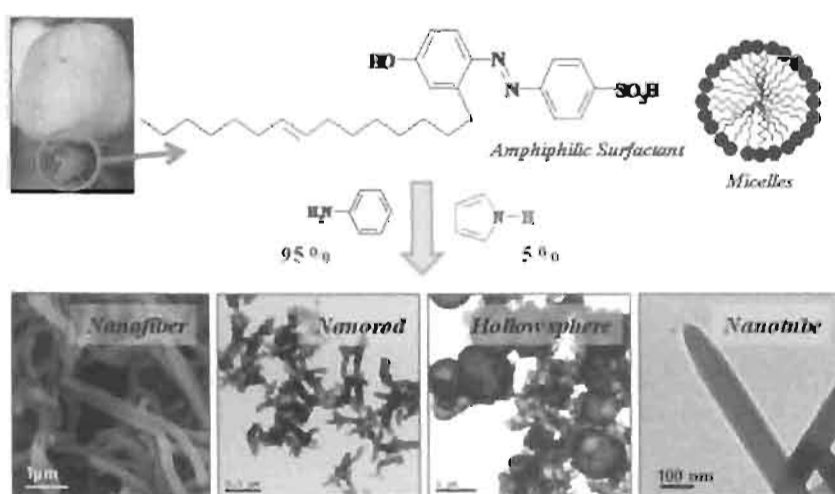
microscopic analysis (SEM and TEM) confirmed the formation of uniform size polypyrrole nanospheres. The nanomaterials formation was unperturbed by the variation of the oxidation agents such as ammonium persulphate (APS) or ferric chloride (FeCl_3). WXR D analysis of the nanomaterials indicated that the anionic surfactant effectively penetrated into the polypyrrole chains to produce highly ordered polymer chains. Absorbance and FT-IR analysis also revealed the highly doped state of the nanomaterials. The conductivity of the samples was obtained in the range of 0.01 to 0.1 S/cm by four-probe conductivity measurements.



The third chapter deals with template selectivity in three structurally different anionic surfactants having same polar head but variation in the hydrophobic tail. They were utilized for achieving size and shape control in polyaniline, polypyrrole, and their polyaniline-co-polypyrrole random copolymer nanomaterial synthesis. All anionic surfactants produce polypyrrole nanospheres, however, they interacted differently with aniline to form cylindrical aggregates, which exclusively template for nanofibers of 180 nm in diameter with length up to 3–5 μm . The unique template selectivity of surfactants toward aniline and pyrrole was used to tune the nanostructure of the polyaniline-co-polypyrrole random copolymers. Interestingly, the morphologies of the nanomaterials underwent transformation from nanofibers to nanospheres via short nano-rod intermediates. Dynamic light scattering technique and electron microscopes were used to study the mechanistic aspects of the template-assisted copolymerization process. Four probe conductivities of the copolymers showed a nonlinear trend and the conductivity passes through minimum at 60–80% of pyrrole in the feed. The unexpected trend in the conductivities of the copolymers was correlated to the difference in the solid state ordering of the copolymer nanomaterials.

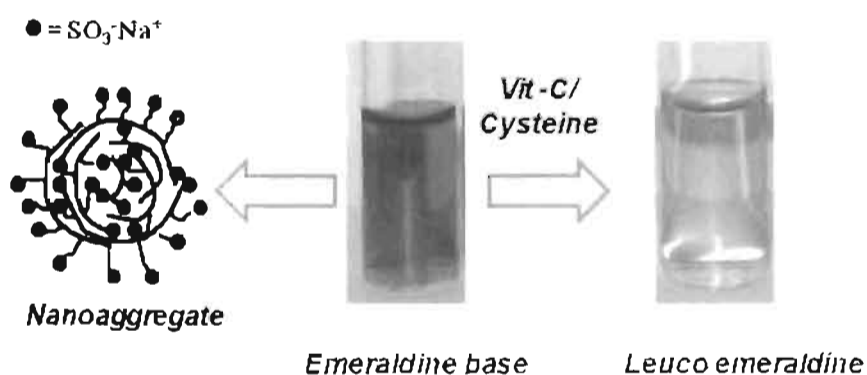


The fourth chapter describes the evolution of the different types of nanomaterial morphologies such as nanofiber, nanorod, nanosphere, and nanotube in a single system without changing their chemical composition or polymerization route. Anionic surfactant was self-organized with fixed composition of aniline (95%) and pyrrole (5%) and the resultant white emulsion was diluted with water to induce cylindrical to vesicular aggregate transformation. The chemical oxidation of the cylindrical templates produced nanofibers and nanorods, whereas hollow spheres and nanotubes were produced by vesicular templates. The size and shape of the template aggregates matched very well with that of the synthesized nanomaterials thereby providing direct evidence for the template-assisted evolution of the morphology. NMR, FT-IR and UV-visible spectroscopies were utilized to confirm the structure and electronic properties of the nanomaterials. Wide angle X-ray diffraction and transmission electron microscopy-electron diffraction analysis revealed that the nanotubes possessed three-dimensional lamellar type solid state ordering with high percent crystallinity up to 60 %. Variable temperature four-probe conductivity



measurements of all samples showed typical $I-V$ plots. The conductivity of the nanofibers was found one order higher than that of nanorod, hollow sphere, and nanotubes at all temperatures. The present approach enabled to establish the role of various types of nano morphologies on properties of nanomaterials such as conductivity and solid state ordering without change in their chemical composition.

In the fifth chapter, self doped polyaniline nano-aggregate was developed based on custom designed N-sulfopropyl aniline monomer via chemical oxidative polymerization. Poly-N-sulfopropyl aniline could be characterized by NMR, MALDI, IR and UV-Vis owing to its solubility in water. Doped sodium salt of polymer was used for the colorimetric sensing of vitamin-C and cysteine. Based on the Job's plot method, the stoichiometry of vitamin-C and cysteine with polymer was determined as 3:2 and 4:1, respectively. Molar ratio method and Benesi-Hildebrand equations were used to determine the association (or binding) constants: $K = 2.1 \times 10^3$ and $1.5 \times 10^3 \text{ M}^{-1}$ for vitamin-C and cysteine, respectively. The polymers possessed typical amphiphilic structure and Zeta potential of the polymer nano-aggregates were found to show negative surface charges in the range of -10 to -30 V. The analytes are typical organic molecules and preferentially occupied the hydrophobic cavity provided in the nano-aggregates for efficient colorimetric sensing in water at biological conditions.



The last chapter summarizes the outcome of the research work in the Ph. D thesis.

Chapter-1

Introduction

1.1. Introduction to nanomaterials

Materials possessing sizes ranging from 1-100 nm are generally classified as nanomaterials [Mirkin, C. A *et al* 2005]. Nanomaterials are distinct from the bulk materials and small molecules in terms of their size dependant properties [Whitesides, G. M *et al* 1991; Goddard III, W. A. *et al* 2007; Rao, C. N. R. *et al* 2004; Huck, W. T. S. *et al* 2005]. Nature is a great source of nanomaterials like proteins, DNA and RNA which is having size in the nanometer regime. Feynman envisaged the changing magnitude of various physical phenomena if we can able to manipulate and arrange individual atoms and molecules down to a smaller needed scale [Goddard III, W. A. *et al* 2007]. Although Feynman statements popularized nanotechnology, however its rapid progress happened only after the arrival of sophisticated instrumentation which can manipulate and view the material in nanoscale. For a clear understanding of size ranges, a comparison of various commonly known objects was given in figure 1.1.

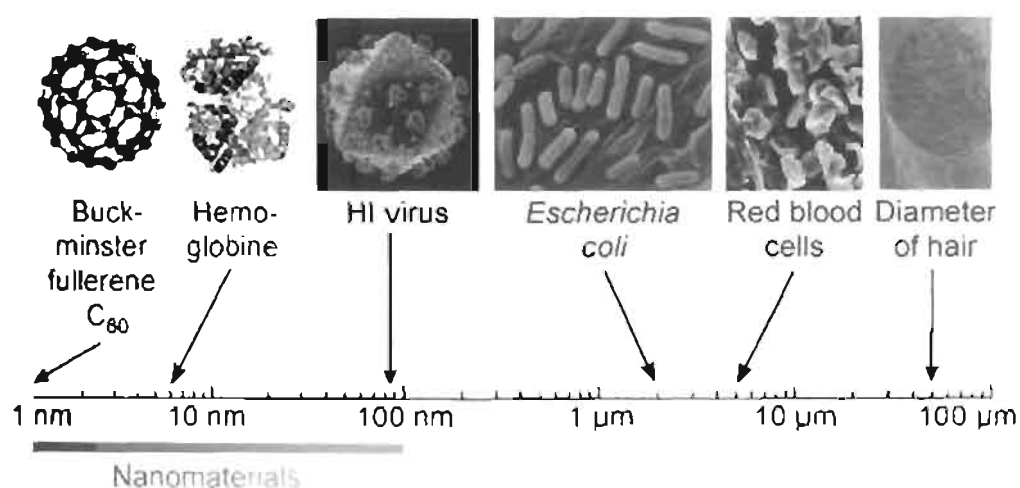


Figure 1.1. Length scale for classifying nanomaterials [adapted from Goesmann, H. *et al* 2010].

Nanomaterials possess large surface area per unit volume which is ideal for catalytic and sensor applications. Damage on biological systems like DNA *ca* 2.5 nm and proteins of size 1-20 nm could be cured by artificial nano components having same size [Fahlman, B. D. *et al* 2007]. Nanomaterials are capable of varying the fundamental properties like magnetization, optical properties (color), melting properties and hardness relative to the bulk materials without change in chemical composition [Fahlman, B. D *et al* 2007]. The physical phenomena of nanomaterials

become pronounced in nano domain due to statistical mechanical effects, as well as quantum mechanical effects [Nalwa, H. S. *et al* 2000]. These effects do not come into play by going from macro to micro dimensions, but it becomes dominant only when the nanometer size range is reached. Currently nanoscience has grown up to a fully fledged fascinating interdisciplinary area of research because of the novel quantum and surface phenomena exhibited by these new classes of materials at the nano-scale which enabled a wide range of applications in the field of physics, chemistry, biology, material science and engineering.

Nanomaterials are synthesized via two approaches, (a) top down and (b) bottom up approaches (see figure 1.2.) [Rao, C. N. R. *et al* 2004; Xia, Y. *et al* 1999]. In top down approach larger size particle were mechanically fractionated to form 'nanomaterials' with desired size, shape and alignment via etching or grinding and deposition method. Etching are usually carried out using high energy ultraviolet light, x-rays or electron beams, whereas deposition was done via important methods like atomic layer deposition (ALD) techniques and dip pen nanolithography [Goesmann, H. *et al* 2010]. An atomic force microscope tips can be used as a nanoscale "write head" to deposit a chemical upon a surface in a desired pattern. In parallel to the top-down approaches which was developed by engineers, molecular chemists developed bottom up approach for fabrication of desired nano-object via molecular self-assembly. This method is inexpensive and simple for producing nanomaterials. Molecular self-assembly seeks to use the concepts of supramolecular chemistry, and molecular recognition in particular, to cause single-molecule components to automatically arrange themselves into some useful conformation [Whitesides, G. M. *et al* 1991].

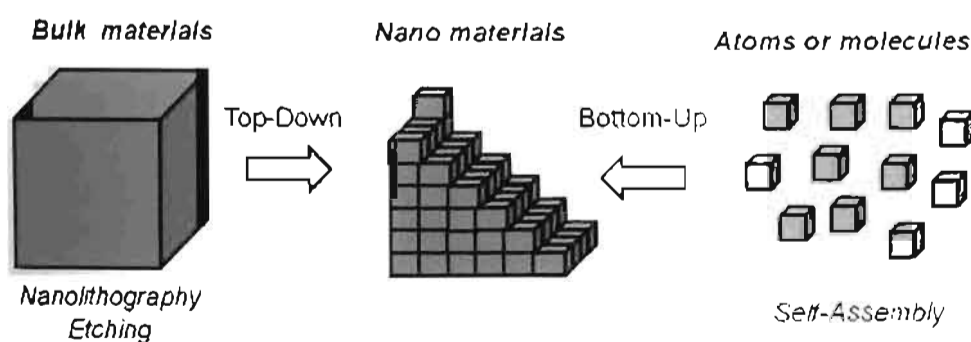


Figure 1.2. Schematic representation of top-down and bottom-up methods.

1.2. Self-assembly approach for nanomaterials

Molecular self-assembly is one of the key tools for the bottom-up approach of organic nanostructures. It is the spontaneous association of molecules under equilibrium conditions into stable, structurally well-defined aggregates joined by noncovalent bonds [Whitesides, G. M. *et al* 1991; Hamley, I. W. *et al* 2007; Atwood, J. L. *et al* 2008; Zhang, X. *et al* 2010]. Key to this type of synthesis is to understand and control the noncovalent connections between molecules and to overcome the intrinsically unfavourable entropy involved in bringing many molecules together in a single aggregate. The concept of self assembly originates from nature, which is observed in a wide variety of biological processes, such as folding of protein in native structure, substrate binding to a receptor protein, protein-protein complexes, antigen-antibody association, enzymatic reaction, transduction of signal, cellular recognition. translation and transcription of the genetic code are excellent examples of the ingenuity of biological processes governed by such interaction [Seal, S. *et al* 2008; Hamley, I. W. *et al* 2007]. Molecular self-assembly is also ubiquitous in chemistry and material science, since the formation of surfactant micelles, molecular crystals, gels, liquid crystals, semi crystalline polymers, colloids, phase-separated block polymers, and self-assembled monolayers are unique examples [Seal, S. *et al* 2008; Ariga, K. *et al* 2006]. Thus, the self-assembled structure is the result of a delicate balance of competing short-range attractive and long-range repulsive interactions in diverse physical and chemical systems. Some of the classical examples for the non covalent supramolecular interaction which is leading to self-organisation are described as below.

Table 1.1. Different type of supramolecular interaction, energies and examples.

Type of Interaction	Strength (KJ mol ⁻¹)	Examples
Ion-Ion	200-300	Quaternary ammonium salt
Ion-Dipole	50-200	Sodium[15] Crown-5
Dipole-dipole	5-50	Acetone
Hydrogen-bonding	4-120	Acids, DNA
Cation- π	5-80	K ⁺ in Benzene
π - π	0-50	Benzene, graphite
Van der Waals	<5	Molecular crystals
Hydrophobic	Depends on solvation	Inclusion compounds

In general, all the secondary interaction forces are weak; however, they may lead molecules from some random state to a highly complex final ordered state. Co-operative effects among different secondary interactions are also common. Nevertheless, the knowledge and understanding to control the mechanism of the process is the key to developing new functional materials of novel performance by self assembly [Seal, S. et al 2008]. In a specific case, a single interaction may play major role; however, in general the supramolecular structures are established by mutual interplay of combination of several of the above forces and quantitative assessment of their relative contribution is very difficult.

1.2.1. Self-assembly by ionic interaction

The ionic self-assembly represents the association due to the interaction between two ionic species and involves the interaction between ion-ion, ion-dipole or dipole-dipole, which are based on the coulombic attraction between opposite charges [Seal, S. et al 2008; Huck W. T. S. et al 2005]. Strongest interaction is ion-ion, which is comparable to that of covalent interaction. The ion-ion interactions are non-directional and strong, whereas the ion-dipole and dipole-dipole are directional and weak. These electrostatic interaction plays major role in understanding the factors influencing the binding affinity biological process like proteins and enzymes. A typical example for self assembly via electrostatic attraction (ion-ion) which involves charge transfer was shown in figure 1.3. The interactions are due to the formation of electrostatic complex formation between viologen linked electron acceptor amphiphile (RV) and the pH responsive electron donor 8-hydroxypyrene-1, 3, 6-trisulfonic acid (DHPS) [Wang, C. et al 2010]. In contrast to the vesicular structure made from RV itself, RV-DHPS forms ultra-long nanofibers by self-assembly in water. Interestingly, the nanofibers exhibit pH responsiveness: at pH 10, DHPS is negatively charged and the adjacent charged moieties would repel each other, making the coiled nanofiber straight; at pH 9 the straight nanofibers become coiled once again.

1.2.2. Self-assembly by hydrogen bonding

The hydrogen bonding force is a special class of dipole-dipole interaction and is predominantly an electrostatic interaction between a weakly acidic donor group (C-

H, O-H, N-H, F-H) and an acceptor atom that has a lone pair of electron with distance of separation $\sim 3 \text{ \AA}$ [Seal, S. et al 2008]. The strong directionality of the hydrogen bond reflects the anisotropy of charge distribution (lone pair) of the acceptor atom. The reversible hydrogen-bond formation is a critical feature in biological system for creation of complex functional materials such as proteins, carbohydrates and in particular, nucleic acids. Hydrogen bonding can be purposefully designed and used as a general strategy for controlling molecular association to create novel material with predictable architecture and properties. A classical example for the hydrogen bonded structures formed between melamine and isocyanuric acid were shown in figure 1.4. [Kimizuka, N. et al 1998].

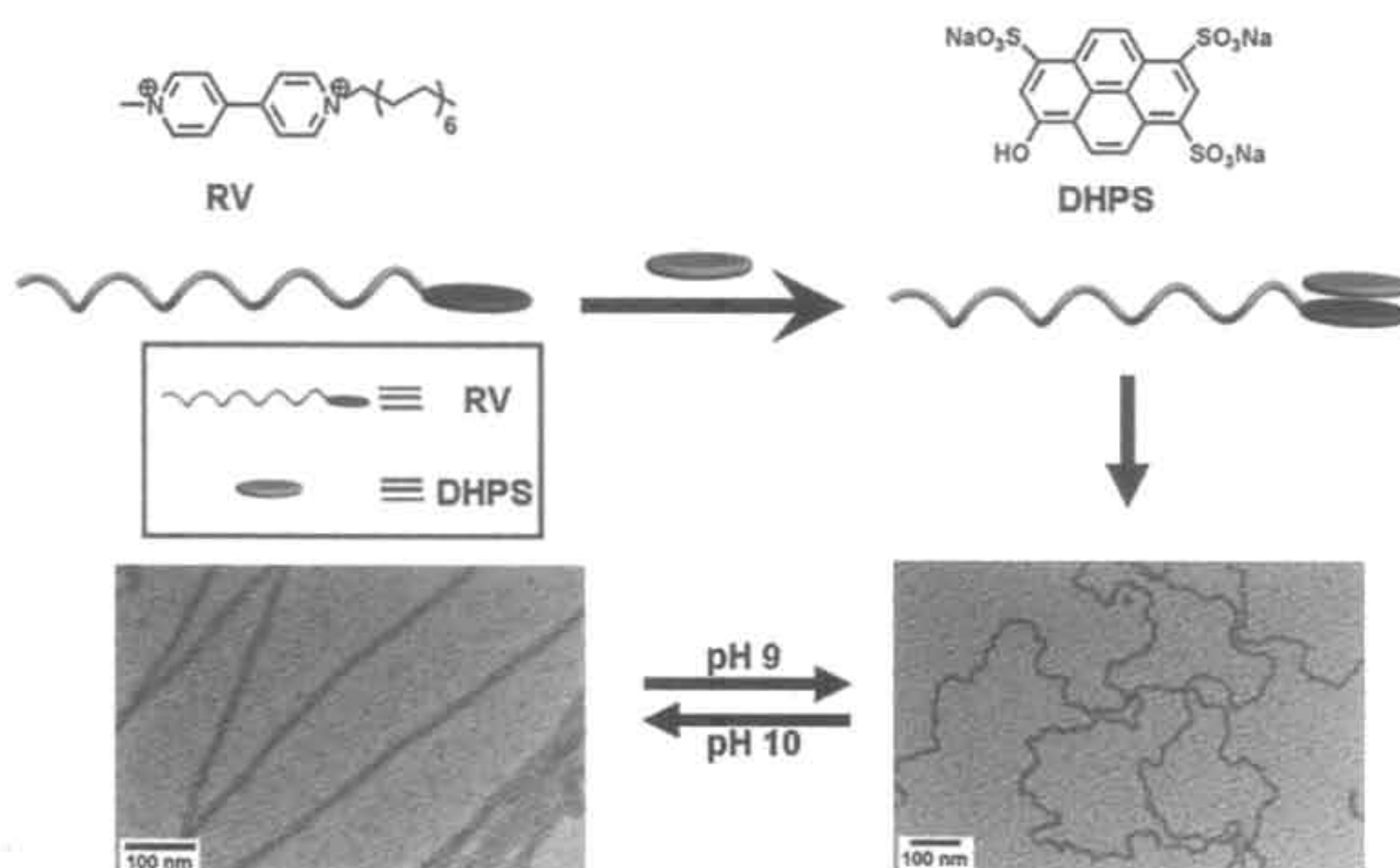


Figure 1.3. *pH responsive electrostatic self assembly via electron donor-acceptor molecules. [adapted from Wang, C. et al 2010]*

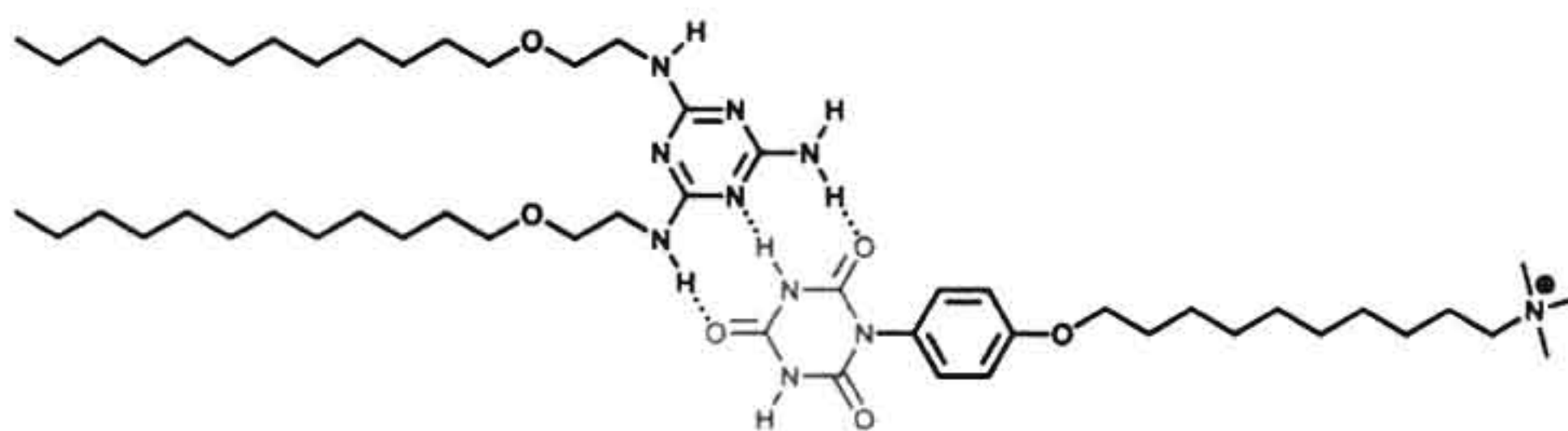


Figure 1.4. *Hydrogen bonding interaction between melamine and isocyanuric acid derivatives. [adapted from Kimizuka, N. et al 1998]*

1.2.3. Self assembly by π - π interaction

The π - π interactions are partial charge interactions and play a role in the association of conjugated molecules. For example benzene and other condensed aromatic rings display a partial negative charge in the plane of the ring within the π -system, and partial positive charge on the hydrogen atoms. Consequently, the parallel stacking of such rings is hindered by the repulsive interaction, results an edge-to-face arrangement for successive rings [Seal, S. et al 2008; Ariga, K. 2006]. However, in solution the energy difference between the edge to face and face to face arrangement appears to be negligible. By proper electrostatic compensation, the interaction may also be surmounted. It is also possible to program π - conjugated molecules such as oligo-(p-phenylenevinylene)s to self-assemble into cylindrical aggregate in solution and in solid, which may be of significant promise in supramolecular nano-size optoelectronic devices. Ajayaghosh and co-workers from our institute have reported π -conjugated organogels from self-assembled oligo-p-phenylenevinylene see figure 1.5. [Praveen, V. K. et al 2008]. The fiber like morphology of the OPV xerogels are a result of multilayer lamellar assemblies of molecules through π - π stacking, hydrogen bonding, van der waals interactions.

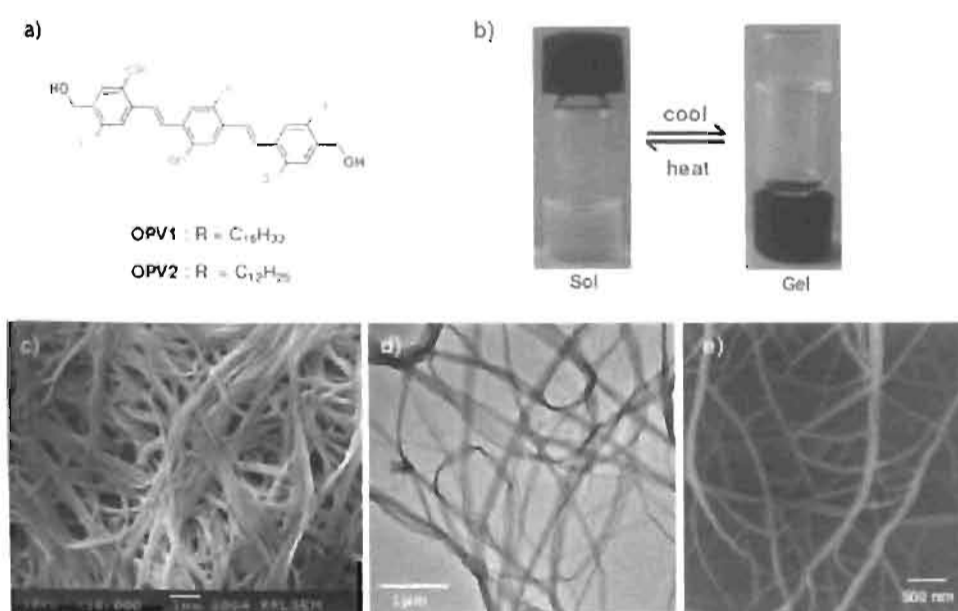


Figure 1.5. Self-assembly of oligophenylenevinylene gels via supramolecular interaction. [adapted from Praveen, V. K. et al 2008]

1.2.4. Self-assembly by van der waals force

The noncovalent interactions between electrically neutral molecules are collectively known as van der waals forces that arise from electrostatic interactions among permanent and/or induced dipoles [Seal, S. et al 2008; Hamley, I. W et al 2007]. These interactions are generally much weaker than the charge-charge interaction of ion pairs. These energies vary with r^{-3} , so they rapidly decrease with distance. Van der waals forces are of two types **a)** Dipole induced dipole interaction: A permanent dipole also induces a dipole moment on a neighbouring group and consequently forms an attractive interaction force. Such interaction is generally much weaker than dipole-dipole interaction. **b)** London dispersion force: At any instant, even non-polar molecules exhibit a dipole moment resulting from the rapid fluctuation of their electron cloud density. The resulting transient dipole moment polarizes the electrons in a neighbouring group. These forces are very weak attractive force and only significant for contacting groups (near their van der Waals contact distance). However, the London dispersion force significantly influences the conformation of polymers and proteins due to the large number of inter atomic contacts.

1.2.5. Self-assembly by solvophobic and incompatibility effects

The solvophobic effect is the influence that causes exclusion of the solvophobic segments of a molecule to minimize their contact with solvent and derives from the property of the solvent. The formation of micelles by amphiphilic molecule in water is a well-known example [Hamley, I. W. 2007]. The unfavourable free energy of hydration of the nonpolar segment in soap causes its ordering and has the net effect of exclusion from the aqueous phase. By doing so it minimizes the overall entropy loss of the entire system. The free energy change to remove a $-CH_2-$ group from an aqueous solution is about 3 kJ by thermodynamic measurements. This is a relatively small quantity of free energy; however, considering the large number of contacts involved in a supramolecular assembly, the cumulative solvophobic interaction is significant. In fact, the hydrophobic force is a key driver in folding proteins into native conformations.

1.2.6. Metal-ion directed self-assembly

Transition metal centers and their coordination chemistry are widely used as a strategy for self-assembly [Fujita, M. et al 1999; Piepenbrock, M, M. *et al* 2010]. Through the directional bonding, they provide highly predictable corners or side units that result in various geometric shapes such as triangles, squares, rectangles, cubes, etc, and it is a widely used strategy to develop novel functional materials. Considering the many coordination environment, the metal centers can adopt and a vast range of geometries available from coordinating ligands, a variety of complexes are accessible through metal-ion-directed self-assembly. The catalytic performance of the encapsulated transition metal complexes is significantly different from a non-encapsulated analogue; they are more active and highly selective in nature. A classical example which leads to a supramolecular metal coordinated polymer is shown in figure 1.6. A bisterdentate bridging ligand was reported to bind to transition metal in an octahedral geometry with a 1:1 stoichiometry as well as to lanthanides with a higher coordination number with a stoichiometry of 1.5:1 [Piepenbrock, M, M. *et al* 2010]. Interestingly, this coordination polymer has shown gelation properties in solvents.

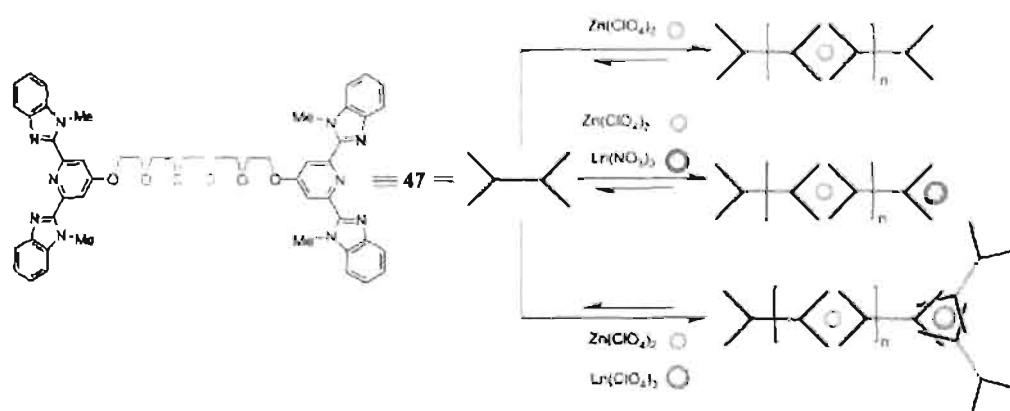


Figure 1.6. Representation of metallosupramolecular polymers formed from the ditopic ligand end-capped monomer with transition metal [adapted from Piepenbrock, M, M. *et al* 2010].

1.3. Amphiphilic surfactants in self-assembly

Surfactants are the simplest class amphiphilic molecules which undergoes spontaneous self organisation in solution (see figure 1.7). In general, surfactants can

be classified into cationic surfactants, anionic surfactants, zwitterionic and non-ionic surfactants [Hamley, J. W. 2007; Luck W. J. S. *et al* 2005]. The cationic surfactants are molecules with positively charged head groups. These surfactants are usually made of long-chain amines and long-chain ammonium salts. Anionic surfactants are molecules with negatively charged head groups. Examples include carboxylic acid salts and sulfonic acid salts (sulfonates). Zwitterionic surfactants are molecules with head groups containing both a positive group (ammonium) and a negative group (carboxylic or sulfonate). Non-ionic surfactants are molecules with neutral head groups, such as polyethylene oxides. Surfactants form micelles in water above a particular concentration called critical micelle concentration (CMC) and the size of the molecular micelles can vary from 5-20 nm depending on the length of surfactant. Surfactants above critical micellar concentration organize in such a way that the polar head groups become oriented towards the water, while at the same time the hydrophobic tails cluster together. This can lead to various superstructures such as micelles, vesicles, multilayers and lyotropic liquid crystalline phases see figure 1.7.

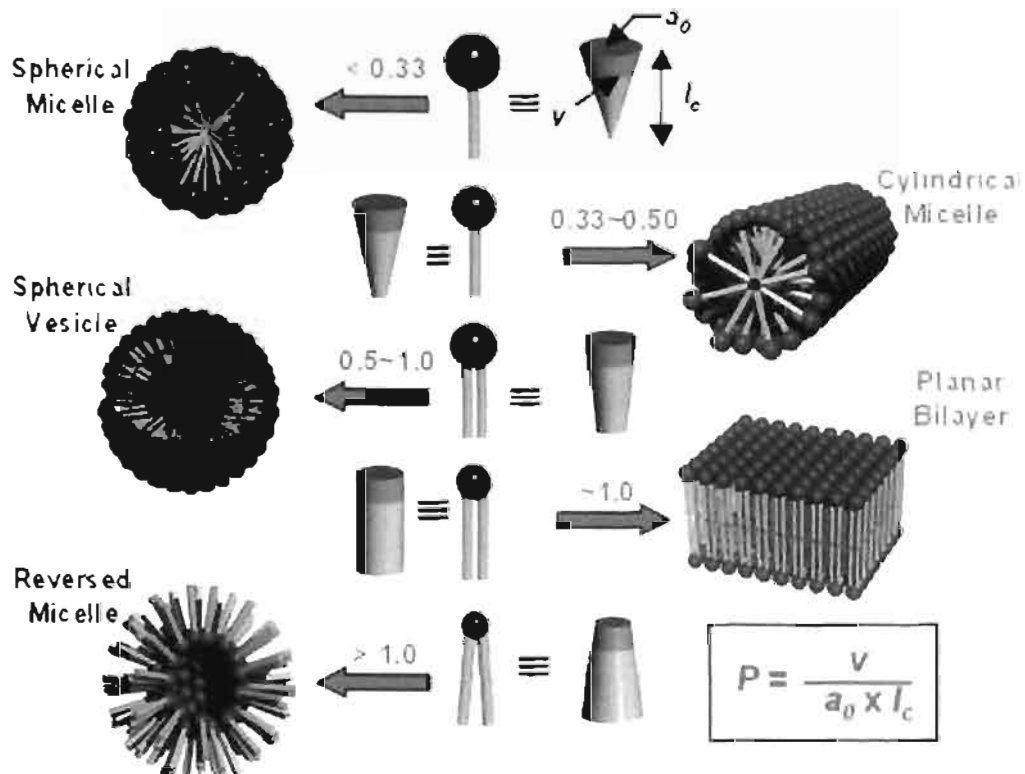


Figure 1.7. Molecular self assembly of surfactant molecules [adapted from Shimizu, T. *et al* 2005].

A theoretical model predicting the shape and structure relationship between the monomeric units and their aggregates was developed by Israelachvili based on statistical mechanics of phospholipids [Israelachvili, J. N. *et al* 1976; Huck W. T. S. *et al* 2005]. This model predicts the type of the aggregate formed on the basis of the packing parameter (P), which relates the volume of the molecule (V) to its length (l) and to the mean cross-sectional (effective) head group surface area (a) by an equation:

$$P = V/al \quad \dots\dots\dots (1)$$

Packing parameter deduced from the above formula can be used for the theoretical predictions of the shape of micelles shown in table 1.2. For spherical amphiphiles, $P < 0.33$, cylindrical micelles $0.33 < P < 0.5$, spherical vesicles $0.5 < P < 1$ and reverse micelles $P > 1$ are formed. The predictions of this model are in agreement with most of the experimental results for phospholipids, and small amphiphiles with conventional aliphatic chains as well as for several more complicated molecules such as diblock copolymers.

Table 1.2. Surfactant packing parameter for various surfactant aggregates

Aggregate Morphology	Packing Parameter (P)	Shape of surfactant
Spherical micelles	< 0.33	cone
Cylindrical micelles	$0.33 < P < 0.5$	Truncated cone
Bilayers vesicles	$0.5 < P < 1$	Truncated cone
Lamella	~ 1	Cylinder
Inverted micelles	$P > 1$	Inverted cone

Vesicles and micelles are representing two of the important classes of self-assembled structures that can be formed by amphiphiles in dilute or semi-dilute solution [Hamley, I. W. *et al* 2007]. Vesicles are hollow spheres enclosed by a bilayers of the amphiphiles and are commonly used to encapsulate labile hydrophilic molecules within their interior. Micelles tend to occur in a range of morphologies, including spherical, ellipsoidal, and cylindrical structures. Cylindrical micelles that are very long and flexible are referred to as “wormlike micelles”, and their formation

is linked to the emergence of viscoelasticity in the solution. Due to their viscoelastic properties, wormlike micelles have found applications in many areas, such as in personal care products and in the oil-field industry. Raghavan and co-workers have reported the formation of unilamellar vesicles from aqueous solutions of the cationic surfactant, cetyl trimethylammonium bromide (CTAB), when 5-methyl salicylic acid (5mS) is added at slightly larger than equimolar concentrations [Davies, T. S. *et al* 2006]. When these vesicles are heated above a critical temperature, they transform into long, flexible wormlike micelles see figure 1.8.

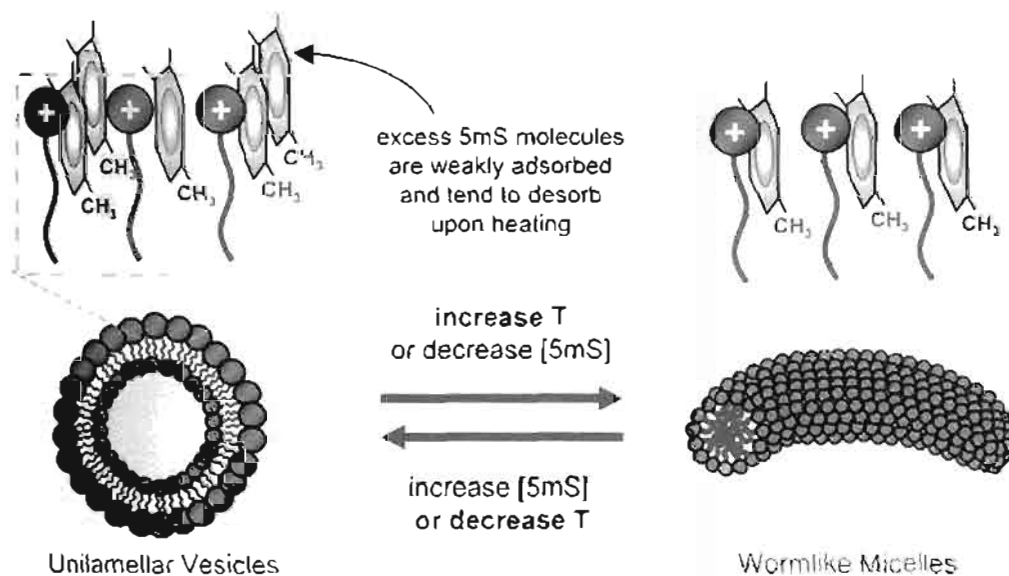


Figure 1.8. Formation of vesicles and worm like micelles with addition of 5 mS [adapted from Davies, T. S. *et al* 2006].

The cationic surfactant cetyltrimethylammonium bromide (CTAB) is exclusively used for the seed-mediated, surfactant-assisted gold nanorod synthesis [Murphy, C. A. *et al* 2002; Smith, D.K. *et al* 2008]. This method relies on the initial preparation of ~1.5 nm diameter gold nanoparticles formed by mixing aqueous solutions of CTAB, hydrogen tetrachloroaurate (III) hydrate and sodium borohydride. These gold nanoparticles are then added to a growth solution of concentrated CTAB, silver nitrate, hydrogen tetrachloroaurate (III) hydrate, and ascorbic acid. Ascorbic acid is a weak reducing agent that induces heterogeneous gold deposition at the surface of the seed particle. Anisotropic nanorod growth results from facet-selective gold deposition promoted by the silver ions, which adsorb to the gold surfaces. The

nanorod aspect ratio can be increased to a certain extent, up to 4.5, by increasing the silver concentration, and the absence of Ag^+ from the reactions leads to only a very low yield of Au nanorods. CTAB coats the nanorod surface as a bilayer that prevents aggregation (see figure 1.9.). The purity of CTAB also determines the reproducible formation of the gold nanorods [Smith, D.K. *et al* 2008].

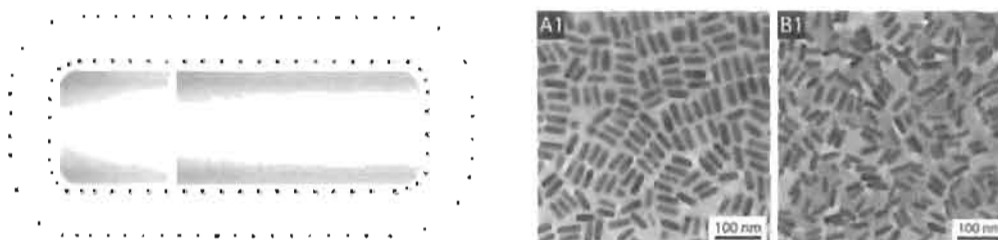


Figure 1.9. Surfactant mediated gold nanorod synthesis [adapted from Smith, D.K. *et al* 2008].

1.4. Self-assembly in polymeric systems

The self-assembly of amphiphilic polymers in solution and melt were well studied mainly by using linear chain block copolymers, owing to their synthetic accessibility [Forster, S. *et al* 2002]. Block copolymers form a large number of super lattices with characteristic dimensions in the range of a few nanometers up to several micrometers by self-organization. The interplay of supramolecular physics and chemistry opens up new approaches for the production of inorganic, organic, and biological structures and to their integration into functional units. Block copolymers find numerous applications from the production of inorganic nanoparticles (metals, semiconductors, magnets) and mesoporous materials up to take-up/ release systems in chemo- and gene therapy, drug delivery etc [Forster, S. *et al* 2002; Huck W. T. S. *et al* 2005]. For their self-assembly, solvents plays an important role in increasing the solvent affinity of a block copolymer, behaving as a selective solvent for a block. Major differences between surfactant micelles and block copolymers micelles are (1) the critical micellar concentration (cmc) of the latter is usually much lower and (2) block copolymer micelles are more stable and their exchange dynamics are substantially slower. This is a result of a number of factors, such as the higher molecular weight, chain entanglement and the decreased mobility of the polymer chains in the core of the micelle. The self-assembled morphologies depend on a

number of structural factors and experimental conditions: block chain lengths, ratios of blocks, molecular weights and their distribution, chain composition, the stereochemistry of the polymer chain, solvent composition, temperature, incubation time, concentration, and preparation order [Forster, S. *et al* 2002]. Block copolymers with large soluble blocks, that is, with small curvature radii R , form spherical micelles preferably, whereas cylindrical micelles or vesicles result from smaller soluble blocks, that is, with greater curvature radii. Cylindrical micelles of poly(butadiene-*b*-ethylene oxide) (PB-PEO) may have lengths of several micrometers see figure 1.10. [Forster, S. *et al* 2002]. Block copolymer vesicles were observed with diameters from 100 nm up to several micrometers. Polymer vesicles (polymersomes) are mechanically and thermodynamically much more stable than the well investigated lipid vesicles, and are well suited for the encapsulation and the release of substances. The vesicles of poly-(2-vinylpyridine-*b*-ethylene oxide) (P2VP-PEO) with diameters of more than 10 μm (giant vesicles) into which, for example, fluorescent dyes can be encapsulated see figure 1.10. [Forster, S. *et al* 2002]

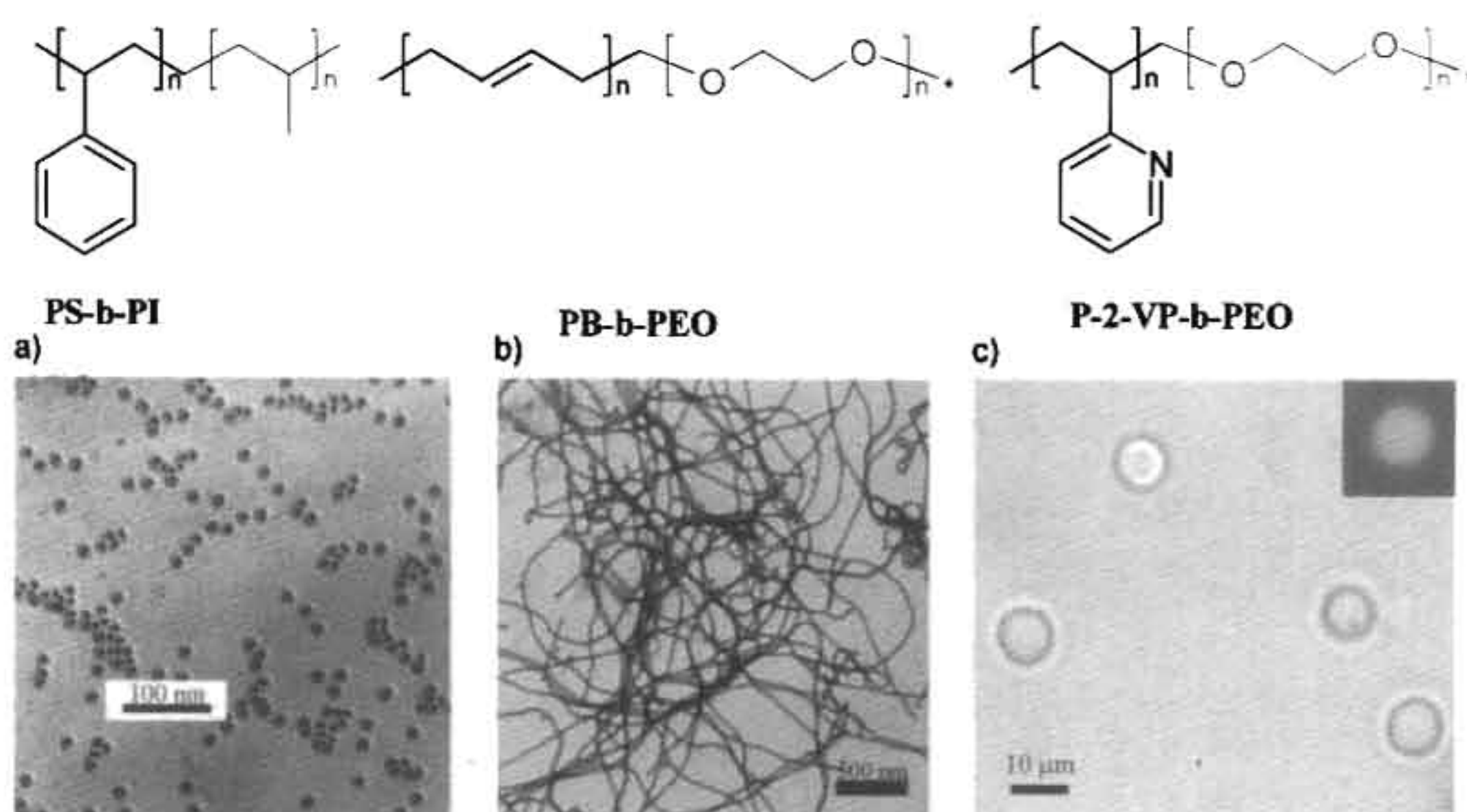


Figure 1.10. Block copolymer self-organization: a) *spherical micelles (PS-PI/DMF)* b) *cylindrical micelles (PB-PEO/water)* and c) *vesicles (P2VP-PEO/water)* [adapted from Forster, S. *et al* 2002].

The surfactant induced approach can be useful for both homo-polymers and block-co-polymers [Tiitu, M. *et al* 2004; Ikkala, O. *et al* 2002; Valkama, S. *et al* 2004]. In this approach the supramolecular interaction between polymer chain and

amphiphiles are utilized. The polymer-amphiphile complex is formed by the attractive physical interaction (e.g. hydrogen bonding, ionic interaction etc.) of the head group of amphiphile with the polymer backbone. In the case of homo-polymers, these complexes can form comb-shaped supramolecular structures in the solid state. The self-assembly of polymer-amphiphile complexes can be combined with diblock copolymers also, which leads to hierarchy of structures, i.e. structure-*within*-structure [Brinke, G. T. *et al* 2004]. In this case one block has an attraction with the amphiphile and the other block has not, so the self-assembly now takes place at two length scales. The morphology depends on several parameters such as the volume fraction of domains, the degree of complexation, alkyl tail lengths of the amphiphiles, and temperature. In short, principles of self assembly and supramolecular chemistry is not only restricted to small molecules, however knowledge can be easily used as tool for the synthesis of hard materials like metal nanorods and larger polymer systems like block copolymer self assembly, self assembled monolayers (SAM's), surfactant induced polymer self assembly, self assembled polymer films etc.

1.5. Origin of conducting polymers

Polymers are typically insulating material and they find exclusive applications in commercial and technological products due to their mechanical properties and low cost production [Brydson, J. A. 1999; Odian, G. 2004]. However, the major break through in conducting polymers research was started with the discovery of conducting polyacetylene. This discovery was pioneered by three eminent professors, Alan Mac Diarmid, Alan. J. Heeger and Hideki Shirakawa in 1977 and they were awarded Nobel Prize in chemistry in 2000 [Skotheim, T. A. *et al* 1998; MacDiarmid, A. G. *et al* 2001]. Polymers which pass electric current with applied potential are called conducting polymers. Conjugated polymers are systems with alternate single and double bonds which can delocalize π -electrons. However, the conjugated polymers are not conductive material due to the considerably high band gap unlike metal. Conducting polymers are produced from conjugated polymer through a method called doping [Shirakawa, H. *et al* 1977]. Doping involves the use of dopants which injects charges on the polymer conjugated backbone. Doping allows the formation of conducting bands with narrow band gap. Both n-type and p-type dopants have been utilized to induce an insulator to conductor transition in conducting polymers

[Skotheim, T. A. *et al* 1998]. Doping of these materials results in rearrangements of polymer chains and induces ordered structure conductivity, processability. The doping of polyacetylene with iodine was shown in the figure 1.11.



Figure 1.11. Doping of polyacetylene with iodine.

Trans polyacetylene has a high conductivity as that of metallic copper, but its poor environmental stability hampers practical applications. This has led to the development of large number of other conducting polymers such as polypyrrole (PPy), polythiophene, poly-p-phenylene, poly-p-phenylenevinylene (PPV), polyaniline (PANI). Some of the commonly known conducting polymers with its structure are summarized in figure 1.12. Major conducting polymers with its conductivity, dopants used, processability and cost were shown in table 1.3. Recently large amount of research work are pertained to conjugated polymers to develop light emitting diodes, solar cells, conducting and semi conducting circuits, field effect transistors and so on. Conjugated polymer based technologies can potentially replace the existing technologies in terms of their superior performance, low cost and mechanical stability and so on.

Table 1.3. Conducting polymers, Dopants used, conductivity, processability, stability and cost of some common conducting polymers.

Polymer	Dopants	Conductivity (S/cm)	Stability	Processability	Cost
Polyacetylene	I ₂ , Br ₂ , Li, Na	10000	Poor	Limited	High
Polypyrrole	BF ₄ ⁻ , ClO ₄ ⁻	500-7500	Good	Good	Low
Polythiophene	BF ₄ ⁻ , ClO ₄ ⁻	1000	Good	Excellent	High
Polyphenylene	AsF ₆ ⁻ , Li, Na	1000	Poor	Limited	High
Polyaniline	HCl, R-SO ₃ H	200	Good	Good	Low

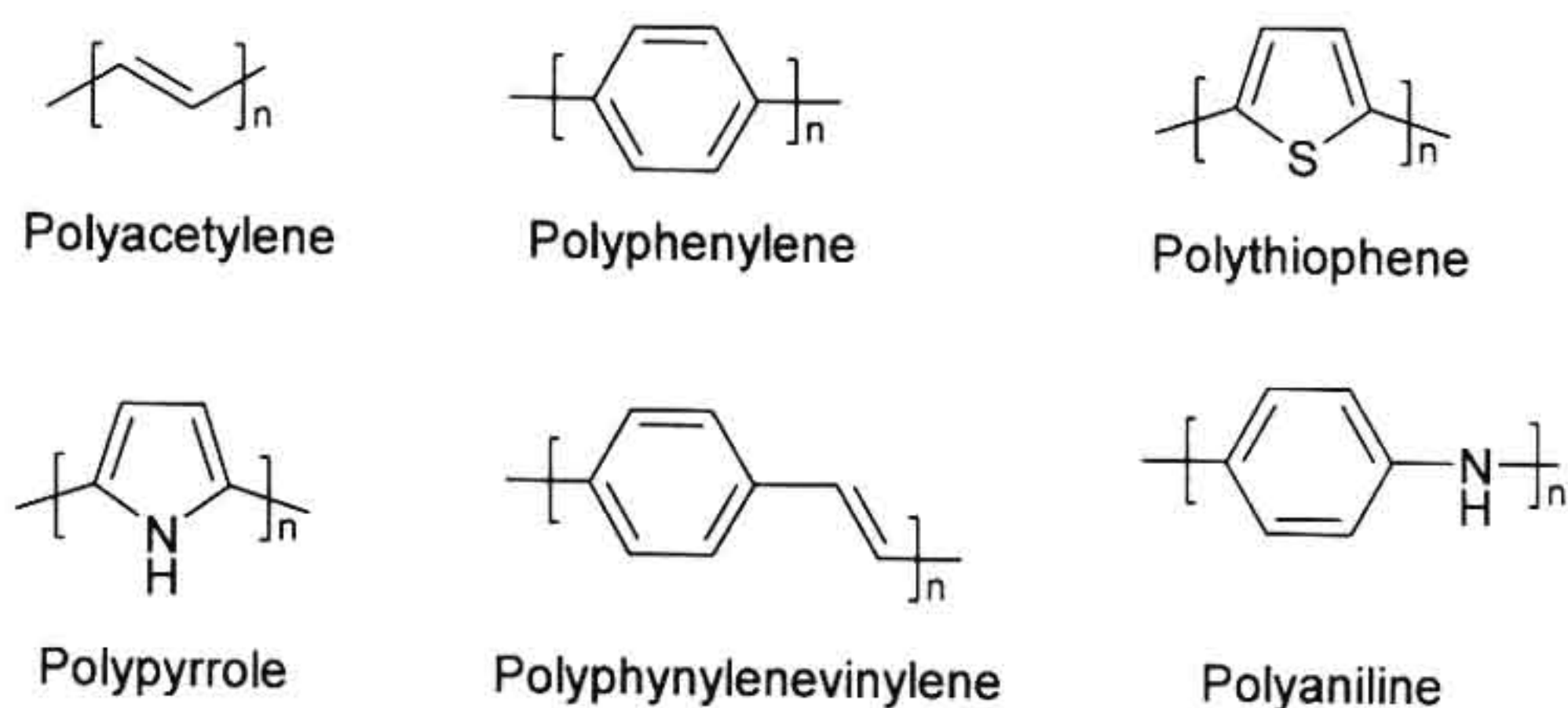


Figure 1.12. Various types of conducting polymers with structures.

Among different conducting polymers, polypyrrole and polyaniline are well-known conducting polymer for its ease of synthesis, environmental stability, and unique acid/base doping-dedoping and oxidation/reduction chemistry [Li, D. *et al* 2009; Skotheim, T. A. *et al* 1998; Chandrasekhar, P. 1999]. Polyaniline can be readily synthesized by either chemical oxidation or electrochemical polymerization of aniline under mild conditions. Polyaniline exists mainly in four different forms, a) completely reduced leucoemeraldine base b) completely oxidized pernigraniline form c) emeraldine base form and, d) emeraldine salt form [Kang, E.T *et al* 1998]. In its emeraldine salt form, polyaniline becomes electrically conducting when doped with an acid. The doping level can be tuned simply by controlling the pH of the dopant. With the rapid emergence of nanoscience and nanotechnology in recent years, synthesizing nanostructures of this unique conducting polymer, especially making nanofibers, has attracted growing attention. In general, the idea behind making nanomaterial is to improve efficiency of the material [Virji, S. *et al* 2006]. Soft template methods like micelles, gels, liquid crystals, seeding, and hard template method like porous template and physical methods like electrospinning were developed for synthesizing polyaniline nanofibers [Li, G. *et al* 2004; Wei, Z. X. *et al* 2002; Skotheim, T. A. *et al* 1998.; Chiou, N. R *et al* 2005.; Chiou, N. R *et al* 2005.]. The polyaniline nanomaterial finds superior applications in batteries, sensors, actuators, electromagnetic shielding, corrosion protection, electro-optic and electrochromic devices compared to bulk material [Janata, J. *et al* 2003; Li, D *et al* 1999]. Earlier, Anilkumar P *et al* from our group have reported the synthesis of

polyaniline nanofiber using renewable resource cardanol derived surfactant for the synthesis of polyaniline nanofibers via emulsion route see figure 1.13. [Anilkumar, P. *et al* 2006]. Detail investigation reveals that nanofibers were formed due to the oxidation of self assembled aniline + surfactant cylindrical template. The nanofiber formation was facile for wide range of [aniline]/ [surfactant] concentration which was rarely reported in literature for synthesis of polyaniline nanofibers. Interfacial polymerisation was also carried out using the same anionic surfactant - oxidant in aqueous layer and aniline in organic layer resulted formation of nanospheres [Anilkumar, P. *et al* 2008]. The formation of the spherical aggregates between surfactant and oxidant ammonium persulfate and subsequent monomer intake at the interface created the polyaniline nanospheres.

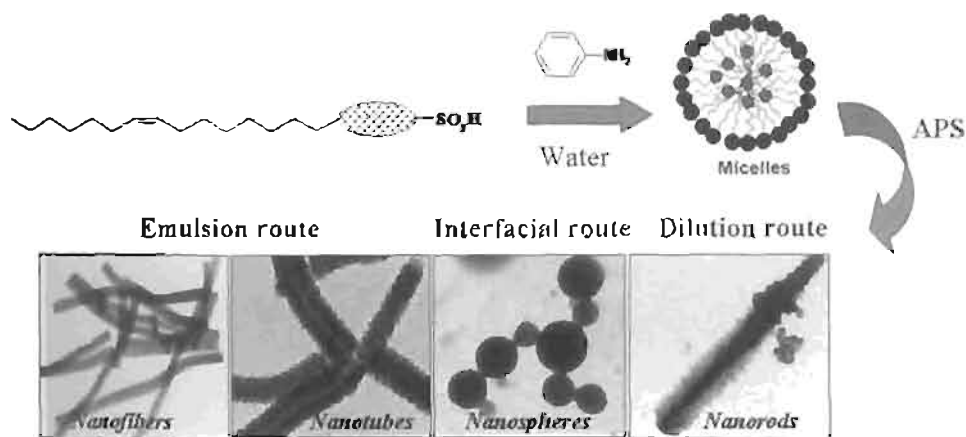


Figure 1.13. Synthesis of Polyaniline nanostructures using different methods of polymerisation route [Adapted from 'Anilkumar, P. *et al* 2010].

In general, the sound knowledge of the polyaniline structure and chemical properties, with reasonably good solubility and processability, thermal and environmental stability and facile nanomaterial formation makes this polymer front runner in conducting polymer nanomaterials. Similar to polyaniline, polypyrrole is another interesting conducting polymer with good conductivity and thermal stability. However polypyrrole has a major drawback in solubility and processability. In addition to that the nanomaterial formation was not understood properly unlike polyaniline. Hence, here we find a unique opportunity to address some of the basic understanding of the polypyrrole nanomaterial formation by surfactant self assembly approach.

1.6. Polypyrrole (PPy)

Polypyrrole (PPy) has attracted great attention because of its high electrical conductivity and good environmental stability [Skotheim, T. A. *et al* 1998]. PPy has been considered as the key material to many potential applications such as electronic devices, electrodes for rechargeable batteries and supercapacitors, solid electrolytes, electromagnetic shielding materials, sensors, corrosion protecting materials, actuators, electrochromic devices, or membranes [^aBre'das, J. L. *et al* 1984; ^bBre'das, J. L. *et al* 1984] The conductivity of the neutral PPy is remarkably changed from an insulating regime to a metallic one by doping. Polypyrrole is doped simultaneously during polymerization and counter anions in the reaction medium are incorporated into the growing PPy chains to maintain the electrical neutrality of the polymer system. Neutral PPy consists of benzenoid rings and upon extraction of a negative charge from a neutral segment of a PPy chain by the doping process, a local deformation to the quinoid structure occurs see (figure 1.14.).

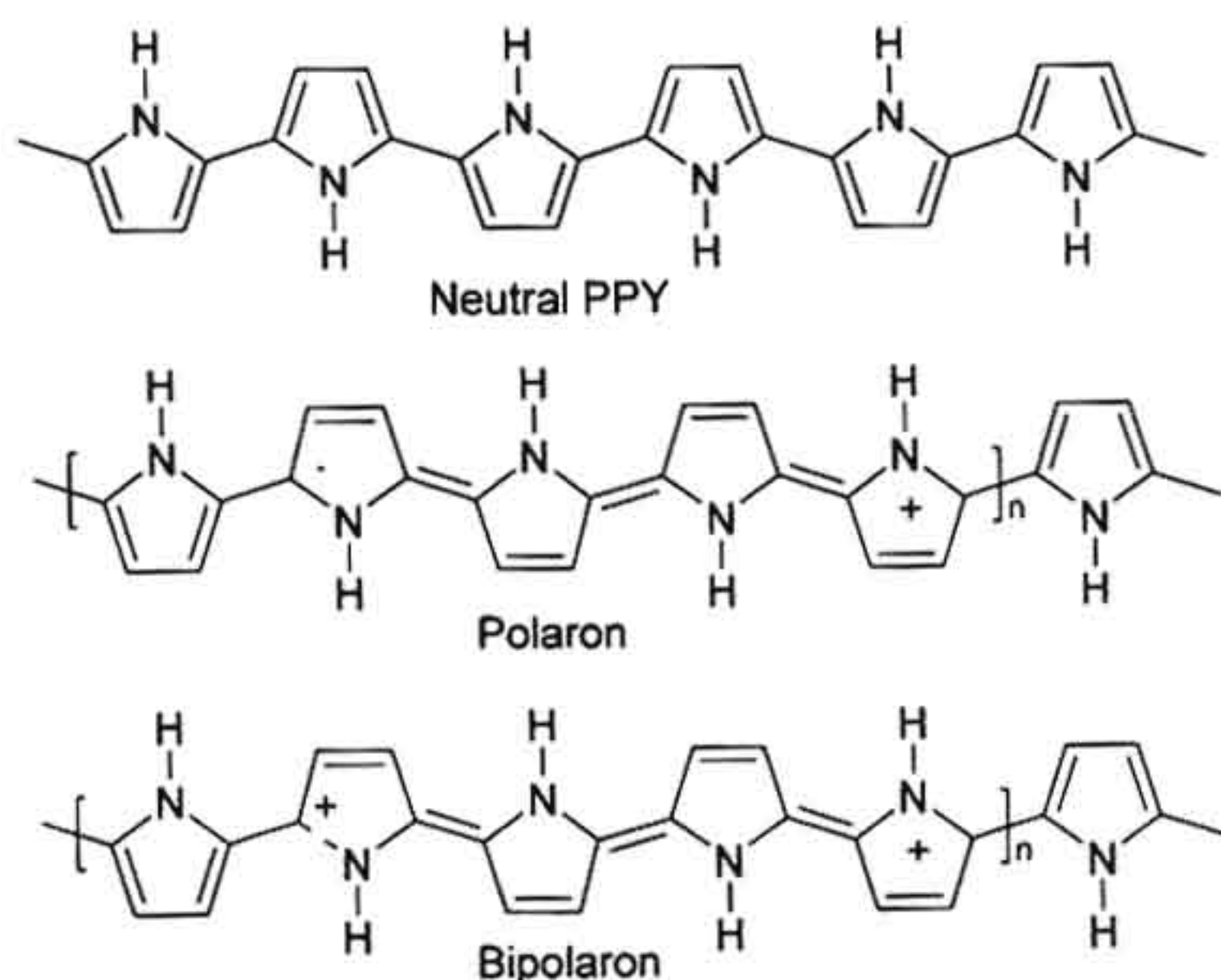


Figure 1.14. Chemical structure of the PPy in neutral and doped state.

The formation of a polaron induces two new intermediate states (bonding and antibonding) within the band gap while unpaired electron occupies the bonding (low energy) state, thus giving the polaron of spin 1/2. In combination with the quinoid structure, the positive charge and the unpaired spin are referred to as a polaron. As oxidation continues further, another electron has to be removed from a PPy chain that

already contains a polaron, resulting in the formation of a bipolaron which is energetically preferred to the formation of two polaron shown in figure 1.14. A bipolaron is known to extend over about four pyrrole rings. The lower energy state of the bipolaron is empty, thus the species has a zero spin. As the degree of oxidation increases, the bipolaronic energy state overlaps, resulting in the formation of narrow intermediate band structures shown in figure 1.15. The energy diagram of bipolaron shown corresponds to a doped state of about 33 mol %, which is close to the maximum value found in electrochemically oxidized PPy [Skotheim, T. A. *et al* 1998].

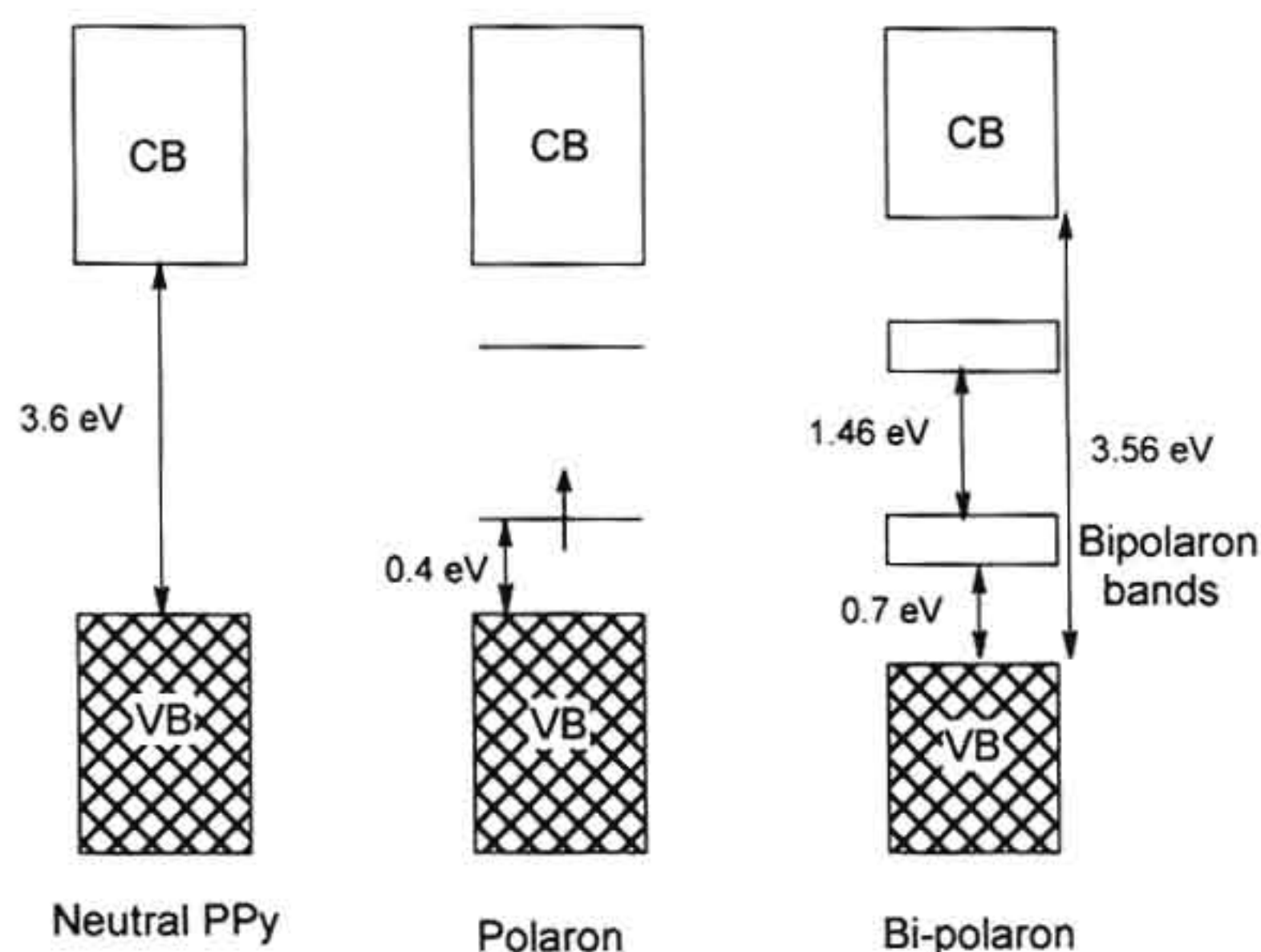


Figure 1.15. Schematic representation of conduction and valence bands of PPy in neutral and in doped state.

1.6.1. General methods of polypyrrole synthesis

Polypyrrole may be prepared by either chemical or electrochemical oxidation of pyrrole monomer (see figure 1.16.). In the chemical oxidation method, oxidizing agent such as, ferric chloride or metal salts of persulfate is added to the pyrrole and a dopant dissolved in a suitable solvent, resulting in the precipitation of doped PPy powder [Omastova, M *et al* 2003; Omastova, M *et al* 2004]. Nevertheless, the chemical oxidation method is suitable for commercial mass production of PPy and may produce processable PPy. Since this method has much greater feasibility to control the molecular weight and structural feature of the resulting polymer than the

electrochemical oxidation method. It is well known that various properties such as the electrical conductivity, stability, and morphology of synthesized PPy strongly depend on various reaction conditions, concentrations of oxidant and dopants or surfactant, polymerization temperature and time, stoichiometry and solvent. Chemical polymerization with surfactants is meant to improve conductivity, stability or solubility in organic solvents. In electrochemical oxidation method, pyrrole and electrolyte salt are dissolved in a suitable solvent and then the solution is subjected to oxidation, resulting in the growth of a conducting PPy film on the anodic working electrode. Diaz *et al.* manufactured free-standing PPy films with excellent electrical and mechanical properties by the electrochemical method [Diaz, A. F *et al* 1977]. The electrochemical polymerization is a fast, easy, and clean method to obtain highly conductive PPy films. It was also reported that PPy could be polymerized using supercritical fluids like carbon dioxide which is non-toxic, non-flammable, and environmentally acceptable compared to organic solvents [Abbett, K. F. *et al* 2003] or to use magnetic ionic liquid (MIL) like butyl-3-methylimidazolium tetrachloroferrate, (Bmim [FeCl₄]) as the solvent or electrolyte for chemical and electrochemical polymerisation [Kim, J. Y. *et al* 2008]

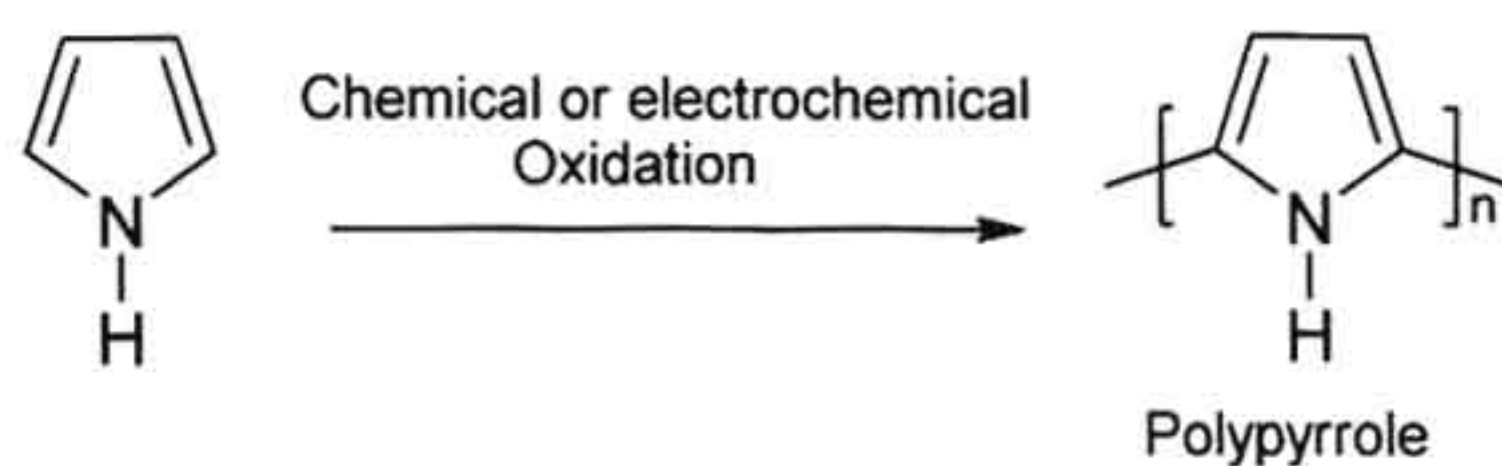


Figure 1.16. Synthesis of polypyrrole via oxidation of pyrrole monomer.

The most widely accepted polymerization mechanism of PPy is the coupling between radical cations [Skotheim, T. A. *et al* 1998]. In the initiation step, the oxidation of a pyrrole monomer yields a radical cation. Coupling of the two generated radical cations and deprotonation produces a bipyrrrole. The bipyrrrole is oxidized again and couples with another oxidized segment. In the propagation step, re-oxidation, coupling, and deprotonation continue to form oligomers and finally PPy. The radical coupling between oligomeric pyrrole species is favoured since the oxidation potential of oligomeric or polymeric pyrrole species is lower than that of the monomer. Once the chain length of the oligomers exceeds the solubility limit of the

solvent, precipitation of polypyrrole occurs. The termination step has not been fully elucidated but is presumed to involve nucleophilic attack on the polymer chain.

1.7. Polypyrrole (PPy) nanomaterials

PPy nanomaterials have been extensively explored because of their easy synthesis, tunable conductivity, reversible redox property, and environmental stability [Skotheim, T. A. *et al* 1998; Jang, J. *et al* 2006]. A variety of fabrication methods have been developed for conducting polymer nanomaterials. Among the various synthetic strategies, template methods are very promising and powerful tool to fabricate conducting polymer nanomaterials. Template method involves the inclusion of monomer inside the template so as to achieve the template shape. In general, template method is classified by soft and hard templates. Soft templates include surfactant, gels, lipids, cyclodextrin, liquid crystal, etc, whereas anodic aluminium oxide (AAO) membrane, track-etched polycarbonate (PC) and zeolite can be used as hard templates. In template-free method represents the synthesis of conducting polymer nanomaterials without the template. Important methods employed for the synthesis of polypyrrole nanomaterials are described as follows.

1.7.1. Soft template method

Soft templates have been used for the fabrication of various morphologies of polypyrrole nanomaterials. There are several soft templates such as surfactant, liquid crystals, gels, cyclodextrin and functionalized polymer [Wu, A *et al* 2005; Hulvat, J. F. *et al* 2003]. Among them, surfactants, which imply cationic, anionic and non-ionic amphiphiles, are mostly used as a nanoreactor. Microemulsions formed by surfactants with monomer are macroscopically homogeneous mixtures of monomer, water and surfactant, which on the microscopic level consist of individual domains of oil and water separated by a monolayer of amphiphile [Lindman, J. *et al* 1998]. Microemulsions are thermodynamically stable (i.e., indefinitely stable) with droplet sizes varying from 10 to 100 nm. Microemulsions act as attractive media for polymerization reactions. In general, microemulsion polymerization has been widely accepted for synthesizing conducting polymer nanoparticles, hollow nanospheres, core-shell nanostructures and nanofibers. Synthesis of 1-D Polypyrrole nanofibers, nano wires and nanoribbons was developed using a lamellar mesostructure formed in-

situ between cationic surfactant and ammonium persulfate as oxidising agent [Wu, A. *et al* 2005]. The diameter of as-prepared polypyrrole nano wires was in the range of 20–65 nm, and the length was up to several micrometers see figure 1.17. In general, anionic surfactants like DBSA and SDS produce polypyrrole nanospheres [De Armit, C. *et al* 1993; Haung, K. *et al* 2005]. Since the oxidative polymerization of corresponding monomers produces cationic intermediates, the anionic assemblies acted as an excellent template owing to the mutual electrostatic attractive force. The helical superstructures of PPy could be prepared via the electrochemical polymerization using anionic synthetic lipid assemblies [Matano, T. *et al* 2004]. A bulk synthesis of PPy nanofiber (diameter: 60–90 nm) was performed using nanofiber seeds as a template [Zhang, X. *et al* 2005]. V_2O_5 nanofiber (diameter ~15 nm), which was chemically treated with pyrrole monomer, was used as a reactive seed template, and pre-polymerization reaction on the surface of fibrillar template provided the evolution of bulk fibrillar morphology with subsequent addition of the oxidizing agent.

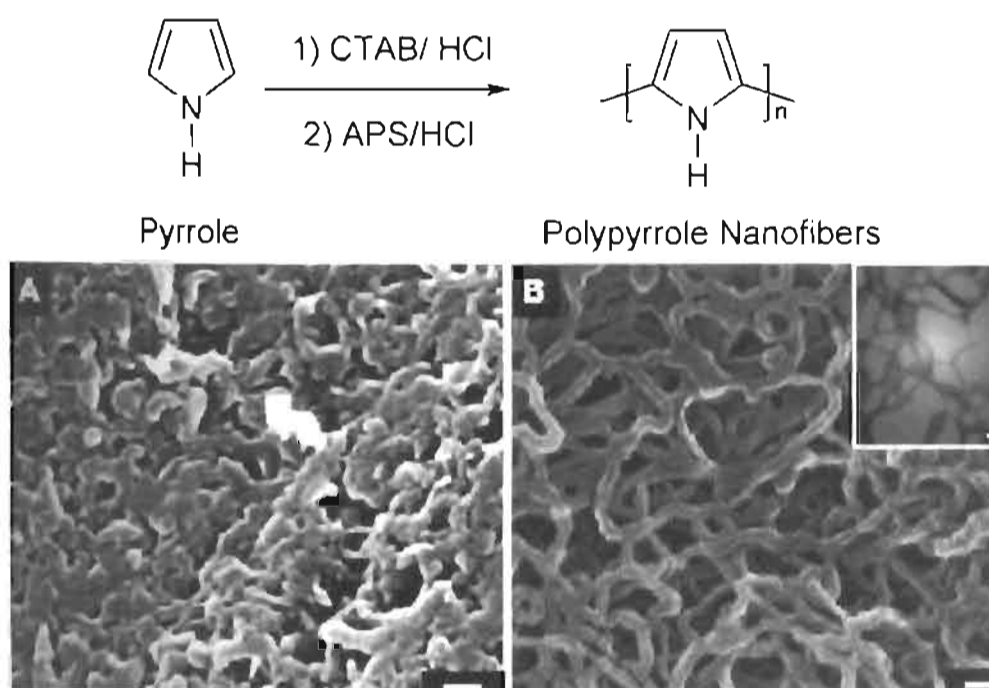


Figure 1.17. Synthesis of polypyrrole nanofibers using CTAB as surfactant: APS as oxidising agent [adapted from Zhang, X. *et al* 2005]

1.7.2. Template-free method

Template-free techniques have been extensively studied for the fabrication of conducting polymer nanomaterials. Compared with hard and soft template methods, these methodologies provide a facile and practical route to produce pure, uniform, and high quality nanofibers. Template free methods encompass various methods such as electrochemical synthesis, chemical polymerization, aqueous/organic interfacial polymerization, radiolytic synthesis, and dispersion polymerization. PPy microtubes and nanofibers have been synthesized in the presence of β -naphthalene sulphonic acid (β -NSA) by electrochemical polymerization [Jang, J. *et al* 2006]. Recently, Zhong, W *et al* reported superhydrophilic polypyrrole (PPy) nanofiber network synthesized by electrochemically in an aqueous solution using phosphate buffer solution (PBS) in the absence of templates, surfactants and structure-directing molecules (see figure 1.18.).

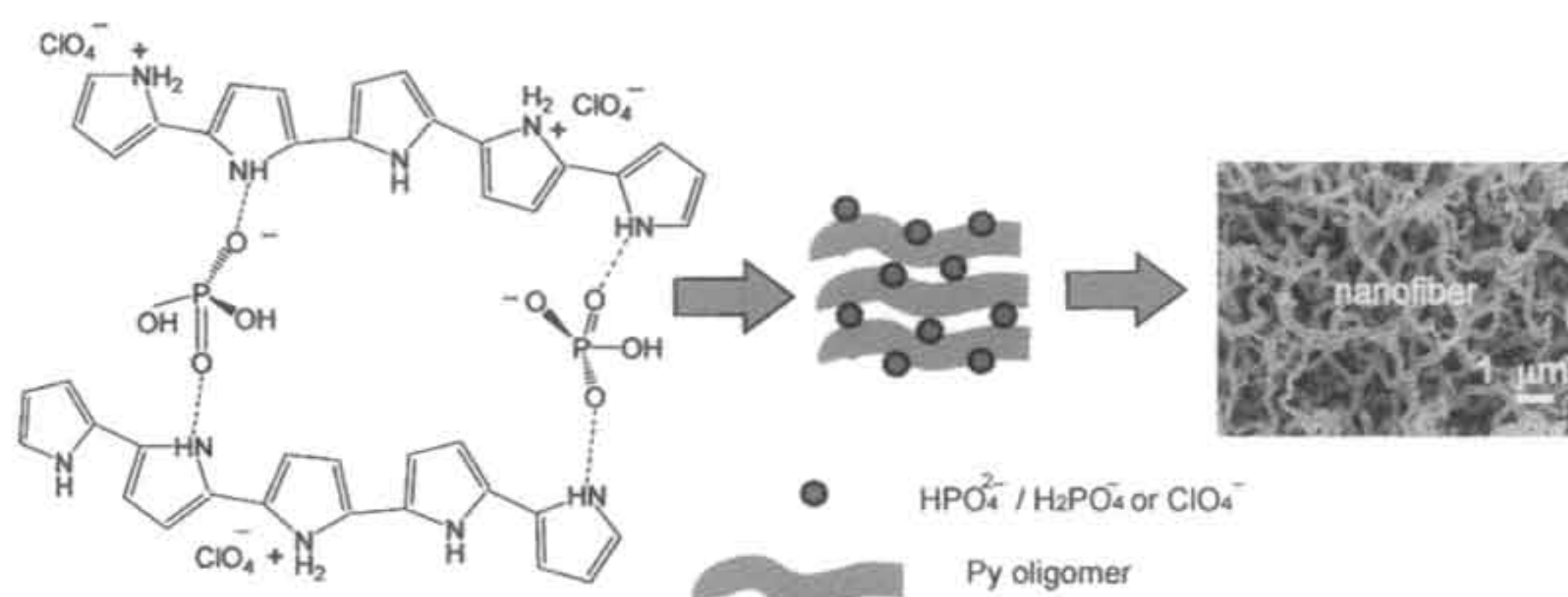


Figure 1.18. Template free electrochemical polymerisation of polypyrrole nanofibers in phosphate buffer [adapted from Zhong, W. *et al* 2008].

1.7.3. Hard template method

Hard template method has been used for the 1-D nanostructures such as nanotubes, nanorods and nanofibers of conducting polymers. The commonly used templates are AAO membrane, and track-etched PC membrane, whose pore size ranges from 10 nm to 100 μ m [Martin, C. R *et al* 1994; Martin, C. R *et al* 1995]. In general, the polymerization of a conducting monomer has been performed at nanochannel as a nanoreactor and hard templates are removed after polymerization in order to fabricate 1-D conducting polymer nanomaterials. Martin, C *et al.* have used

hard template method for preparing polymer nanomaterials. Recently, Jang *et al* produced PPy nanotube with highly uniform surface and controlled wall thickness by one-step Vapour deposition polymerisation (VDP) technique using AAO membrane see figure 1.19. The template mediated vapour phase polymerization provides facile and effective method to fabricate highly uniform tubular walls and with control wall thickness [Jang, J. *et al* 2004]. One of the major challenges in this type of synthesis is to retain the purity and stability of the nanomaterial after the removal of the hard template.

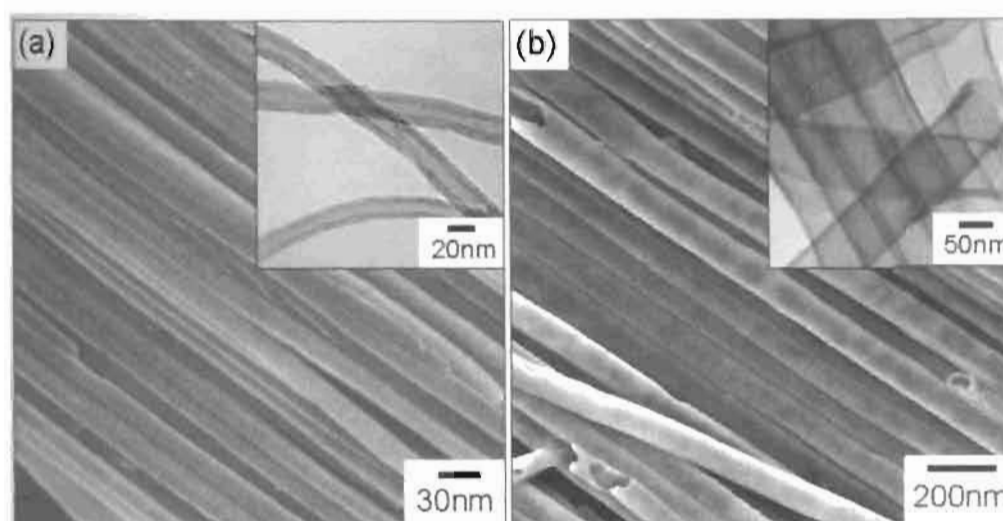


Figure 1.19. Polypyrrole nanotube synthesized using AAO via vapour deposition technique [adapted from Jang, J. *et al* 2004].

1.7.4. Electrochemical synthesis

Electrochemical method is widely accepted for the synthesis of polypyrrole nanomaterial in presence of template like micelles, liquid crystals, lipids, starch, heparin, porous material and also without any template [Jang, J. *et al* 2006; Qu, L. *et al* 2003]. Various types of morphologies like nanofibers, tubules, spheres, nano bowls or containers were produced by this route. The influence of experimental parameter like working electrode, concentration and shape of template, monomer concentration, current density, and polymerisation time plays important role in determining the morphology and properties of the nanomaterial. One of the advantage of electrochemical route is deposition of the nanomaterial can be done very easily to the sensor electrode.

1.7.5. Dispersion route

There are three categories of dispersion polymerization in order to fabricate the conducting polymer colloids. The first approach, utilizes sterically stabilized polymer like polystyrene sulfonic acid (PSS) and polyvinyl alcohol (PVA) for conducting polymer nanoparticle [Qi, Z. *et al* 2006]. In this case, the monomer and oxidant are dissolved in a sterically stabilized polymer medium and conducting polymer nanoparticles are formed as polymerization proceeds. Processability and solubility was found to be very good for the conducting polymer synthesized via this method, however the conductivity loses due to presence of steric stabilizer. The other approach involves in-situ polymerization of monomer is performed in the presence of silica nanoparticles and the conducting polymer is adsorbed onto the silica nanoparticles as seed [McCarthy, G. P. *et al* 1997; Maeda, S. *et al* 1995] The particle size and morphology of silica-conducting polymer can be readily varied by adjusting size of silica, concentration of silica and monomer, and type of oxidant and monomer. Third category involves the use some metal colloidal particle as a stabilizer medium for the polypyrrole. Fujii *et al* reported the one pot synthesis of polypyrrole coated silver core shell material using the oxidation polypyrrole with silver nitrate see figure 1.20.)



Figure 1.20. Polypyrrole spherical core-shell nano material via by dispersion route. [adapted from Fujii, S. *et al* 2007]

1.7.6. Other routes

Other important routes for the production of polypyrrole with special purpose like making thin films, improvement of solubility and conductivity are as follows:

a) Interfacial route: Thin polypyrrole film could be prepared by chemical polymerization at the interface of chloroform solution of pyrrole and aqueous solution of ammonium persulfate [Lu, Y. *et al* 1998]. There are several conditions for the solvents to be used for interfacial polymerization of pyrrole. The oxidant and monomer should be soluble in different solvents for the reaction to occur only at the interface. To prevent PPy from depositing as powder or floating on the aqueous surface, the upper layer solvent should have lower density than PPy. The conductivity and other solid state properties of the polypyrrole material synthesized via interfacial route are poor in comparison to the chemical and electrochemical method. The films of polypyrrole formed at the interface of the 'organic' aqueous layer were usually undergoes over oxidation due to the insolubility materials in either organic or aqueous solution.

b) Plasma route: Plasma polymerization has been recognized as an important process to obtain thin films of conductive polymer, which are formed by reactions in gas phase without any chemical oxidants [John, R. K. *et al* 2002]. The chemical structure of plasma-polymerized polypyrrole is different from that obtained by conventional chemical or electrochemical polymerization processes because of fragment formation, trapped radicals, and a higher degree of branching and cross linking.

c) Copolymerization: Even though polypyrrole may be used in many application fields, its poor processability, mechanical, and physical properties have been a large obstacle. To improve the processability, mechanical and other properties, various kinds of PPy copolymers have been polymerized with many other conducting and conventional polymers [Simmons, M.R. *et al* 1998]. To improve the processability of PPy, the sterically stabilized colloidal PPy particles have been synthesized using a tailor-made reactive copolymer. Electroactive random copolymer was produced by the electrochemical copolymerization of pyrrole and aniline in acetonitrile and supporting electrolyte [Sari, M. *et al* 1998; Fusalbu, F. *et al* 1999; Li, X. G *et al* 2001; Stejskal, J. *et al* 2004; Lim, V. W. L. *et al* 2001; Kim, J. W. *et al* 2003; Cho, C. H *et al* 2004; Zhou, C. *et al* 2008]. It was also reported that there was a clear dependency of polymerization rate and yield, solubility, ability to form films,

molecular weight, thermal stability, and conductivity of the copolymers on the comonomers ratio. Interestingly, literature report suggests that chemical and electrochemical copolymerisation of pyrrole and aniline has not produced well defined nanomaterials. More detailed review on copolymers were discussed in chapter-3. There was no major attempts to understand the polyaniline-co-polypyrrole nanomaterial formation due to the following reasons 1) the unclear understanding of formation mechanism homopolymer nanomaterials especially polypyrrole 2) poor stability of the soft templates for both aniline and pyrrole monomer. Hence, to address these issues in detail, we have explored polypyrrole-polyaniline random copolymer nanomaterials via self assembly approach.

1.8. Applications of polypyrrole nanomaterials

1.8.1. Sensors

Polypyrrole nanomaterials are widely used as chemical and biological sensors [Geetha, S. *et al* 2006; ⁸Jang, J. *et al* 2006]. The sensing action of polypyrrole sensors are based on the variations in conductivity, color, mass, volume, and so forth which are easily influenced by their inherent reversible doping-dedoping /oxidation-reduction mechanisms. It is noteworthy that the nanostructures including nanorods, nanofibers, and nanotubes not only provide a high surface-to-volume ratio but also allow rapid diffusion of analytes into and out of the material. Gas sensors were fabricated by spin-casting polymer films onto pre-patterned glass electrodes see figure 1.21 [An, K. H. *et al* 2004]. PPy nanomaterials have been applied to various sensors such as toxic gas noses, non-toxic gas noses, aroma sensors, humidity sensors, and microbial noses [Lellouche, J. P, *et al* 2005]. Upon cyclic exposure to ammonia gas, the PPy wire sensor was at least six times more sensitive than the PPy bulk film sensor. The electrochemical behaviour of the electrodes modified with PPy nano wires was described as a chemical sensor. The modified electrodes had good activity towards nitrite reduction and the electro-reduction current depended linearly on the concentration of nitrite and increased with increasing the PPy thickness, acidity of electrolyte solution, temperature, and scan rate [Tian, Y. *et al* 2004; Tian, Y. *et al* 2005]. Glucose biosensor has been developed using polypyrrole/enzyme nano junctions and demonstrates the signal transduction mechanism based on the change in

the nanojunction conductance as a result of glucose oxidation induced change in the polymer redox state see figure 1.21. [Forzani, E.S. *et al* 2004]. Furthermore, an amperometric enzyme electrode was prepared based on the co-immobilization of CNT and glucose oxidase within an electro polymerized PPy film [Kros, A. *et al* 2002; Gao, M. *et al* 2003; Wang, J. *et al* 2005]. Such a simultaneous incorporation of CNT and glucose oxidase imparted biocatalytic and electrocatalytic properties onto amperometric sensor. This research was further extended to the fabrication of PPy nano-wire biosensor for label-free bio-affinity sensing [Ramanathan, K. *et al* 2005]. The one-step incorporation of functional biological molecules into PPy nanowires during its electropolymerization was a critical advantage of a novel fabrication method over the CNT and silicon nanowire biosensors that required post-synthetic modification and positioning.

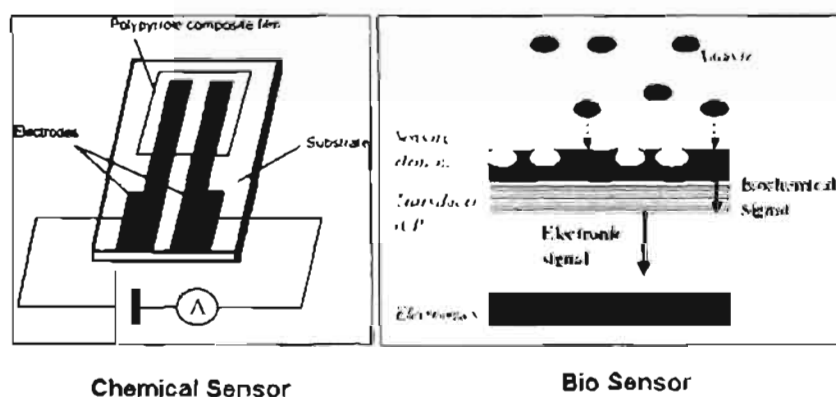


Figure 1.21. Schematic representation of chemical and biosensor based on conducting polymer. [adapted from Ma, X. *et al* 2008; Guimard, N. K. *et al* 2007]

1.8.2. Electrochromic device

Electrochromism can be defined as a reversible color change in a material induced by an electric field. Early studies of electrochromism focused on inorganic (e.g., WO_3) compounds and organic molecules (e.g., bipyridiliums). However, recent researches have fairly focused on conducting polymers such as PPy, PANI, and PT [Argun, A. A. *et al* 2003]. Conducting polymers have advantages over the other electrochromic materials, including ease of processing, fast switching time, high

contrast and coloration efficiency, tunable band gap, and so forth. In particular, nanostructured conducting polymers can provide a much faster switching time compared with bulk counterparts. The electrochromic devices with fast switching speeds could be recently fabricated based on well-defined PEDOT nanotube arrays [Cho, S. I. *et al* 2005]. Recently, Smella, E *et al.* microfabricated movable electrochromic pixel based on polypyrrole see figure 1.22.

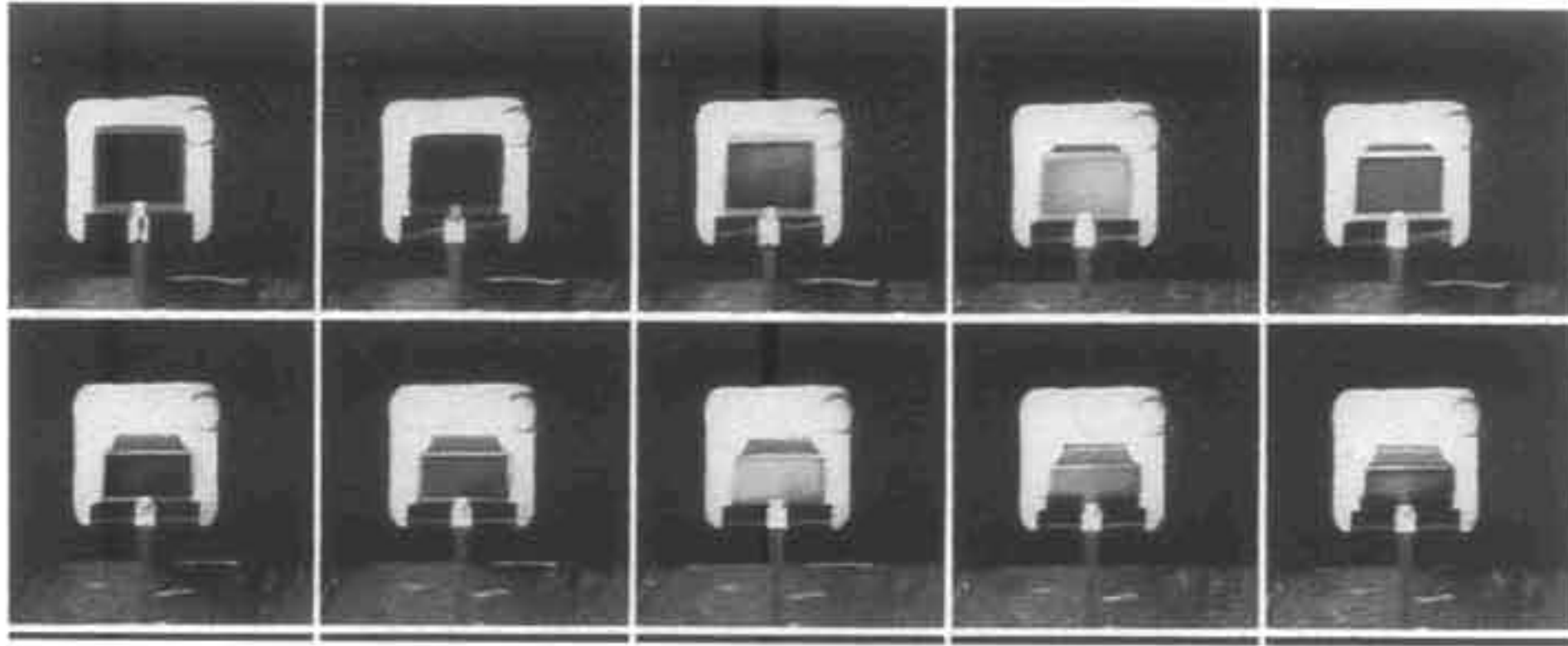


Figure 1.22. *Microfabricated movable electrochromic pixel based on polypyrrole [adapted from reference Smela, E. *et al* 1999].*

1.8.3. Actuator

Polypyrrole nanomaterials have been considered as excellent material for actuator applications, because it undergoes reversible volume changes (expansion and contraction) during oxidation and reduction [Berdichevsky, Y. *et al* 2006]. Recent research trends concerning conducting polymer actuators have been reviewed by Smela. PPy exhibited several advantages including large strain like 3 % in-plane and > 30 % out-of-plane, high strength, low voltage operation, biocompatibility, and so forth (see figure 1.23.). Microactuator consists of PPy-Au bilayers and Au layer acted both as structural layer and an electrode. These micromuscles were used to lift plates, to open and close boxes. In addition, the microrobotic arms could pick up, lift, move, and place micrometer-size objects within an area of about $250 \times 100 \mu\text{m}^2$. The controlled movement of the robot arm was due to individually controlled microactuators [Smela, E. *et al* 2003; ^aJager, E. W. H. *et al* 2000; ^bJager, E. W. H. *et al* 2000; ^cJager, E. W. H. *et al* 2001].

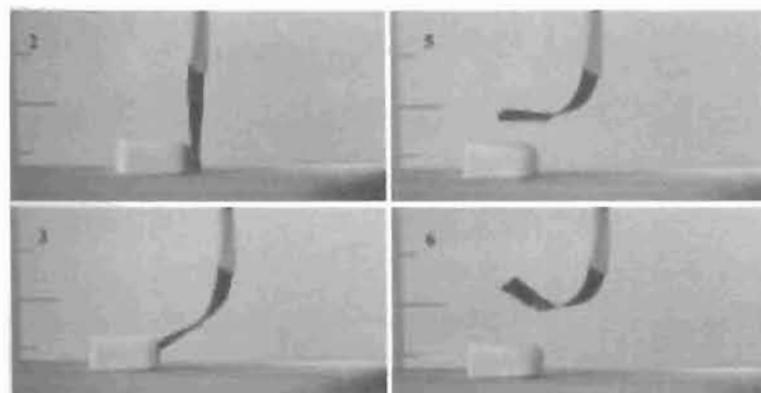


Figure 1.23. *Snapshots showing the mechanical actuation in polypyrrole actuator [adapted from reference Otero, T. F. et al 2003]*

1.9. Aim of the thesis

Based on the detail review discussed in this chapter, it is evident that polypyrrole nanostructures are produced using different kinds soft as well as hard template method. However, there is a large discrepancy in the synthesis of nanostructured polypyrrole with controllable morphologies, sizes and proper understanding of formation mechanisms. In general, synthetic approaches developed for PPy and PANI were found not suitable for the synthesis of polypyrrole-copolyaniline nanomaterials. Development of copolymer nanostructures is unexplored due to limitation of existing molecular templates to stabilise both aniline and pyrrole for new nanostructure formation. In this thesis, new molecular amphiphile based on renewable resource starting material were designed to address above issues. The idea of interconnecting both renewable resources and conducting nanomaterials is very new and have tremendous opportunities for fundamental and applied research. Renewable resource raw material based on cardanol, which is an industrial waste and pollutant from cashew nut industry, was utilized as novel amphiphilic dopants for conducting polypyrrole and polypyrrole-polyaniline nanomaterials. Additionally, colorimetric sensing approach of polyaniline was undeveloped technique due to its insolubility and mismatch of redox potential for some of the biomolecules. A water soluble self-doped polyaniline sulfonic acid colorimetric sensing approach was developed for vitamin-C and cysteine using redox chemistry polyaniline.

The work consists of following five important parts:

- (i) Synthesis and utilization of amphiphilic azobenzene sulfonic acid from renewable resource cardanol for size control synthesis polypyrrole nanomaterials
- (ii) Synthesis of polyaniline-polypyrrole random copolymer for understanding the morphology transformation and conductivity.
- (iii) Dilution of emulsion templates of aniline (95 %) + pyrrole (5%) for evolution of new morphologies like rods to hollow spheres to nanotubes
- (iv) Self-doped polyaniline sulfonic acid for the colorimetric sensing of biomolecules like vitamin-C and cysteine.

A amphiphilic surfactant molecule, 4-[4-hydroxy-2 ((Z)-pentadec-8-enyl) phenylazo]-benzene sulfonic acid (surfactant-1), synthesized from cardanol and utilized as structure-directing agent for polypyrrole nanomaterials (in Chapter-2). The micellar behavior and critical micelle concentration (CMC) of the surfactant was analyzed by dynamic light scattering (DLS), surface tension, conductance measurements. The role oxidizing agents on the morphology was also investigated. A dilution route has been carried out to control the size of the polypyrrole nanospheres from 500 nm to 60 nm. Earlier, the same renewable resource amphiphilic surfactant-1 was used to produce polyaniline nanofibers. Template selectivity of pyrrole and aniline monomers was utilized to tune the morphology of polyaniline-polypyrrole copolymer nanomaterial (in chapter-3). Copolymer nanomaterials showed a morphology transformation from fibers to rods to spheres predominantly at lower pyrrole concentration. Four probe conductivity measurements showed a non-linear trend in conductivity. Control experiments with structurally different surfactants showed that solid state ordering of the copolymer plays a crucial role in determining the conductivity. Morphology evolution of the copolymer nanomaterial was achieved from fiber to rods to hollow spheres to nanotubes at a fixed copolymer composition. The dilution of the fixed co-emulsion composition (5 mole % pyrrole + 95 mole % aniline) in water resulted in the transformation of short cylindrical to vesicular aggregates (in chapter-4). The chemical oxidation of the cylindrical templates produced nanofibers and nanorods whereas hollow spheres and nanotubes were produced by vesicular templates. The size and shape of the template aggregates

matched very well with that of the synthesized nanomaterials. The conductivity of the nanofibers was found one order higher than that of nanorods, hollow spheres and nanotubes at all temperatures due to one dimension electrical conduction. In chapter 5, self-doped polyaniline was synthesized from N-sulfopropyl aniline (monomer) via chemical oxidative polymerization. Poly-N-sulfopropyl aniline (PSPA) was structurally characterized by NMR, MALDI, IR and UV-Vis, owing to its water solubility. Dedoped polymer (PSPANa) was used for the colorimetric sensing of vitamin-C and cysteine. With the addition of the analytes the blue colored PSPANa becomes colourless. The mechanism of sensing of was due to electron transfer from the analyte to the emeraldine base form of the self doped polyaniline. The size and zeta potential of the micellar aggregates were determined by DLS and zeta-potential measurements. Jobs plot method was utilized to calculate the stoichiometry of complexation vitamin-C and cysteine with polymer in solution (formation of leucoemeraldine) and found 2:3 and 1:4 respectively. Finally, the overall outcome of the thesis is summarised in last chapter.

Chapter-2

Renewable Anionic Amphiphilic Surfactant for Polypyrrole Nanomaterials

2.1. Introduction

Polypyrrole nanomaterials have good electrical conductivity, environmental stability and biocompatibility and find wide range of applications in electronic and optical devices, chemical and electrochemical sensors, electrochromic devices, actuators and field emission applications etc [Wallace, G. G. *et al* 2002; Berdichevsky, Y. *et al* 2006; Otero, T. F. *et al* 2003; Wang, J. *et al* 2000; Bidon, G. *et al* 2000; Giroto, E. M. *et al* 1998; Korri-Youssoufi, H *et al* 1997; Ramanathan, K. *et al* 2005; Cosnier, S. *et al* 2005; Yoon, H *et al* 2005]. Polypyrrole nano-materials were synthesized using hard porous polymeric templates, electro-spinning, seeding technique, electrochemical polymerization, dispersion polymerization, interfacial polymerization, copolymer methodology or surfactant assisted micelles [Menon, V. P. *et al* 1996; Ikegame, M. *et al* 2003; Kang, T. S. *et al* 2005; Zhang, X *et al* 2005; Qu, L. *et al* 2003; Lu, G. *et al* 2006; Acik, M *et al* 2006; Vito, S. D. *et al* 1998; ^eLi, X. G. *et al* 2007; Jang, J *et al* 2005]. The surfactant-assisted chemical route is particular interesting because of easy removal of templates after the polymerization, potential for large scale-up reactions and ability to distribute reactants between the micellar and solvent phases, which direct the reaction pathways for specified size and shape of the nanomaterials. Polystyrene-co-poly(2-vinylpyridine) or polystyrene-co-poly(4-vinylpyridine) block copolymers, and cationic or anionic surfactants were employed as templates for the polypyrrole nanomaterial [^bZhang, X. *et al* 2006; Goren *et al* 2001; Yoo, S. I; *et al* 2004; Wu, A *et al* 2005; Zhong *et al* 2006; ^eJang *et al* 2005; ^bJang *et al* 2002]. Cetyltrimethylammonium bromide (CTAB) and dodecyltrimethylammonium bromide (DTAB) were good examples for cationic surfactants and produced nanofibers or spheres either in the presence of dopant-like HCl or under neutral conditions (see figure 2.1.). In general, it was noticed that the removal of the cationic or neutral surfactant molecules during the purification step significantly influences the properties of the nanomaterials such as solubility, conductivity, and processability [Wu, A *et al* 2005; Zhong *et al* 2006]. On the other hand, anionic surfactants are very attractive for polypyrrole because they behave both as micelles for polymerization as well as counter anion dopant for the positively charged polypyrrole matrix. The anionic surfactants permanently bind to the polymer chains and become part of the resultant nanomaterials, and thus the properties of polypyrrole nanomaterials were maintained even after purification via standard

protocols [De Armitt, C. *et al* 1993; Omastova, M. *et al* 2003; Stejskal, J. *et al* 2003; Shen, Y *et al* 1998; Lee, J. Y *et al* 1995; Haung, K. *Et al* 2005; Wie, Z *et al* 2005; Liu, J. *et al* 2001; Shen, Y. *et al* 1997; Cassagnol, C. *et al* 1998]. Polypyrrole nanotubes, nanofibers, and nanospheres were synthesized using anionic surfactants such as bis-(2-ethylhexyl)sulfosuccinate (AOT), sodium dodecylsulfate (SDS), dodecylbenzenesulfonic acid (DBSA), azobenzenesulfonic acid (ABS), and β -naphthalenesulfonic acid (NSA) [Omastova, M. *et al* 2004; Shen, Y *et al* 1998; Omastova, M. *et al* 2003; Lee, J. Y *et al* 1995; Haung, K. *Et al* 2005; Wie, Z *et al* 2005; Shen, Y. *et al* 1997] .

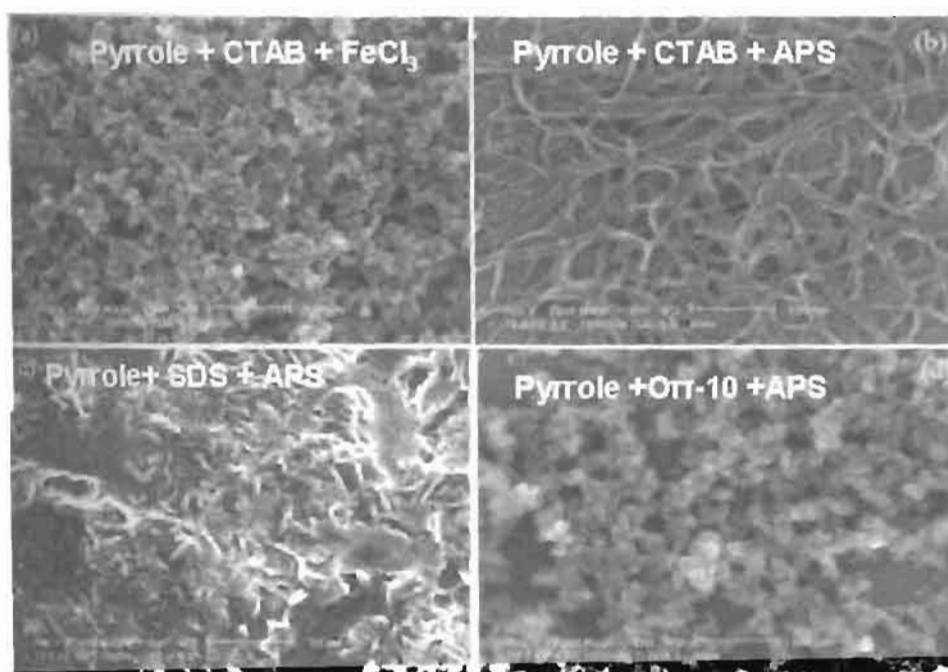


Figure 2.1. Polypyrrole morphology under different surfactants and oxidizing agents a) nanospheres b) nanowires c) no morphology d) nanospheres.

Most often, the synthesis of polypyrrole nanomaterials using anionic surfactants was found very sensitive to the pyrrole/surfactant ratio and good quality of nanomaterials was produced for only a few selective compositions [Haung, K. *et al* 2005; Lee, J. Y *et al* 1995; Shen, Y. *et al* 1997] see figure 2.1. The reason for the inhomogeneity in the nanomaterials formation was associated to the poor micelles formation of the anionic surfactants with pyrrole in water. Unlike in the case of cationic surfactants, unfortunately, the mechanism of the anionic surfactant-mediated

polypyrrole synthesis was not investigated in detail, which is a very crucial factor for reproducible nanomaterials synthesis [Zhang, X. *et al* 2006; Carswell, A.D *et al* 2003]. It is very important to stabilize the micelles in water and understand their polymerization mechanism for precise control of polypyrrole nanomaterial formation. Therefore, design and development of new amphiphilic anionic surfactant is very much in need for the synthesis of polypyrrole nanomaterials with good solubility, morphology, high solid-state ordering, and precise control over the structure-property relationships.

In this thesis, a renewable resource strategy has been developed for conducting polymer nanomaterials research. The building blocks used for nanochemistry are synthesized mainly from petroleum-based products. However, plant resources have distinct advantages for the generation of new building blocks of nanomaterials, because (a) they are obtainable from renewable resources and (b) they are cheap and abundant in nature [Vemula, P. K. *et al* 2008; John, G. *et al* 2001]. Additionally, the idea of interconnecting both renewable resources and conducting nanomaterials is very new and have tremendous opportunities for fundamental and applied research. This study is an effort to combine the principles of green chemistry and nanochemistry by making use of renewable plant-derived resources as the starting materials for the synthesis of conducting polymer nanomaterials. Renewable resource raw material cardanol, which is an industrial waste and pollutant from cashew nut (*Anacardium occidentale*) processing industry [Santos, M. L. *Et al* 2001], was utilized for the synthesis of new amphiphilic sulfonic acid, which template for polypyrrole nanomaterials. Cashew nut shell liquid (CNSL) is a natural source for unsaturated long-chain cardanol, obtained from thermal decarboxylation of anacardic acid, the main component of CNSL. Cardanol consists of four types *meta*-alkyl phenols with alkyl chains differing in their degree of unsaturation like 8-ene, 8, 11- dienes, 8, 11, 14-trienes and saturated side chain (see figure 2.2.). The amount and types of these components vary depending up on the species of the plant [Vemula, P. K. *et al* 2008; Santos, M. L. *Et al* 2001] This renewable material has wide applications in the form of adhesives, composites, flame retardants, surface coatings, paints and varnishes [C. K. S. Pillai *et al* 1990.; Menon, A. R. R *et al* 1995]

The hydroxyl group of cardanol is reactive and readily available for further functionalization leading to some new cardanol based molecular and polymeric

materials. For example, cardanyl acrylate was synthesized by the reaction of cardanol with acryloyl chloride, which produced a linear polymer upon solution polymerization in toluene using radical initiator [John, G. *et al* 1989; John, G. *et al* 1993] (see figure 2.3.). Upon removal of solvent and exposure to either air or UV light, the polymer underwent cross-linking to produce an insoluble transparent film.

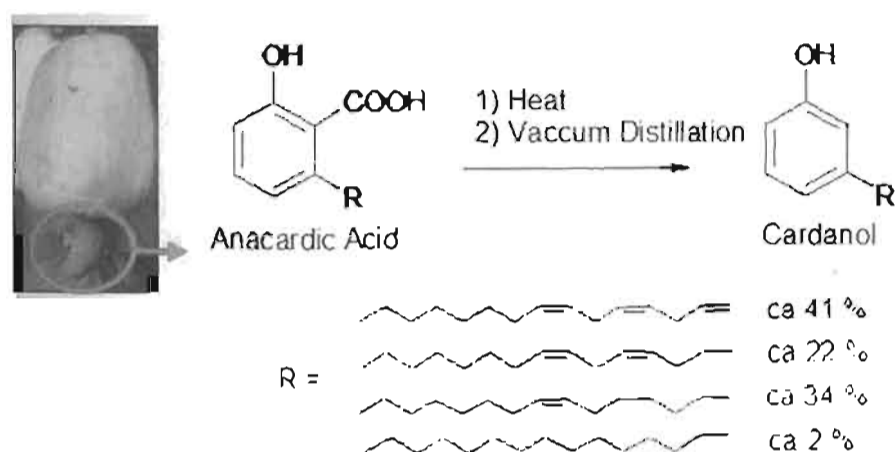


Figure 2.2. Cardanol from renewable resource CSA

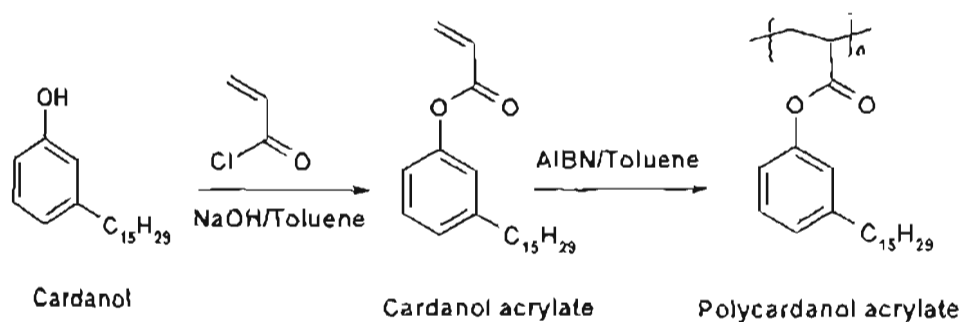


Figure 2.3. Synthesis of Poly cardanyl acrylates from cardanol.

S.K. Asha and co-workers have introduced hydrogen bonding urethane group as a spacer between hydrophobic cardanol unit and poly acrylate unit to induce self-assembly properties (see figure 2.4.). These polymers were undergone self assembly in different organic solvents into pores, spheres, vesicles, tubes etc. John, G. *et al* reported the synthesis of cardanyl glycolipids by attaching glucopyranose to cardanol (see figure 2.5.). Self-assembly properties of glycolipids have been extensively

investigated in hot aqueous solution to generate nanostructures, such as helical and twisted fibers and nanotubes [Yui, H. *et al* 2005; John, G. *et al* 2002].

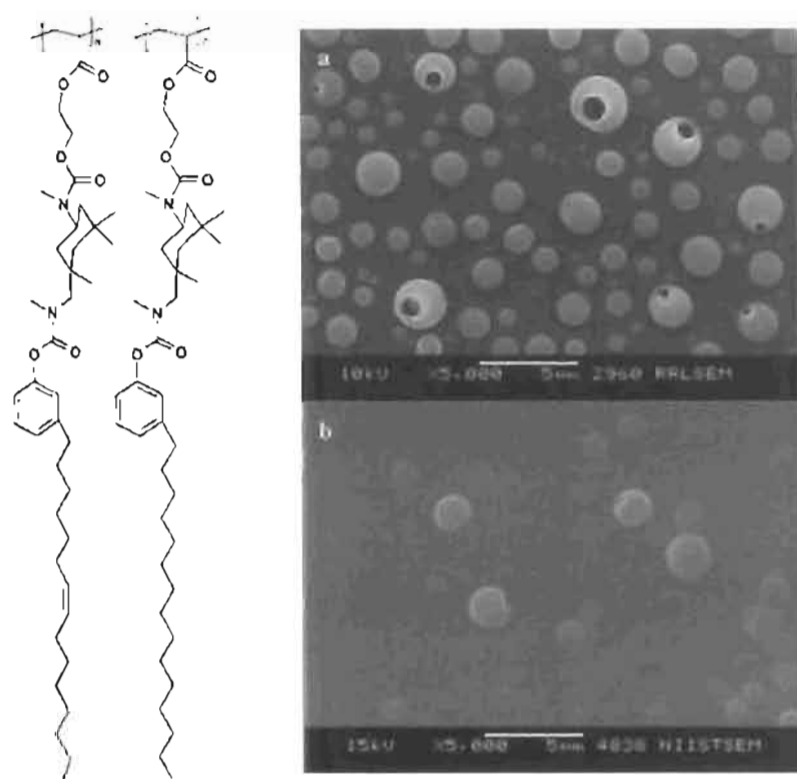


Figure 2.4. Cardanol-based side chain urethane methacrylates [Adapted from Rekha, N *et al* 2009].

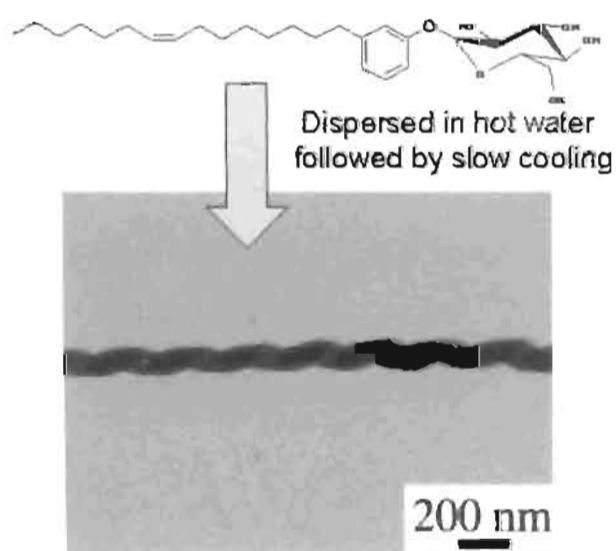


Figure 2.5. Cardanol based glycolipids [adapted from Vemula, P. K. *et al* 2008].

The synthesis of novel amphiphilic sulfonic and phosphoric acids from cardanol based materials was established by C. K. S Pillai and co-workers from our institute [Paul, R. K. *et al* 1999; Antony, R. *et al* 1990]. It was found that when cardanol was treated directly with H₂SO₄, the resin formation takes place instead of ring sulfonation due to the presence of unsaturation in the pentadecyl side chain. Hydrogenation of cardanol was carried out to saturate the side chain and the saturated cardanol was sulfonated to give the sulfonic acids. These dopants are insoluble in water (due to stiff packing of hydrophobic saturated side chain) at room temperatures and not explored as soft templates for polyaniline nanomaterials. Therefore, the direct utilization of cardanol based dopants as soft templates for conducting nanomaterials is a challenging problem to be addressed. Similarly, renewable resource lignosulfonic acid (LSA), a waste from the paper pulp industry, was used for the preparation of conducting polyaniline, polyaniline-ferromagnetic composites and exploration of polyaniline for biomedical applications [Jayakannan, M. *et al* 2006; Roy, S. *et al* 2002]. The complex formation of lignosulfonic acid sodium salt (LSA) with polyaniline has been studied and found that lignosulfonic acid was showing the doping behaviour like any other dopants and yields highly conducting polyaniline. However, so far no attempts were reported for synthesizing and controlling the properties of polypyrrole nanomaterials based on renewable resource materials.

In this chapter, a renewable resource amphiphilic surfactant [4-[4-hydroxy-2((Z)-pentadec-8-enyl) phenylazo]-benzenesulfonic acid (surfactant-1) has developed from cardanol. The new dopant possesses unique amphiphilic geometry with a hydrophilic polar head and hydrophobic alkyl chain to produce micelles in water. These micellar aggregates behaved as template for polypyrrole nanosphere synthesis in emulsion and dilution route. The micellar behaviour and critical micelle concentration (CMC) of the dopant was obtained from the dynamic light scattering (DLS), surface tension, and ionic conductance studies. The results revealed that the anionic surfactant exists in the form of 4.3 nm size micelle in water. The interaction of surfactant with pyrrole produces aggregated micelles. The composition of the pyrrole: anionic surfactant was varied from 1: 1/3 to 1: 1/100 (up to 100 times lower amount of surfactant with respect to pyrrole) in the feed, and the polypyrrole nanospheres were produced through controlled and self-organized micellar-mediated templates in water. The role of the oxidizing agents was also investigated for the

wider pyrrole: surfactant composition using ammonium persulfate (APS) and ferric chloride (FeCl_3). Additionally, an effort has been made to find out the role of dilution on the polymerisation for controlling size of polypyrrole nanospheres ranging from 0.5 μm to 50 nm. Dynamic light scattering, electron microscopy and particle size measurements are used to propose the mechanism of formation of polypyrrole nanomaterial formation. The schematic representations of the above approach are shown in Figure 2.6.

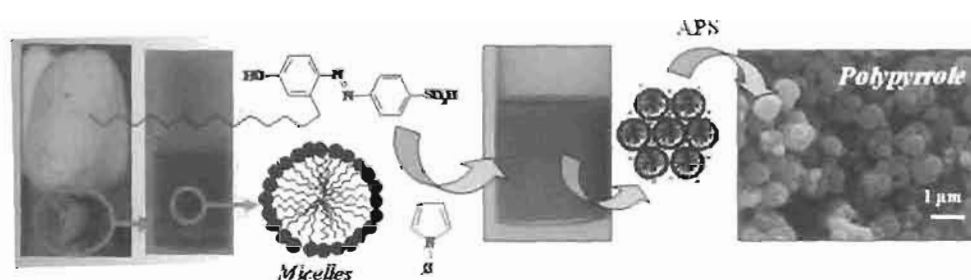


Figure 2.6. Synthesis of polypyrrole nanospheres via emulsion route.

The polypyrrole nanospheres were characterized by SEM, TEM, UV-visible, DLS, particle size analyzer, and wide-angle X-ray diffractions, etc. In a nut shell, we have successfully utilized amphiphilic anionic surfactant for the size controlled synthesis of polypyrrole nanospheres and to establish the mechanism of formation.

2.2. Experimental procedures

2.2.1. Materials: Pyrrole, ammonium persulfate (APS), sulfanilic acid and ferric chloride hexahydrate were purchased from sigma aldrich. Cashew nut shell liquid (CNSL) used in this study was obtained from Vijayalakshmi cashew company, in Kollam district of Kerala, India. Cardanol was purified by double-vacuum distillation at 3-4 mm of Hg, and the fraction distilled at 220-235 $^{\circ}\text{C}$ was collected.

2.2.2. General procedures: NMR spectra of the compounds were recorded using a 500-MHz Bruker NMR spectrophotometer in d_6 -DMSO containing tetramethylsilane (TMS) as the internal standard. Infrared spectra of the polymers were recorded using a Perkin-Elmer precisely spectrum one FT-IR spectrometer in the range of 4000-400

cm^{-1} . The purity of the compounds was determined by fast atom bombardment high-resolution mass spectrometry (FAB-HRMS: JEOL JSM 600). For SEM measurements, polymer samples were subjected to a thin gold coating using a JEOL JFC-1200 fine coater. The probing side was inserted into a JEOL JSM-5600 LV scanning electron microscope for taking photographs. TEM analysis was recorded using a Hitachi H-600 instrument at 75 kV and Tecnai 30 G² S-twin 100 KV HR-TEM. For TEM measurements a suspension of nanospheres was prepared in ethanol and deposited on a formvar coated copper grid. UV-Vis spectra of the polypyrrole nanospheres were recorded using a Perkin-Elmer Lambda-35 UV-Vis spectrometer. For conductivity measurements, the polymer samples were pressed into a 10 mm diameter pellet and analyzed using a four-probe conductivity instrument by applying a constant current. The resistivities of the samples were measured at five different positions. WXR D of the finely powdered polymer samples were recorded by a Philips analytical diffractometer using Cu-K α emission. The spectra were recorded in the range of $2\theta = 2-40$ degrees and analyzed using X'Pert software. Particle size analysis was done by Malvern U.K. Zetasizer 3000 HAS (static light scattering) and DLS measurement (DLS) was done by Nano ZS Malvern instrument employing 4 mW He-Ne laser ($\lambda = 632.8$ nm) and equipped with a thermo stated sample chamber. The thermal stability of polymers were determined by using a TGA-50 Shimadzu thermogravimetric analyzer at a heating rate of 10 °C /min in nitrogen.

2.2.3. Synthesis of surfactant-1

Purification of cardanol: CNSL (1.25 L) was taken in a 2 L round bottom flask equipped with a distillation set up. The contents were allowed to boil for 1 h at 120 °C under sufficient vacuum. During this time most of the anacardic acid was decarboxylated to form cardanol. This conversion was indicated by the evolution of plenty of smoke due to the generation of carbon dioxide. Finally, the temperature of the mixture was elevated to 180 °C and distilled out the clear yellow liquid at 230 °C under vacuum (5 mm of Hg). The collected yellow liquid was re-distilled (230 °C, under 5 mm of Hg) to get 500 mL of pale yellow coloured pure cardanol. ¹H-NMR (500 MHz, CDCl₃), δ : 7.19 (t, 1H, Ar-H), 6.80 (d, 2H, Ar-H), 6.70 (m, 2H, Ar-H), 5.45 (b, 2H, CH=CH), and 2.9-0.6 ppm (m, 27H, aliphatic- H). ¹³C-NMR (125 MHz,

CDCl₃) 155.5, 144.9, 130, 129.4, 120, 115.4, 112.6, 35.8, 32.6, 31.9, 31.8, 29.8, 29.5, 29.4, 29.3, 29.1, 28.9, 27.3, 22.8 and 14.5. FT-IR (KBr, cm⁻¹): 3353, 3006, 2929, 1590, 1305, 1456, 1265, 984, 873, 811, 702 and 515. FAB-MS (MW: 302.0): *m/z* = 303.1 (M⁺).

Synthesis of 4-[4-Hydroxy-2((Z)-pentadec-8-enyl)phenylazo]-benzenesulfonic acid (Surfactant-1): Sulfanilic acid (6.9 g, 39.7 mmol) and sodium carbonate (1.6 g, 14.7 mmol) were dissolved in water (70 mL) by heating to 60-70 °C. It was then cooled to 5 °C, and a cold solution of sodium nitrite (2.4 g, 35.4 mmol) in water (8 mL) was added. The resultant yellow solution was poured into ice (50.0 g) containing concentrated HCl (8 mL) and stirred using a mechanical stirrer for 30 min at 5 °C. The cold diazonium salt was added dropwise into an aqueous solution containing cardanol (10.0 g, 33.1 mmol) and sodium hydroxide (4.0 g, 100 mmol) in water (30 mL). The reaction was continued with stirring for 3 h in ice-cold conditions using a mechanical stirrer. The reaction mixture was neutralized by the addition of concentrated HCl (40 mL) in crushed ice (70.0 g). The red precipitate was filtered using a Buchner funnel and washed with water. The crude dried product (13.0 g) was further purified by passing through silica gel column using 5% methanol in ethyl acetate. The solvent was removed to obtain the product as a red-orange solid. Yield = 7.8 g (49 %). ¹H NMR (500 MHz, *d*₆-DMSO) δ: 7.75 ppm (s, 4H, Ar-H), 7.57 ppm (d, 1H, Ar-H), 6.75 ppm (s, 1H, Ar-H), 6.70 ppm (d, 1H, Ar-H), 5.24 ppm (2H, CH=CH), 3.1-0.06 ppm (m, 27H, aliphatic- H). ¹³C NMR (125 MHz, *d*₆-DMSO) δ: 161.3, 152.6, 149.1, 145.8, 142.9, 129.7, 126.8, 121.8, 116.9, 116.4, 114.2, 31.8, 31.2, 30.8, 29.1, 28.9, 28.6, 26.7, 26.6 and 25.3. FT-IR (KBr, cm⁻¹): 3006, 2923, 2852, 2852, 1600, 1533, 1498, 1369, 1338, 1263, 1174, 1116, 1033, 1007, 820, 706, and 559. UV-Vis (in H₂O, λ max) 365 and 463 nm. FAB-MS (MW: 486): *m/z* 486.3 (M⁺).

2.2.4. Synthesis of polypyrrole nanomaterials

Emulsion route synthesis of polypyrrole nanomaterials: Typical procedure for the preparation polypyrrole nanospheres is given for **P-100a**. The surfactant **1** (70 mg, 0.144 mmol) (for **P-100a**, pyrrole: surfactant is 1:1/100) was added to 25 mL of double distilled water in a 100 mL round-bottom flask and stirred for 15 min. Freshly

distilled pyrrole (1.0 mL, 14.4 mmol) was added to the above solution and stirred for 45 min in ice-cold condition to obtain a dark red viscous solution. Ammonium per sulphate (0.9 g, 4 mmol) in double distilled water (15 mL) was added drop by drop to the above solution, and stirring was continued for 8 h under ice-cold condition. The resulting polypyrrole was purified by pouring into a large excess of distilled water, filtered, and washed with distilled water and methanol until the filtrate become colorless. The black powder sample was dried under vacuum (0.1 mm of Hg) for 12 h prior to further analysis. Yield = 33 (%). FT-IR (KBr, cm^{-1}): 1540, 1460, 1360, 1295, 1190, 1172, 1090, 1036, 960, 905, 783, 670 and 612. UV-Vis (water, λ max): 480 nm, 1000 nm.

A similar procedure was adopted by varying the amount of [pyrrole]: [surfactant] ratio from 1:1/3 to 1:1/75 using APS as oxidizing agent to prepare polypyrrole nanomaterials **P-3a** to **P-75a** (**a** for series using APS).

Alternatively, ferric chloride (14.4 mol, 3.9 g) was employed as oxidizing agent instead of APS for pyrrole: surfactant ratio from 1:1/5 to 1:1/100 to prepare polypyrrole nanomaterials **P-5b** to **P-100b** (**b** for series using FeCl_3).

Dilution route synthesis of polypyrrole nanospheres: A dilution route has been carried out on the fixed composition of P-100 (1: 1/100; pyrrole: surfactant) to investigate the role of concentration on morphology. Typical procedure for the synthesis of P-1 is given below. Surfactant (70 mg, 0.144 mmol) was taken in 10 mL water and stirred in a sonicator (From Aldrich, Bransonic 3510E-MTH) for 15 min. Pyrrole (1 mL, 14.4 mmol) was added to the surfactant solution and sonicated for 45 min. At the end of stirring, the polymerization mixture turned into a pale yellow thick emulsion. APS (3.28 g, 14.4 mmol) in water (5 mL) was added drop wise to the solution and continued the stirring under sonicator for 1 h. Then the reaction was allowed to continue for 8 h without further disturbance at 25 °C. The sample was filtered, washed with water and methanol till the filtrate become colorless. The polypyrrole nanomaterial was dried under vacuum oven for 12 h at 50 °C. Yield = 89 %. FT-IR (KBr, cm^{-1}): 1540, 1460, 1360, 1295, 1181, 1090, 1036, 960, 905, 783, 670, and 612. UV-Vis (water, λ max): 480 nm, 1000 nm.

Polymers **P-2**, **P-3**, **P-4**, **P-5**, **P-6**, **P-7**, and **P-8** were synthesized by adopting similar procedure with the amount of water ranging from 15, 20, 50, 100, 150, 200,

and 250 mL, respectively (same amount of pyrrole, dopant, and APS). Various amount of water was added to the reaction mixture and stirred using sonicator before the polymerization by APS.

2.3. Results and discussion

2.3.1. Synthesis of new azobenzene amphiphilic surfactant

Cashew nut shell liquid (CNSL) is plant based renewable resource and by-product of the cashew processing industry [Vemula, P. K. *et al* 2008]. CNSL contains anacardic acid as major component, which on heat treatment and followed by vacuum distillation (230 °C at 5 mm of Hg) undergo decarboxylation to yield pure cardanol. Cardanol was purified by double vacuum distillation at 5 mm of Hg and the fraction distilled at 230 - 235 °C was collected [Santos, M. L. *Et al* 1999]. The NMR and mass spectrum confirms this molecule has only one double bound at 8th carbon atom in the side chain. We adopted a diazotization coupling reaction in water using diazonium salt of sulfanilic acid and coupled with cardanol under basic conditions to yield, 4-[4-hydroxy-2((Z)-pentadec-8-enyl)phenylazo]-benzenesulfonic acid (surfactant-1). Under above reaction conditions, the side chain double bond is inactive and does not affect the diazotization reactions. The synthesis of surfactant-1 is represented in figure 2.7.

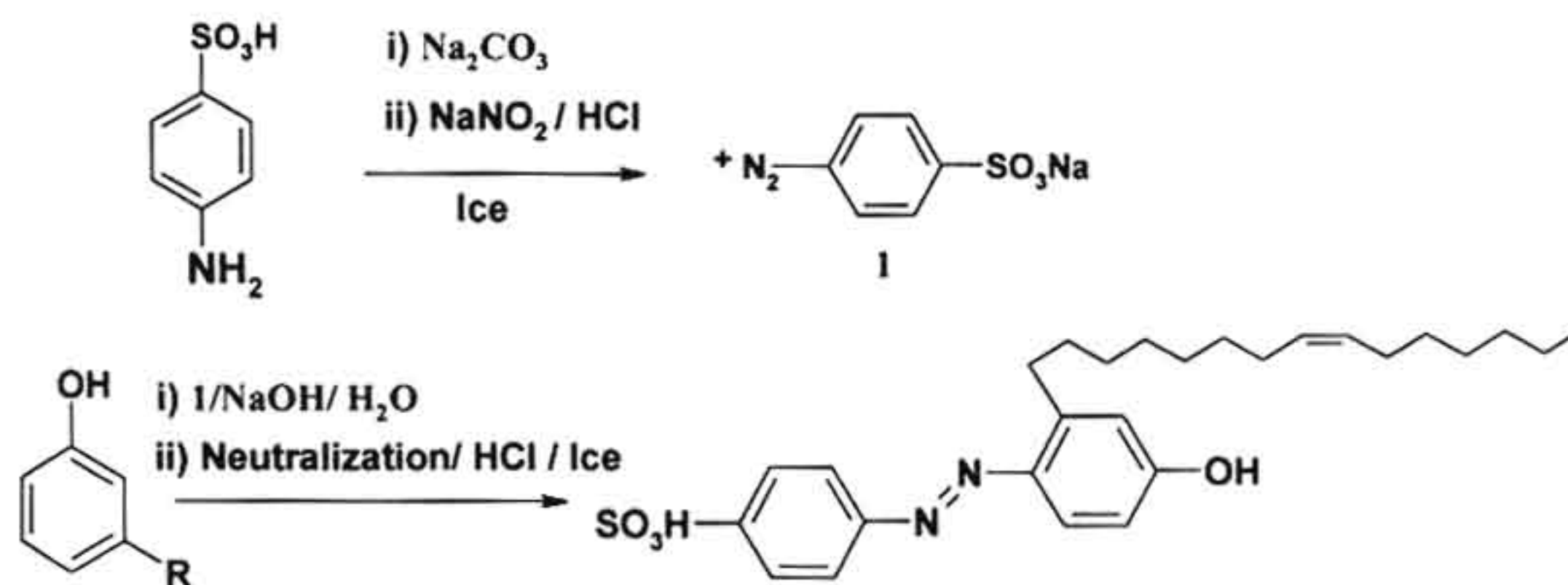


Figure 2.7. Synthesis of amphiphilic azobenzene surfactant from cardanol.

The structure of the cardanol and surfactant was confirmed by NMR and mass techniques were shown in figure 2.8. Cardanol has shown four aromatic protons at

7.19, 6.80, 6.70 and 6.68 ppm and unsaturated double bonds in the side chains appear at 5.43 ppm. The rest of the protons in the side chain appear from 2.9 to 0.76 ppm. The integration of the peaks was very well matched with the required number of protons and it confirms (Z)-(pentadec-8-enyl) phenol. The $^1\text{H-NMR}$ spectrum of surfactant-1 shown all different types aromatic and aliphatic protons are assigned with alphabets. The four protons in the aromatic ring containing the sulfonic acid group appears together at 7.75 ppm (e+ f), whereas the aromatic protons from the other phenolic ring appears with characteristic splitting pattern at 7.57, 6.75 and 6.70 ppm. The double bond in the side chain appears at 5.24 ppm and all other aliphatic protons appear below 3.2 ppm. The $^{13}\text{C-NMR}$ spectrum also showed all peaks corresponding to the number carbon atoms of surfactant see figure 2.9. The peak intensities are in accordance to the expected structure, which confirm the formation of the expected amphiphilic dopant. FT-IR analysis surfactant showed a broad peak at 3444 cm^{-1} corresponds to the -OH stretching of the sulfonic acid group. The C-H stretching vibration bands appeared at 2923 and 2852 cm^{-1} . The peak at 1600 cm^{-1} is for the C=C vibrations. The peak at 1496 cm^{-1} was due to stretching vibrations of aromatic rings and the peak at 1033 cm^{-1} is due to sulfonic acid vibrations (see figure 2.14.).

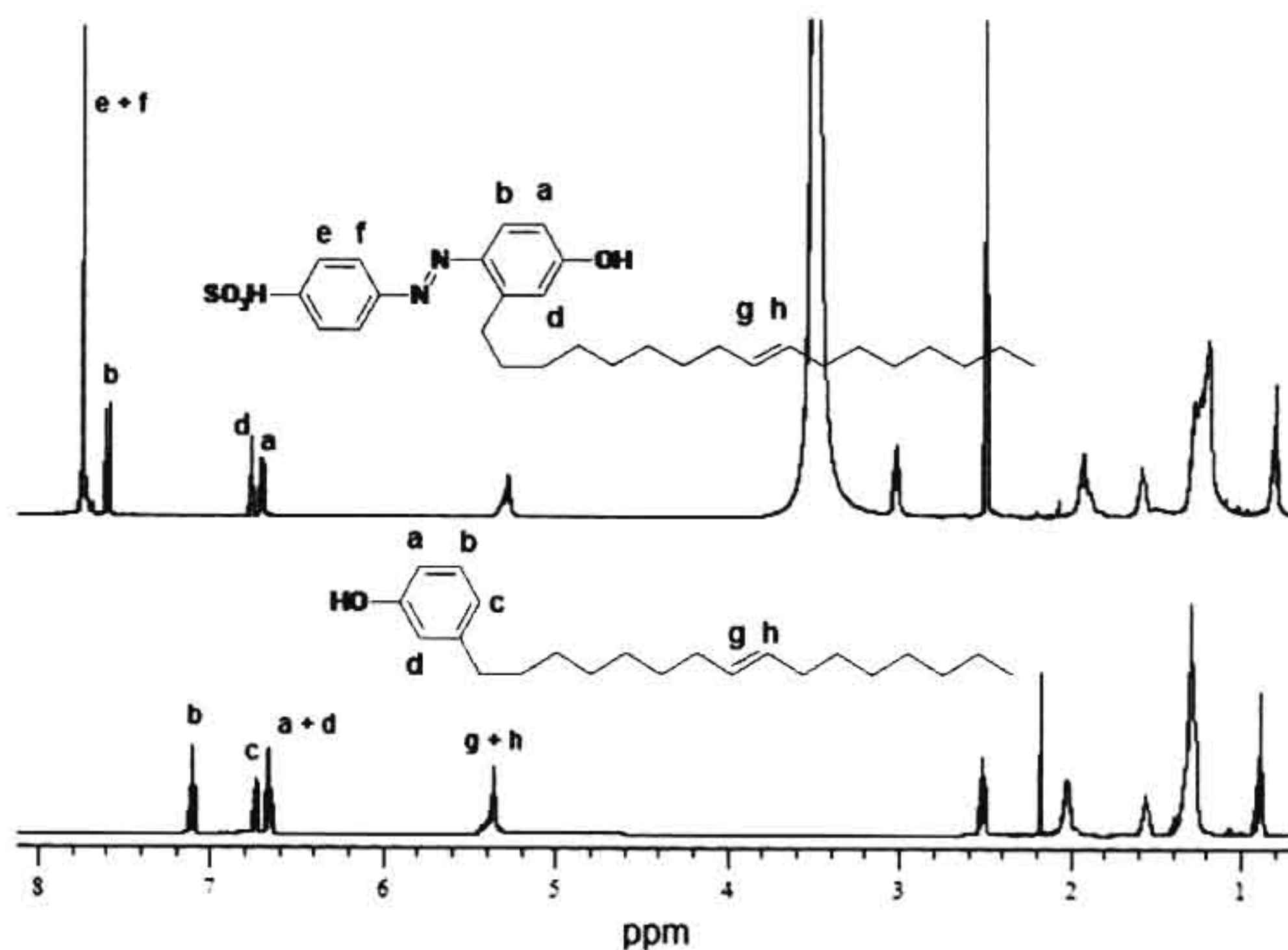


Figure 2.8. $^1\text{H-NMR}$ of cardanol and surfactant-1

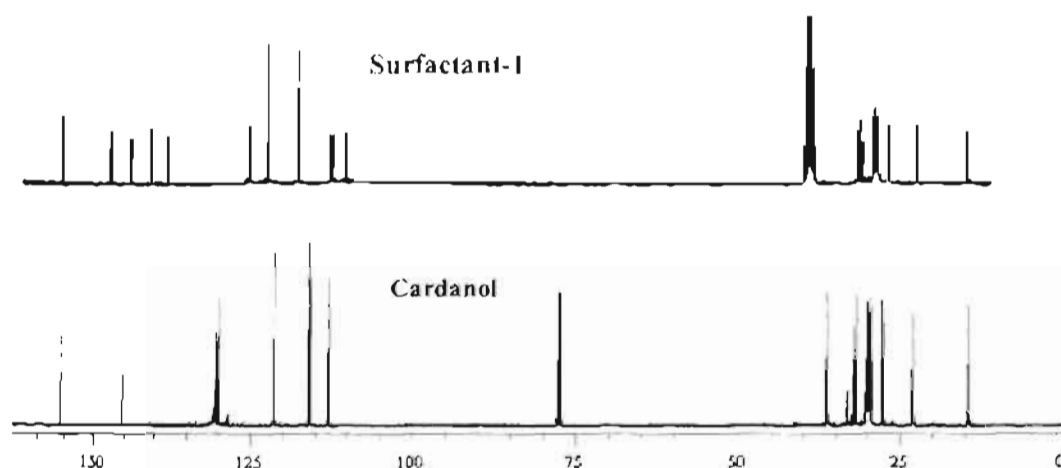


Figure 2.9. ^{13}C -NMR of cardanol and surfactant-1

2.3.2. Micellar behaviour of the surfactant

Surfactant-1 is soluble in water and forms foam like solution with gradual increase of concentration. In order to find out the existence of micellar behaviour, the surfactant was subjected to dynamic light scattering (DLS) studies in water at (1×10^{-3} M) see figure 2.10 [Buchholz, Y. *et al* 2008; Zhang, X. *et al* 2006]. DLS analysis revealed that more than 99.4 % of the azobenzene surfactant molecule in water exists in the form of the micelles and their average diameters were obtained as 4.29 nm. In emulsion polymerization route, the shape and dimensions of the nano-materials are highly depended on their micellar state. The theoretical size of the surfactant molecule was calculated using AM1 calculations and found that the end-to-end distance of the polar head to hydrophobic tail was obtained as 24.4 Å or 2.44 nm (see figure 2.10.). The diameter of the tightly packed spherical micelles is always equal to the double the length of surfactant molecule. The theoretical diameter of the micelle is equal to $2 \times 2.44 \text{ nm} = 4.88 \text{ nm}$, which is almost matching with that of the values obtained experimentally by DLS. In order to get more insight in to the dopant packing factor, we have utilized energy minimized AM1 structure (see figure 2.11.). The molecule has a bend shape with a head group radius of 1.36 nm, tail length of 2.01 nm with overall molecular length of 2.44 nm. It appears as a cone shape with large head and a long hydrophobic tail. The P_c for the new amphiphilic dopant molecule was calculated

equation (1) of chapter 1 obtained as 0.34, which predicts the shape of the aggregates as spherical one [Israelachvili, J. N. *et al* 1976].

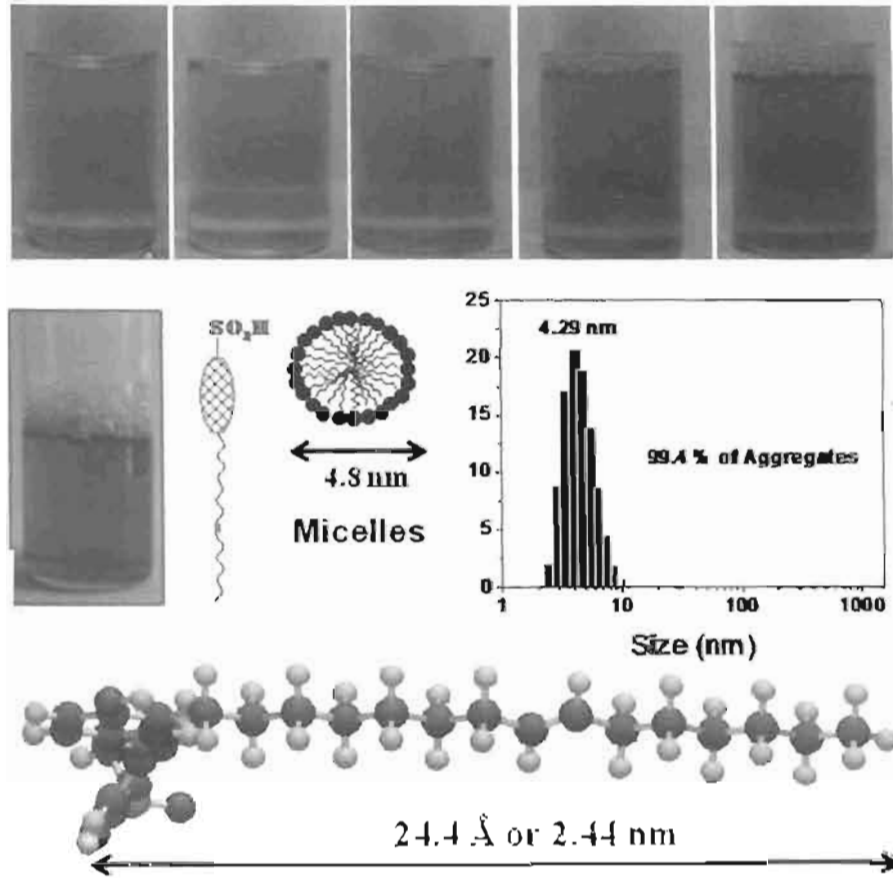


Figure 2.10. DLS histogram of the surfactant and energy minimised structure.

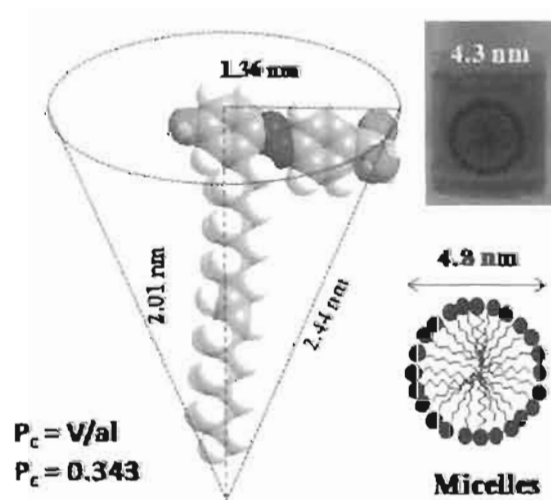


Figure 2.11. Molecular geometry and theoretical packing factor.

The surfactant molecule was subjected to surface tension and ionic conductance measurements to determine CMC. The surface tension measurement was carried out by Wilhelmy Plate method in double distilled water at 27°C at various concentrations [Franke, D. *et al* 2005]. The plot of surface tension against surfactant concentration revealed that the surface tension decreased with increase in surfactant concentration and after a particular concentration surface tension remains unchanged (see figure 2.12). The CMC was taken as the concentration where the surface tension changes its trend and is found to be 4×10^{-4} M. Another important physical property which gives an idea about the CMC as well the structural changes in anionic surfactant molecules is its specific conductance measurements [Atkins, P. *et al* 2002]. The plot of specific conductance versus concentration of the dopant is given in figure 2.12. Specific conductance was very low at 1×10^{-5} M surfactant concentration, which may be due to the less number of molecules to carry the ionic charge. As the concentration of the surfactant increases above 1×10^{-4} M, the specific conductance showed gradual increment marking the transformation of loose aggregates to spherical micelles, which can conduct more current. The break point of specific conductance plot directly gives the CMC as $\sim 4 \times 10^{-4}$ M. These two independent experiments also confirmed that the surfactant forms micelles above its CMC $\sim 4 \times 10^{-4}$ M.

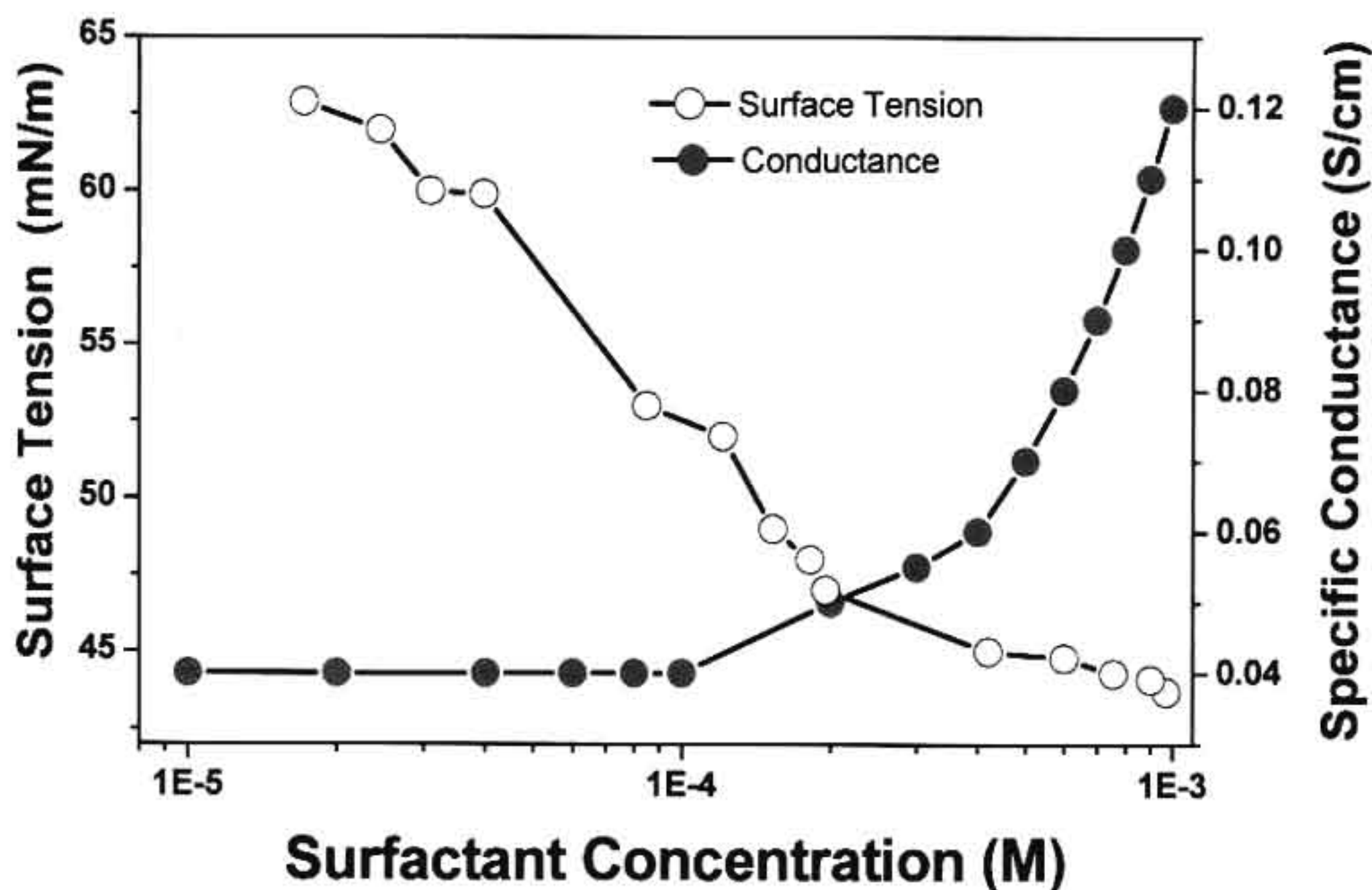


Figure 2.12. Concentration dependent changes in surface tension and ionic conductance of the surfactant solution.

2.3.3. Polypyrrole nanospheres via emulsion route

The surfactant has unique built-in amphiphilic design in which the hydrophilic sulphonic acid behaves as polar head and the long alkyl chain as hydrophobic tail. The new surfactant is freely soluble in water and various water loving organic solvents, which have an added advantage for preparing polypyrrole nano-structures under micellar mediated self-organization approach. The polypyrrole nano-materials were synthesized by varying the pyrrole : surfactant composition over a wide range from 1: 1/3, 1:1/4, 1:1/5, 1:1/10, 1:1/25, 1:1/50, 1:1/75 to 1:1/100 (up to 100 moles less amount of surfactant with respect to pyrrole) in water at ambient conditions (see figure 2.13.). The concentration of the pyrrole was fixed as 3.6×10^{-1} M for all the compositions and the concentration of surfactant was varied by dissolving various amounts in water (1.2×10^{-1} M to 3.6×10^{-3} M, see table 2.1). Typically, the polymerization was carried out by taking pyrrole and surfactant in water and stirred using mechanical stirrer under ice cold conditions for 1 h. The resultant viscous red solution was oxidized by adding aqueous solution of ammonium per sulfate or ferric chloride at 0-5 °C under mechanical stirrer for 30 minutes. The polymerization was continued for 8 h and the green nano- material was filtered and purified by washing with water and methanol until the filtrate become colorless. It was dried under vacuum for 24 h (0.05 mm of Hg) at 60 °C in vacuum oven prior to further analysis.

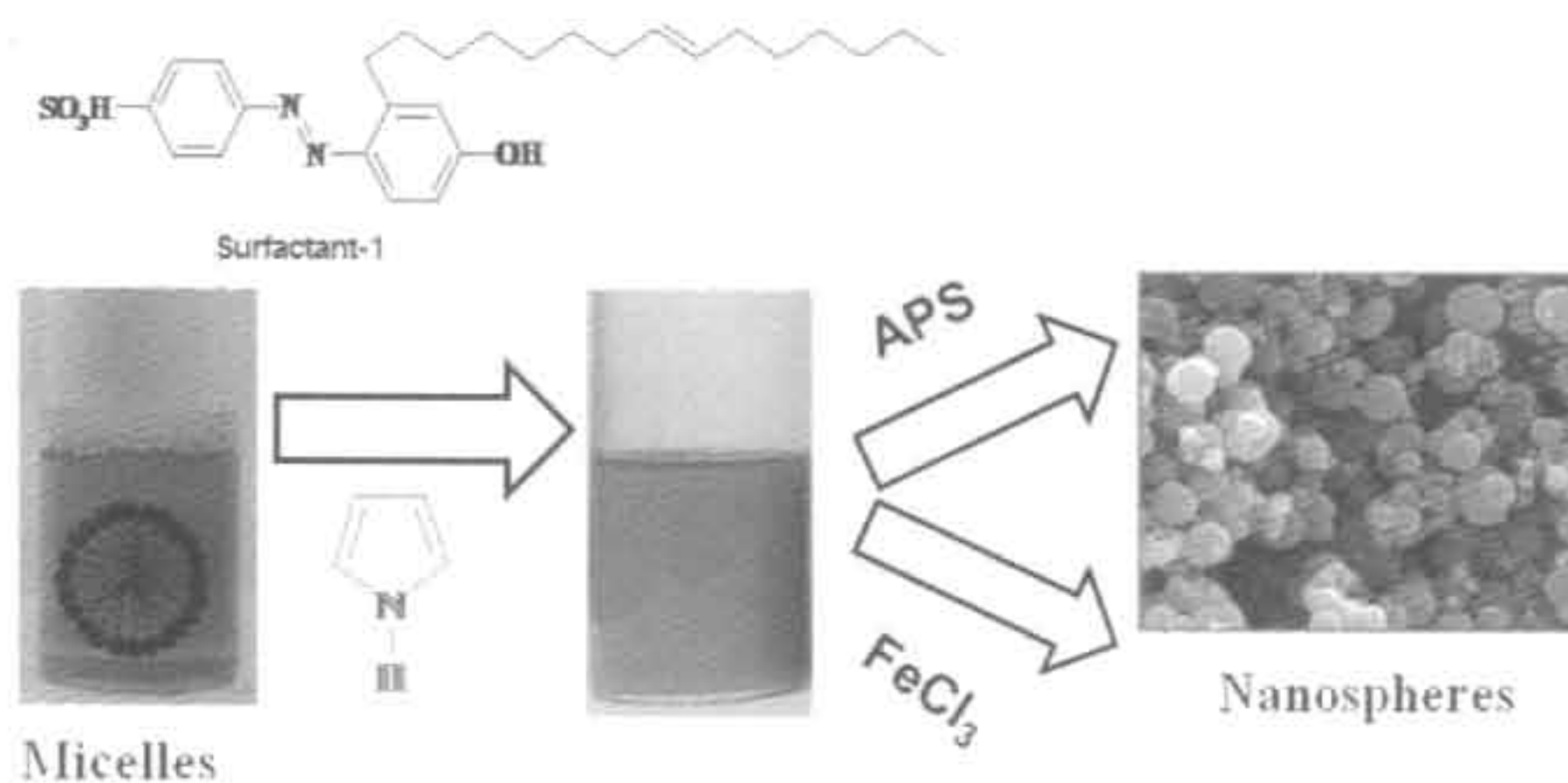


Figure 2.13. Synthesis of polypyrrole nanospheres via emulsion polymerization using APS and $FeCl_3$ as oxidising agents.

The polymers are denoted as **P-Xa** or **P-Xb**, where 'X' is corresponding to the pyrrole/dopant (in moles) in the feed and 'a' and 'b' represent the nano-materials prepared using APS or FeCl₃ as oxidizing agents, respectively. The yield and composition of the polypyrrole nano-materials, **P-3a** to **P-100a** and **P-5b** to **P-100b** are summarized in table 2.1. The degree of doping is obtained from the elemental analysis of the nano-materials. The sulphur/nitrogen (S/N) ratios were summarized in table 2.1 for all the polymer samples. The S/N values were matching with earlier reports of polypyrrole nano-materials prepared using anionic surfactants.

Table 2.1. Concentration of the reactants used for synthesis, yield and elemental analysis of nanomaterials.

Sample ^a	Conc. of dopant (M)	Dopant: Pyrrole (moles) ^b	Yield ^c (%)	S/N ratio ^d
P-3a	1.2×10^{-1}	1:3	27	0.34
P-4a	9.0×10^{-2}	1:4	24	0.32
P-5a	7.2×10^{-2}	1:5	23	0.30
P-10a	3.6×10^{-2}	1:10	23	0.29
P-25a	1.4×10^{-2}	1:25	38	0.26
P-50a	7.2×10^{-3}	1:50	29	0.25
P-75a	4.8×10^{-3}	1:75	30	0.26
P-100a	3.6×10^{-3}	1:100	33	0.25
P-5b	7.2×10^{-2}	1:5	51	0.32
P-10b	3.6×10^{-2}	1:10	55	0.24
P-25b	1.4×10^{-2}	1:25	58	0.21
P-50b	7.2×10^{-3}	1:50	56	0.12
P-75b	4.8×10^{-3}	1:75	57	0.11
P-100b	3.6×10^{-3}	1:100	58	0.08

^a Polypyrrole synthesized using ammonium persulfate (series-a) or FeCl₃ (series-b) as oxidizing agents.

^b Concentration of pyrrole was maintained as $3.6 \times 10^{-1} M$ for all the polymerization reactions. ^c Yield calculated for isolated product. ^d Sulphur/ Nitrogen ratio was obtained by elemental analysis.



The polypyrrole nano-materials were subjected to FT-IR analysis to confirm the structure of the doped polymers see figure 2.14. The FT-IR spectra have showed clear characteristic peaks at 1548 and 1466 cm^{-1} with respect to symmetric and anti-symmetric aromatic ring-stretching modes [Zhang, X. *Et al* 2006; Omastova, M. *et al* 2004]. The peaks at 1050 and 1300 cm^{-1} are corresponding to the C-H and C-N stretching vibrations, respectively [Omastova, M. *et al* 2004]. The presence of two peaks at 1190 cm^{-1} was attributed to the SO_3 -aromatic ring in doped state of polypyrrole. The peak at 915 cm^{-1} is corresponding to the O=S=O stretching vibration in the sulfonic acid groups of the dopant. All the peaks are in accordance with the literature reported for polypyrrole materials.

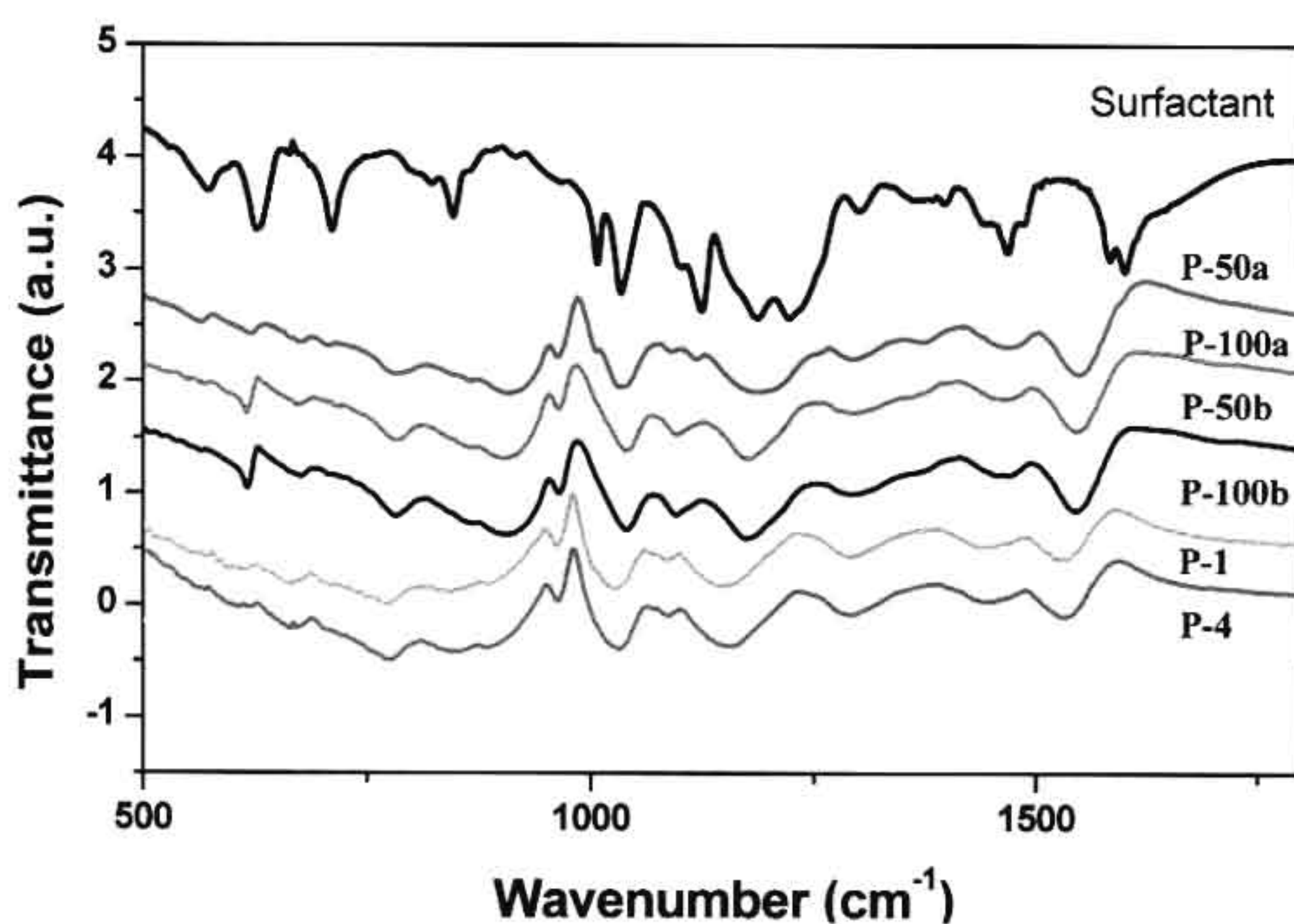


Figure 2.14. FT-IR spectra of polypyrrole nanospheres

2.3.4. Morphology of polypyrrole nanomaterials

The morphologies of the nano-materials were recorded using JEOL JSM-5600 LV scanning electron microscope and SEM images of the polypyrrole samples are given in figure 2.15. The anionic azobenzenesulfonic acid surfactant mediated polypyrrole nano-materials were highly sensitive to the pyrrole: surfactant ratio and different morphologies were produced depending upon their amount in the feed. At higher surfactant concentration (1.2×10^{-1} to 9.0×10^{-2} M) (for P-3a to P-5a), coral-

like morphology was obtained. As the surfactant amount further decreases in the feed (3.6×10^{-2} to 3.6×10^{-3} M, from **P-10a** to **P-100a**), the reaction mixture was found more homogeneous which resulted in the formation of uniform polypyrrole nano-spheres of diameter in the range of 150-250 nm.

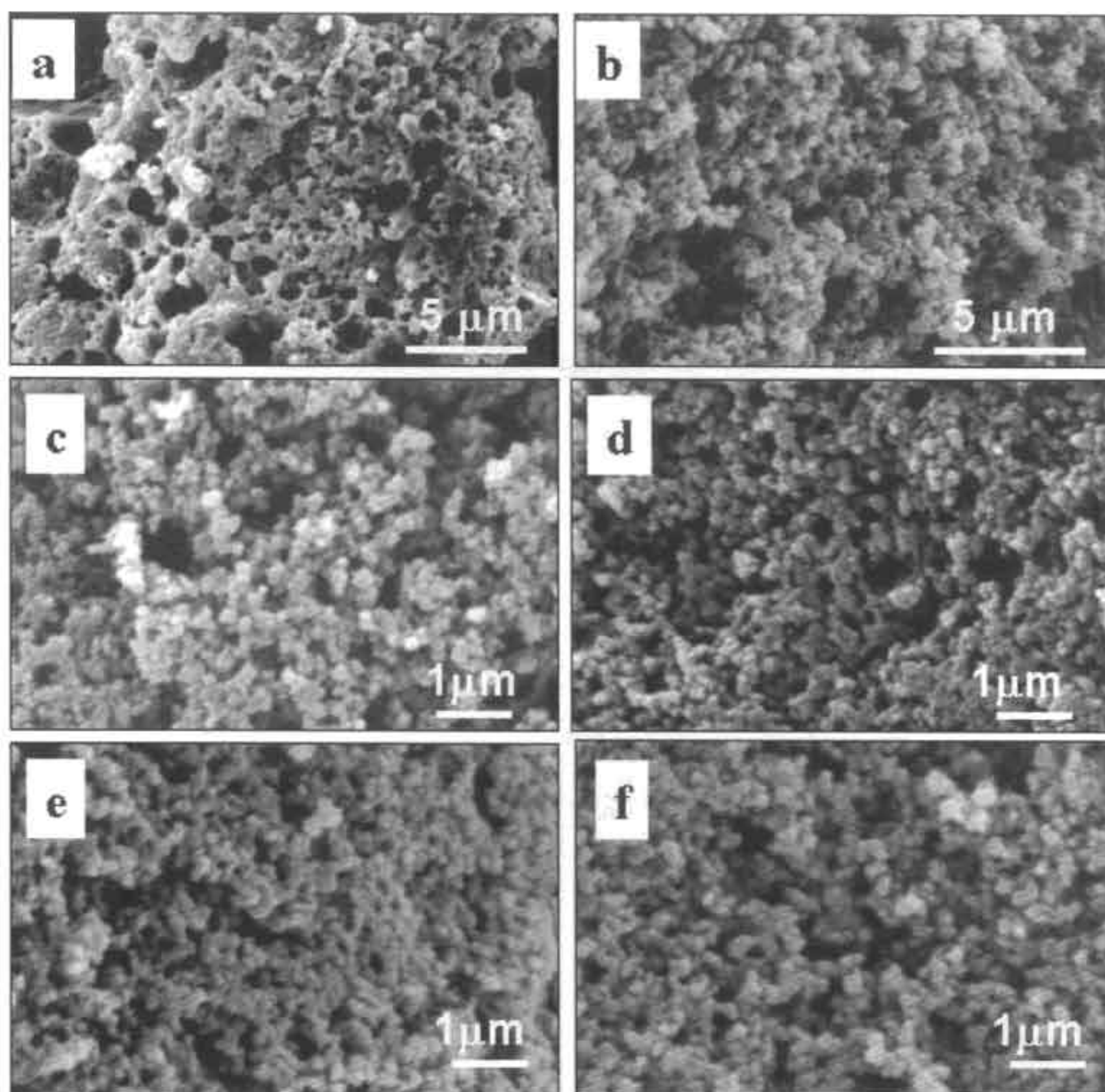


Figure 2.15. SEM pictures of polypyrrole nanomaterials prepared using APS as oxidizing agent : **P-3a** (a), **P-5a** (b), **P-25a** (c), **P-50a** (d), **P-75a** (e), and **P-100a** (f)

SEM images of polypyrrole nano-materials produced using FeCl_3 as oxidizing agent under the identical conditions were shown in figure 2.16. The sample **P-5b** has spheres plus coral-like morphology whereas the samples **P-10b** to **P-100b** have predominantly 0.5-0.9 sub-micrometer spheres. However, the diameters of the nanospheres were much higher for the series-a (prepared using APS) compared to series-b (prepared using FeCl_3). SEM technique has the limitation for very small size

nano-materials (< 150 nm range) which account for the poor resolution of SEM images for series-a sample (small spheres) in figure-2.15.

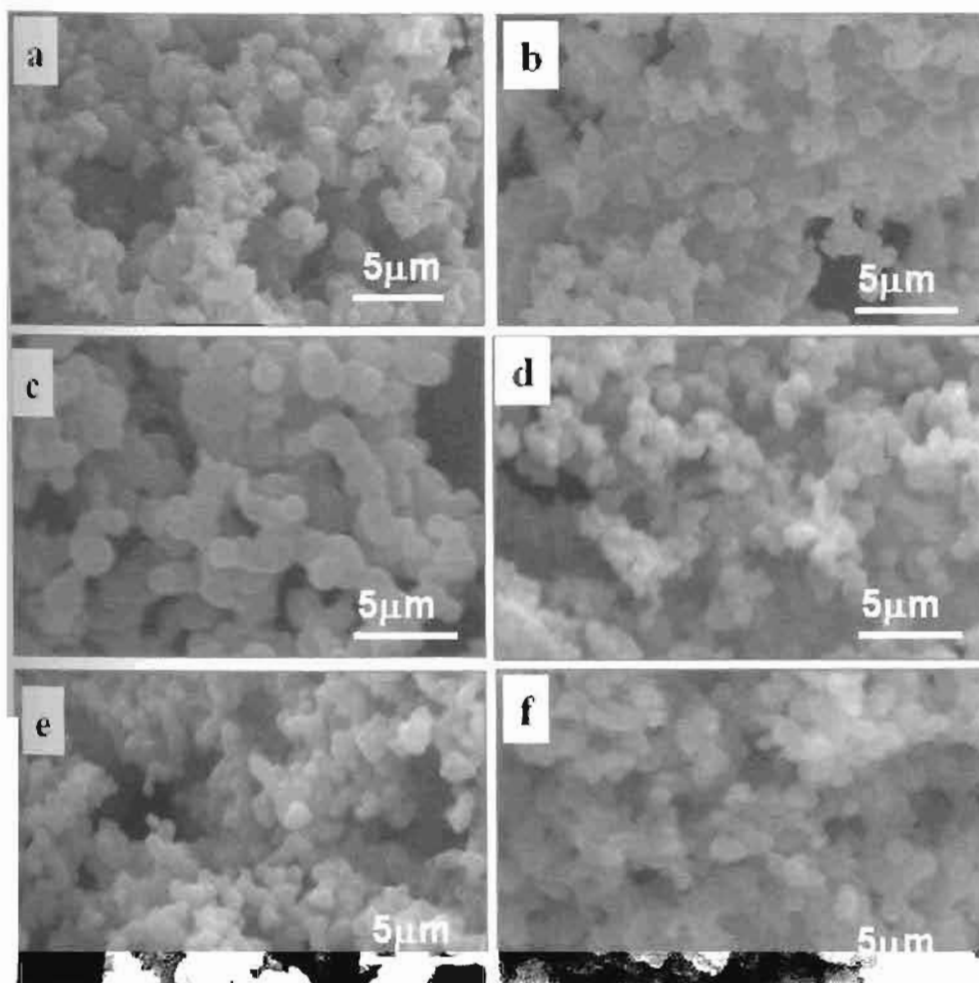


Figure 2.16. SEM pictures of polypyrrole nanomaterials prepared using $FeCl_3$ as oxidizing agent: P-5b (a), P-10a (b), P-25b (c), P-50b (d), P-75b (e), and P-100b (f).

The samples were subjected for transmission electron microscopic (TEM) analysis to get better morphology of these nano-materials. TEM images of P-50a and P-100b are shown in figure 2.17. TEM-images of the samples clearly indicate that the entire materials have uniform solid nano-spheres (no hollow spheres or fibers) and their diameters are in the range of 150 nm and 800 nm for P-50a and P-100b, respectively. The comparison of the TEM and SEM images of these samples reveals that the nano-spheres diameters are almost comparable in both techniques.

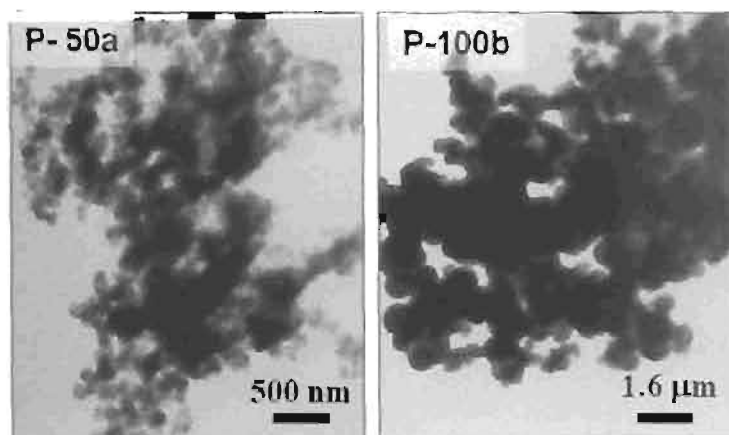


Figure 2.17. TEM pictures of polypyrrole nanomaterials.

Thus, specially designed renewable resource amphiphilic molecule is very efficient anionic surfactant for polypyrrole nanospheres, and for the first time, we have shown that the size and nature of the nano-materials can be fine-tuned for a wide composition range of pyrrole: dopant in the feed. Though there is a difference in the sizes of the nano-spheres produce by oxidizing agents, interestingly both routes produced only nano-spheres and no traces of fibers were found in the entire materials. It indicates that the mechanism of the nano-spheres formation is mainly controlled by the surfactant-pyrrole complexes in water rather than the types of the oxidizing agents employed. It is quite opposite to the observations reported by Wu *et al.* and Zhang *et al.* in the cationic surfactant mediated polypyrrole synthesis [Zhang, X. *et al* 2006; Wu, A. *et al* 2005]. They found that FeCl_3 oxidation of CTAB-pyrrole complex produced spheres whereas wire-like network morphology was obtained for APS oxidation [Zhang, X. *et al* 2006] (see figure 2.1). Interestingly, in the present system neither changes in the amount of pyrrole: surfactant ratio (for wide range of 1: 1/5 to 1: 1/100 in the feed) or oxidizing agent disturbs the morphology of the nano-materials. It is very surprising to notice that nano-spheres were produced even at very low concentration of the surfactant, which is almost 1/100 lower than that of pyrrole in the feed. Further, the polypyrrole nano-spheres P-50a, P-75a and P-100a were dispersed in water and subjected to particle size analysis. The nano-particle sizes and their distribution are plotted and shown in figure 2.18. P-50a has two distributions with average diameter of the nano-spheres centered at 400 nm and 1.6 μm . P-75a has also showed a broad distributions centered at 450 nm, but the average particle size is

much lower than that of **P-50a**. Interestingly, sizes of the nano-spheres were found uniform in the case of **P-100a** with average diameter of 300 nm. The average size of the nano-spheres determined by this method is almost comparable with that of SEM and TEM. The change in the bi-model (in **P-50a**) to broad (**P-75a**) to uniform distribution (in **P-100**) of nano-spheres, indicates that large size nanospheres are formed at higher [pyrrole]/[surfactant] composition than lower composition. Thus, by controlling the [pyrrole]/[surfactant] composition in the feed one can precisely control the size of the polypyrrole nanomaterials. However, it is important to indicate that the micellar mediated systems not only depends on the composition it also reflects on the concentration of the species.

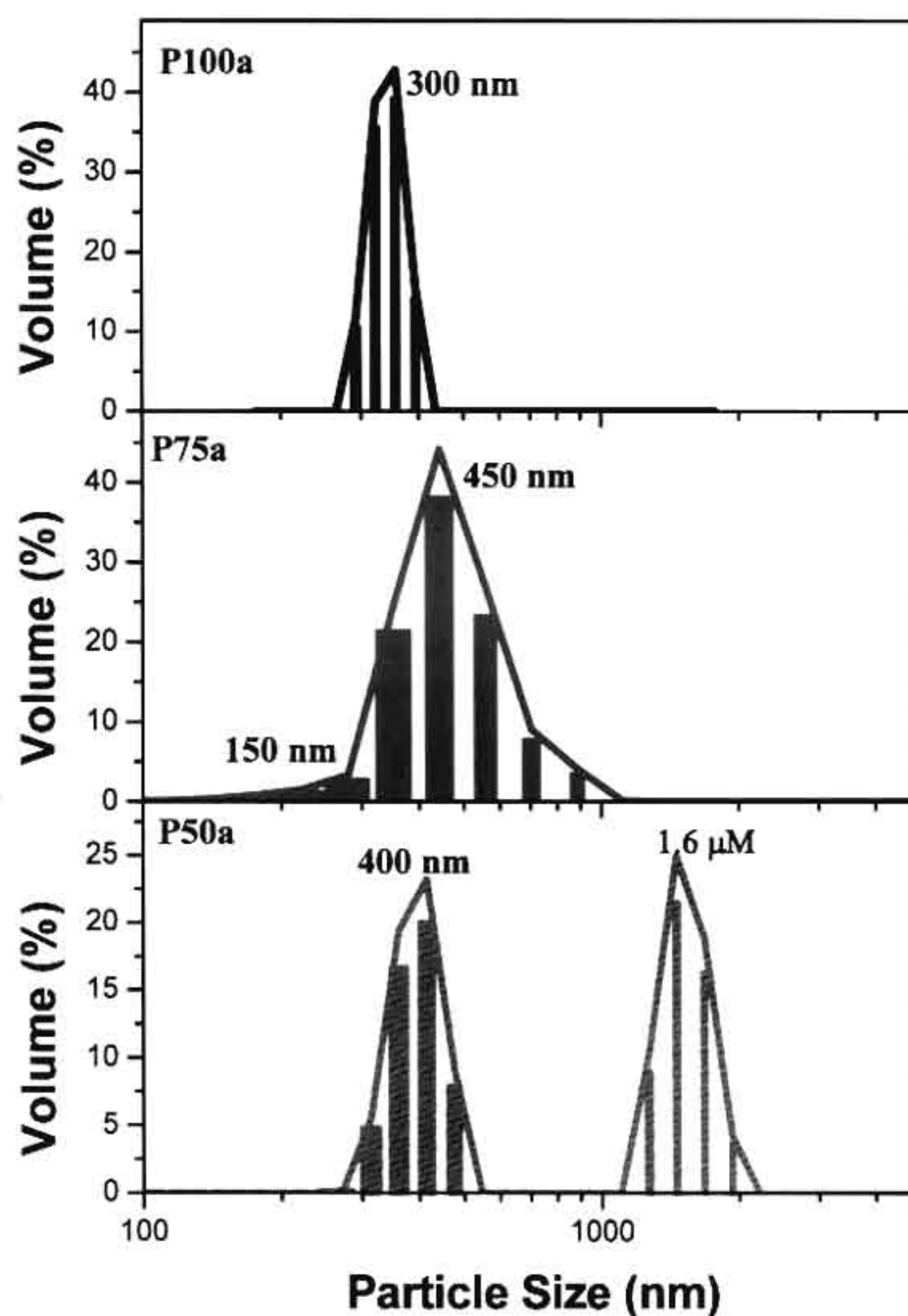


Figure 2.18. Particle size distribution of polypyrrole nanospheres

2.3.5. Polypyrrole nanospheres via dilution Route

A dilute route polymerization was carried out by varying the concentrations of both surfactant and pyrrole to produce polypyrrole nanospheres. Nano-sphere (~ 150 nm) formation were almost invariant for $[\text{pyrrole}]/[\text{surfactant}] = 100$. Based on this experience, the composition of $[\text{pyrrole}]/[\text{surfactant}]$ was fixed as 100 for the dilution route. Initial concentration of pyrrole and surfactant was fixed as 9.6×10^{-1} and 9.6×10^{-3} M respectively and then for dilute polymerization, the concentrations of the surfactant (9.6×10^{-1} to 5.8×10^{-1} M) and pyrrole (9.6×10^{-1} to 5.8×10^{-2} M) were varied by adding required amount of water from 15 to 250 mL to the pre-formed emulsion (see table 2.2.). Upon dilution, that thick yellow emulsion turned turbid and then became a clear yellow solution without any phase separation (see figure 2.19.). The emulsion and dilute polymerization samples were found stable for more than 2 days under ambient conditions. These solutions were stirred for 45 minutes in sonicator and then oxidized by adding aqueous solution of ammonium persulphate in ice cold condition under sonication for 1 h. The polymerization was continued for 8 h and the resulting nano- material was filtered and purified by washing with water and methanol until the filtrate became colorless. It was dried under vacuum for 24 h (0.05 mm of Hg) at 50 °C in a vacuum oven prior to further analysis. The polymers are denoted as P-1, P-2, P-3, P-4, P-5, P-6, P-7, and P-8 (see table 2.2).

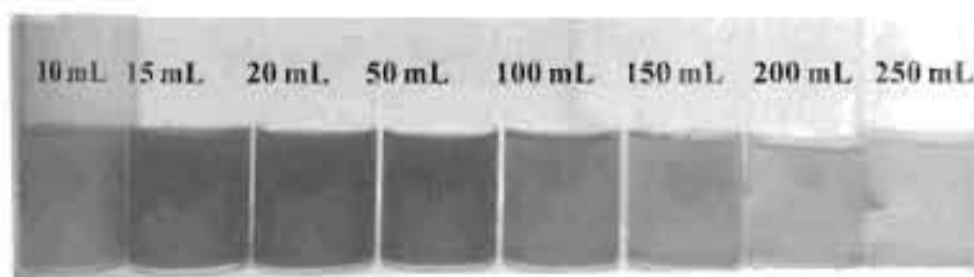


Figure 2.19. Dilution of the thick emulsion from 10ml. to 250 mL.

Table 2.2. Concentration of the surfactant and pyrrole, yield and elemental analysis of nanomaterials synthesized via dilution route.

Sample	Conc. of pyrrole (M)	Conc. of Surfactant (M)	Water ^a in (mL)	Yield ^b (%)	S/N ^c Ratio
P-1	9.6×10^{-1}	9.6×10^{-3}	10	89	0.31
P-2	7.2×10^{-1}	7.2×10^{-3}	15	85	0.30
P-3	5.7×10^{-1}	5.7×10^{-3}	20	80	0.29
P-4	2.6×10^{-1}	2.6×10^{-3}	50	88	0.30
P-5	1.4×10^{-1}	1.4×10^{-3}	100	75	0.31
P-6	9.6×10^{-2}	9.6×10^{-4}	150	90	0.32
P-7	7.2×10^{-2}	7.2×10^{-4}	200	95	0.27
P-8	5.8×10^{-2}	5.8×10^{-4}	250	92	0.30

^a Amount of water used for dilution. ^b Yield calculated for isolated product. ^c Sulphur/ Nitrogen ratio was obtained by elemental analysis.

2.3.6. Morphology of polypyrrole nanomaterial via dilution route

The morphologies of the nano-materials were recorded using JEOL JSM-5600 LV scanning electron microscope and SEM images of the polypyrrole samples are given in figure 2.20. Sample **P-1** had spheres of sizes in the range of 550 ± 100 nm. Dilute polymerization samples showed a significant decrease in the size of the nano-spheres and they were obtained as 350-250 nm for **P-2** and **P-3**, respectively. At larger dilution, the size of the resulting nano-spheres became very small and sizes were found in the range of 60-80 nm diameter (for **P-4** to **P-7**). The samples were subjected for high resolution TEM and the images are shown in figure 2.21. TEM images confirmed the sizes of the spheres of **P-2** are in the range of 0.5 - 0.7 μm and **P-4** (also **P-7**) in the range of 60-80 nm. TEM and SEM morphology of the nano-spheres clearly indicated that non-uniform larger spheres were produced from higher pyrrole-surfactant concentration (thick emulsion) whereas uniform nano-spheres (~60 nm) were produced at dilute conditions.

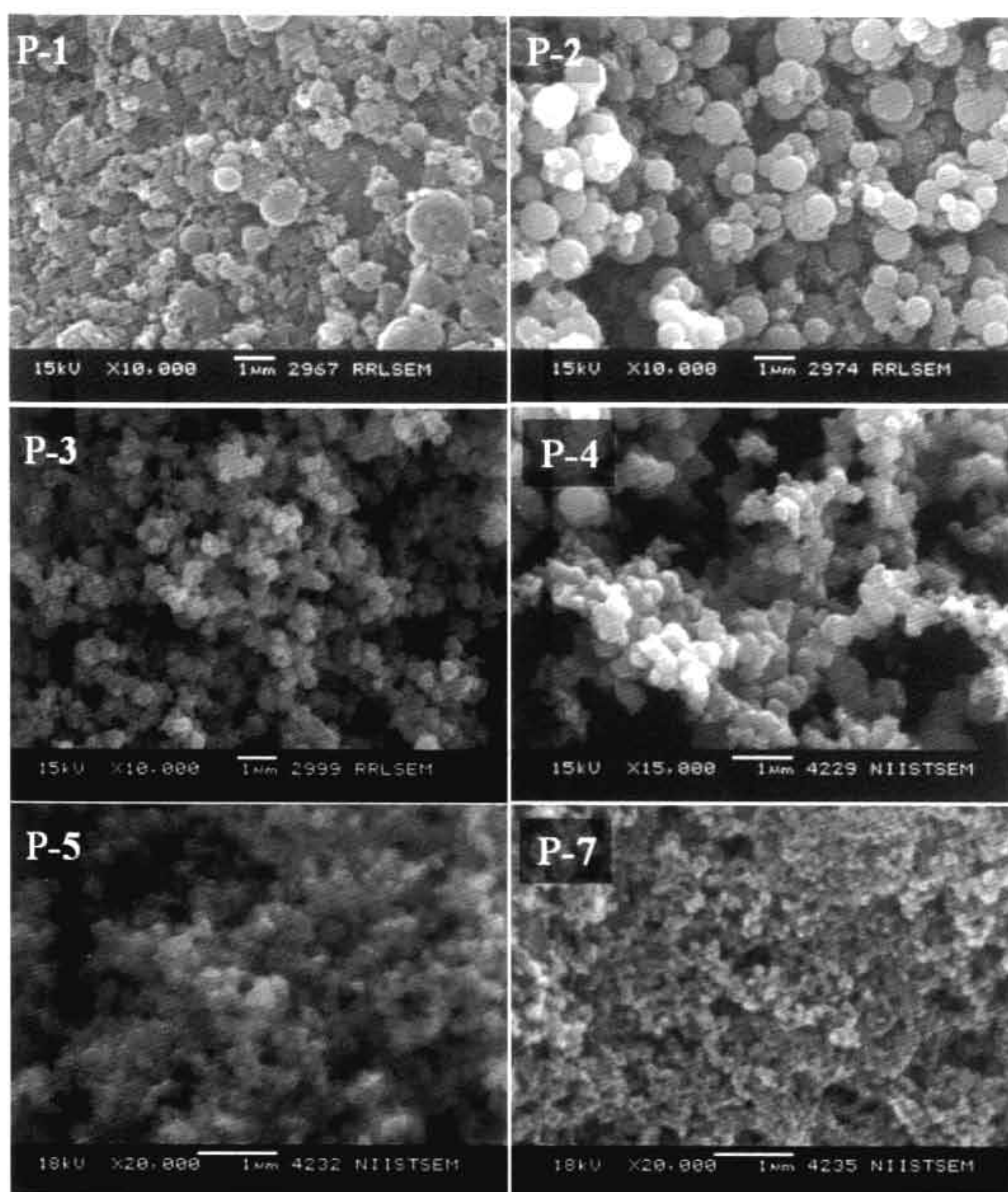


Figure 2.20. SEM images of polypyrrole nanospheres synthesized via dilution route.

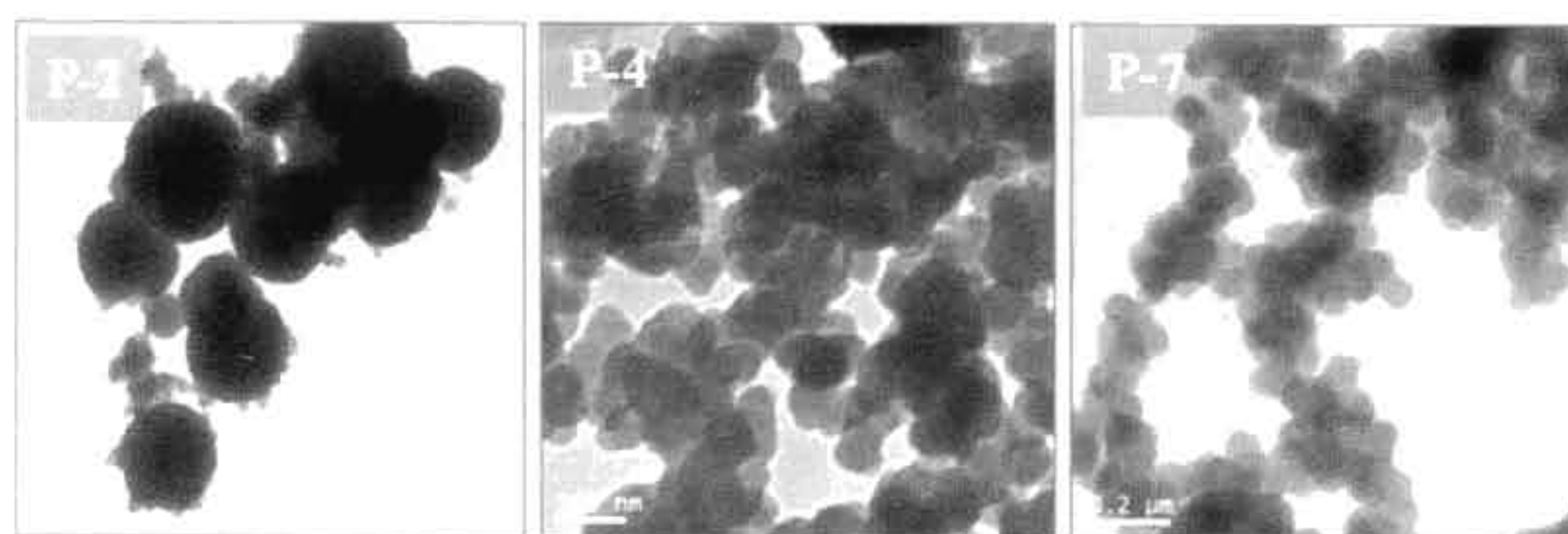


Figure 2.21. TEM images of polypyrrole nanospheres prepared under dilution route.

2.3.7. Mechanism of nanomaterial formation

Dynamic light scattering studies on the pyrrole surfactant complex have been carried out to trace the size of the complex at various concentrations. The addition of pyrrole into surfactant in water induces self-organization of surfactant micelles which resulted in the formation of strong aggregates of 500-600 nm in size (see **P-1** in figure 2.22.). Pyrrole is a weak base and interacts with the acidic anionic surfactant through weak acid-base interactions. Upon dilution by water, the micelles were well separated and the sizes of the aggregates gradually decreased and showed a bi-modal distribution with maxima at 300 and 50 nm (see **P-2** and **P-3**), at larger dilution (in **P-7**), the population of smaller aggregate increases and finally formed a uniformly distributed 20-30 nm pyrrole + surfactant complex.

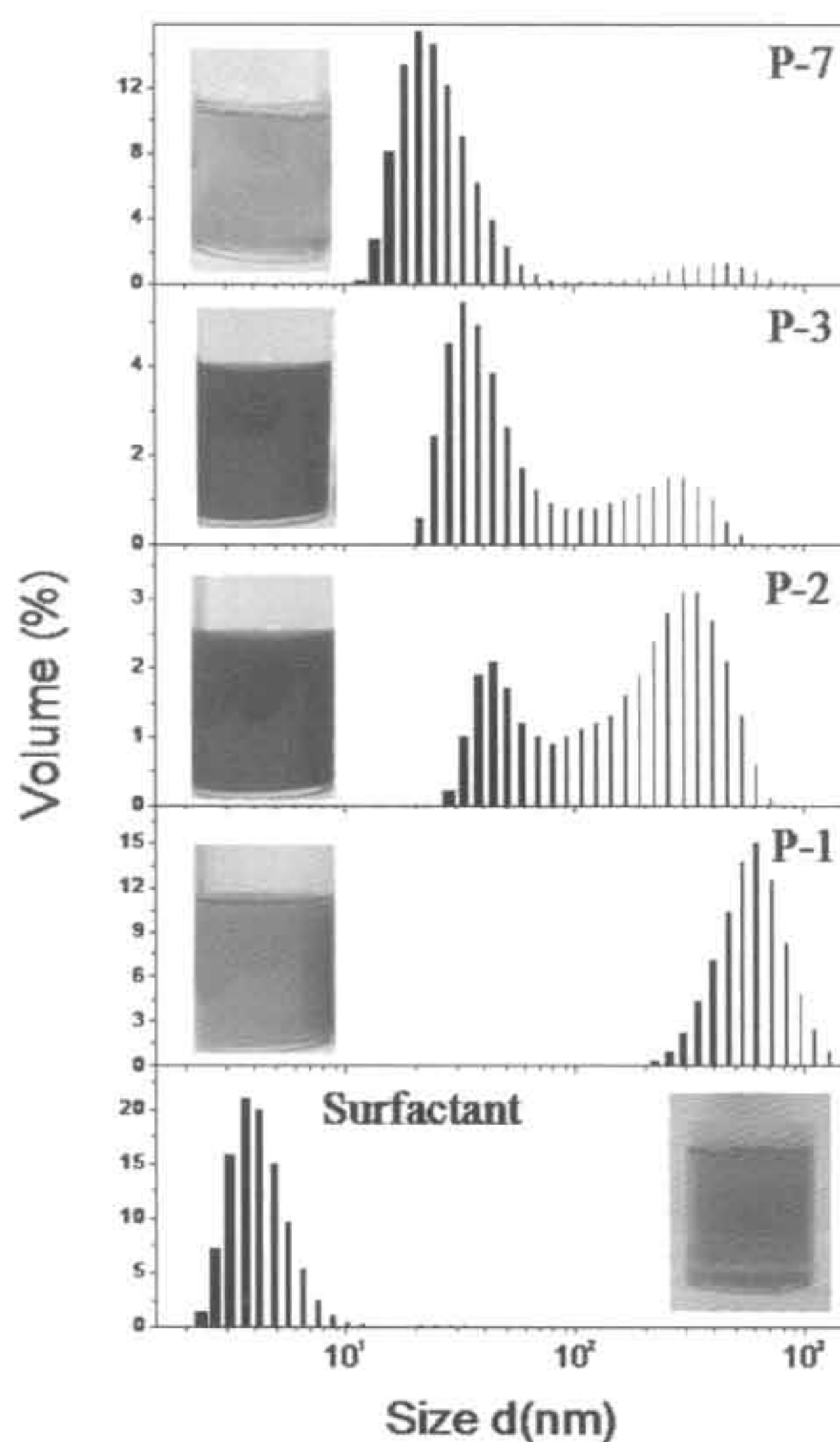


Figure 2.22. DLS histogram of the polymerisation templates.

It is very clear from the DLS histograms of surfactant + pyrrole complexes in water that the size of the aggregates in the anionic surfactant + pyrrole can be precisely controlled (from 600 to 30 nm) by diluting the emulsion template. The concentration of **P-8** (5.8×10^{-4} M) was also slightly lower than that of CMC, but the concentration lie within the experimental error of various techniques used for CMC determination. Therefore, the sample **P-8** was also expected to show the micellar behaviour in the polymerization process like other cases in **P-1** to **P-7**.

Though the DLS gives evidence for the formation of large size aggregates for pyrrole + dopant complex in water, it could not provide information on the shape of the micellar aggregates (cylindrical or spherical). A drop of the pyrrole + dopant complex was slowly evaporated on the SEM grid and subjected to SEM analysis. The SEM image (see figure 2.23.) of the **P-2** (at higher concentration) complex showed spherical aggregates of 0.6- 0.7 μm . The dilute polymerization samples (**P-7**) also showed the presence of spherical aggregates, however, their sizes were obtained in the range of 150-200 nm. It is clearly evident that upon dilution the size of the micelle aggregates were drastically reduced from sub-micron to nano-meter without altering the spherical geometry. The size of the aggregates both in SEM and DLS studies were comparable and it supported that surfactant + pyrrole aggregates behaved as templates for producing polypyrrole nano-spheres.

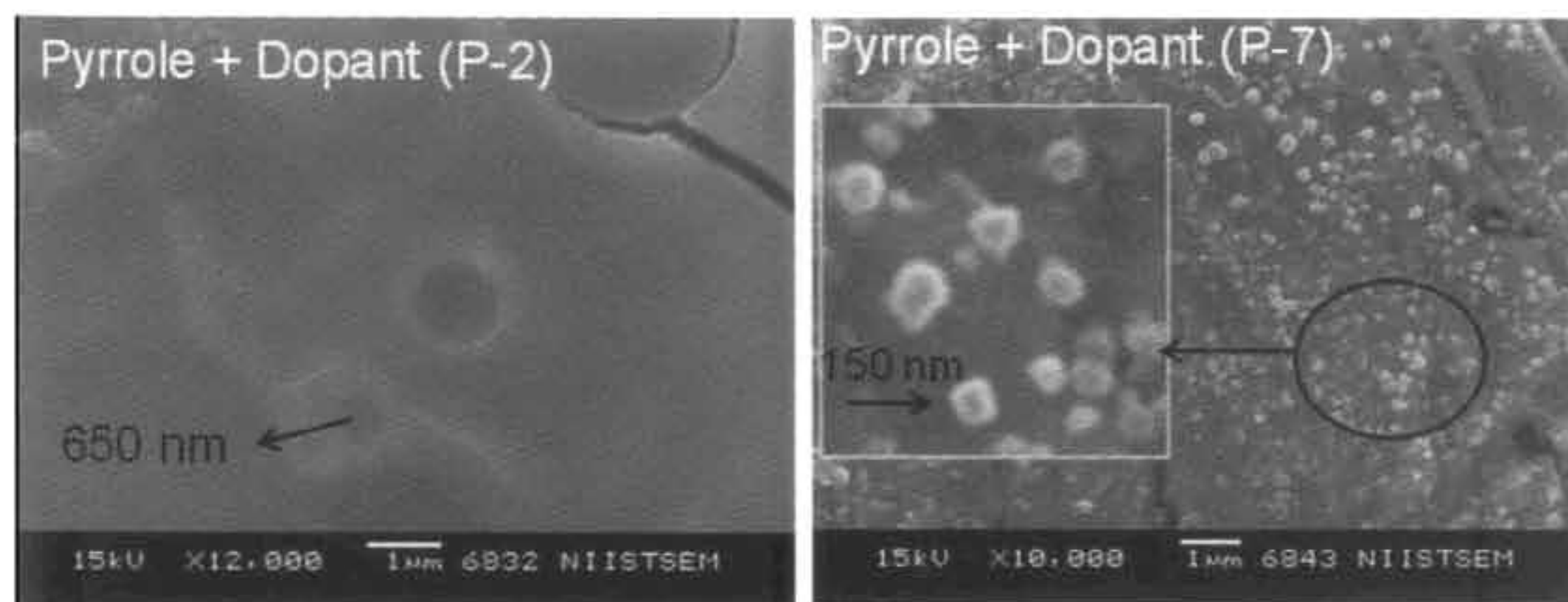


Figure 2.23. SEM image of the emulsion template.

The nano-materials synthesized through dilution route (**P-1** to **P-7**) were dispersed in water and subjected to particle size analysis (static light scattering) to determine the size of the synthesized polypyrrole nano-spheres. The nano-particle

sizes and their distribution are shown in figure 2.24. **P-1** showed a very broad distribution (from 750 – 300 nm) of spheres with a peak maximum at 500 nm. **P-2**, **P-3** and **P-6** showed a relatively less broad distribution with their size distribution having maxima at 350, 300 and 225 nm, respectively. The sample **P-7** showed narrow distribution with uniform particle size in the range of ~ 70 nm. The particle sizes of the spheres clearly indicate the formation of more uniform and small nano-spheres upon dilution of emulsion templates. The average particle size of the nano-spheres from SEM images for all the samples were determined by averaging more than 20-25 spheres.

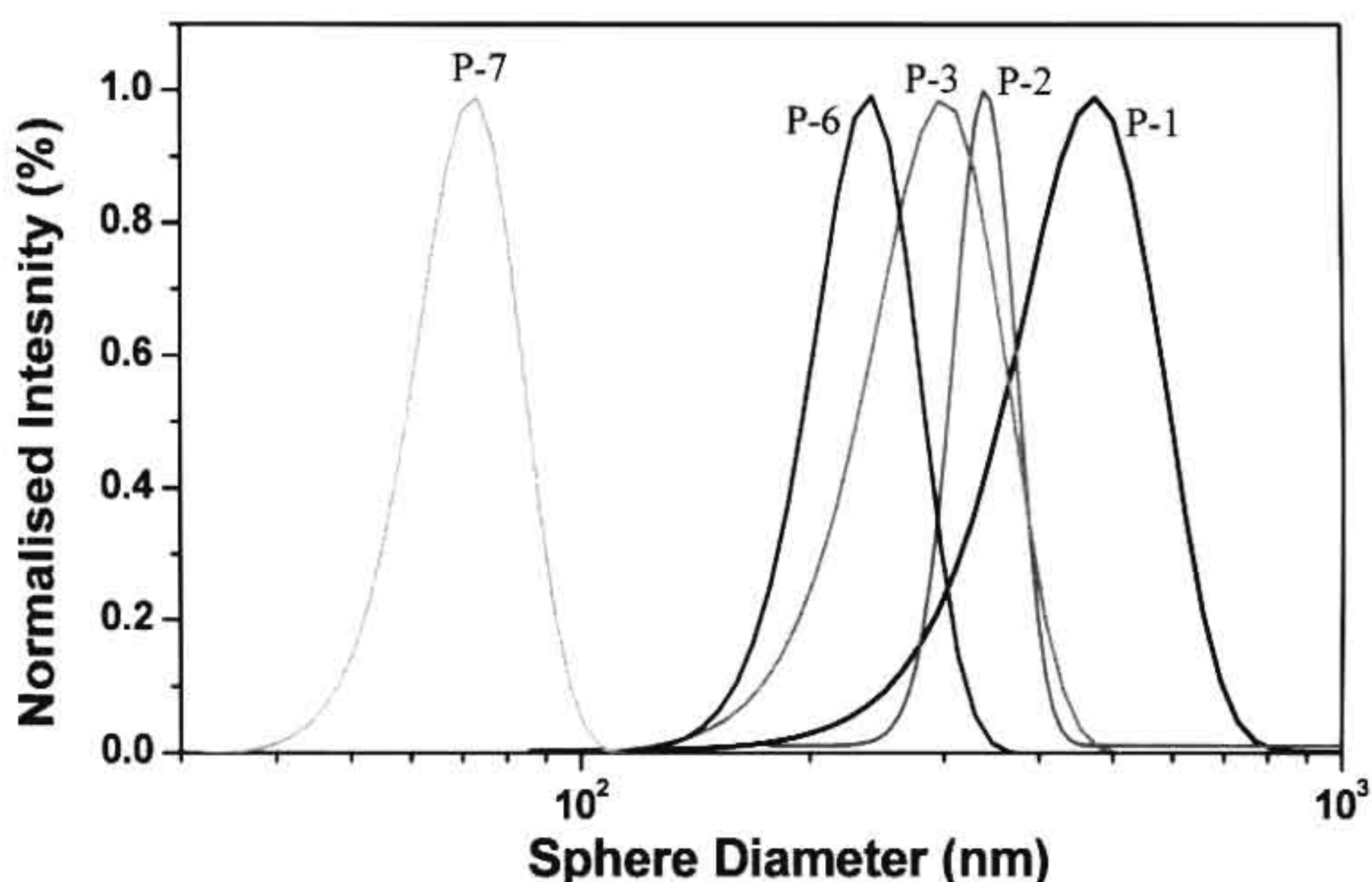


Figure 2.24. Particle size of polypyrrole nanospheres prepared under dilution route.

Under the micelle controlled template synthesis, one would expect a good correlation between the sizes of the templates to the dimensions of the synthesized nano-spheres. To prove this correlation, micelle template sizes (from solution DLS studies, figure 2.22), average sizes of nano-spheres determined from SEM image (from figure 2.20) and peak maxima of the particle size analyzer data (figure 2.24) and average sizes from TEM are plotted against the concentrations of surfactants and shown in figure 2.25. Both the size of the templates and nano-spheres (from SEM and particle size) increased with the increase in the surfactant concentration. The size of

the templates matched very well with that of the synthesized nano-spheres for the samples of **P-1** and **P-2**, but slightly deviated for highly diluted samples **P-3** to **P-7**. At higher concentration, surfactant + pyrrole complex formed stable and strong aggregates of 600 nm in size, which can directly template for the same size nano-spheres. The deviation in the size difference for the nano-materials (from SEM data) and templates in the diluted samples may be the result of poor resolution sub-nanometer spheres by SEM. For this purpose, the average sphere sizes were calculated based on TEM image for the samples **P-1**, **P-3**, **P-7** and **P-8** and plotted in figure 2.25. The size of the spheres calculated based on TEM images matches well with that of the template sizes within the experimental error. The sizes of the synthesized nano-particles determined by particle size analyzer were found almost 2-3 times higher than that of the polymerization templates. This difference was attributed to the agglomeration of polymer nano-particles due to their partial solubility in water.

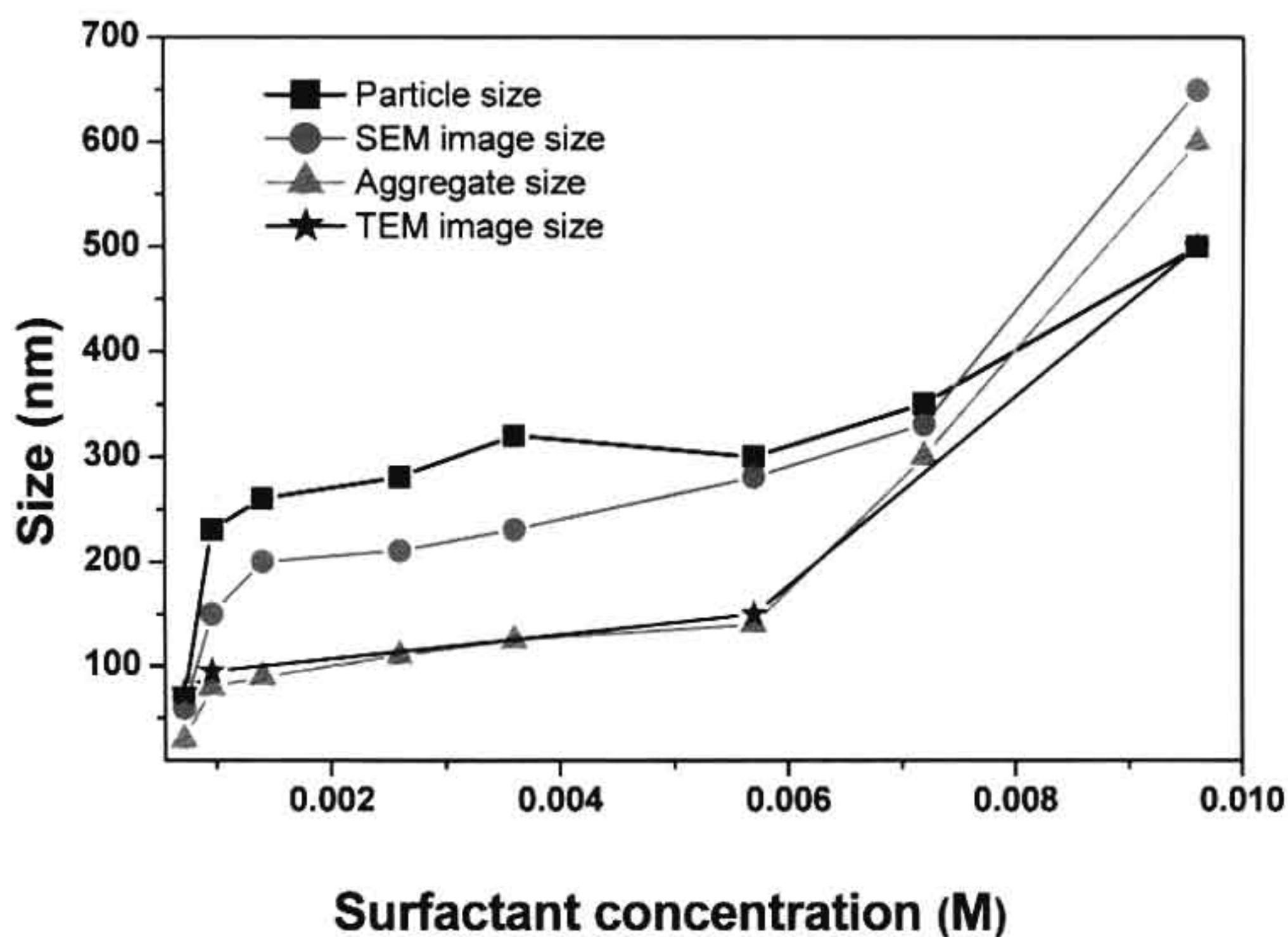


Figure 2.25. The plots of size of the aggregate, average nanoparticle size, average size taken from SEM pictures and TEM pictures versus the surfactant concentration in the feed.

In order to test the role of the sonication in the nano-material synthesis, the sample **P-8** was also prepared with magnetic pellet stirring, ultra sonication and without ultra sonication. The morphology of these controlled experiment samples indicated that the nano-sphere morphology was not affected by any of these stirring conditions like ultra sonic or magnetic pellet stirring (see figure 2.26.). Therefore, the synthesis of the nano-materials in the current work is mainly driven by the self-organization route rather than any other external stimuli like sonication. The sonication process mainly helps in the formation of homogeneous mixture in the nano-materials synthesis.

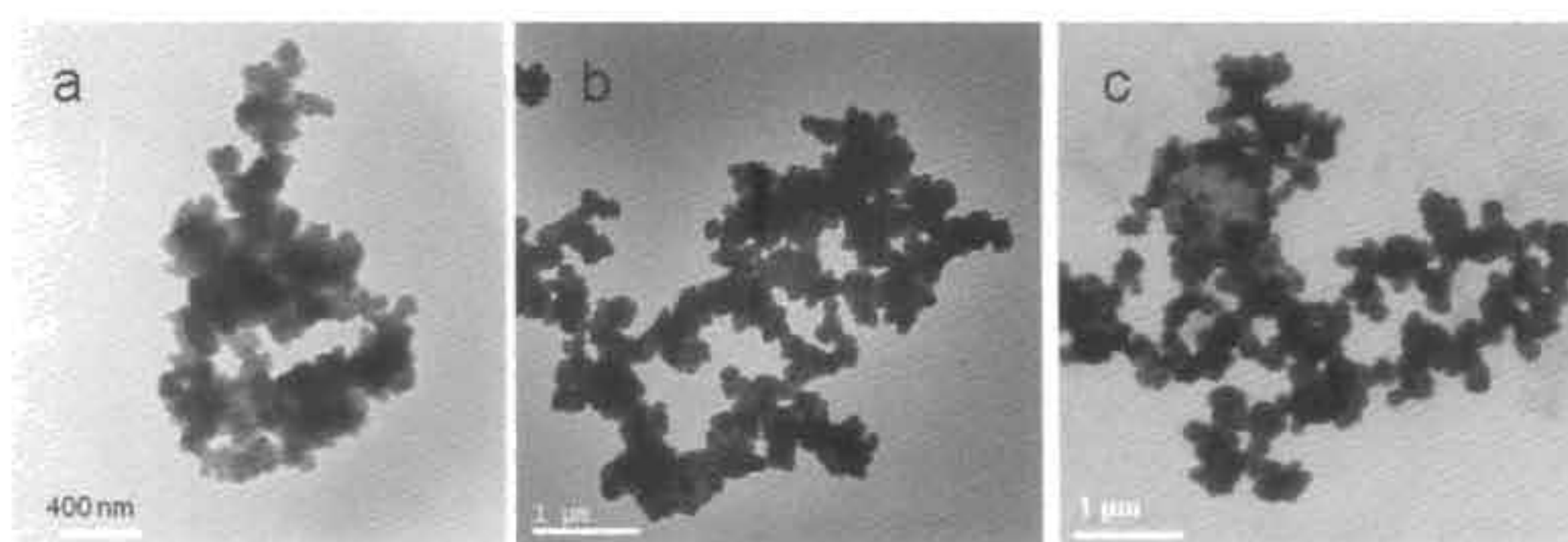


Figure 2.26. TEM images of polypyrrole nanospheres synthesized (a) magnetic stirring (b) sonication, c) without sonication.

Based on these analyses, the mechanism for the size control of the nanospheres in the polypyrrole synthesis was proposed in figure 2.27. The surfactant micelles exist in the form of 4.3 nm micelles in water. The addition of pyrrole into the surfactant in water produces 600 nm size aggregated micelles (evident from DLS and SEM image), which template the synthesis of large sized spheres. The dilution of emulsion micelle template produces smaller aggregates depending upon the amount of water added for the dilution. The weakly aggregated micelles of 30-40 nm behave as template for the formation of tiny nano-spheres at very dilute polymerization conditions. It is clearly evident from the present investigation that the renewable resource anionic surfactant is an effective structure directing agent for polypyrrole nano-spheres with precise control over their size ranging from 600 to 50 nm.

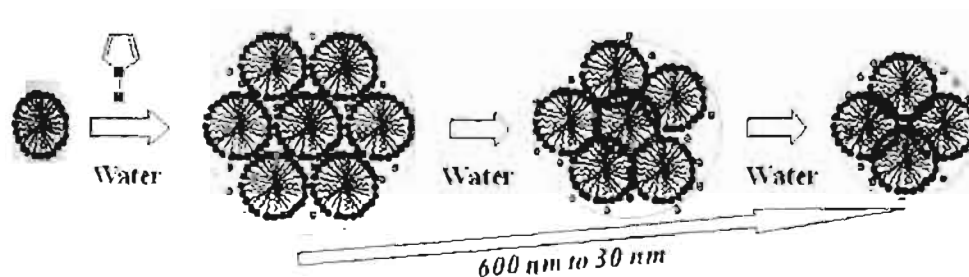


Figure 2.27. Mechanism of size control in polypyrrole nanospheres.

2.3.8. Properties of Polypyrrole Nanomaterials

The thermal analysis of the polypyrrole samples was carried out by thermogravimetric analysis (TGA) as shown in figure 2.28. Polymer samples doped by the new azobenzene sulfonic acid were thermally stable up to 280° C, similar to camphor sulfonic acid doped samples [Li, X. G. *Et al* 2004].

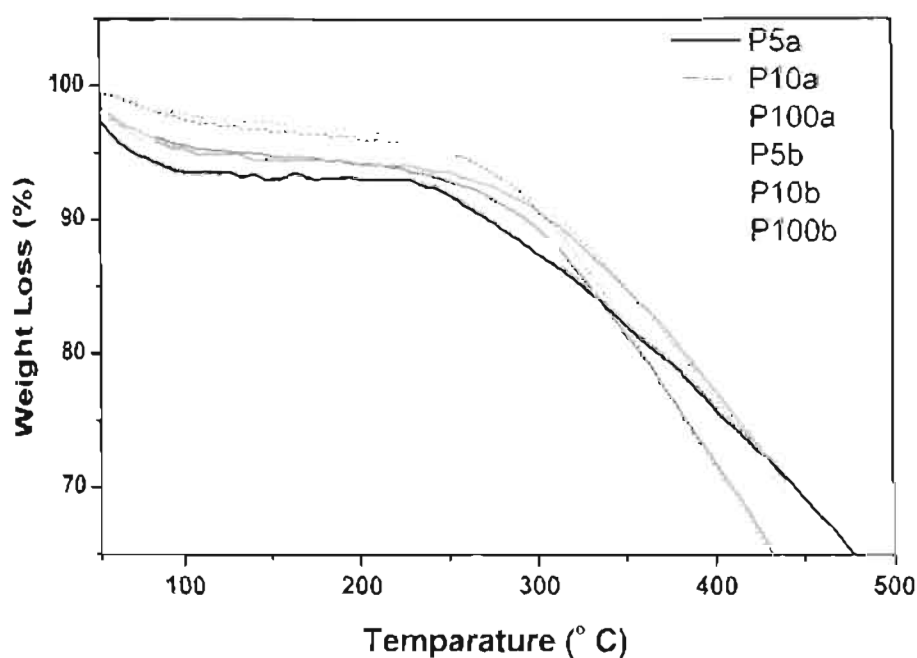


Figure 2.28. TGA of polypyrrole nanospheres.

The polypyrrole nano-materials were freely suspended in water by stirring under ultrasonic at room temperature. Polypyrrole nano-materials prepared using APS as oxidant were found to be more dispersible in water whereas the samples prepared using FeCl_3 found insoluble and less dispersible in water. UV-visible spectra of the

samples P-3a to P-100a and P-5b to P-100b were shown in figure 2.29. The absorption spectra of azobenzenesulfonic acid surfactant showed strong transition at 360 and a shoulder at 450 nm corresponding to the π - π^* and n - π^* transitions of trans and cis azobenzene isomers [Janitkumar *et al* 2007]. The UV-visible spectra of polypyrrole nano-materials showed three distinct bands at 400 nm, 475 nm and a free tail above 1000 nm in the NIR region [Menon, V. P. 1996; Cabala, R. 2002]. These three transitions were corresponding to the transitions from valence bond to polaron, anti-bipolarons and bipolarons of the oxidized form of polypyrrole. The increase in the intensity of the low energy transition in the NIR for samples P-25a to P-100a revealed that these nano-materials were highly doped compared to that of the P-3a to P-10a.

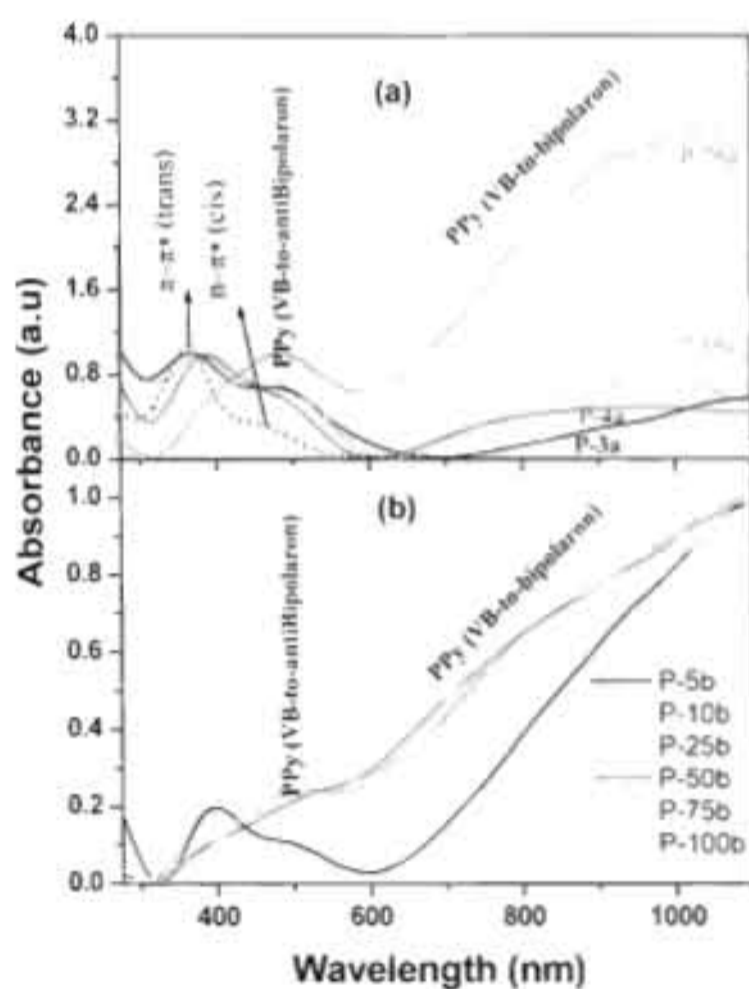


Figure 2.29. Absorption spectra of polypyrrole nanospheres synthesized using (a) APS (b) FeCl₃.

Dilute polymerization samples (P1- P8) have absorption bands at 475 nm and 1000 nm and it was similar to P-100a. The peaks obtained are in accordance with the doped polypyrrole peaks reported in literature. Absorption properties of the dilute polypyrrole nanospheres (P1-P7) did not produce profound changes with dilution of pyrrole-surfactant complex.

Table 2.3. Size of the nanomaterials, electrical conductivity and WXR D data of polypyrrole nanomaterials synthesized using APS and FeCl₃.

Sample ^a	(S/cm) ^b	Spheres ^c Diameter (nm)	WXR D data ^d	
			2θ values	d-spacing (Å)
P-3a	0.001	Coral-like	20.26	4.38
P-4a	0.002	Coral-like	20.04	4.43
P-5a	0.02	150-220	9.02,21.55	9.8, 4.12
P-10a	0.04	180-220	8.96,21.55	9.8, 4.12
P-25a	0.01	180-220	7.66,26.41	11.5, 3.37
P-50a	0.01	180-220	6.87,26.41	12.9, 3.37
P-75a	0.02	180-220	6.86,26.81	12.9, 3.32
P-100a	0.02	180-220	6.23,26.80	14.2, 3.31

^a Polypyrrole synthesized using ammonium persulfate (series-a) or FeCl₃ (series-b) as oxidizing agents.

^b Conductivity of the nanomaterials measured using four probe conductivity meter at 30 °C. ^c Size of the nanomaterials calculated from SEM images. ^d WXR D analysis of the nanomaterials using powder method

The conductivity of the polypyrrole nanostructures were determined by four probe conductivity measurement using compressed pellets at room temperature (see table 2.3.) The conductivity values for the samples P-5a to P-100a were obtained in the range of 1×10^{-2} S/cm, whereas P-3a and P-4a showed conductivity one order lower compared to other samples [1., X. G. *et al* 2004; Omastova, M. *et al* 2003]. The low conductivity of samples P-3a and P-4a reflect on their UV-Vis spectra that these samples have weak peaks corresponding to the bipolaron transitions compared to P-10a to P-100a (figure 2.29). Additionally, the morphology of the P-3a to P-5a were also highly porous (see figure-2.9), which may also accountable for their low conductivity. The polymers P-5b to P-100b prepared using FeCl₃ showed much higher conductivity (up to the range of 1×10^{-1}) compared to APS series. The

conductivity of the polymers synthesised via dilution (P1-P8) have shown conductivity in the range 10^{-1} S/cm which is in accordance with conductivity values reported for polypyrrole. Li *et al* reported the conductivity of [Cl] doped polypyrrole copolymer micro-spheres (using APS as oxidant) in the range of 10^{-1} S/cm, which is one order higher than that of polypyrrole nano-spheres (150-220 nm) obtained in the present system for the same oxidizing agent (see series-a, in table 2.3.).

The solid-state properties of polypyrrole nano-spheres were studied for finely powdered samples using wide angle X-ray diffraction analysis (WXR D). Polypyrrole is a highly rigid polymer because of their linear structure and less flexible chain folding to induce crystalline domain. In the presence of organic surfactants, the surfactant-polymer undergoes various interactions, which tend to organize the polymer chains in three-dimensional highly ordered fashions. The WXR D patterns of polypyrrole nano-spheres were shown in figure 2.30. The WXR D patterns showed two characteristic peaks in the regions at $2\theta = 20-26$ (d-spacing 4.12 to 3.32 Å) and $2\theta =$ below 10 (d-spacing = 11.5 to 14.2 Å) [Jayakannan, M. *et al* 2005]. Decreasing the amount of surfactant drastically affect the nature of the peaks in the WXR D-plots. While moving from P-5a to P-100a, the peak at $2\theta = 20$ showed shift towards higher angle (from $2\theta = 20.04$ to 26.37) whereas the peak at $2\theta = 10$ showed a opposite trend, i. e., (towards lower angle (from $2\theta = 9.1$ to 6.3). The peaks centered at $2\theta = 20.04$ (d spacing = 4.43 Å) and 26.37 (d spacing = 3.37Å) are assigned to scattering from pyrrole-counter ion or inter-counter ion interactions and pyrrole-pyrrole inter-planar distance [Wernet, W. *et al* 1984; Song, M. K. *et al* 2004]. The shift from 4.43 Å to 3.37 Å in the higher angle region may be due to the difference in the doping level and related to the pyrrole-pyrrole and pyrrole-counter ions. The lower angle peak (d-spacing = 14.2 Å) is particular very interesting because both the intensity as well as inter planner distance (d-spacing values) increases while moving from P-25a to P-100a. It indicates that the decrease in the amount of surfactant in the feed increase the inter-planar distance in the nano-materials and produce highly ordered polypyrrole nano-spheres. Surprisingly, the FeCl₃ series samples did not show any significant peak in the low angle region. It suggests that the samples P-25b to P-100b are poorly ordered and it may be the reason for the low solubility of these samples compared to that of the P-25a to P-100a in water. In the P-3a to P-100a, the penetration of the surfactant molecule increase the inter-planner distance, and

therefore, the solvent molecules easily enter into the lattices to dissolve the polymer chain in water.

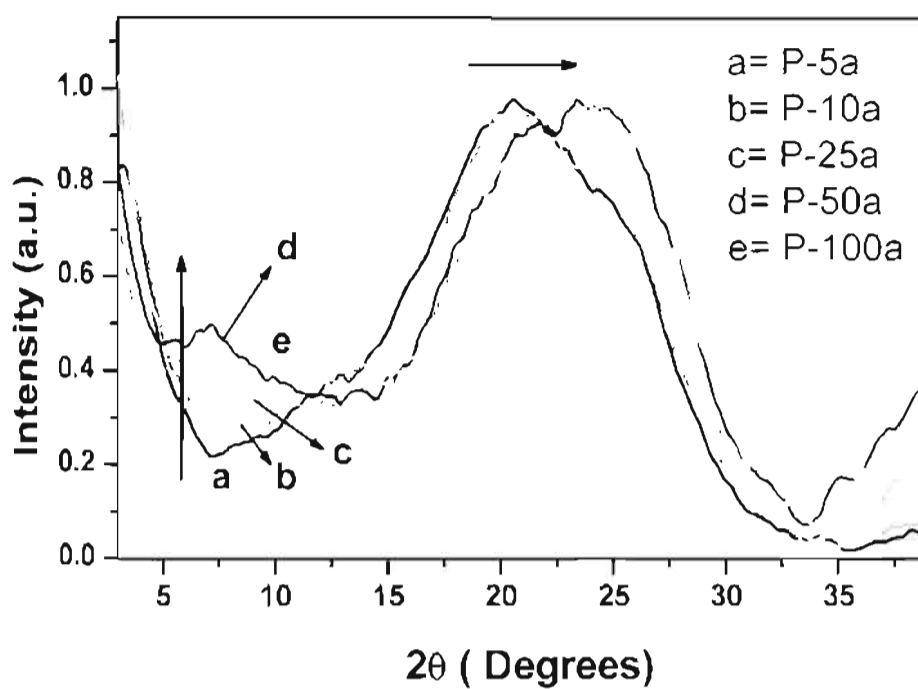


Figure 2.30. WXR D of polypyrrole nanomaterial synthesized using APS.

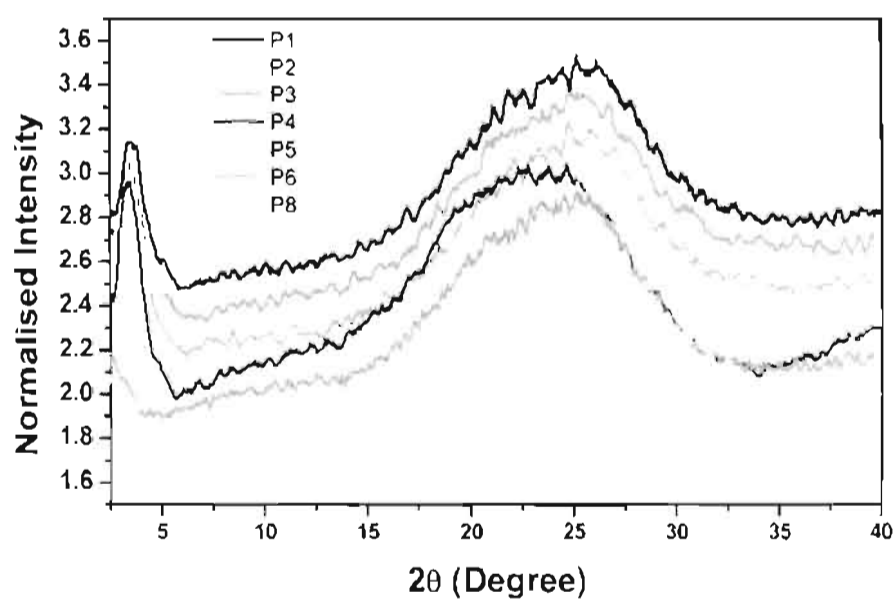


Figure 2.31. WXR D of polypyrrole nanomaterial synthesized via dilution route.

Table 2.4. Polypyrrole nanomaterials synthesised using APS via dilution route electrical conductivity, size of the nanomaterials and WXRd.

Sample ^a	σ^b (S/cm)	Size of Nano-materials ^c	WXRd data ^d	
			2 θ values	d-spacing (Å)
P-1	0.11	S, 550±100	3.64, 25.20	25.51, 3.52
P-2	0.12	S, 350±30	3.53, 25.16	25.02, 3.54
P-3	0.13	S, 230±30	3.65, 25.16	25.53, 3.54
P-4	0.10	S, 220±30	3.43, 23.93	25.70, 3.71
P-5	0.10	S, 200±30	3.53, 24.39	25.02, 3.62
P-6	0.04	S, 150±30	24.93	3.62
P-7	0.03	S, 80±30	25.20	3.53
P-8	0.05	Wire like	25.61	3.54

^a Polypyrrole nanomaterials synthesized via dilution using ammonium persulfate. ^b Conductivity of the nanomaterials measured using four probe conductivity meter at 30 °C. ^c Size of the nanomaterials calculated from SEM images. ^d WXRd analysis of the nanomaterials using powder method

WXRd patterns of the **P1, P-2, P-3, P-4, P-5, P-6 and P-8** have shown in figure 2.31. and two characteristic peaks in the regions at $2\theta = 20-26$ (d-spacing 4.12 to 3.32 Å) and $2\theta = \text{below } 5$ (d-spacing =23.4 to 29.1) were present in the samples. The peaks centered at higher angle were assigned to scattering from pyrrole-counter ion or inter-counter ion interactions and pyrrole-pyrrole inter-planar distance. The lower angle peak at $2\theta = 3.5$ values showed that an ordered arrangement of dopant in the polymer chain causes lamellar ordering as reported by others. The intensity of the low angle peak vanished completely in **P-6 to P-8**. The reason for the disappearance of the low angle peak in **P-6 and P-8** is attributed to the lower dopant concentration at highly diluted polymerization samples. The solid state conductivity of the dilute polymer samples decreases with concentration see table 2.4. The poor solid state packing of the **P-6 and P-8** contributes to the one order decrease in the conductivity of the samples.

24. Conclusion

In conclusion, we have developed a renewable resource amphiphilic azobenzene sulfonic acid and utilized as an anionic surfactant for synthesis of polypyrrole nanospheres. Pyrrole: surfactant ratio in the feed was varied from 1:1/3 to 1:1/100 (using surfactant up to 100 times lower than that of pyrrole) to systematically control the aggregation of pyrrole + surfactant micelles for tuning the properties of polypyrrole nano-materials. Further, a dilution route has been adopted to synthesize polypyrrole nanospheres with size ranging from 600 nm to 60 nm. The present approach has many advantages: (i) a new renewable resource anionic surfactant was synthesized and utilized as structure directing agent for tuning the properties of polypyrrole nano-materials, (ii) the critical micellar concentration (CMC) of the new renewable surfactant was determined from surface tension and specific conductance measurements - as $4 \cdot 10^{-4}$ M. (iii) the size of the micelles was found to be 4.3 nm, determined from the DLS measurements and it was in good agreement with the theoretically calculated micelle size. (iv) the surfactant micelles has the tendency to undergo self-organization with pyrrole to form spherical aggregates, which template for the polypyrrole nanospheres, (v) the size of the polypyrrole nanospheres were systematically controlled from 600 to 50 nm by dilution polymerization techniques. (iv) DLS analysis on template, particle size measurements on nanospheres, SEM and TEM were used propose the mechanism of formation. (v) very good correlation between the nano-materials particle size with that of the polymerization templates were obtained for emulsion/dilution route. (v) large spherical aggregate were formed at higher concentration, which on dilution (lower concentration) changes to small spherical aggregates at lower pyrrole + surfactant concentration. (vi) The solid state properties reveals polypyrrole synthesized by nanomaterials are highly ordered in comparison to the FeCl₃ samples. (vii) The formation of the polypyrrole nanospheres are not affected by the external stimuli like ultra sonication, magnetic stirring and without stirring, which confirms the self organisation process. In a nut shell, a renewable resource amphiphilic surfactant was developed for the synthesis of the polypyrrole nanospheres and the mechanism of the nanosphere formation was properly understood by the studies carried on the polymerisation templates in dilution route, which resulted in the control of polypyrrole nanospheres size ranging form 600 nm to 60 nm.

Chapter-3

Micellar Template Approach for Polypyrrole-Co-Polyaniline Nanomaterial

3.1. Introduction

Morphology of polypyrrole and polyaniline were found to be almost intrinsic to their structures and produce nanospheres and nanofibers, respectively. In particular, cationic surfactant helps to produce polypyrrole nanofibers with pyrrole, whereas anionic surfactant produces polyaniline nanofibers with aniline [Wu, A. *et al* 2005; Zhong, W. *et al* 2006; ^bZhang, X. *et al* 2004; Li, D. *et al* 2009] Special efforts such as monomer functionalization and reverse-emulsion are required to make either polyaniline nanospheres or polypyrrole fibers [Ko, S. *et al* 2007; Zhang, L. *et al* 2005; ^eAnilkumar, P. *et al* 2008; ^cJang, J *et al* 2003, ^fJang, J *et al* 2005]. Some of the properties the homopolymer PANI and PPy nanomaterials taken from literature were shown in table 3.1. Efforts to use the knowledge available in both these nanomaterials for tuning size, shape, and morphology in polyaniline-co-polypyrrole copolymer nanomaterials are highly attractive. These copolymers based nanomaterials are very important because they may possess properties of both polypyrrole and polyaniline which may not be available in either of their homopolymers.

Table 3.1. Properties of the conducting polymer obtained from the literature.

Name	Template	Solubility	Shape	σ (S/cm)	Crystalline	Ref. (et al)
PANI	β -NSA	Partial	Nanotubes	0.032	Partially	Wei, Z 2002
PANI	FeCl ₃	Partial	Nanofibers	-	Partially	Kim, B. J. 2008
PANI	Interface	Partial	Nanofibers	-	Partially	Du, X. S 2000
PPy	OTAB	Dispersible	Nanospheres	2.1	Crystalline	Jang, J 2002
PPy	CTAB	-	Nano Wires	0.007	-	Zhang, X 2006
PPy	β -NSA	Dispersible	Nano Tubes	2	Amorphous	Liu, J 2001
PPy	ABSA	-	Nano fibers	50	Amorphous	Huang, K 2005

Copolymerization of pyrrole with aniline has been reported by both electrochemical and chemical approach for tuning the conductivity and other physical properties [Sari, M. *et al* 1998; Fusalba, F. *et al* 1999; ^aLi, X, G. *et al* 2001; Stejskal, J. *et al* 2004; Lim, V. W. L. *et al* 2001; Kim, J. W. *et al* 2003; Cho, C. H *et al* 2004; Zhou, C. *et al* 2008; ^bLi, X. G. *et al* 2001; ^cLi, X. G. *et al* 2001; ^dLi, X. *et al* 2007].

However, so far no effort has been taken to tune the morphology of polypyrrole-co-polyaniline copolymers. The development of copolymer nanomaterials was limited because of the non-availability of anionic surfactant which can be used as a template for both polyaniline and polypyrrole in the copolymer synthesis. The anionic surfactant should stabilize the pyrrole and aniline emulsions for all aniline + pyrrole composition ranges. Therefore, it is very important to identify or develop new amphiphilic anionic sulfonic acids which can act as good dopant-cum-surfactant for polyaniline and polypyrrole as well as their copolymers under identical conditions for tuning the morphology in their nanomaterials.

Recently, P Anilkumar *et al* from our group have reported the emulsion polymerization of aniline with surfactant-1 to produce exclusively polyaniline nanofibers of ~ 200 nm width with length up to $6-8 \mu\text{m}$ [^aanilkumar, P. *et al* 2006], see figure 3.1. Efforts were made to study the effect of composition of [aniline]/[surfactant] in the feed on the morphology and the results suggested that the surfactant was very efficient structure directing agent for wider composition to produce fibrous morphology. The mechanistic aspects of the nanofiber formation was proposed on the basis of DLS, TEM and SEM studies carried out on aniline + surfactant complexes revealed that aniline-surfactant complex forms cylindrical self assembled templates [^canilkumar, P *et al* 2006]. Polyaniline nanofiber formation was highly reproducible and nanomaterials are easily scalable up to 100 g, which is very rarely reported in literature [^eAnilkumar, P. *et al* 2009]. Alternately, a new series of amphiphilic cardanol derivatives were utilized as gel template and dispersion polymerization for producing polyaniline nanofibers and nanotapes respectively [^hAnilkumar, P. *et al* 2009; ⁱAnilkumar, P. *et al* 2010].

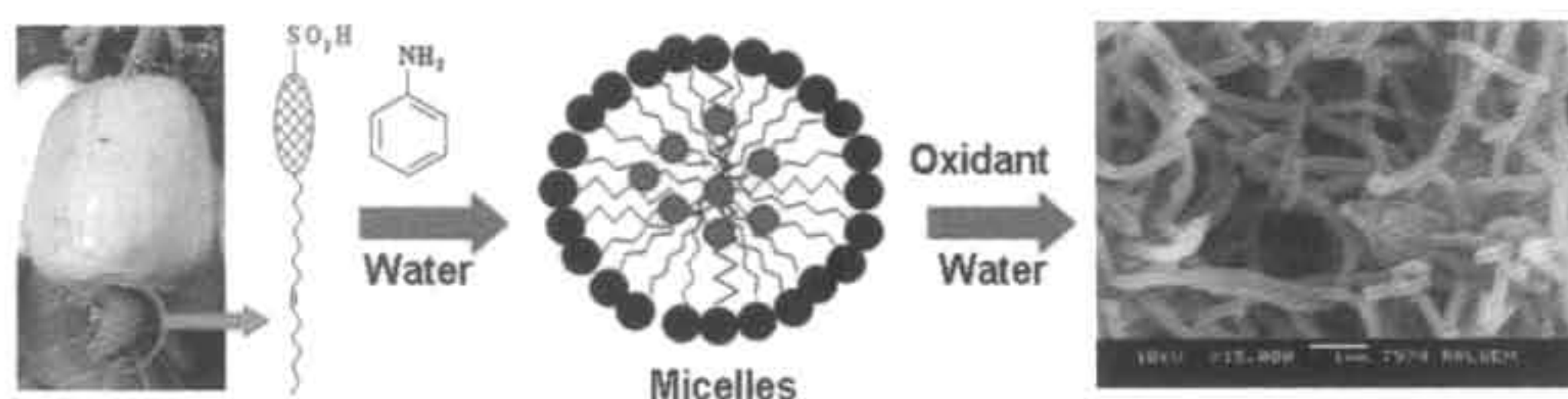


Figure 3.1. Synthesis of polyaniline nanofibers using cardanol azobenzene sulfonic acid surfactant-1.

In chapter-2, the same anionic surfactant was utilized to produce polypyrrole nanospheres, irrespective of the composition and concentration. It is very rare in literature that the same amphiphilic anionic surfactant could selectively act as template for aromatic monomers like aniline and pyrrole to produce exclusively one particular nanomaterial morphology (see figure 3.2.). Therefore, the custom designed renewable resource surfactant provides right choice to understand effect of monomer competition (pyrrole versus aniline) in copolymer nano-materials formation. Detail investigation on role of surfactants played on conductivity, morphology and solid state properties and their interdependent relations are very important aspects to be discussed.

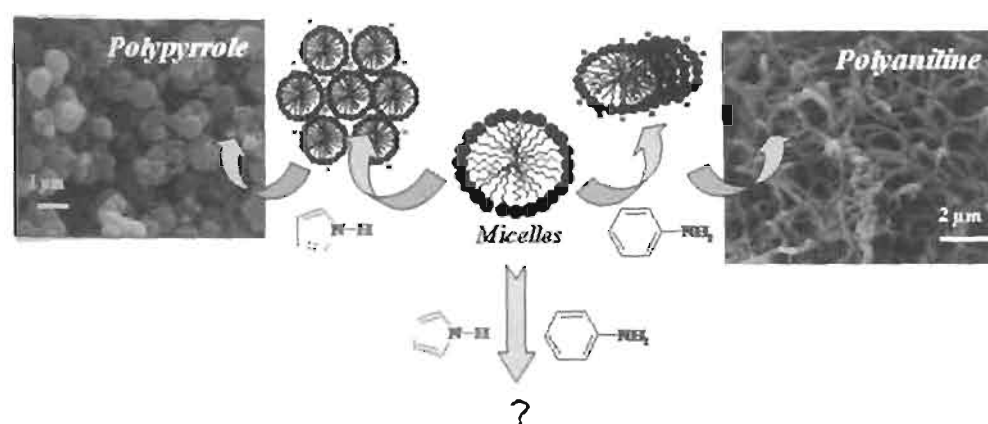


Figure 3.2. Template selectivity of the anionic surfactant micelles for the formation of polypyrrole nanospheres and polyaniline nanofibers.

The renewable resource surfactant-1 was utilized for the copolymer nanomaterial synthesis and morphology was transformed from nanofibers to nanorods to nanospheres. The present approach is an attempt to address the following important aspects: (i) understand the role of the selective templating ability of surfactant micelles with pyrrole and aniline, (ii) study the mechanism of the morphological transformation and (iii) understand the conductivity and solid state properties of the nanomaterials. The conductivity of the copolymers produced from surfactant-1 has shown a non-linear trend, and loss was of the order of 10^2 - 10^3 S/cm with respect to homopolymers, particularly at 70-80 % feeds of pyrrole. Two new anionic surfactants were synthesized to investigate the non-linear behaviour of conductivities in detail. All the anionic surfactants possess same azo head group with hydrophilic sulfonic

acid, however they differ structurally from surfactant-1 by a double tail for surfactant-2 and without any tail for surfactant-3. Surfactants employed for copolymer synthesis have produced similar morphology transformation from fiber to rod to sphere at identical composition. Conductivity measurements of copolymer series made by double tailed surfactant were shown good conductivity without any non-linear conductivity behaviour. Detailed investigations reveals that the good solid state packing and higher crystallinity of the copolymer synthesized using the later case produce good conductivity, whereas large amorphous domains present in single tail series contributes to the poor electrical conductivity. The synthesized nanomaterials were characterized by particle size analyzer, scanning and high resolution transmission electron microscopes (SEM and HR-TEM), UV-visible, FT-IR, four probe conductivity and wide-angle X-ray diffractions (WXR) to study the structure property relationship. The mechanism of the polymerization was also investigated using dynamic light scattering (DLS) technique. The present investigation revealed that the size, shape, and the properties of the nanomaterials can be precisely formulated by controlling the surfactant template in solution.

3.2. Experimental procedures

3.2.1 Materials: Pyrrole, aniline, ammonium persulfate (APS), sulfanilic acid and dodecyl bromide were purchased from sigma aldrich. Hydrochloric acid, dimethyl sulfoxide and sodium hydroxide were purchased locally. Cardanol was purified by double-vacuum distillation at 3-4 mm of Hg, and the fraction distilled at 220-235 °C was collected. 4-[4-Hydroxy-2((Z)-pentadec-8-enyl) phenylazo]-benzenesulfonic Acid (Surfactant 1) was synthesized using the same procedure given in chapter-2.

3.2.2. General procedure: NMR spectra of the compounds were recorded using a 300-MHz Bruker NMR spectrophotometer in d_6 -dimethyl sulfoxide (DMSO) containing small amount of tetramethylsilane (TMS) as internal standard. $^1\text{H-NMR}$ analysis of the polymer samples were carried out in 500-MHz Bruker Avance II NMR Spectrometer using d_6 -DMSO as solvent at 30 °C. Infrared spectra of the polymers were recorded using Perkin Elmer Spectrum one FT-IR Spectrometer in the

range of 4000-400 cm^{-1} . The purity of the compounds was determined by fast atom bombardment high-resolution mass spectrometry (FAB-HRMS: JOEL JSM 600). For SEM measurements, polymer samples were subjected to a thin gold coating using a JEOL JFC-1200 fine coater. The probing side was inserted into a JEOL JSM -5600 LV scanning electron microscope for taking photographs. TEM analysis was recorded using a Tecnai 30 G² S-twin 300KV high resolution transmission electron microscope. For TEM measurements a suspension of nanospheres was prepared in ethanol and deposited on a Formvar-coated copper grid. UV-visible spectra of the polypyrrole nano spheres and copolymers are recorded using a Perkin-Elmer Lambda- 35 UV-visible spectrometer. Particle size analysis was done by Malvern U.K. Zetasizer 3000 HAS (static light scattering) and DLS measurement (dynamic light scattering) was done by Nano ZS Malvern instrument employing a 4 mW He-Ne laser ($\lambda=632.8$ nm) and equipped with a thermo stated sample chamber. For conductivity measurements, the polymer samples were pressed into a 10 mm diameter pellet and analyzed using a four-probe using Keithley 6221 DC and AC current source and 2181A nano-voltmeter. The resistivities of the sample were measured at five different positions. Wide angle X-ray diffraction (WXR) patterns of the finely powdered polymer samples were recorded by a Philips analytical Diffractometer using Cu-K α emission. The spectra were recorded in the range of $2\theta = 0- 40$ and analyzed using X'Pert software. The thermal stability of the polymers was determined using TGA-50 Shimadzu Thermo gravimetric Analyzer at a heating rate of 10 $^{\circ}\text{C}/\text{min}$ in nitrogen. The TGA instrument was calibrated with calcium oxalate monohydrate as standard.

Preparation of polyaniline (PANI) nanofiber via emulsion route using surfactant-1: Typical procedure for the synthesis of polyaniline nanofiber using surfactant-1 is shown below. Surfactant-1 (70 mg, 0.144 mmol) was taken in 10 mL water and stirred under sonicator for 15 minutes. Aniline (1 mL, 11 mmol) were added to the surfactant solution and sonicated for 45 minutes. At the end of stirring, the polymerization mixture turned into a pale yellow thick emulsion. Ammonium persulfate (3.28 g, 14.4 mmol) in water (5 mL) was added drop wise to the solution and continued the stirring under sonicator for 1h. The polymerization was continued

without disturbance for 12 h at 25 °C. The sample was filtered, washed with water and methanol till the filtrate become colorless. The green nano-material was dried under vacuum oven for 12 h at 50 °C. Yield = 97 %. ¹H-NMR (500 MHz, *d*₆-DMSO) δ: 7.40 (m, 2H, PANI), 7.44 (m, 2H, PANI), 7.78 (s, 4H, Ar-H Dopant). FT-IR (KBr, cm⁻¹): 1560, 1494, 1346, 1193, 1111, 1050, 923, 811, 783, and 612. UV-visible (in water, nm) λ max: 350, 450 and 900.

A similar procedure was adopted for the synthesis of polypyrrole nanospheres using 1mL pyrrole instead of aniline and rests of the procedures same (see P1 in chapter 2)

Preparation of pyrrole-aniline copolymers using surfactant-1: Typical procedure for the synthesis of **P-Co-13** is given below. Surfactant 1 (70 mg, 0.144 mmol) was taken in 10 mL water and stirred under sonicator for 15 minutes. Pyrrole (0.1 mL, 1.4 mmol) and aniline (0.9 mL, 9.9 mmol) were added to the surfactant solution and sonicated for 45 minutes and rest of the procedure are similar to polyaniline nanofiber synthesis. Yield = 75 %. ¹H NMR (500 MHz, *d*₆-DMSO) δ: 7.45 (m, 2H), 7.37(m, 2H), 7.27 (d, 2H). FT-IR (KBr, cm⁻¹): 1560, 1494, 1346, 1193, 1111, 1050, 923, 811, 783, and 612. UV-visible (water, nm) λ max: 350, 450 and 900.

Polymer **P1-Co-6**, **P1-Co-36**, **P1-Co-57**, **P1-Co-75**, **P1-Co-84**, **P1-Co-92** and **P1-Co-97** were synthesized using the above procedure with various mole ratios of pyrrole and aniline (see table 3.2).

Polypyrrole seeded by polyaniline nanofibers: Surfactant 1 (70 mg, 0.144 mmol) is taken in 10 mL water and stirred using sonicator for 15 minutes. Pyrrole (1 mL, 14.4 mmol) and 50 mg of powdered polyaniline nanofibers is added to the surfactant solution and the rest of the procedure was identical to that of **P-1**. Yield = 91 %. FT-IR (KBr): 1550, 1460, 1295, 1181, 1110, 1036, 960, 905, 783, 670 and 612. UV- Vis (water, nm) λ max: 480 and 1000.

A similar procedure was adopted for the preparation of polyaniline by seeding polypyrrole nanospheres using 50 mg polypyrrole nano-spheres and aniline (1 mL, 11 mmol). Yield =82 %. FT-IR (KBr, cm⁻¹): 1560, 1490, 1360, 1298, 1246, 1130, 1036, 890 815, 700, 621 and 509. UV-Vis (water, nm) λ max: 360, 425 and 900 nm.

Synthesis of 4-[4-dodecyloxy-2((Z)-pentadec-8-enyl) phenylazo]-benzenesulphonic acid (Surfactant-2): Surfactant-1 (5.0 g, 10.3 mmol) was added to a powdered suspension of KOH (1.1 g, 20.4 mmol) in 10 mL DMSO solution. Dodecyl bromide (3.2 g, 12.9 mmol) was added drop by drop to the above reaction mixture at 60° C for 12 h. The sodium salt of the product was precipitated in acetone solution and filtered through suction pump. Sodium salt of the product is acidified using 2 M HCl and filtered and dried in vacuum oven. Surfactant was column purified using 30 % methanol in ethyl acetate. Yield = 3.3 g (49 %). ¹H NMR (500 MHz, *d*₆-DMSO) δ: 7.76 (s, 4H, Ar-H), 7.64 (d, 1H, Ar-H), 6.90 (s, 1H, Ar-H), 6.83 (d, 1H, Ar-H), 5.24 (2H, CH=CH), 4.04 (t, 2H, -O-CH₂), 3.1-.06 (m, 50 H, aliphatic-H). ¹³C NMR (125 MHz, *d*₆-DMSO) δ: 161.3, 152.2, 149.6, 145.0, 143.6, 129.7, 126.6, 121.7, 116.7, 115.0, 112.5, 69.7, 68.8, 31.0, 31.24, 30.77, 29.14, 28.85, 26.9, 25.4, 22.0 and 13.5. FT-IR (KBr, cm⁻¹): 2923, 2854, 2852.9, 1600, 1533.7, 1472, 1397, 1338, 1228, 1136, 1016, 852, 716 and 636. UV-vis (in H₂O, nm) λ max: 365. FAB-MS (MW: 654.99): m/z = 654.44 (M⁺).

Preparation of Polyaniline nanofibers by surfactant-2: Surfactant-2 (94 mg, 0.144 mmol) was taken in 10 mL water and stirred under sonicator for 15 minutes. Aniline (1 mL, 11 mmol) were added to the surfactant solution and sonicated for 45 minutes. At the end of stirring, the polymerization mixture turned into a pale yellow thick emulsion. Ammonium persulfate (3.28 g, 14.4 mmol) in water (5 mL) was added drop wise to the solution and continued the stirring under sonicator for 1h. The polymerization was continued without disturbance for 12 h at 25 °C. The sample was filtered, washed with water and methanol till the filtrate become colorless. The green nano-material was dried under vacuum oven for 12 h at 50 °C. Yield = 97 %. ¹H-NMR (500 MHz, *d*₆-DMSO) δ: 7.40 (m, 2H, PANI), 7.44 (m, 2H, PANI), 7.78 (s, 4H, Ar-H Dopant). FT-IR (KBr, cm⁻¹): 1560, 1494, 1346, 1193, 1111, 1050, 923, 811, 783, and 612. UV-visible (in water, nm) λ max: 350, 450 and 900.

A similar procedure was adopted for the synthesis of polypyrrole nanospheres using 1mL pyrrole instead of aniline and rests of the procedures same

Preparation of polyaniline-polypyrrole copolymer nanomaterials using surfactant-2: Typical procedure for the synthesis of **P2-Co-13** is given below. Surfactant-2 (94 mg, 0.144 mmol) was taken in 10 mL water and stirred under sonicator for 15 minutes. Pyrrole (0.1 mL, 1.4 mmol) and aniline (0.9 mL, 9.9 mmol) were added to the surfactant solution and sonicated for 45 minutes and rest of the procedures are similar to that of polyaniline nanofiber synthesis.. Yield = 89 %. ¹H NMR (500 MHz, *d*₆-DMSO) δ: 7.45 (m, 2H), 7.37(m, 2H), 7.27 (d, 2H). FT-IR (KBr, cm⁻¹): 1540, 1460, 1360, 1295, 1181, 1090, 1036, 960, 905, 783, 670 and 612. UV-Vis (water, nm) λ max: 480 and 1000.

Polymer **P2-Co-6**, **P2-Co-13**, **P2-Co-36**, **P2-Co-57**, **P2-Co-75**, **P2-Co-84**, **P2-Co-92** and **P2-Co-97** are synthesized using the above procedure with various mole ratio of pyrrole and aniline (see table 3.2).

Synthesis of 4-[4-hydroxy phenylazo]-benzene sulphonic acid (Surfactant-3): Sulphanilic acid (11.0 g, 53.28 mmol) and sodium carbonate (2.8 g, 26.6 mmol) were added into a 50 mL of water and heated to 60-70°C to dissolve the entire solid. It was then cooled to 5°C, and a cold solution of sodium nitrite (4.0 g, 58.5 mmol) in water (8 mL) was added. The resultant yellow solution was poured into ice (50 g) containing concentrated HCl (8 mL) and stirred using a mechanical stirrer for 30 min at 5 °C. Phenol (5.0 g, 53.2 mmol) and sodium hydroxide (6.38, 159.6 mmol) in 30 ml water and cold diazonium chloride solution was added dropwise at 5 °C. The reaction was continued with stirring for 3 h in the ice cold conditions using a mechanical stirrer. The reaction mixture was neutralized by the addition of concentrated HCl (50 mL) in crushed ice (70 g). The red precipitate was filtered using a Buchner funnel and washed using with water. The dried product weighed 12.0 g (crude product). It was further purified by passing through silica gel column using 50 % methanol in ethyl acetate. The solvent was removed to obtain the product as red-orange solid. Yield = 10.35 g (70 %). ¹H NMR(500 MHz, *d*₆-DMSO) δ: 7.85 (d, 2H, Ar-H), 7.8 (s,4H,Ar-H), 6.95 ppm (d, 2H, Ar-H). ¹³C NMR (125 MHz, *d*₆- DMSO) δ: 161.2, 151.8, 149.74, 145.1,126.8, 125.1, 121.4 and 116.5. FT-IR (KBr, cm⁻¹): 2923, 2853, 1602, 1486, 1388, 1244, 1184, 1129, 1048, 852, 714 and 639 cm⁻¹. UV-Vis (in CH₃OH, nm): λmax = 330. FAB- MS (MW: 278): m/z = 278.28 (M⁺).

Preparation of polyaniline (PANI) nanofiber via emulsion route using surfactant-3: Typical procedure for the synthesis of polyaniline nanofiber using surfactant-3 is shown below. Surfactant-3 (40 mg, 0.144 mmol) was taken in 10 mL water and stirred under sonicator for 15 minutes. Aniline (1 mL, 11 mmol) were added to the surfactant solution and sonicated for 45 minutes. At the end of stirring, the polymerization mixture turned into a pale yellow thick emulsion. Ammonium persulfate (3.28 g, 14.4 mmol) in water (5 mL) was added drop wise to the solution and continued the stirring under sonicator for 1h. The polymerization was continued without disturbance for 12 h at 25 °C. The sample was filtered, washed with water and methanol till the filtrate become colorless. The green nano-material was dried under vacuum oven for 12 h at 50 °C. Yield = 97 %. ¹H-NMR (500 MHz, *d*₆-DMSO) δ: 7.40 (m, 2H, PANI), 7.44 (m, 2H, PANI), 7.78 (s, 4H, Ar-H Dopant). FT-IR (KBr, cm⁻¹): 1560, 1494, 1346, 1193, 1111, 1050, 923, 811, 783, and 612. UV-visible (in water, nm) λ max: 350, 450 and 900.

A similar procedure was adopted for the synthesis of polypyrrole nanospheres using 1mL pyrrole instead of aniline and rests of the procedures same (see P1 in chapter 2)

Preparation of pyrrole-aniline copolymers using surfactant-3: Typical procedure for the synthesis of **P-Co-13** is given below. Surfactant-3 (40 mg, 0.144 mmol) was taken in 10 mL water and stirred under sonicator for 15 minutes. Pyrrole (0.1 mL, 1.4 mmol) and aniline (0.9 mL, 9.9 mmol) were added to the surfactant solution and sonicated for 45 minutes and rest of the procedures are similar to that of copolymer synthesis.. Yield = 75 %. ¹H NMR (500 MHz, *d*₆-DMSO) δ: 7.45 (m, 2H), 7.37(m, 2H), 7.27 (d, 2H). FT-IR (KBr, cm⁻¹): 1560, 1494, 1346, 1193, 1111, 1050, 923, 811, 783, and 612. UV-visible (water, nm) λ max: 350, 450 and 900.

Polymer **P1-Co-6**, **P1-Co-36**, **P1-Co-57**, **P1-Co-75**, **P1-Co-84**, **P1-Co-92** and **P1-Co-97** were synthesized using the above procedure with various mole ratios of pyrrole and aniline (see table 3.2).

3.3. Results and discussion

3.3.1. Synthesis of polypyrrole-polyaniline copolymers nanomaterials

Surfactant-1 forms unique anionic amphiphilic micelles in water which acts as self assembled templates for polyaniline nanofibers and polypyrrole nanospheres via emulsion Polymerization. Selective templating of the surfactant micelles could be further extended to produce copolymer nanomaterials. Polypyrrole-co-polyaniline copolymers were prepared by varying the amount of pyrrole and aniline from 0 to 100 % (in moles) in the feed. Concentration of pyrrole and aniline were varied from 4.8×10^{-2} to 9.6×10^{-1} M and 7.3×10^{-1} to 3.6×10^{-2} M respectively, whereas surfactant concentration remains constant (9.6×10^{-3} M) see table. 3.2. The emulsion mixtures were oxidized by APS to obtain the polyaniline, polypyrrole and polypyrrole-co-polyaniline copolymers (see figure 3.3.). The copolymers are denoted as **PX-Co-Y**, where Y= mole fraction of pyrrole in the feed [Y= 6, 13, 36, 57, 75, 84, 92 and 96] (see table 3.2). The ratio of [aniline + pyrrole]/[dopant] was maintained as ~ 75 for the copolymer series.

Table 3.2. Concentration of reactants used for synthesis and S/N ratio of the nanomaterials.

Sample	Conc. of ^a pyrrole (M)	Conc. of aniline (M)	Conc. of surfactant	S/N Ratio ^b
PANI	0	7.3×10^{-1}	9.6×10^{-3}	0.48
P1-Co-6	4.8×10^{-2}	6.9×10^{-1}	9.6×10^{-3}	0.41
P1-Co-13	9.6×10^{-2}	6.6×10^{-1}	9.6×10^{-3}	0.41
P1-Co-36	2.8×10^{-1}	5.1×10^{-1}	9.6×10^{-3}	0.28
P1-Co-57	4.8×10^{-1}	3.6×10^{-1}	9.6×10^{-3}	0.23
P1-Co-75	6.7×10^{-1}	2.2×10^{-1}	9.6×10^{-3}	0.26
P1-Co-84	7.7×10^{-1}	1.5×10^{-1}	9.6×10^{-3}	0.26
P1-Co-92	8.6×10^{-1}	7.3×10^{-2}	9.6×10^{-3}	0.28
P1-Co-96	9.1×10^{-1}	3.6×10^{-2}	9.6×10^{-3}	0.28
PPy-1	9.6×10^{-1}	0	9.6×10^{-3}	0.28

^a Concentration of the monomers, ^b Sulphur Nitrogen ratio from elemental analysis

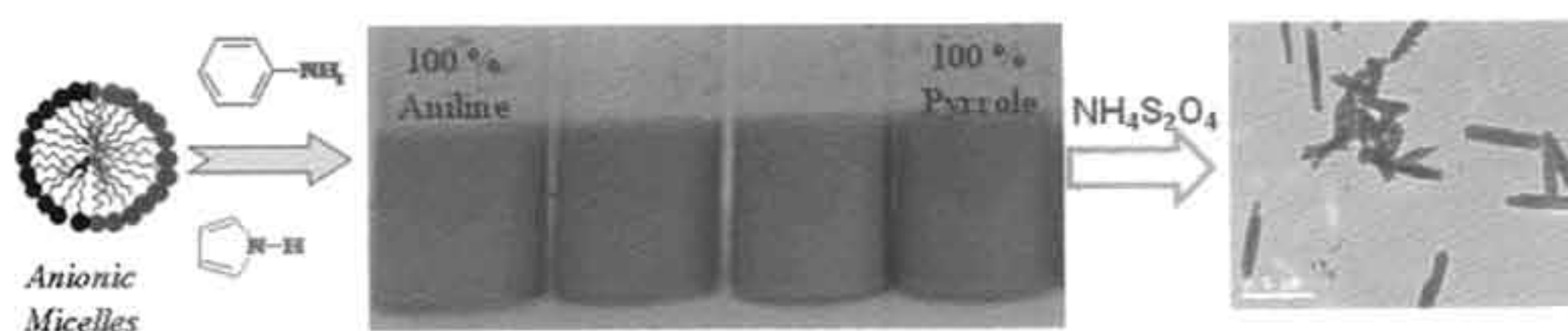


Figure 3.3. Synthesis of polypyrrole-polyaniline copolymer nanomaterials.

3.3.2. Structural characterization of copolymer nanomaterials

The structural analysis of polyaniline-co-polypyrrole samples were done by FT-IR and ¹H-NMR spectroscopy. FT-IR spectra of the copolymers were recorded by making samples into thin pellet with KBr and spectra of copolymers are shown in figure 3.4. and the peaks are assigned with appropriate band structures (A = aniline and P = pyrrole). The polyaniline sample **PANI** has two peaks at 1580 and 1490 cm⁻¹ with respect to stretching vibration of benzenoid and quinoid in polyaniline chains, respectively [^aAnilkumar, P. *et al* 2006; ^bAnilkumar, P. *et al* 2007]. Three additional peak were assigned at 1300, 1148 and 820 cm⁻¹ to C-N stretching of secondary amine group, O=S=O stretching of the sulfonic acid dopant, and C-H in the 1,4-disubstituted ring out- of plane stretching, respectively [Ping, Z. J. *et al* 1996; Christensen, P.A. *et al* 1991; Stejskal, J. *et al* 2004]. A weak band at 1714 cm⁻¹ in the polypyrrole is assigned to C=O, which arise from the hydroxyl functionality introduced by the nucleophilic attack of water and the subsequent conversion of carbonyl by keto-enol tautomerism. The peaks at 1550, 1195, 1040, 965 and 923 cm⁻¹ are assigned to C=C stretching in pyrrole, breathing vibration of the pyrrole rings, N-H (or C-H) in-plane deformation vibration, C-C out of ring deformation and C-H out of plane deformation vibrations, respectively. It is very interesting to note that with increase in the amount of aniline in the feed, the peaks at 1580, 1490, 1300, 1148 and 820 cm⁻¹ were increasing (move downwards) and attained the value of homopolymer, polyaniline. Similarly, the polypyrrole peaks at 1714, 1550, 1195, 1040, 965 and 923 cm⁻¹ were increasing with the amount of pyrrole in the feed (move upwards). The increase in the intensity of the respective peaks with increase in the amount of monomer in the copolymer confirmed the formation of expected structure. The FT-IR spectra of the copolymer nanomaterial synthesized by double tailed surfactant also shown similar peaks confirming the formation of the copolymers materials.

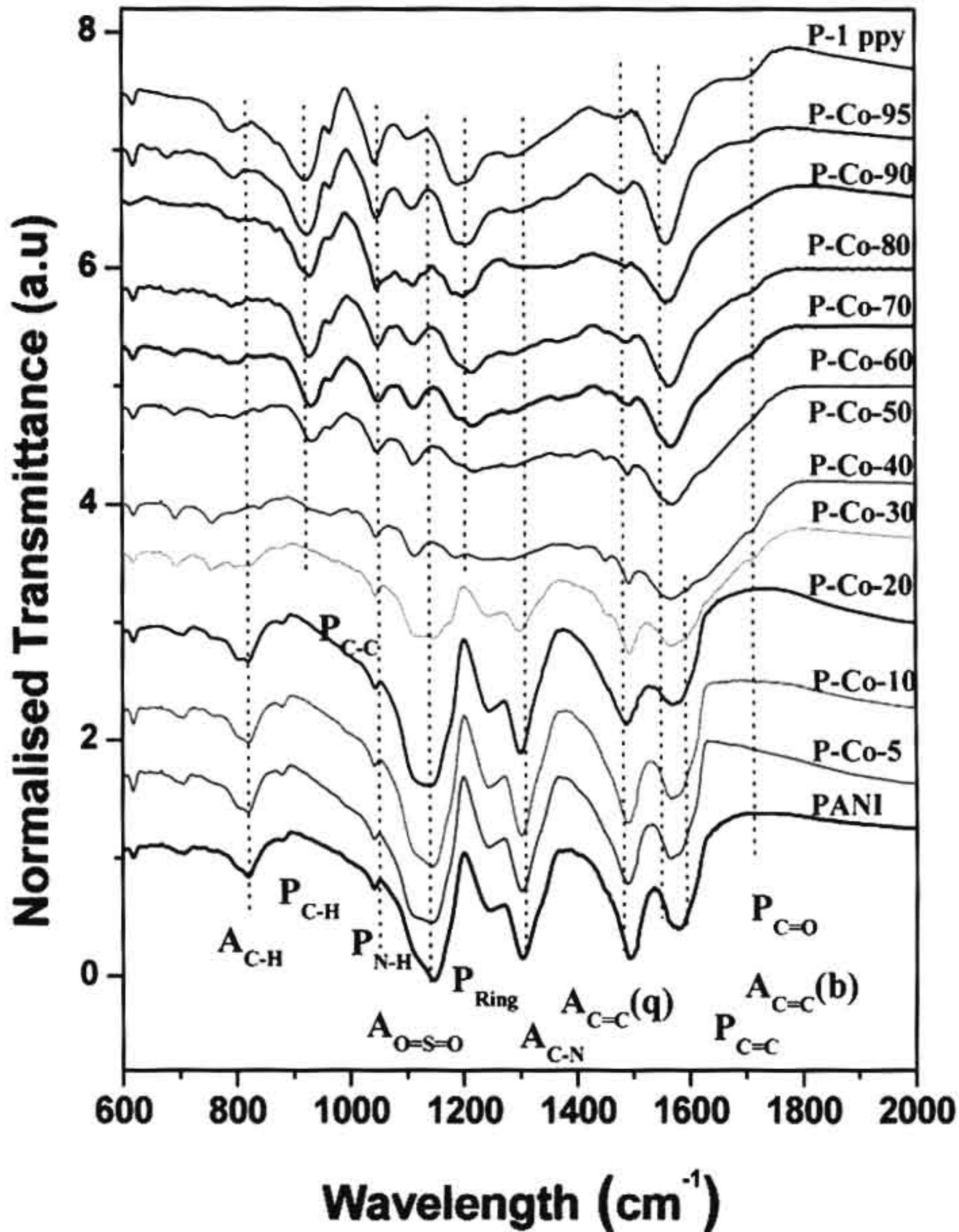


Figure 3.4. FT-IR spectra of the copolymer nanomaterials synthesized using surfactant-1.

$^1\text{H-NMR}$ spectra (500 MHz) of polymers and surfactant were recorded in d_6 -DMSO and shown in figure 3.5. The different types of aromatic protons in the surfactant were assigned with alphabets. Polyaniline showed two peaks at 7.50 and 7.45 ppm with respect to two types of aromatic protons in the aromatic ring. All the polymer spectra showed three equally strong signals at 7.26, 7.15 and 7.05 ppm corresponding to the N-H protons in the conducting polymer chains. The NMR spectrum of polypyrrole sample showed a peak at 7.39 ppm, which was assigned to

the β - hydrogen in the aromatic ring [Zhou, C. *et al* 2008; ^bLi, X. G. *et al* 2001; ^cLi, X. G. *Et al* 2001; ^dLi, X. G. *et al* 2004]. The copolymers **P-Co-57** and **P-Co-84** showed new peaks at 7.34 and 7.28 ppm corresponding to pyrrole-aniline copolymer units. The chemical shift values of the samples were well in accordance to reported values [Zhou, C. *et al* 2008]. The NMR spectra clearly evident that the copolymers are produced by the reacting constituent monomers pyrrole and aniline. The polymers were also showed peaks corresponding to the dopant which confirmed the strong binding ability of the azobenzene sulfonic acid anionic dopant with the polymer chains.

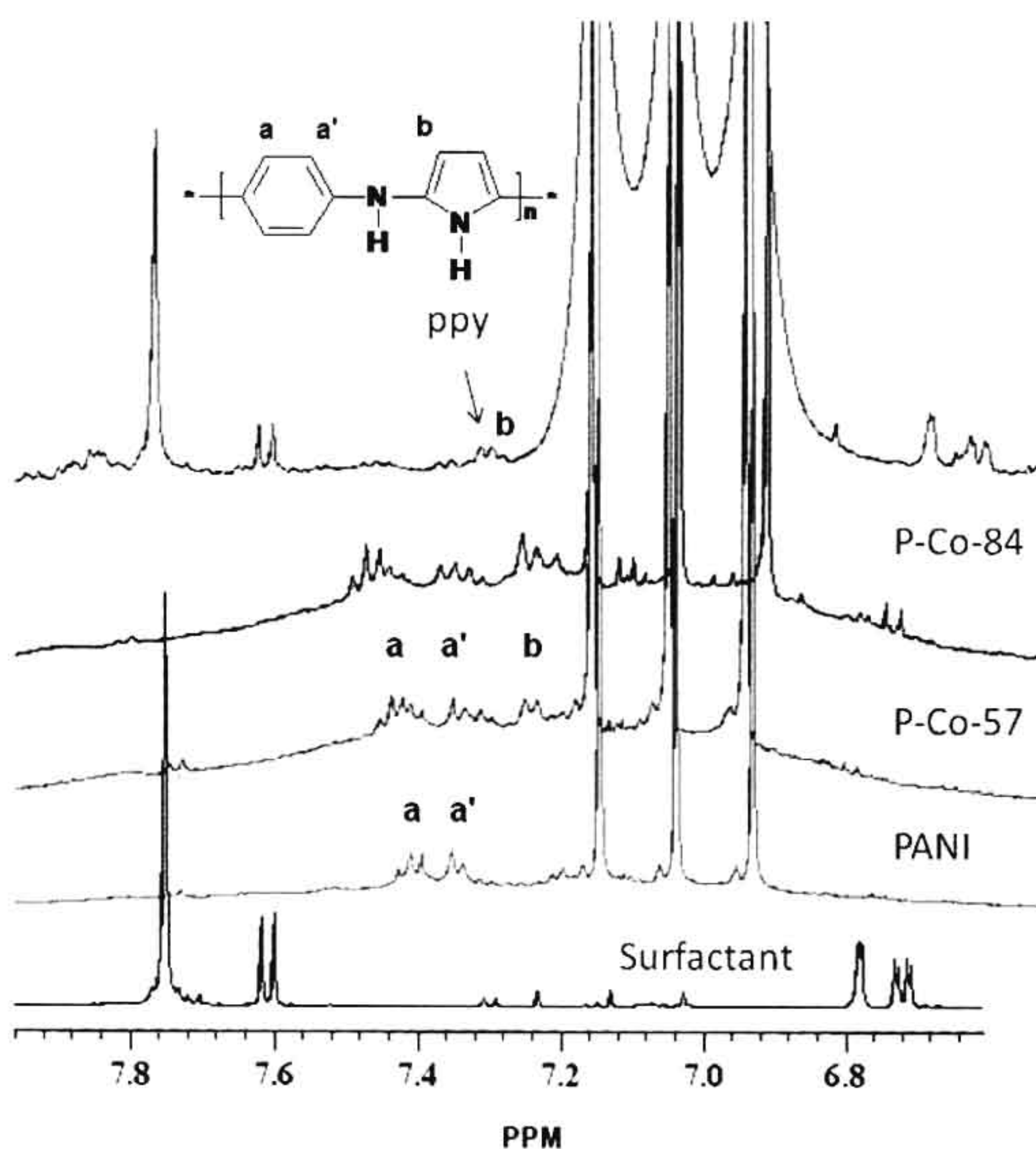


Figure 3.5. ¹H NMR spectra of surfactant, PANI, PPy and copolymers.

3.3.3. Morphology of nanomaterials

SEM images of the polyaniline (**PANI**) and representative copolymers were given in figure 3.6. The morphology of the polyaniline (**PANI**) was found as fibrous with ~ 180 nm in diameter with length up to 3-5 μM . The copolymer **P-Co-6** (with 6.4 % pyrrole and 93.6 % aniline) was found to have nano-fibers but relatively thin and shorter in size compared to that of pure **PANI** nano-fibers. Further increase in the pyrrole was increased to 35 % (**P-co-36** and above) the morphology was completely transformed to a spherical one and no traces of nano-fiber was noticed in the entire sample.

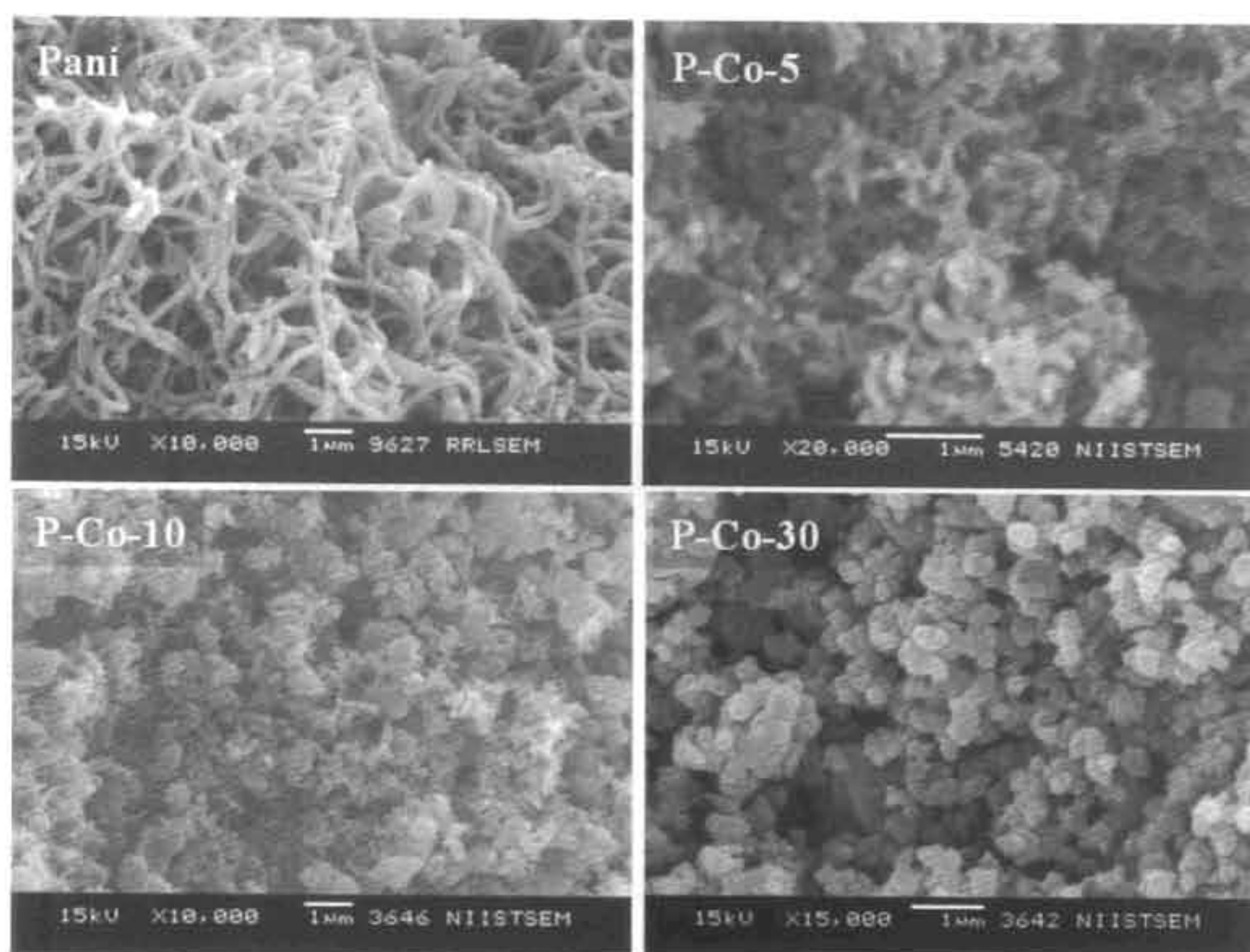


Figure 3.6. SEM images of the **PANI** and Copolymers

TEM images of the copolymer series were recorded and shown in figure 3.7. **PANI** contained only solid nano-fibers of 200 nm diameter with length up to 3 μM . The morphology of the **P-Co-6** showed the appearance of very short nano-rods of 80-100 nm diameter with length up to 0.5-0.7 μM . The nano-rods were separated (not connected together) and almost uniform in size in the entire sample. **P-Co-36** was

found to be full of nano- spheres of 150-180 nm. It is directly evident from the SEM and TEM images that the increase in the pyrrole content in the feed induced the transformation of long nano-fibers to short nano-rods and then to nano-spheres.

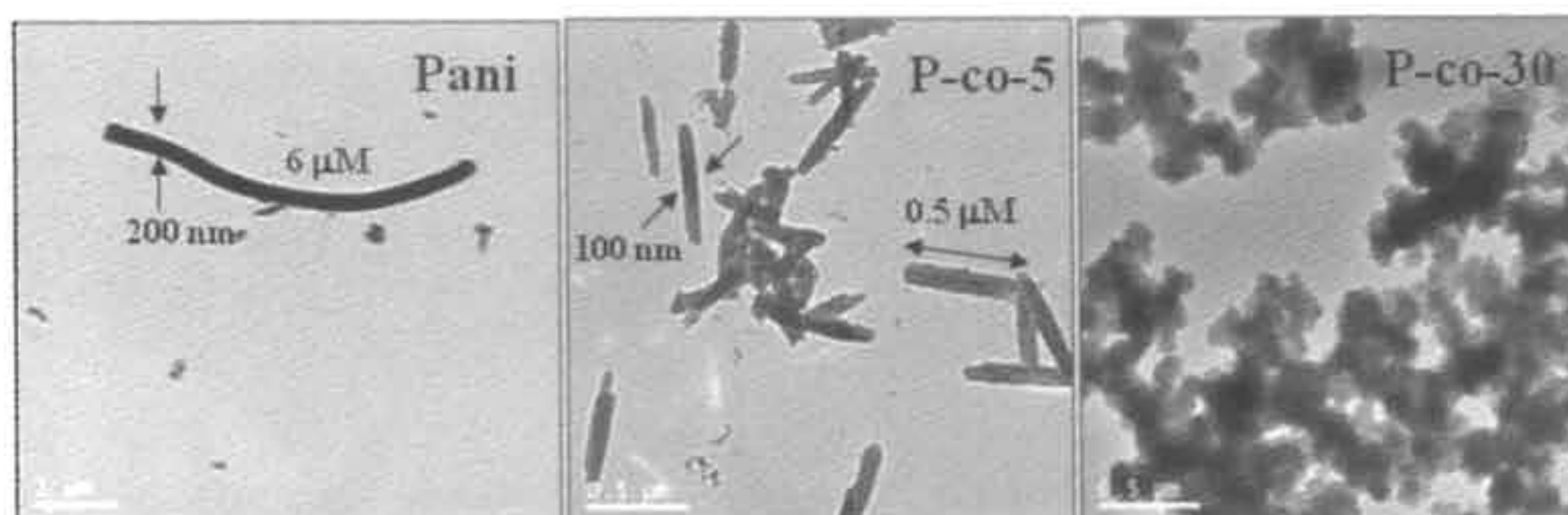


Figure 3.7. TEM images of the **PANI** and Copolymers

3.3.4. Mechanism of the nano-structure transformations

The polymerization of both aniline and pyrrole follow oxidative step-condensation route, both the monomers get oxidized to form aryl radical, which attack on either same or other monomer to produce homo or hetero oligomers. However, the composition of the repeating units in the copolymer was highly dependent on the reactivity of the monomers. The monomer reactivity of the aniline and pyrrole were reported as $r_{An} = 0.13$ and $r_{py} = 2.16$, and therefore, always the pyrrole has higher reactivity over aniline in the copolymerization [Lim, V. W. L. *et al* 2001]. In a size control nano-material synthesis of copolymers, the copolymerization route is not only influenced by the reactivity differences of the monomers but also by the template associated with each monomer. Therefore, interaction of anionic surfactant with the mixture of aniline and pyrrole monomers in the copolymer route is expected to be different compared to that of their homo polymerization. Two pathways are possible in the copolymerization route: (i) predominant self-organization and polymerization of one of the monomer over other to form either spherical or cylindrical aggregates, which template (or seeding exclusively) for one particular nanostructures or (ii) combined self-organization of both monomers to produce new short range intermediate (cylindrical + spherical) aggregates, which template for new morphology.

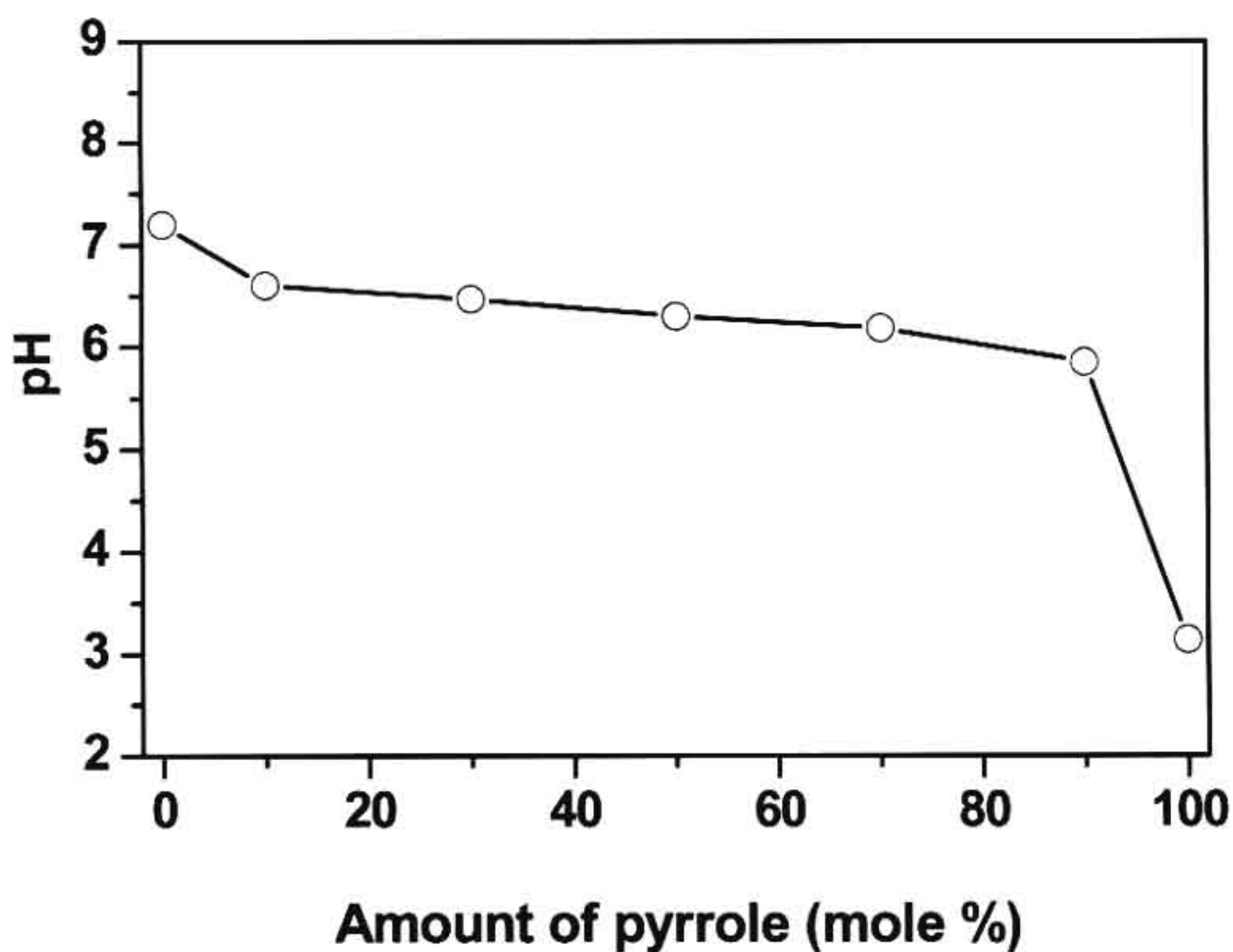


Figure 3.8. *pH profile pyrrole-aniline emulsion templates at different composition.*

In order to understand the interactions of aromatic moieties like aniline and pyrrole with surfactant in water, the pH of the polymerization mixtures were measured (see figure 3.8.). Since, the surfactant is sulfonic acid its interactions with bases like aniline and pyrrole are expected to reflect in the pH of the solution. Under the polymerization condition, the pH of the surfactant (alone), surfactant + pyrrole and surfactant + aniline in water were obtained as 2.86, 3.14 and 7.29, respectively. As expected, the surfactant was highly acidic in nature in water. Aniline is a moderate base and effectively reacted with the surfactant to form the neutral anilinium-salt which drastically increased the pH of the solution from 2.86 to 7.29 (towards neutral). On the other hand, pyrrole is relatively weak base compared to aniline and the complex solution was found acidic (small changes from 2.86 to 3.14). The pH of the copolymer mixtures was shown gradual decrease with increase in pyrrole concentration. DLS analysis of the copolymerization mixtures were carried out in water, the plots were shown in figure 3.9. DLS distribution of the **PANI**, **P-Co-10**, **P-Co-30** and **P-Co-70** indicates that monomer form strong sub micrometer aggregate

with surfactant with their distribution maxima centered on 400-500 nm. The DLS histograms of the copolymer mixtures were almost identical to that of the homopolymers, which confirmed that both aniline and pyrrole are compatible with the surfactant and form strong aggregates without any phase separation.

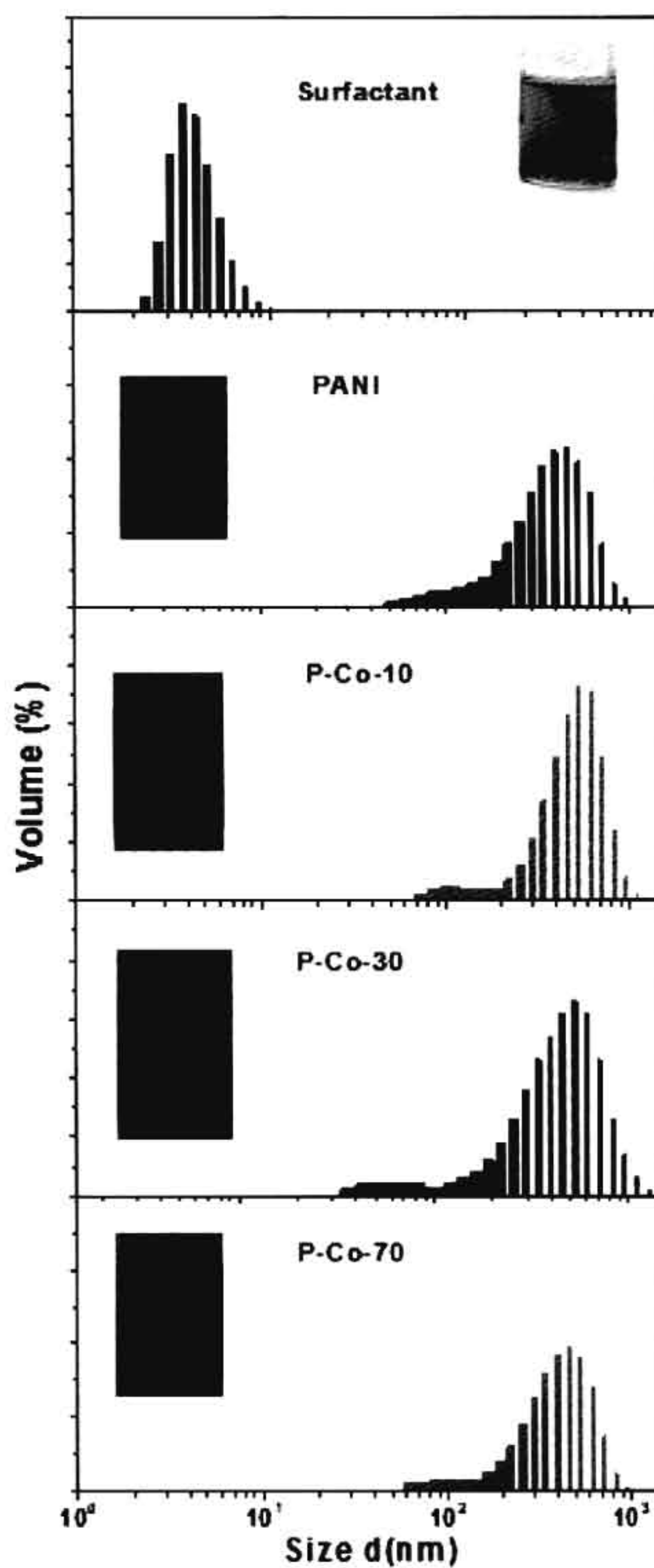


Figure 3.9. DLS histogram of emulsion templates.

The shape of the aggregated micelles could not be predicted by the DLS distribution, hence the thick emulsion was cast on the SEM grid and subjected to morphology analysis (see figure 3.10.). The morphology of the aniline + surfactant complex was found completely different from that of the pyrrole + surfactant. The aniline complex existed in the form of long fibrous network compared to that of spherical geometry observed for pyrrole complexes. The addition of 6.4 % pyrrole truncates the long range self-organization of cylindrical template and produce short cyclical-flake like aggregates, which upon oxidation produce well defined short conducting nano-rods. When the amount of pyrrole was increased further, the truncation became predominant and resulted in the formation of spherical micelles, which lead to the formation of small nano-spheres (see chapter 2). It is very important to note that the addition of ~13 % of pyrrole was sufficient enough to disturb the long range ordering of remaining of ~90 % aniline self-organization with surfactant molecules.

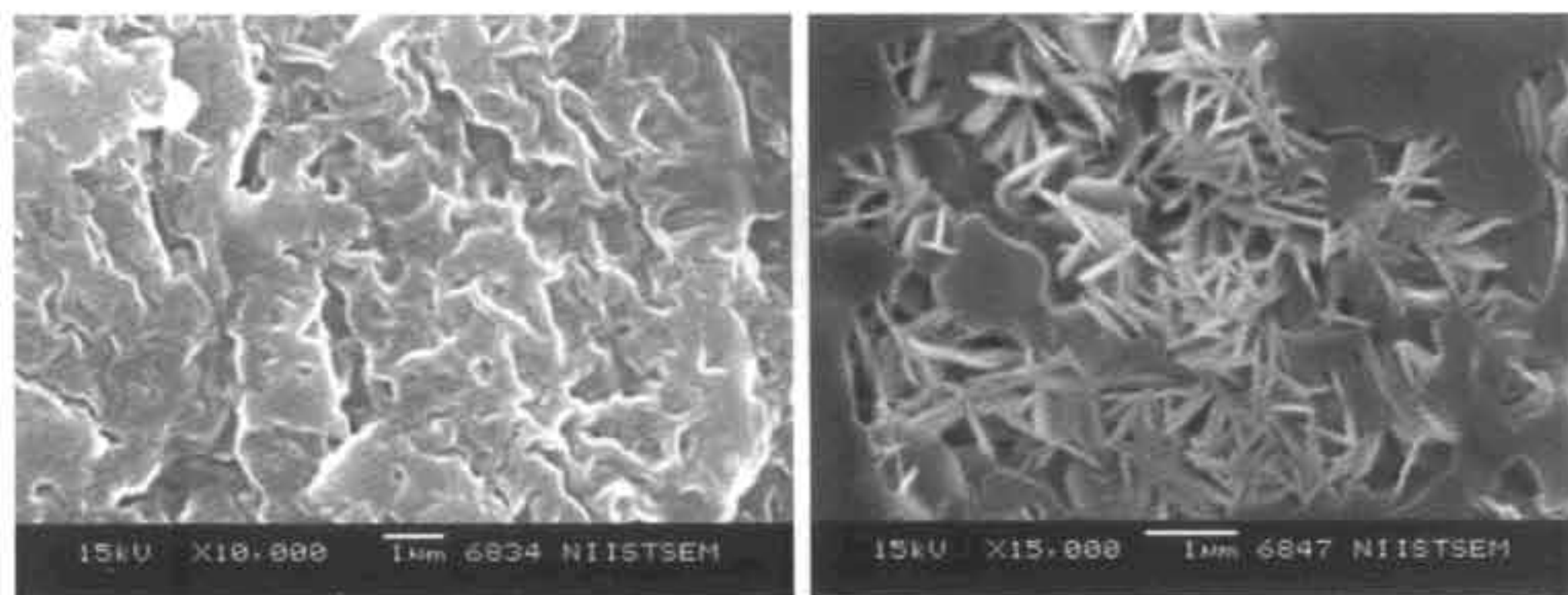


Figure 3.10. SEM image of emulsion templates.

One may assume that the formation of nano-rod may be the result of seeding of initially polymerized polypyrrole nano-spheres (6 % monomer) and further growth of the polyaniline chains (94 % monomer) rather than the combined self-organization of pyrrole + aniline with surfactant, which template for nano-rods. In order to rule out the seeding possibility, selective seeding polymerizations were carried out by seeding polyaniline by polypyrrole nano-spheres and polypyrrole by polyaniline nano-fibers (see figure 3.11.). The morphology of the polyaniline sample seeded by nano-spheres is fibrous in nature and it exactly matches with that of its homopolymers PANI. Similarly the polypyrrole sample seeded by polyaniline nano-fiber was found to be

full of spheres and matched with its homopolymer P-1 (in chapter-2). It clearly evident that the seeding was not predominant process in the anionic surfactant template mediated nano-materials synthesis.

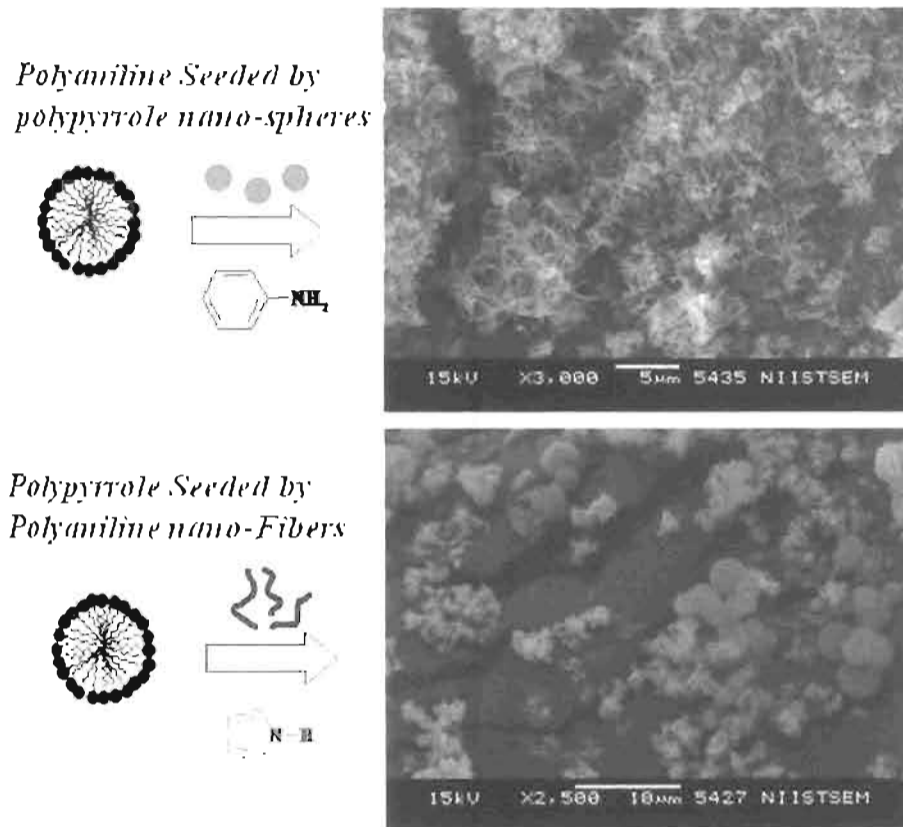


Figure 3.11. Seeding Polymerization PANI and PPy using nanomaterials.

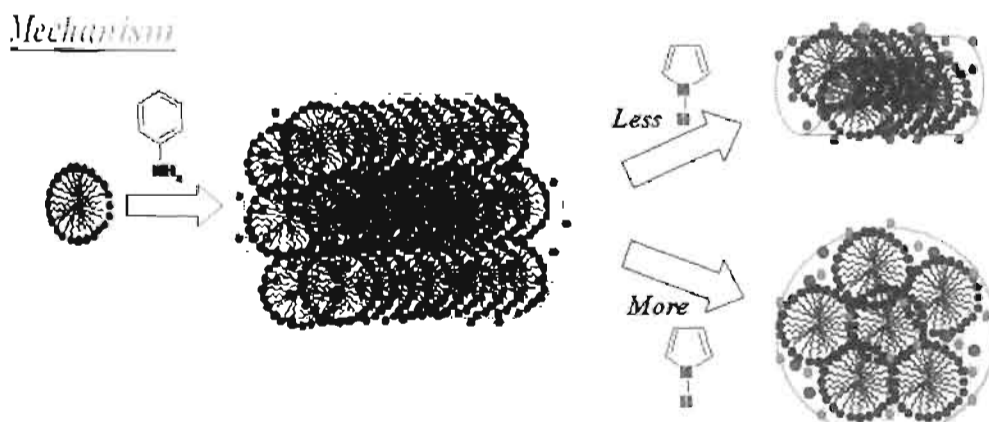


Figure 3.12. Mechanism of copolymer nanomaterials.

Based on the above studies, the following mechanism has been proposed for the morphology transformation of the copolymer nanomaterials (see figure 3.12.). Amphiphilic azobenzene sulphonic acid forms micelles of size 4.3 nm in water. Surfactant micelles in presence of aniline (aromatic primary amine) self-assemble as aggregated cylindrical micelles which produce nanofibers (PANI). Aniline monomer effectively neutralizes polar head of the surfactant (screens the negative charge of surfactant micelles) in addition to their inclusion to the aromatic core of the micelles. Long cylindrical micelles are formed due to the aggregation of the spherical surfactant micelles in a cylindrical manner. With the introduction of co-monomer pyrrole in feed (5 mole %), long range order cylindrical aggregates were truncated into short and thin cylindrical aggregates. The transformation from long cylindrical to small cylindrical micelle was clearly visible in the template morphology and pH change. With increase in pyrrole content greater than 30 %, the all the cylindrical template has truncated completely into spherically aggregated micelles. Thus, in the present investigation, morphology of the nanomaterial was precisely controlled by adjusting the composition of aniline and pyrrole in presence of amphiphilic anionic surfactant.

3.3.5. Role of anionic structure on copolymer morphology

Surfactant-1 forms stable emulsion with monomers like aniline and pyrrole to produce nanofibers and nanospheres respectively via oxidative Polymerization. Here, in the addition to surfactant-1, two more structurally different surfactants were used to understand the role surfactants played on stability of emulsion, morphology and solid state properties. Diazotization reaction of phenol and cardanol have been carried out with sulphanilic acid for the synthesis of two water soluble amphiphilic dopant cum surfactants, 4-[4-hydroxy phenylazo]-benzenesulphonic acid (surfactant-3) and 4-[4-hydroxy-2((Z)-pentadec-8-enyl) phenylazo]-benzenesulphonic acid (surfactant-1) shown in figure 3.13. Further, surfactant 2 was synthesized via nucleophilic substitution reaction of surfactant-1 with dodecyl bromide to produce double-tailed surfactant 4-[4-dodecyloxy -2((Z)-pentadec-8-enyl) phenylazo]-benzenesulphonic acid surfactant-3. Cardanol is natural phenol with unsaturated side chain, an industrial bye product from cashew nut processing industry. Surfactant 2 and surfactant 3 have unique built-in amphiphilic design in which the hydrophilic sulphonic acid behaves as a polar head and the long alkyl chain as a hydrophobic tail, whereas the surfactant-3

possessed only the head group. This provides an unique opportunity to study the structural effects of surfactants on the synthesis and properties of the conducting copolymers nanomaterials under surfactant assisted emulsion Polymerization.

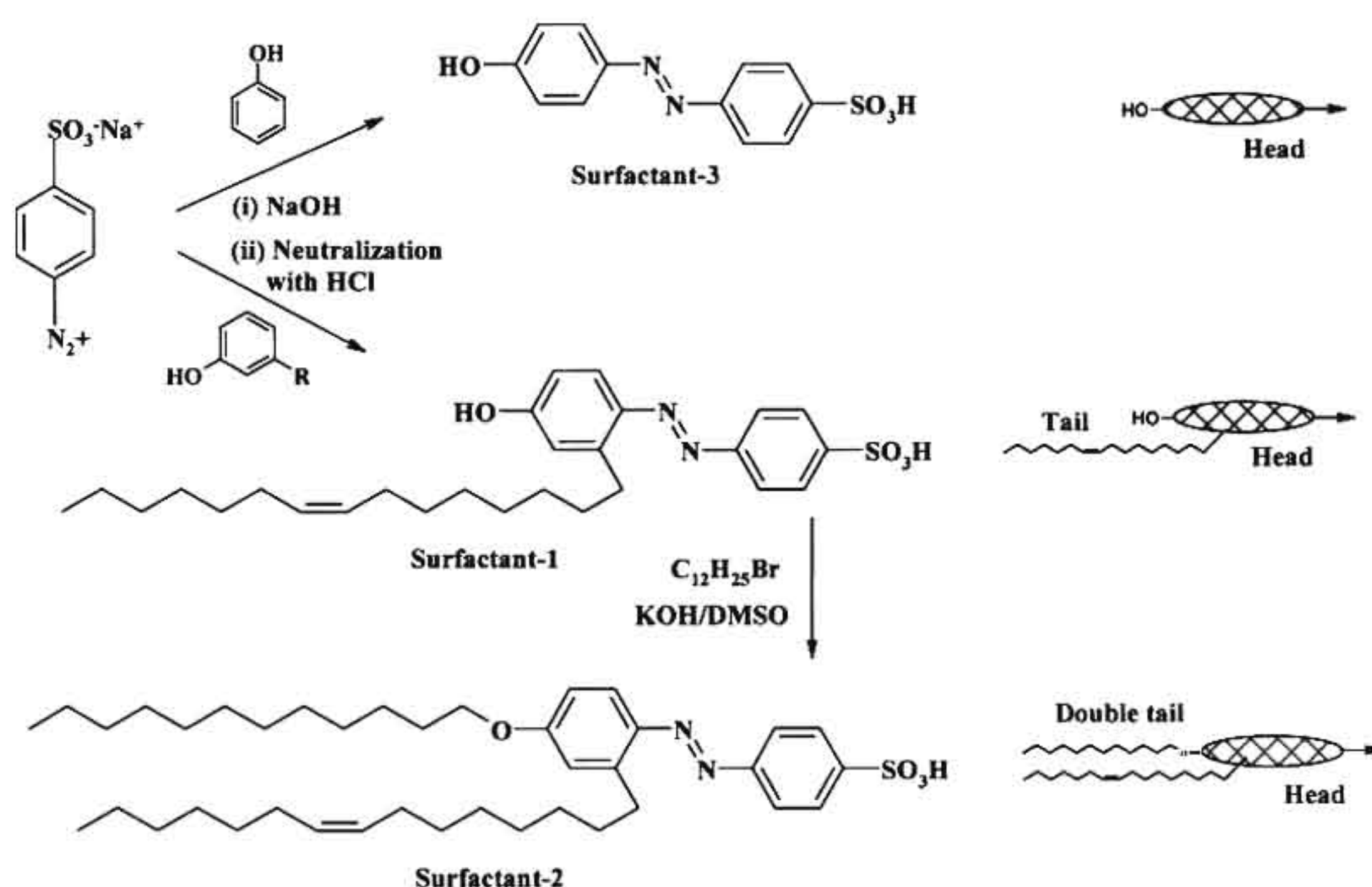


Figure 3.13. Synthetic scheme for surfactant-1, surfactant-2 and surfactant-3.

The purity and structure formation of the synthesized surfactant-cum-dopants were confirmed by ¹H NMR (see figure 3.14.) and other techniques like ¹³C NMR, FT-IR spectroscopy. NMR spectra of surfactant-1 shown four types aromatic protons at 7.8, 6.95, 6.8, 6.75 and protons corresponding to double bonds at 5.3 ppm where as, surfactant-3 have shown three equivalent aromatic proton at 7.85, 7.8 and 7.95 ppm. Surfactant-2 which was derived from surfactant-1 have shown Ar-O-CH₂- protons at 4.02 ppm in addition to the aromatic protons at 7.75, 7.64, 6.92, 6.84 and double bond proton at 5.27 ppm in the chain. The observed intensity and number of protons of the surfactants are matching to the theoretically calculated protons confirming the formation of surfactant. The ¹³C-NMR spectrum shows peaks corresponding to the total number carbon atoms of surfactant and intensities in accordance with the expected structure, which confirm the formation of the amphiphilic surfactants.

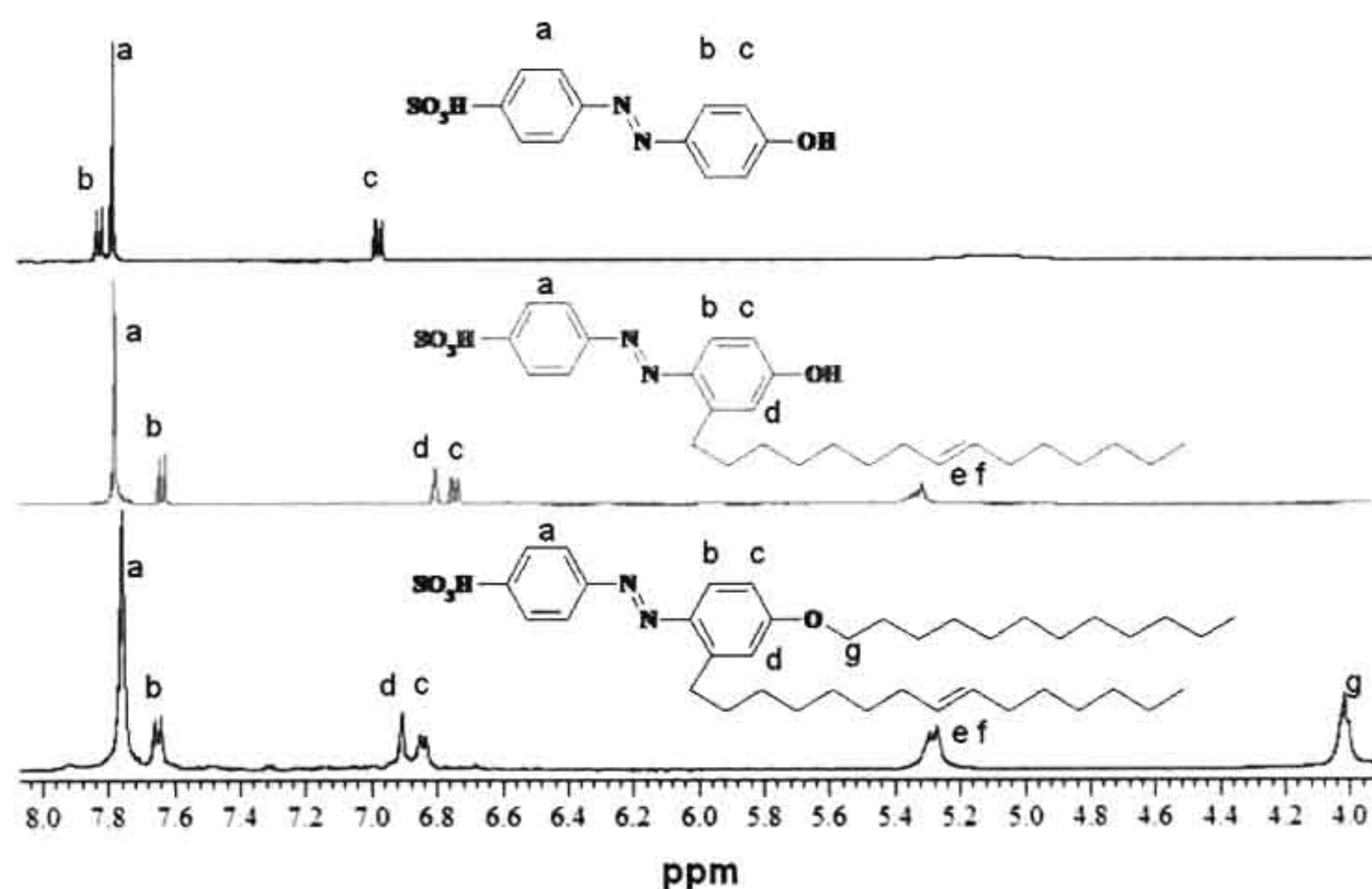


Figure 3.14. ^1H NMR spectra of the surfactants.

Synthesis of new copolymer series using surfactant-2 and surfactant-3 were followed by using the same procedure used for surfactant-1. Polypyrrole-polyaniline copolymers were prepared by varying the amount of pyrrole and aniline from 0 to 100 % (in moles) in the feed. Concentration of pyrrole and aniline were varied from 4.8×10^{-2} to 9.1×10^{-1} M and 7.3×10^{-1} to 3.6×10^{-2} M respectively, whereas surfactant concentration remains constant (9.6×10^{-3} M) see table. 3.3. The concentration of the monomers and surfactant concentration were shown in table 3.3. Emulsion mixtures were polymerized by adding aqueous solution of ammonium persulphate in ice cold condition and keeping the reaction mixture without any disturbance for overnight. The resultant dark green material was filtered, washed with water and methanol until the filtrate became colorless. It was dried under vacuum oven for 24 h (0.05 mm of Hg) at 50 °C prior to further analysis. The copolymers are denoted as **PX-Co-Y**, where **Y** is the mole fraction feed of pyrrole used for copolymer synthesis and where **X**= 1, 2 and 3 for surfactant-1, surfactant-2 and surfactant-3, respectively. Polyaniline (**PANI-X**) was synthesized by polymerizing the thick emulsion of aniline with three surfactants (no pyrrole monomer), where **X**= 1, 2 and 3 for surfactant-1, surfactant-2 and surfactant-3 respectively.

Table 3.3. Concentration of reactants used for synthesis and S/N ratio of the nanomaterials for P2-Co-Y and P3-Co-Y series

Sample	Conc. of pyrrole (M)	Conc. of aniline (M)	Conc. of surfactant	S/N Ratio ^b
Pani-2	0	7.3×10^{-1}	9.6×10^{-3}	0.48
P2-Co-6	4.8×10^{-2}	6.9×10^{-1}	9.6×10^{-3}	0.41
P2-Co-13	9.6×10^{-2}	6.6×10^{-1}	9.6×10^{-3}	0.41
P2-Co-36	2.8×10^{-1}	5.1×10^{-1}	9.6×10^{-3}	0.28
P2-Co-57	4.8×10^{-1}	3.6×10^{-1}	9.6×10^{-3}	0.23
P2-Co-75	6.7×10^{-1}	2.2×10^{-1}	9.6×10^{-3}	0.26
P2-Co-92	8.6×10^{-1}	7.3×10^{-2}	9.6×10^{-3}	0.28
PPy-2	9.6×10^{-1}	0	9.6×10^{-3}	0.33
Pani-3	0	7.3×10^{-1}	9.6×10^{-3}	0.49
P3-Co-6	4.8×10^{-2}	6.9×10^{-1}	9.6×10^{-3}	0.42
P3-Co-13	9.6×10^{-2}	6.6×10^{-1}	9.6×10^{-3}	0.34
P3-Co-36	2.8×10^{-1}	5.1×10^{-1}	9.6×10^{-3}	0.25
P3-Co-57	4.8×10^{-1}	3.6×10^{-1}	9.6×10^{-3}	0.24
P3-Co-75	6.7×10^{-1}	2.2×10^{-1}	9.6×10^{-3}	0.26
P3-Co-92	8.6×10^{-1}	7.3×10^{-2}	9.6×10^{-3}	0.26
PPy-3	9.6×10^{-1}	0	9.6×10^{-3}	0.33

^a Concentration of the monomer and surfactant in water. ^b Obtained from elemental analysis.

The copolymer formation was characterized by ¹H NMR and IR spectra. FT-IR spectra of the copolymers recorded by making samples into thin pellet with KBr powder were shown in figure 3.15. The peaks are assigned with appropriate band structures (A= aniline and P= pyrrole). The polyaniline sample PANI has two peaks at 1580 and 1490 cm⁻¹ with respect to stretching vibration of quinoid and benzenoid in polyaniline chains, respectively. Three additional peaks were assigned at 1300, 1148 and 820 cm⁻¹ to C-N stretching of secondary amine group, O=S=O stretching of the sulfonic acid dopant, and C-H in the 1,4-disubstituted benzene ring out-of plane stretching, respectively [Ping, Z. J. *et al* 1996; Christensen, P. A. *et al* 1991; Stejskal, J. *et al* 2004]. The peaks at 1550, 1195, 1040, 965 and 923 cm⁻¹ are assigned to C=C stretching in pyrrole, breathing vibration of the pyrrole rings, N-H (or C-H) in-plane deformation vibration, C-C out of ring deformation and C-H out of plane deformation vibrations, respectively. It is very interesting to note that with increase in the amount of aniline in the feed, the peaks at 1580, 1490, 1300, 1148 and 820 cm⁻¹ were increasing (move downwards) and attained the value of homopolymer, polyaniline.

Similarly, the polypyrrole peaks at 1714, 1550, 1195, 1040, 965 and 923 cm^{-1} were increasing with the amount of pyrrole in the feed (move upwards). ^1H NMR spectra of copolymers synthesized using surfactant-2 is shown in figure 3.16. PANI-2 has shown two aromatic protons at 7.45 and 7.40 ppm and copolymer P2-Co-57 showed a peak at 7.29 ppm corresponding to β -protons in pyrrole in addition to the polyaniline protons confirming the formation of copolymer nanomaterials [Zhou, C. *et al* 2008; ^bLi, X. G. *et al* 2001; ^cLi, X. G. *et al* 2001; ^dLi, X. G. *et al* 2004]. NMR spectra for P2-Co-75 showed increase of intensity of pyrrole protons indicating higher pyrrole content in copolymers. The NMR spectra of PANI-3 and copolymers were not recorded due to the poor solubility of samples in d_6 -DMSO.

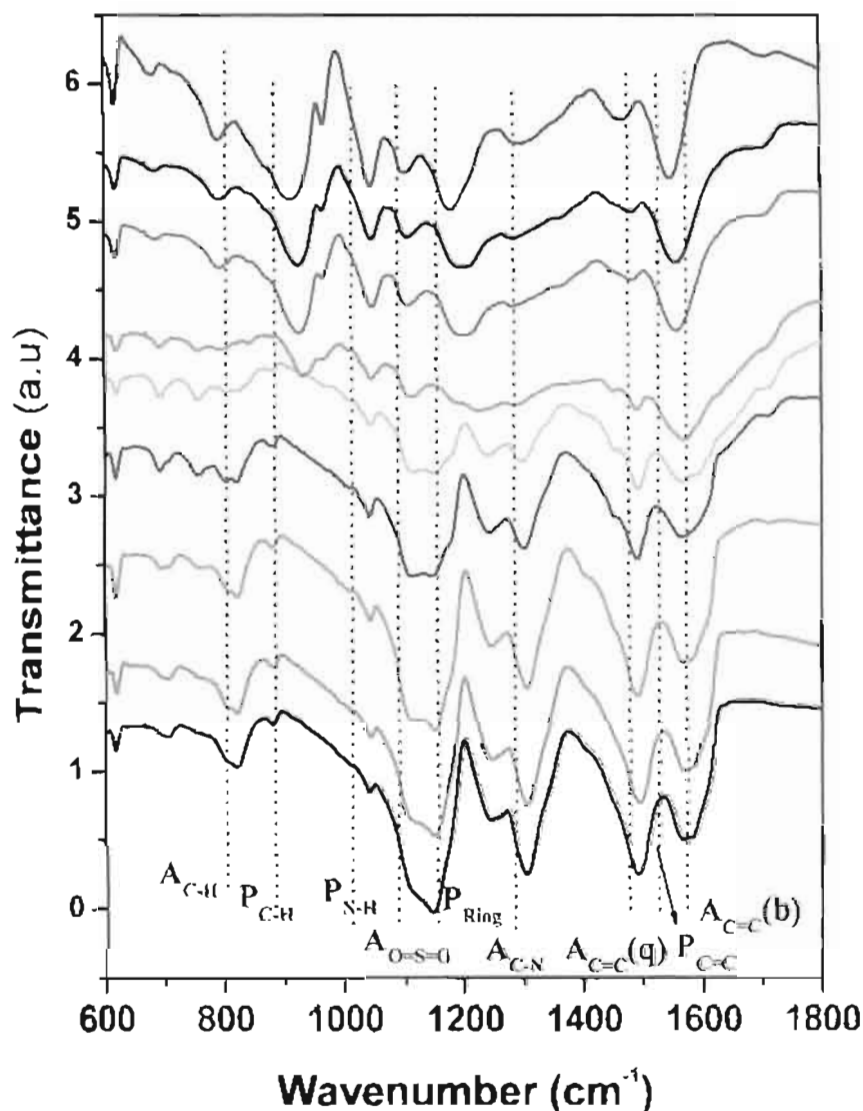


Figure 3.15. FT-IR spectra of the copolymer nanomaterials prepared by surfactant-2.

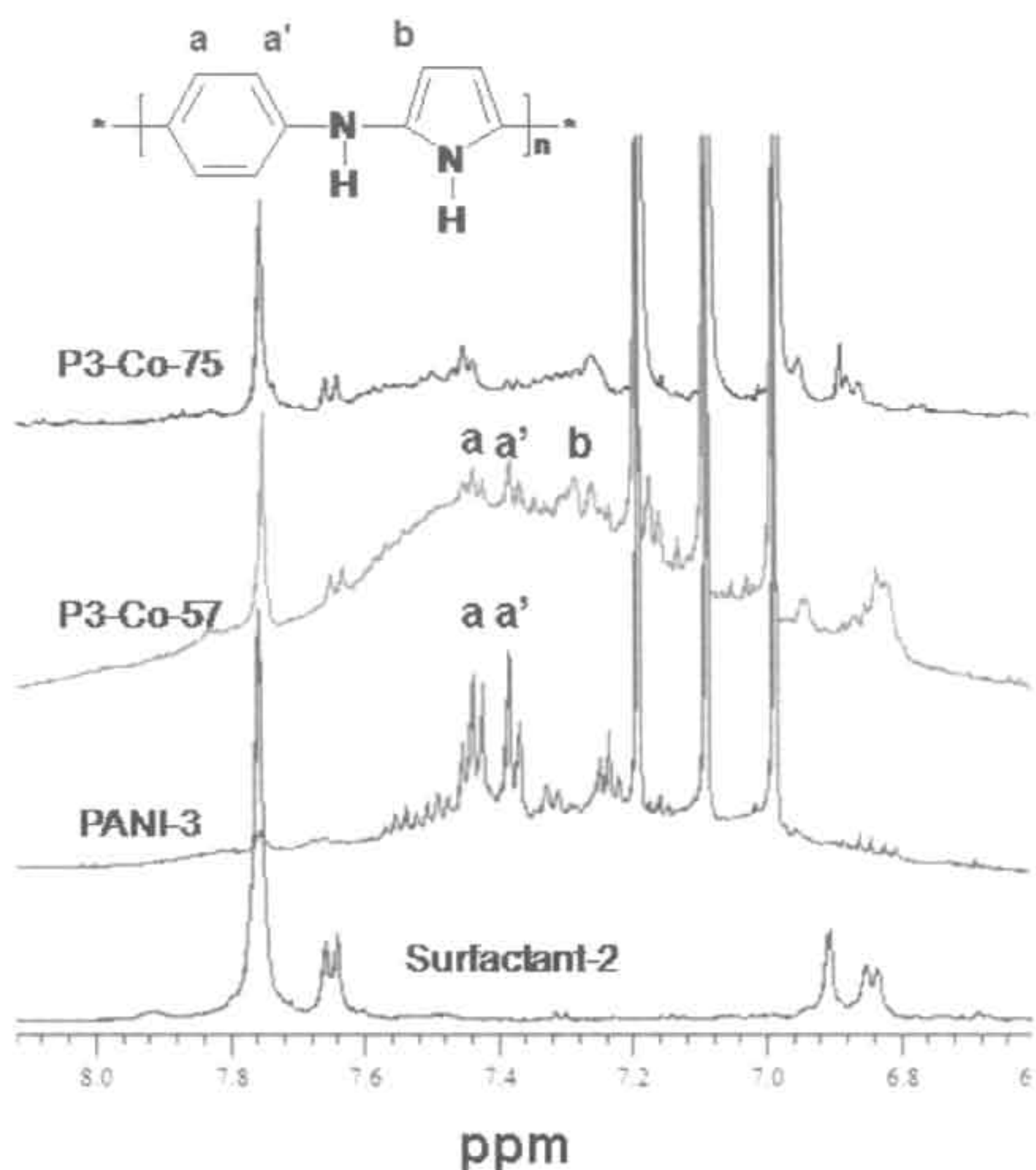


Figure 3.16. ^1H NMR and ^{13}C NMR spectra of surfactant-2

3.3.6. Morphology of copolymer nanomaterial synthesized using surfactant-2

The morphology of the copolymer nano-materials (**P2-Co-Y** and **P3-Co-Y** series) was recorded using JEOL JSM-5600 LV scanning electron microscope (SEM) are shown in figure 3.17. and figure 3.18. respectively. The morphology of **PANI-2** showed thick and long nanofibers of length up to 4-6 μm and width of about 280 nm, whereas the **PANI-3** forms nanofibers of width of 80 nm and length 3-5 μm . The thickness of **PANI-3** was much lower compared to **PANI-1** and **PANI-2**, could be attributed to the smaller cylindrical diameter of the micelles formed with aniline. **P2-Co-5** forms of small and thin rod like structures with length of 500-700 nm and width 100 -120 nm, whereas **P3-Co-5** forms much shorter and thinner nanorods. On further increase in pyrrole content (**PX-Co-30** and above), morphology was transformed to spheres without the traces of fiber or rods. In short the morphology transformation from fiber to rods to spheres was similar in all the copolymer series.

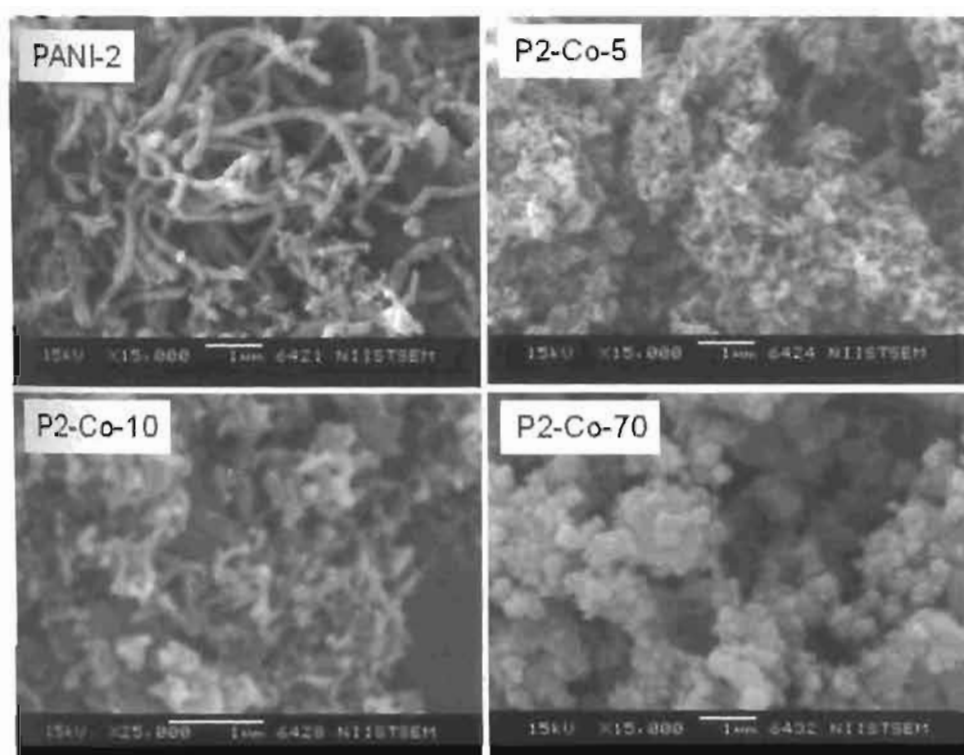


Figure 3.17. SEM images of the PANI and Copolymers prepared using surfactant-2

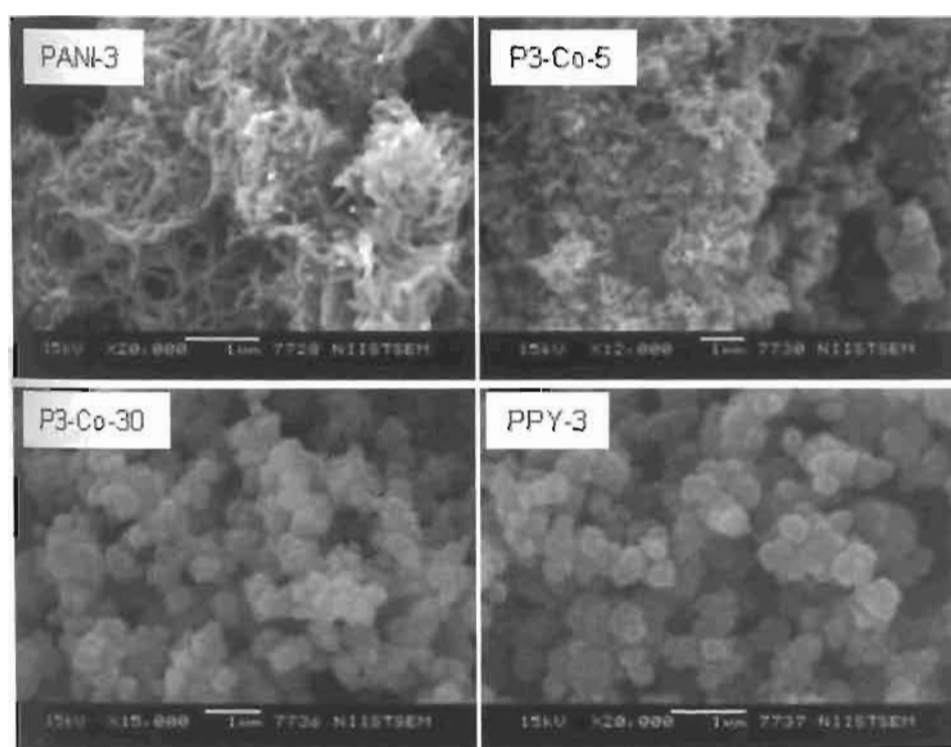


Figure 3.18. SEM images of the PANI and Copolymers prepared using surfactant-3

Further, TEM analysis was carried out on the samples **PANI-2**, **P2-Co-5** and **P2-Co-30** confirms the formation of nanofibers, nanorods and solid spheres respectively, without any tubular structures (see figure 3.19.). Dimensions calculated from SEM and TEM are approximately matching each other. Thus morphology transformation obtained were in full agreement with the mechanism of formation proposed.

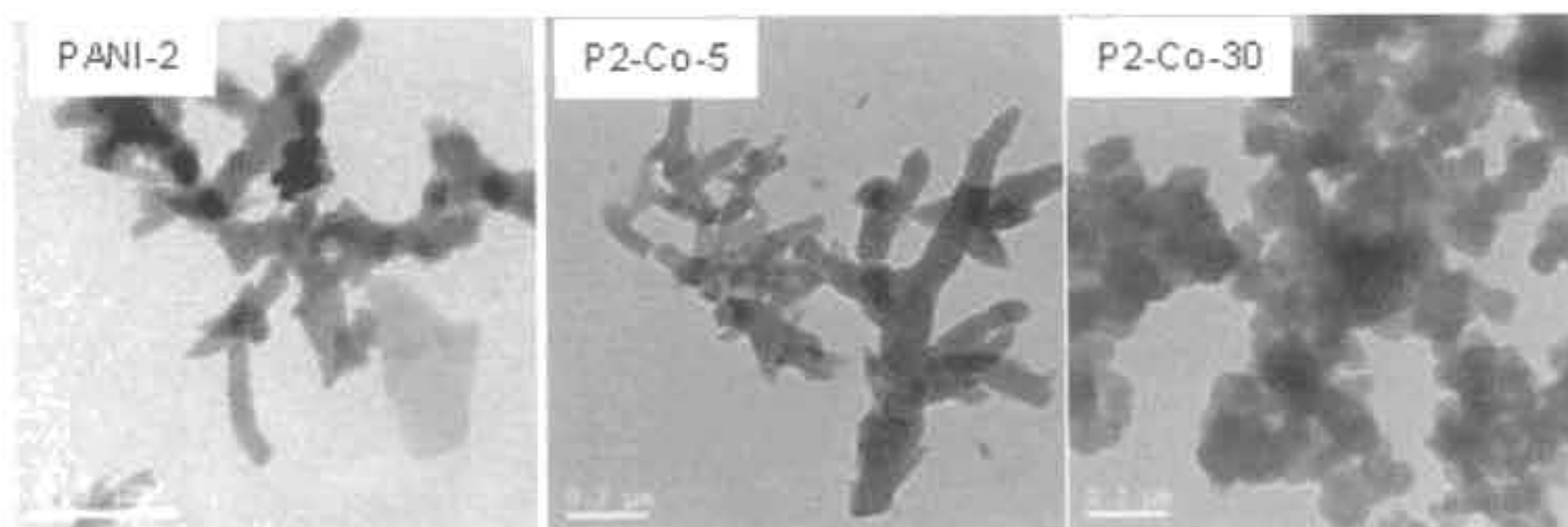


Figure 3.19. TEM images of the *PANI* and Copolymers

3.3.7. Properties of copolymer nanomaterials

Copolymer nano-materials have shown only 10 % weight loss at temperature lower than 280 °C see figure 3.20. Copolymer nanomaterials were doped by azo benzenesulphonic acid were thermally stable as similar to camphorsulphonic acid [Shen, Y. et al 1998; Omastova, M. *et al* 2003].

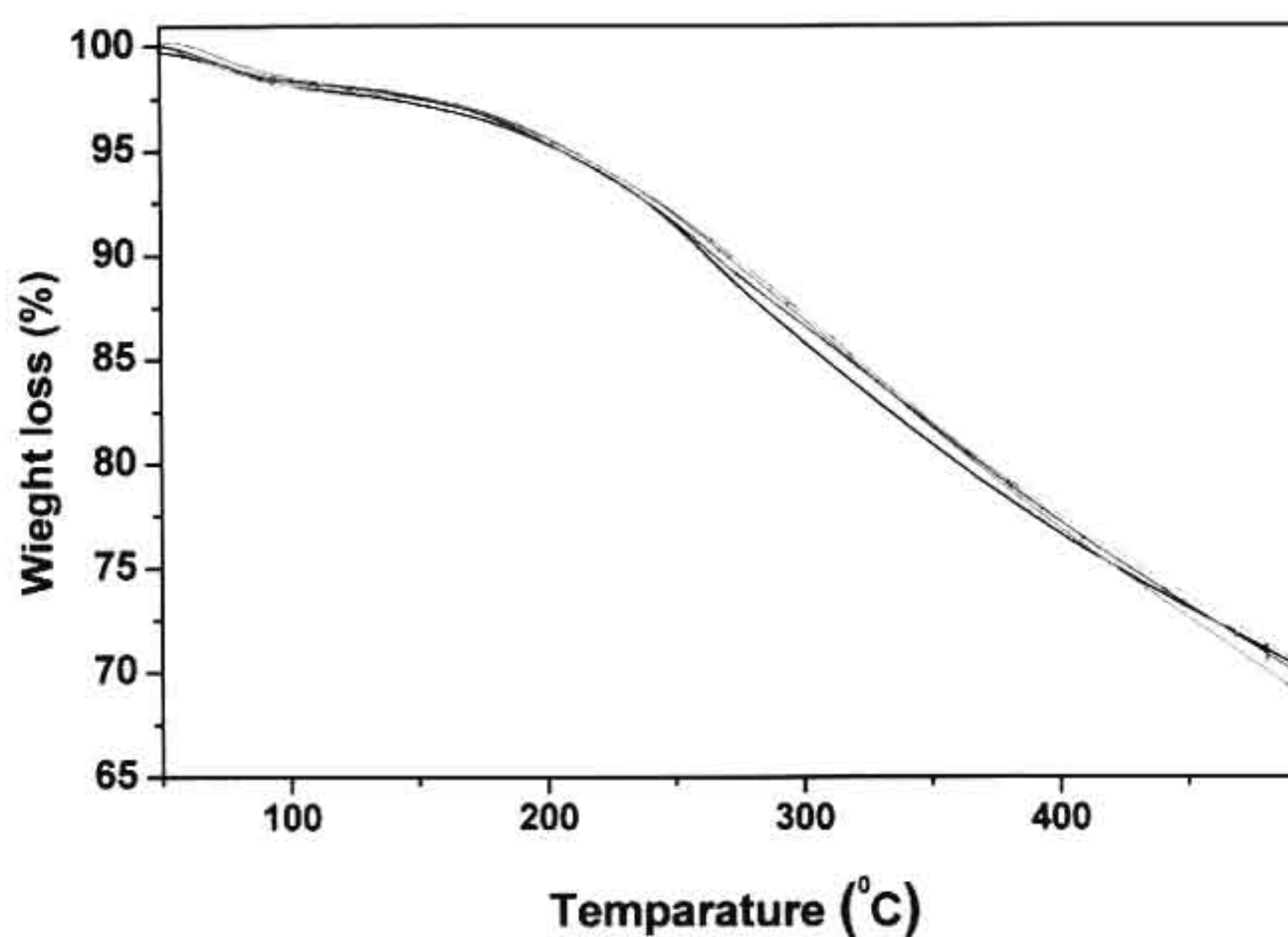


Figure 3.20. TGA profile of the copolymer nanomaterials.

Absorption spectra of the PPy, PANI and copolymers were easily recorded in water due to good dispersibility enhanced by the doped surfactant molecules (see in figure 3.21.). Polypyrrole showed characteristic transitions of doped polypyrrole at 480 nm, and free carrier tail at NIR region (900-1000) corresponding to valence band anti-bipolaron band and valence band to bipolaron band respectively [^aAntony, M. J. *et al* 2007; Cabala, R *et al* 2002]. Polyaniline showed three transitions at 350 nm, 430 nm, and a broad peak at 850 nm with respect to π - π^* transition, polaron to conducting band, valence band to polaron band respectively [^aAnilkumar, P. *et al* 2006, ^banilkumar, P. *et al* 2007, Xia, Y. *et al* 1995]. The decrease in the peak intensity at 380-400 and increase in the peak intensity above 900 nm with increase in the amount of pyrrole in the copolymer confirmed the formation of expected random copolymers. The absorbance characteristics were almost unaltered above 35 % pyrrole, which suggested that less than 35 % pyrrole is sufficient enough to attain the properties of pure polypyrrole. This observation was coinciding with the morphology of the nanomaterials that beyond 35 % of pyrrole in the feed the polypyrrole-polyaniline chains have the morphology of pure polypyrrole (nano-spheres). The absorption spectra of the copolymer nanomaterials synthesised using double tailed surfactant were shown similar absorption peaks.

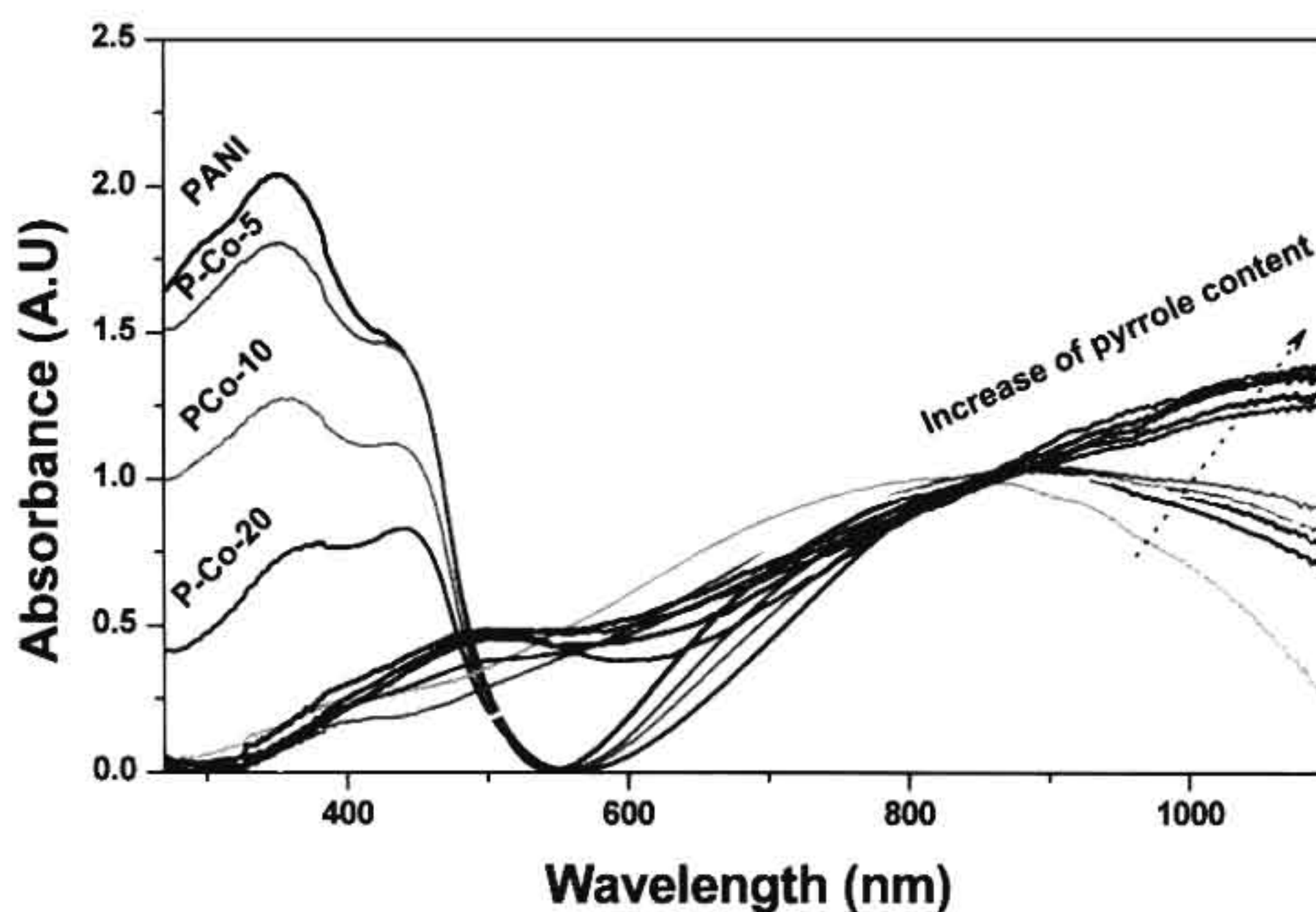


Figure 3.21. Absorption spectra of copolymer nanomaterial series prepared using surfactant-1.

The conductivity of copolymers was determined by four probe conductivity method and is plotted against the mol percentage amount of pyrrole in feed. Conductivity of the copolymer nanomaterials of first series have showed a non-linear trend, the conductivity passed through minimum at 60-80 (%) of pyrrole in the feed (see figure 3.22.). The conductivity of the copolymer units were found more than 100-1000 times lower than that of their respective homopolymers.

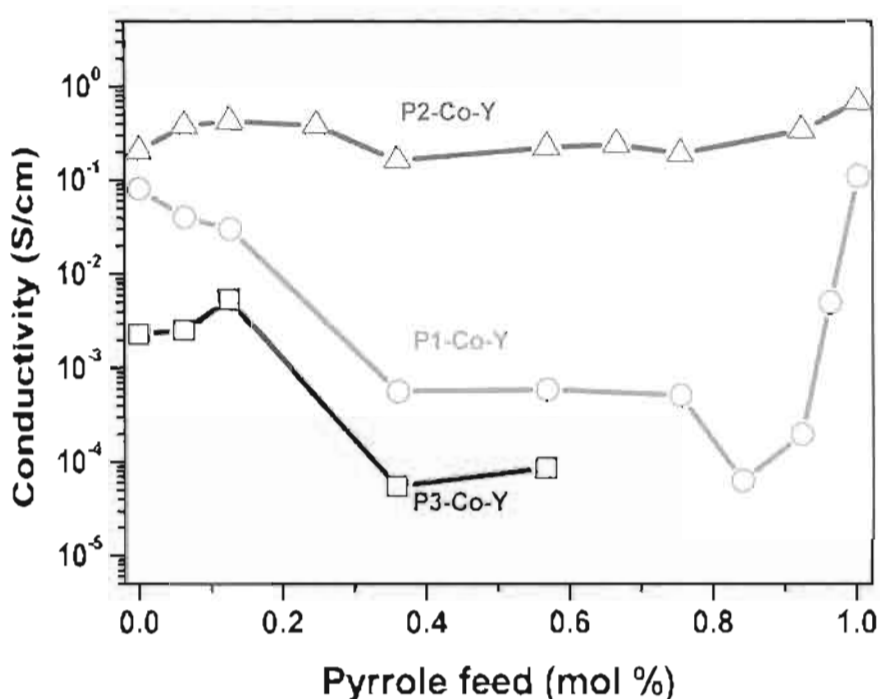


Figure 3.22. Electrical conductivity of copolymer nanomaterials.

Recently, Stejskal *et al.* and Lim *et al* separately reported such non-linear loss in the conductivity in polypyrrole-co-polyaniline (not nano-materials) [Stejskal, J. *et al* 2004; Lim, V. W. L. *et al* 2001] This unusual trend can be explained as suggested by Stejskal and Lim; (i) aniline rich copolymers - at least four aniline units are necessary for materials to be conducting, but with increase with the percentage of pyrrole in the feed, most of the polyaniline chain became shorted and the conductivity deteriorates [MacDiarmid, A. G. *et al* 1999] and (ii) pyrrole rich copolymers - at low aniline concentration, the aniline has the tendency to form heterodiads with pyrrole rather than to form aniline blocks (due to low concentration) and break the conjugation of polypyrrole. The lower conductivity values for the aniline rich polymer

can be understood by the morphology of the nano-materials. With increase in the pyrrole concentration (6 %), the long nano-fibers were shortened to form small nano-rods, which is due to the truncation of long ordered cylindrical micelles by the aniline with surfactant. The truncation of aniline-surfactant micelles by pyrrole disturbs the local concentration of aniline in any particular domain and the subsequent oxidation expected to produce shorter chains compared to that of homopolymers.

Table 3.4. Conductivity and WXR D data.

Sample	σ^a (S/cm)	WXR D ^b	
		2 θ	d-spacing (Å)
PANI-1	0.08	3.5, 21.1, 25.4	25.2, 4.2, 3.5
P1-Co-5	0.04	3.5, 21.1, 25.4	25.2, 4.2, 3.5
P1-Co-10	0.03	20.2, 24.9	4.4, 3.6
P1-Co-30	5.7×10^{-4}	20.7, 25.1	4.3, 3.54
P1-Co-50	4.2×10^{-4}	-	-
P1-Co-70	5.2×10^{-4}	23.5	3.8
P1-Co-80	6.4×10^{-5}	-	-
P1-Co-90	2×10^{-4}	-	-
P1-Co-95	0.005	-	-
PPY-1	0.11	3.4, 25.4	3.8, 3.5
PANI-2	0.20	3.6, 20.4, 24.9	25.3, 4.3, 3.6
P2-Co-5	0.38	3.3, 20.2, 24.9	26.7, 4.4, 3.6
P2-Co-10	0.42	3.3, 20.2, 24.9	26.7, 4.4, 3.6
P2-Co-30	0.38	3.6, 20.4, 25.6	25.3, 4.3, 3.4
P2-Co-50	0.16	-	-
P2-Co-70	0.22	3.3, 23.1	26.7, 3.8
P2-Co-80	0.19	-	-
P2-Co-90	0.34	3.5, 25.8	25.2, 3.5
P2-Co-95	0.33	-	-
PPy-2	0.68	3.5, 25.8	25.2, 3.5

^a conductivity of the samples measured using four probe conductivity meter at 30°C. ^b Wide angle X-ray diffraction studies of the copolymer nanomaterials carried out 25°C

Conductivity of the double tail synthesised copolymers are measured and the results were compared with previous case to investigate the unusual loss of conductivity see table 3.4. Since, both surfactants provided similar morphology transformation from fiber to rods to spheres. The only difference between the two

series was the extra tail contained in the surfactant-2 and hence it is worth to have comparison studies on solid state properties.. **PANI-1**, **PANI-2** and **PANI-3** were shown conductivity in the range of 10^{-1} , 10^{-2} and 10^{-3} S/cm respectively [^aanilkumar, P. *et al* 2006; ^banilkumar, P. *et al* 2007; ^canilkumar, P. *et al* 2007]. Aniline rich copolymer composition like **PX-Co-6** and **PX-Co-13** (in general) were not shown any significant loss in conductivity (see figure 3.22.). However, with increase in pyrrole, the conductivity was drastically reduced approximately to 10^{-4} S/cm in first case. Poor emulsion forming tendency hampers the conductivity studies of copolymer synthesized using surfactant-3, hence we omitted the plot above 50 % pyrrole for obtaining good comparison with others. The conductivity of the copolymer synthesized using double tailed surfactant have not shown any large conductivity loss and conductivity was remains of the order of 10^{-1} S/cm. The unusual decrease in conductivity of copolymers are could due to three reasons (i) due to the structural defects in the copolymers like break of conjugation or cross-link (ii) due to random copolymer formation the copolymer chain can become highly amorphous and hence to show the low conductivity (iii) or poor doping of the surfactant or dopant in the copolymer. Interestingly, in the present case the conductivity of all copolymer series have shown a minimum at ~ 50 % feed indicating the hetero-diad formation in the copolymer. However, conductivity loss was negligible for double-tailed series in comparison with other two series indicates the possibility of large conductivity loss could be due to other factors like solid state packing and extend of doping.

The solid-state properties copolymers were studied by wide angle X-ray diffraction (WXR) method are shown in figure 3.23a. WXR of **PANI-1** showed three peaks at $2\theta = 25$, 19.5 and 3.5 . The lower angle peak is due to the long range lamellar arrangement of dopant molecule in polyaniline [Jayakannan, M. *et al* 2005; Dufour, B. *et al* 2001; Laska, J. *et al* 2002; ^aJana, T. *et al* 2000.; ^bJana, T. *et al* 2000.; ^cJana, T. *et al* 2000]. The copolymers of first surfactant series did not show any ordered peak at lower angle, which indicated that the random copolymers were less crystalline compared to that of homopolymers. In general, the random copolymerization is known to induce large degree of disorder in the crystalline domains than their homopolymer chains. Recently, Zhou *et al.* was also reported a similar observation in the WXR patterns of their polyaniline-polypyrrole copolymer hollow nanospheres. [Zhou, C. *et al* 2008]. Truncation of aniline and the amorphous

nature of the copolymers disturb the local concentration of aniline at any particular domain resulting in decreased crystallinity and electrical conductivity. Therefore, the highly amorphous copolymers have much lower conductivity almost 3 to 4 orders of magnitude lower than that of their highly crystalline homopolymers. The WXR D of copolymers synthesized using double tail series are shown in figure 3.23b. Polyaniline have shown three peaks, one at lower angle 3.5 and two at higher 25 and 19.5 2θ degrees. All the copolymer **P2-Co-10**, **P2-Co-30**, **P2-Co-70** and **PPY** have shown lower peak corresponding to long range lamellar peaks at lower angle. Thus, the WXR D analysis indicate that copolymer of double tailed series are packed very well via the surfactant induced tail packing in comparison to first series.

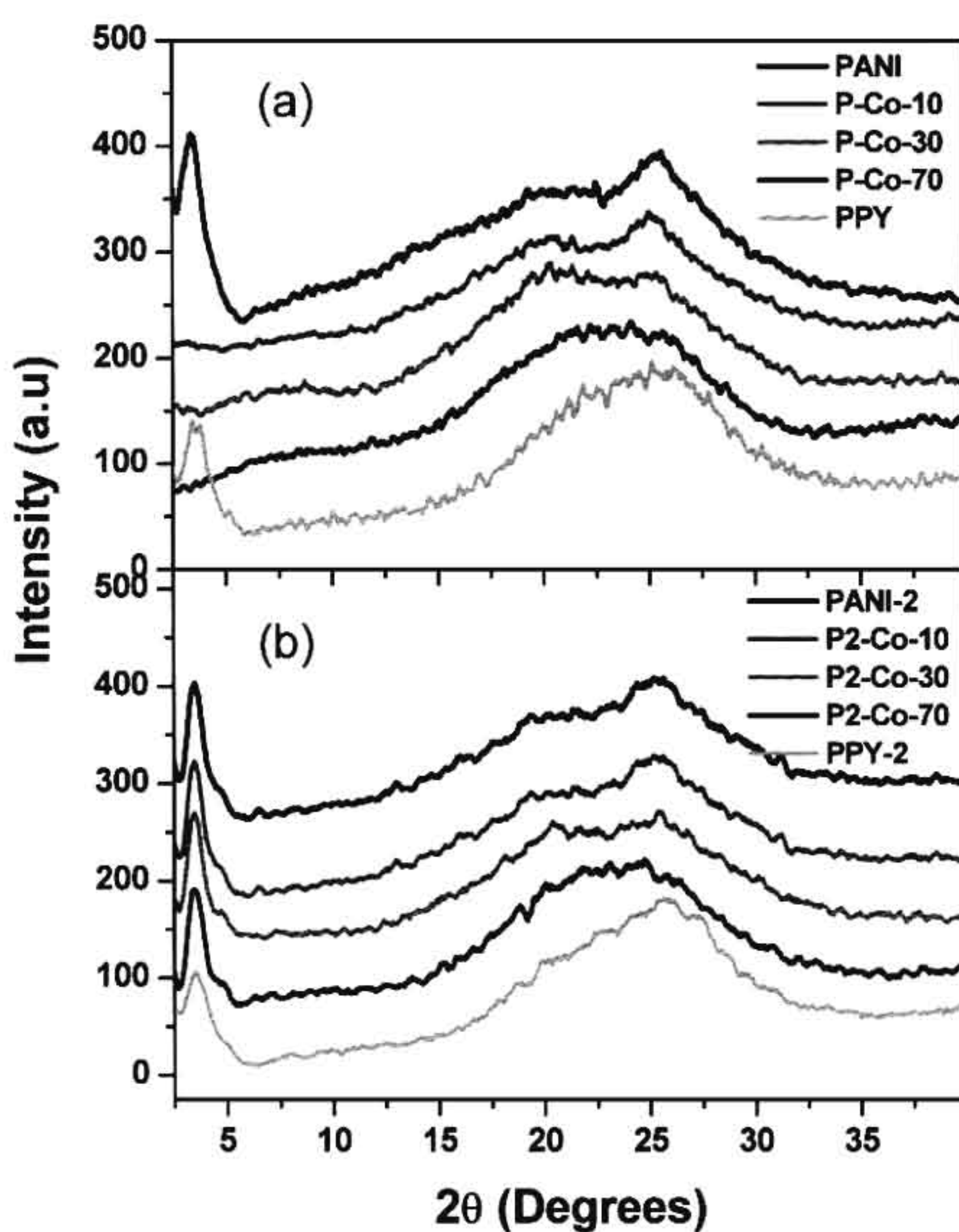


Figure 3.23. WXR D analysis of the copolymers prepared using (a) surfactant-1 and (b) surfactant-2 .

In order to quantify the amount of crystallinity in the copolymer of both series, the amorphous and crystalline peaks were deconvoluted computationally and percentage crystallinity was calculated from the area of crystalline/crystalline + amorphous and plotted versus mole feed of pyrrole (see figure 3.24.). In both cases, the homopolymer have shown crystallinity approximately of 10 %. The crystallinity of the first series decreases with increase in pyrrole content, reaches a minimum at equal feeds and then increases. However in the second series the percent crystallinity of the samples was remains the same range without any large loss in the crystallinity. Interestingly, the trend observed in percentage crystallinity (figure 3.24) and conductivity (figure 3.22) follows same pattern, hence the conductivity changes of the copolymer nanomaterials would have strongly influenced by the solid state packing of the nanomaterial.

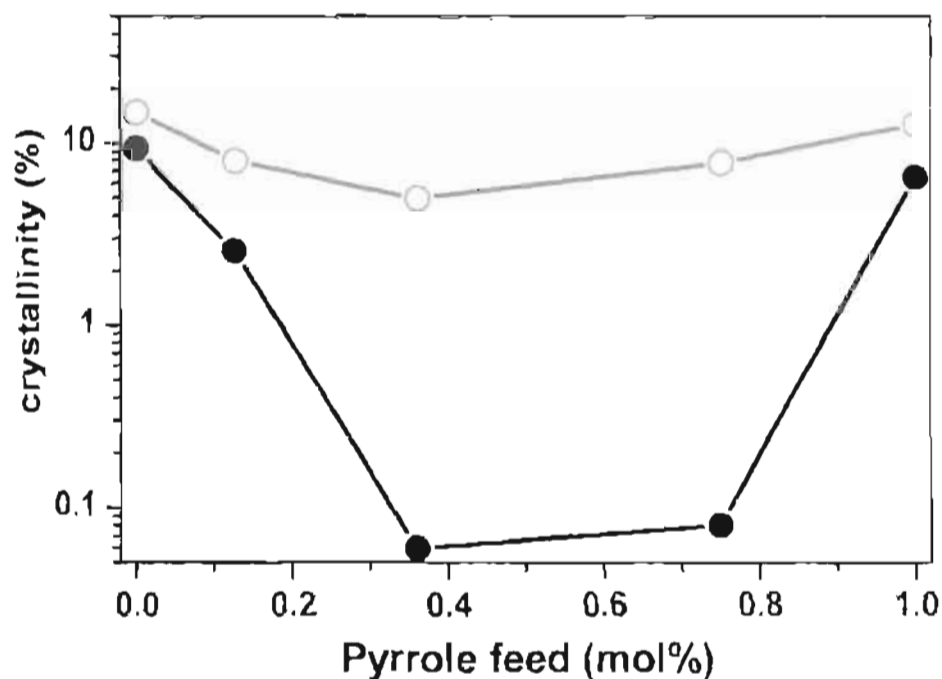


Figure 3.24. Crystallinity versus pyrrole monomer feed plot of copolymer series.

In short, the present investigations on the copolymer nanomaterial synthesized using three anionic amphiphilic micelles revealed morphology transformation from fiber to rod to spheres with monomer composition. Interestingly, the morphology transformation occurred exactly at similar composition, which provides very good

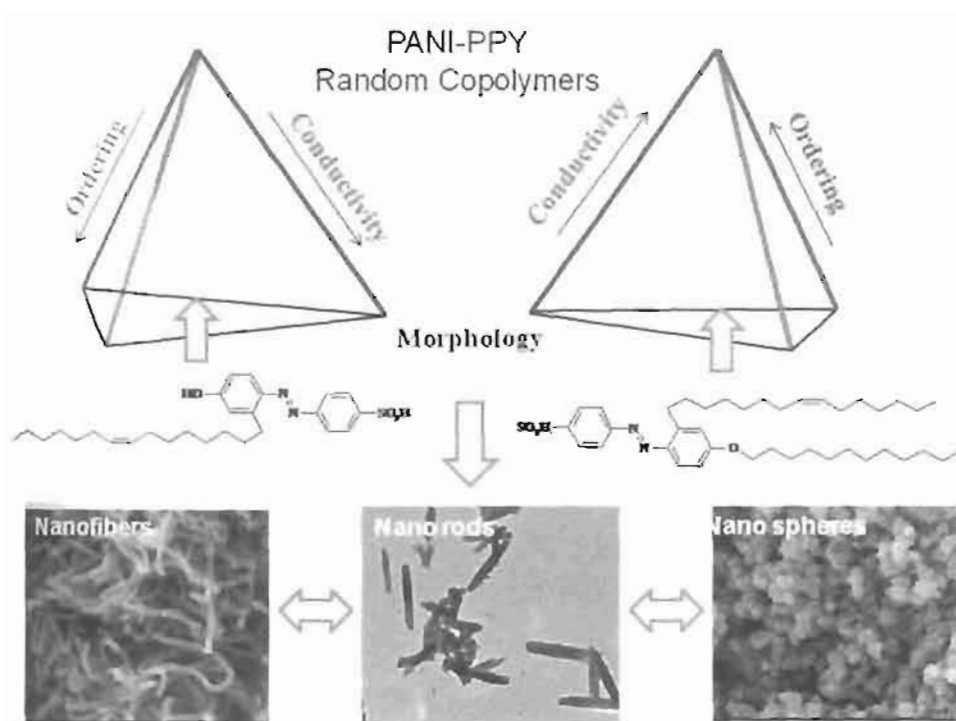


Figure 3.25. Morphology transformation and properties changes in copolymer nanomaterials.

comparison studies of the nanomaterials in conductivity and solid state ordering. In first series of copolymers (single tail), both conductivity and percentage crystallinity passes through a non-linear loss. On the other hand copolymers of double tail surfactant have shown almost linear steady changes in conductivity and crystallinity. The morphology transformation of the nanomaterials being similar, solid state properties of the copolymers synthesised using two structurally different surfactants were schematically shown in figure 3.25. Higher the crystallinity (solid state packing), provided higher the conductivity and vice versa. Since, electron mobility directly contributes to the bulk conductivity of the nano-materials, and therefore, enhanced solid state ordered crystalline domains are known to enhance their conductivity compared to amorphous domains.

3.4. Conclusion

In conclusion, we have developed three structurally different amphiphilic surfactant molecules to fine tune size, shape, and properties of polypyrrole-co-polyaniline nano-materials. The important features of the present approach are as follows following: (i) a renewable resource surfactant-1 was derived from cardanol by diazotization reaction with sulfanilic acid and employed for synthesis of random copolymer nanomaterials (ii) morphology of the copolymer were shown a transformation from fiber-to-rod-to-spheres which was confirmed by electron microscopic analysis (SLM and TEM), (iii) the mechanism of nanomaterial formation was established by DLS, pH and SEM studies on emulsion templates in addition to seeding and control experiments (iv) the conductivity of the copolymer synthesised using single tail surfactant have shown a non-linear loss (10^2 - 10^3 S/cm), particularly at 60-80 % feed of pyrrole in feed with respect to homopolymer (v) two new surfactants one from phenol by diazotization reaction with sulfanilic acid and the other synthesized from surfactant-1 by nucleophilic substitution reaction with dodecyl bromide (vi) all the surfactants have same azo head group with sulfonic acid polar head, while they structurally differ by the hydrophobic tail, (vii) copolymers synthesised using new surfactants were shown a similar morphology transformation, enabling a good comparison studies on conductivity and other properties (viii) the conductivity of the copolymer synthesized from double tail surfactant remains more or less of the order of 10^{-1} S/cm, (ix) the unusual conductivity loss of the copolymer were correlated to poor solid state packing obtained from WXR D measurements and (x) the plot of crystallinity and conductivity of the copolymer nanomaterials versus mole feed of pyrrole reveals that linear conductivity ($\sim 10^{-1}$ S/cm) of the double tail copolymer series would have strongly influenced by the solid state packing. In a nutshell, for the first time, a systematic analysis were carried out based on renewable resource anionic surfactants for development of random copolymer nano-materials and to establish the structure-property relations of the copolymers.

Chapter-4

Evolution of Multiple Nanostructures from Identical Copolymer Composition

4.1. Introduction

One dimensional conducting polymer nanomaterials find numerous applications particularly in electronic, electrochemical, mechanical and biological fields [Wallace, G. G. *et al* 2002, Berdichevsky, Y. *et al* 2006; Otero, T. F. *et al* 2003; Wang, J. *et al* 2000; ^aHuang, J. *et al* 2003; ^bHuang, J. *et al* 2004; Bidon, G. *et al* 1999; Giroto, E. M. *et al* 1998; Korri-Youssoufi, H. *et al* 1997; Ramanathan, K. *et al* 2005]. Shape and size of these nanomaterials were found to be very crucial for their functioning in electronic devices and delivery applications [Lee, J-H. *et al* 2006; Geetha, G. *et al* 2006.]. Among various conducting polymer nanomaterials. polyaniline and polypyrrole are two important classes of conducting polymers having the advantage of good conductivity, environmental and chemical stability [Wu, A. *et al* 2005]. Nanofibers of polyaniline and polypyrrole were usually synthesized using hard porous templates, electrospinning, surfactant micelles and template-free methods [^bJang, J. *et al* 2002; Zhong, W. *et al* 2006; ^bZhang, X. *et al* 2004; Li, D. *et al* 2009; De Armit, C. *et al* 1993; ^aShen, Y. *et al* 1998; Haung, K. *et al* 2005]. Surfactant controlled nanomaterial synthesis have attractive features like low cost production. easy synthesis and bulk scale up etc. Anionic surfactants acts as structure directing agent as well as dopant for cationically charged polymer matrix, which was not possible in other synthetic methods and cationic surfactants or non-ionic surfactant [De Armit, C. *et al* 1993; ^bShen, Y. *et al* 1998; Haung, K. *et al* 2005; Bay, L. *et al* 2002; Liu, L. *et al* 2005]. Anionic surfactant doped nanomaterial possesses good solubility and stability, which allows complete characterisation in solution. Earlier, our custom designed renewable resource anionic surfactant was utilized for emulsion polymerisation of aniline and pyrrole, which produced polyaniline nanofibers and nanospheres respectively [^aAnilkumar, P. *et al* 2006; ^bAnilkumar, P. *et al* 2007; ^cAnilkumar, P. *et al* 2007; ^aAntony, M. J. *et al* 2007]. Morphology of the nanomaterials was controlled via micellar mediated polymerisation of the self organized monomer + surfactant complex. Surfactant forms selective templates like cylindrical micelles and spherical micelles with aniline and pyrrole respectively. Further, template selectivity was efficiently utilized for making copolymer nanomaterials via polymerisation of selected aniline-pyrrole compositions [^bAntony. M. J. *et al* 2009]. Interestingly, the morphology of the copolymer nanomaterials has shown transformation from nanofiber (100 % aniline) to rods (5-10 % aniline) to

spheres (>30 % aniline). Though the composition depended copolymerisation route produced different morphologies, however it is difficult to correlate morphology with solid state conductivity due to different compositions. Hence, it is important to develop some methods for the production of different copolymer nanostructures from identical composition and ingredients.

In this chapter, emphasis is given on the evolution of nanomaterial morphologies like nanorod-to-hollow sphere-to-nanotube via dilution of self-assembled molecular templates in polyaniline-polypyrrole copolymers (see figure 4.1.). The chemical compositions of [aniline]: [pyrrole] and [monomers]/ [dopant] were fixed and concentration was varied by diluting with various amount of water to tune the morphological transformation. The templates were subjected to chemical oxidation using ammonium persulphate to produce copolymer nanomaterials. Electron microscopic analysis of samples revealed that the conducting polymer morphologies underwent transformation from nanofibers to nanorods and further extended to hollow spheres to well defined nanotubes. Thus, our custom designed surfactant provides new opportunities in conducting nanomaterials for tracing the phenomena of evolution of various morphologies in a polyaniline-co-polypyrrole system.

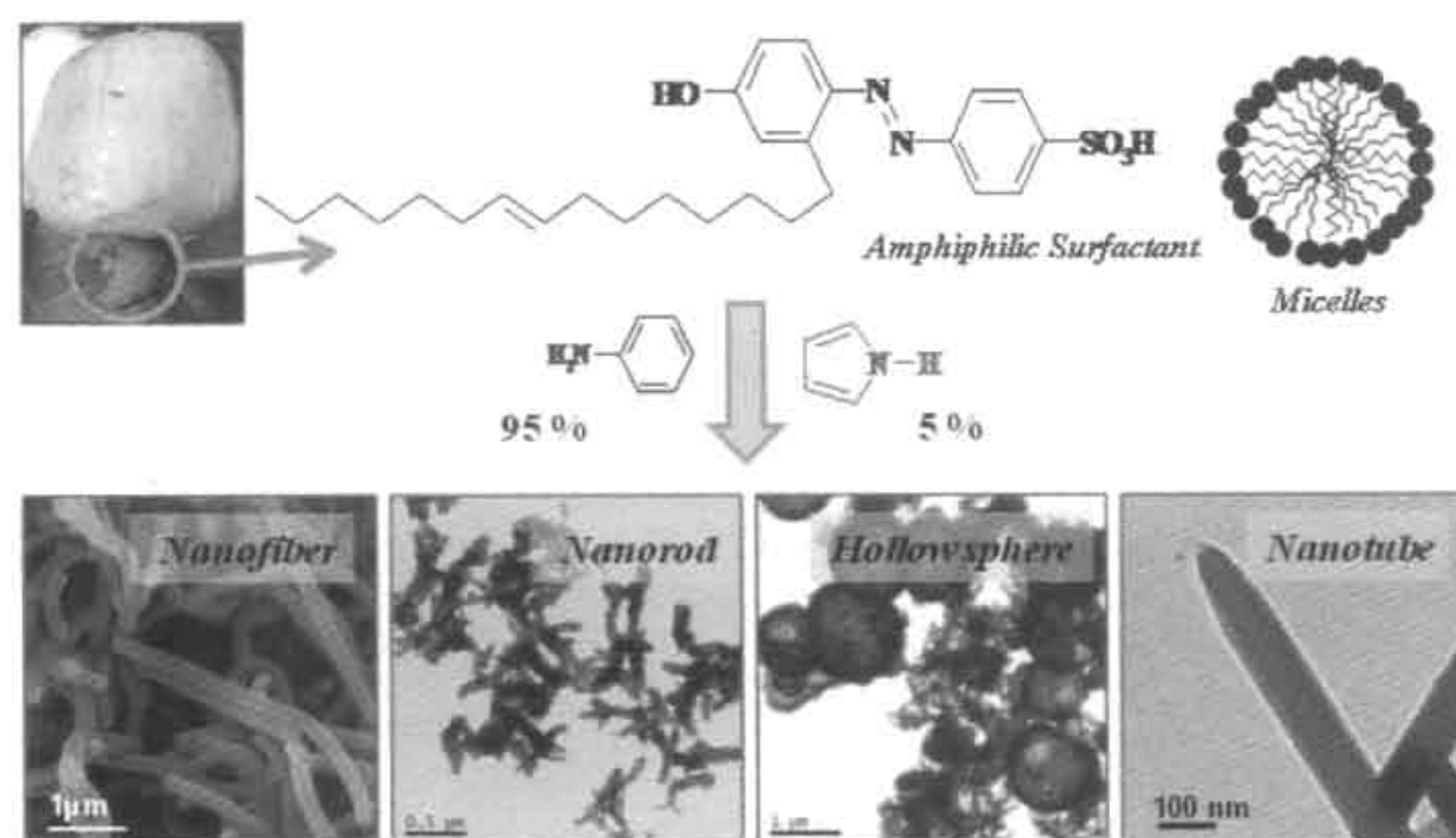


Figure 4.1. Schematic representation of synthesis of copolymer nanomaterials.

This approach was aimed to address the following important aspects in the conducting polymer nanomaterials: (i) for the first time, the evolution of the different types of morphologies such as nanofiber, nanorod, nanosphere and nanotube in a

single polymerization medium without changing their chemical composition or polymerization routes was attained, (ii) to attain the above objective, a dilute polymerization technique was developed for a fixed composition of the surfactant, aniline and pyrrole by varying the concentration of the chemical constituents and (iii) the role of the various nano-morphologies on properties such as conductivity, solid state ordering, percent crystallinity and electronic spectroscopic features was also be established and (iv) the variable temperature I-V techniques to establish the role of the morphology with conductivity. Dynamic light scattering and SEM analysis were utilized to trace the transformation from cylindrical to vesicular aggregates in templates, which account for morphological transformation in nanomaterials. Further, these nanomaterials were submitted to absorption, NMR and FT-IR, temperature dependent four probe conductivity measurements and WXR D analysis to study the structure-property relationship and establish the correlation between the nano-morphology with solid state conductivity. The detailed investigation revealed that the conducting polymer nanofiber morphology was found to show superior conductivity behaviours compared to all other nanostructures such as nanorod, hollow sphere and nanotube for identical chemical composition under same polymerization route.

4.2. Experimental procedures

4.2.1. Materials: Pyrrole, aniline, ammonium persulfate (APS), sulphanic acid, hydrochloric acid, and sodium hydroxide were purchased locally and purified. Cardanol was purified by double-vacuum distillation at 3-4 mm of Hg, and the fraction distilled at 220-235 °C was collected. The amphiphilic dopant 4-[4-hydroxy-2((Z)-pentadec-8-enyl) phenylazo]-benzenesulphonic acid was synthesized from cardanol as per the procedure in chapter 2.

4.2.2. General procedures: ¹H-NMR analysis of the dopant and polymer samples were carried out in 500-MHz Bruker Avance II NMR Spectrometer in *d*₆-dimethyl sulphoxide (DMSO) containing small amount of Tetra methylsilane (TMS) as internal standard. Infrared spectra of the polymers were recorded using Perkin Elmer Spectrum one FT-IR Spectrometer in the range of 4000-400 cm⁻¹. The purity of the compounds

were determined by fast atom bombardment high-resolution mass spectrometry (FAB-HRMS: JOEL JSM 600). For SEM measurements, polymer samples were subjected to a thin gold coating using a JEOL JFC-1200 fine coater. The probing side was inserted into a JEOL JSM -5600 LV scanning electron microscope for taking photographs. TEM analysis was recorded using a Tecnai 30 G² S-twin 300 KV high resolution transmission electron microscope. For TEM measurements a suspension of nanomaterials was prepared in ethanol and deposited on a formvar-coated copper grid. For conductivity measurements, the polymer samples were pressed into a 10 mm diameter and 1 mm thickness pellet and analyzed using a four-probe using Keithley 6221 DC and AC current source and 2181A Nano voltmeter. Resistance of the sample was measured at five different positions. UV-visible spectra of the copolymers are recorded using a Perkin-Elmer Lambda-35 UV-visible spectrometer. DLS measurement was done by Nano ZS Malvern instrument employing a 4 mW He-Ne laser ($\lambda = 632.8$ nm) and equipped with a thermo stated sample chamber. The temperature depended conductivity of the sample is measured with the help of PID controlled heating oven. Wide angle X-ray diffraction (WXRd) patterns of the finely powdered polymer samples were recorded by a Philips analytical Diffractometer using Cu-K α emission. The spectra were recorded in the range of $2\theta = 0-40$ degrees and analyzed using X'Pert software. The thermal stability of the polymers was determined using PerkinElmer STA 6000 simultaneous thermal analyzer at a heating rate of 10°C/min in nitrogen atmosphere.

Preparation of polyaniline-co-polypyrrole nanomaterials via dilution route:

Typical procedure for the synthesis of **P-Co-5** is given below. Surfactant 1 (70 mg, 0.144 mmol) was taken in 10 mL water and stirred under sonicator for 15 minutes. Pyrrole (0.05 mL, 0.7 mmol) and aniline (0.95 mL, 10.5 mmol) were added to the surfactant solution and sonicated for 45 minutes. At the end of stirring, the polymerization mixture turned into a pale yellow thick emulsion. Ammonium persulfate (3.28 g, 14.4 mmol) in water (5 mL) was added drop wise to the solution and continued the stirring under sonicator for 1h. Then the reaction was kept undisturbed for overnight at 25 °C. The sample was filtered, washed with water and methanol till the filtrate become colorless. The copolymer nano-material was dried

under vacuum oven for 12 h at 50 °C. Yield = 75 %. ¹H-NMR (500 MHz, *d*₆-DMSO) δ: 7.40 (m, 2H), 7.44 (m, 2H), 7.29 (d, 2H, PPy), 7.78 (s, 0.4H, Dopant) 1.2 (m, 1H, aliphatic-H), 0.8 (m, 0.2H, Aliphatic-H). FT-IR (KBr, cm⁻¹): 1560, 1494, 1346, 1193, 1111, 1050, 923, 811, 783, and 612. UV-visible (water, nm) λ max: 350, 450 and 900. Polymer **P-20**, **P-50** and **P-100** were synthesized using the above procedure by diluting the polymerization mixture with various amount of water. The concentration of the reactants, amount of water and S/N ratio are provided in table 4.1.

Preparation of polyaniline nanofiber via emulsion route: Synthesis of Polyaniline nanofibers were carried out using a similar procedure in chapter -3.

4.3. Results and discussion

4.3.1 Synthesis of polypyrrole-polyaniline nanomaterials via dilution route

Amphiphilic water soluble anionic surfactant 4-[4-hydroxy-2((*Z*)-pentadec-8-enyl) phenylazo]-benzenesulphonic acid (surfactant-1) has a unique built-in amphiphilic design in which the hydrophilic sulphonic acid behaves as a polar head and the long alkyl chain as a hydrophobic tail. Emulsion polymerization of the anionic amphiphilic surfactant micelles with monomers like aniline and pyrrole produced their corresponding nanofibers and nanospheres, respectively [^aAnilkumar, P. *et al* 2006; ^aAntony, M. J. *et al* 2009]. In the present investigation, the compositions of reaction constituents were fixed and while concentrations were systematically varied by diluting the thick emulsion by known amount of water (see figure 4.2.). The chemical compositions of [aniline]: [pyrrole] and [monomers]/[dopant] were fixed as 95:5 and ~ 75 base on previous experience. The exact concentration of the reaction constituents and amount of water utilized in the dilute polymerization route was summarized in Table 4.1. The aniline concentration is varied from 7.3×10^{-1} to 1×10^{-1} M, while pyrrole concentration is varied from 4.8×10^{-2} M to 6.9×10^{-3} M. The concentration of the surfactant is varied from 9.6×10^{-3} to 1.4×10^{-3} M to carry out the copolymerization polymerization. The concentration of the amphiphilic dopant was maintained always higher than its CMC to retain its micellar behaviour in water [^danilkumar, P. *et al* 2008]. This had facilitated the stabilization of the aromatic monomers (aniline and pyrrole) without phase separation

even at large dilution (at 100 mL). Pyrrole composition was fixed as 5 mole % in the feed because of two reasons: (i) the morphology transformation was predominant at lower composition of pyrrole in the feed and (ii) at higher incorporation of pyrrole, the copolymers were found insoluble which restrict their structural characterization by NMR. The emulsions were found very stable for more than a week at ambient conditions. Polymerization mixtures were oxidized by adding aqueous solution of ammonium persulphate in ice cold condition and keeping the reaction mixture without any disturbance for overnight. The resultant dark green material was filtered, washed with water and methanol until the filtrate became colorless. It was dried under vacuum oven for 24 h (0.05 mm of Hg) at 50 °C prior to further analysis. The copolymers are represented by P-Co-5, P-20, P-50 and P-100. The number in P-Co-5 represent 5 mol % pyrrole feed, which is synthesized in 10 ml water and while the others P-20, P-50 and P-100 represent the amount of water (mL) added for the dilution. Polyaniline nanofiber (PANI) was synthesized by polymerizing the thick emulsion of aniline with dopant (no pyrrole monomer) under identical conditions.

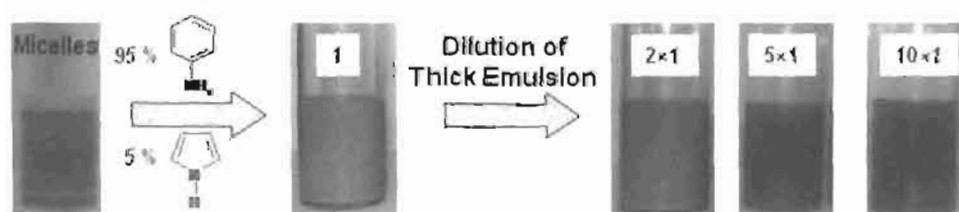


Figure 4.2. Dilution of the thick emulsion template.

Table 4.1. Concentration of the reactants and amount of water used for synthesis, elemental analysis of nanomaterials.

Sample ^a	Conc. of Aniline (M)	Conc. of pyrrole (M)	Conc. of surfactant (M)	Amount of water (mL) ^b	S/N ratio ^c
PANI	7.3×10^{-1}	-	9.6×10^{-3}	10	0.43
P-Co-5	7.0×10^{-1}	4.8×10^{-2}	9.6×10^{-3}	10	0.41
P-20	4.2×10^{-1}	2.9×10^{-2}	5.8×10^{-3}	20	0.40
P-50	1.9×10^{-1}	1.3×10^{-2}	2.6×10^{-3}	50	0.40
P-100	1.0×10^{-1}	6.9×10^{-3}	1.4×10^{-3}	100	0.35

^aPolyaniline and copolymer samples prepared under dilution. ^b Amount of the water used for dilution. ^c Sulphur/ Nitrogen ratio was obtained by elemental analysis.

4.3.2. Structural characterization of copolymer nanomaterials

The structures of the copolymer nanomaterials were characterized by $^1\text{H-NMR}$ and FT-IR spectra. The NMR spectra of dopant, PANI and P-Co-5 were recorded in d_6 -DMSO and were shown in the figure 4.3. The dopant showed peaks at 7.78, 7.60, 6.77, 6.71 ppm corresponding to the different types of aromatic protons. PANI contains two sets of aromatic protons at 7.45 and 7.40 ppm [Mu. S. *et al* 2008; Goto, H. *et al* 2002]. Copolymer P-Co-5 showed a peak at 7.29 ppm corresponding to β -protons in pyrrole [a Li, X. G. *et al* 2001; b Li, X. G. *et al* 2001; c Li, X. G. *et al* 2004; d Li, X. G. *et al* 2004]. The comparison of the integral intensities of polyaniline with β -protons of pyrrole revealed 16 mole % incorporation of pyrrole in the copolymer. A similar composition determination for the other dilute polymerization samples P-20 and P-50 confirmed the pyrrole content in the range of 16-18 %. P-100 was found insoluble in d_6 -DMSO and not possible to record its NMR spectrum. The high incorporation of pyrrole in the copolymer was correlated to the high reactivity ratio of pyrrole ($r_{\text{PY}}=2.16$) over aniline ($r_{\text{AN}}=0.13$) in oxidative polymerization route [Lim, V. W. L. *et al* 2001]. NMR spectra analysis confirmed the incorporation of ~16-18 % pyrrole in the copolymer irrespective of the various levels of dilution in the polymerization mixture.

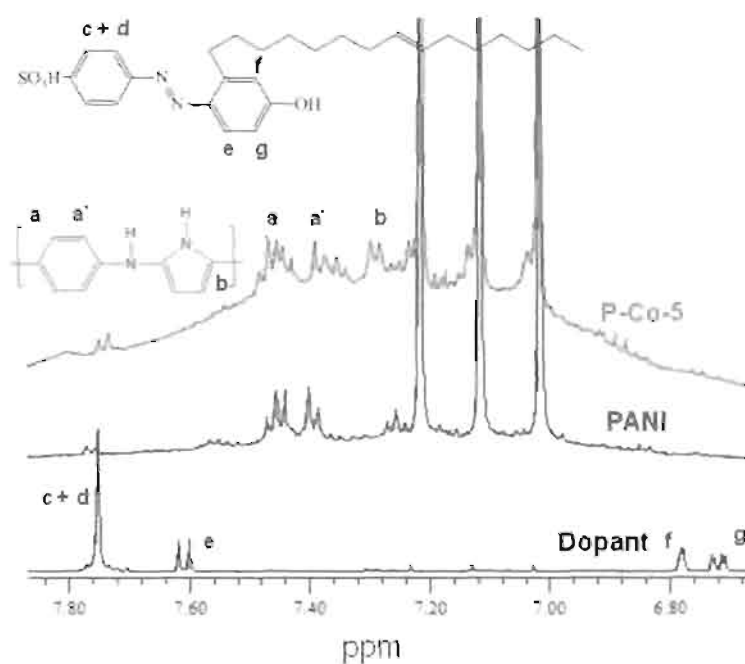


Figure 4.3. $^1\text{H-NMR}$ spectra of surfactant, PANI, and P-Co-5 in d_6 -DMSO.

FT-IR spectra of the copolymers were also recorded by making thin pellet with KBr powder (see figure 4.4.). The polyaniline sample PANI has two peaks at 1580 and 1490 cm^{-1} with respect to stretching vibration of benzenoid and quinoid in polyaniline chains, respectively [Zheng W. *et al* 1997; ³Omastova, M. *et al* 2003]. Three additional peaks were assigned at 1300, 1148 and 820 cm^{-1} to C-N stretching of secondary amine group, O-S-O stretching of the sulphonic acid dopant, and C-H out-of-plane stretching in the 1,4-disubstituted benzene ring respectively [¹Omastova, M. *et al* 2004; ²Zhang, X. *et al* 2006]. Copolymers formation is indicated by in-plane deformation of (N-II or C-II) at 1047 cm^{-1} which increases the intensity from PANI to P-Co-5, P-20, P-50, and P-100 respectively. The peaks at 1580, 1490, 1300 and 1148 cm^{-1} showed a decreasing intensity trend with dilution.

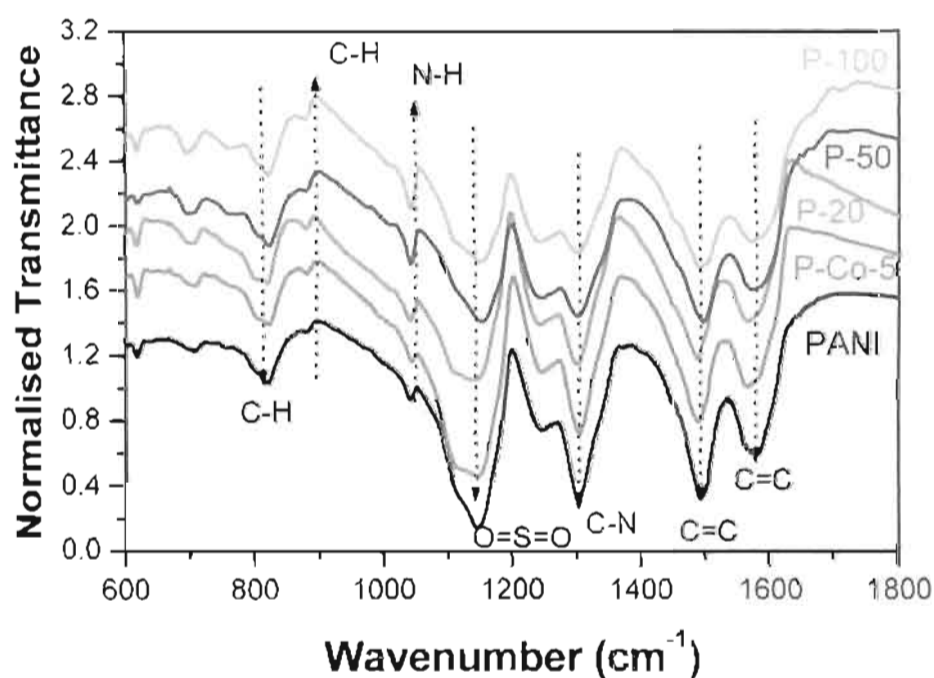


Figure 4.4. IR spectra of the copolymer nanomaterials.

4.3.3. Morphology of Nanomaterials

The morphology of the nano-materials was recorded using JEOL JSM-5600 LV scanning electron microscope (SEM) and images are shown in figure 4.5. The morphology of PANI showed a mat of thick and long nanofibers of length upto 4-6 μm and width of about 200 nm. The morphology of P-Co-5 and P-20 were drastically changed to short nano-rods. Interestingly, at large dilution samples (P-50 and P-100)

were found as hollow materials. The sizes of the nanomaterials of P-Co-5 to P-100 were very small and good pictures were not able to obtain from SEM.

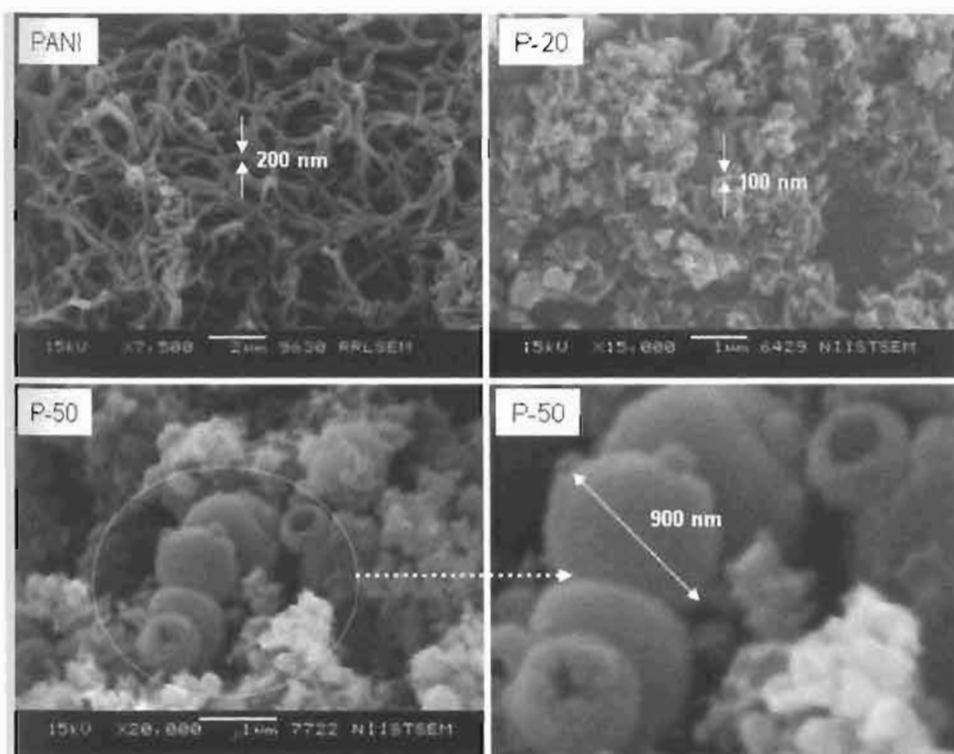


Figure 4.5. SEM image of copolymer nanomaterials

The TEM image of the PANI contained exclusively nanofibers of 4-6 μm length with 200 nm widths which was matching very well with that of its SEM image (see figure 4.6.). P-Co-5 and P-20 samples devoid of any long nanofibers, but showed the presence of short nano-rods of 0.5-0.7 μm length with 80-120 nm diameter. In P-50, a large number of hollow spheres of 1 μm in diameter were found which was almost matching with size and shape of its SEM image. The wall thickness of the hollow sphere was obtained as ~ 80 nm. Interestingly, the largely diluted sample P-100 showed exclusively nano-tubes. The average wall thickness and the inner pore diameter of the nanotubes were obtained as ~ 30 nm and ~ 60 nm, respectively. The nanotubes were very short and their length was varied from 1.2 μm to 1.8 μm . The nanotubes were further found to be highly crystalline and the electron diffraction pattern showed bright spots with periodicity corresponding to highly ordered layer -

like structures in **P-100** [Jang, J. *et al* 2002]. SEM and TEM of nanomaterials clearly gave evidence for the evolution of morphological transformation from long nanofibers to short nanorods and subsequently transferred into hollow spheres to highly crystalline nanotubes. It is very important to note that this is for the first time such an evolution of nanomaterial morphologies were obtained in a single system without change in the polymerization process or composition of the constituents in the conducting polymer nanomaterials.

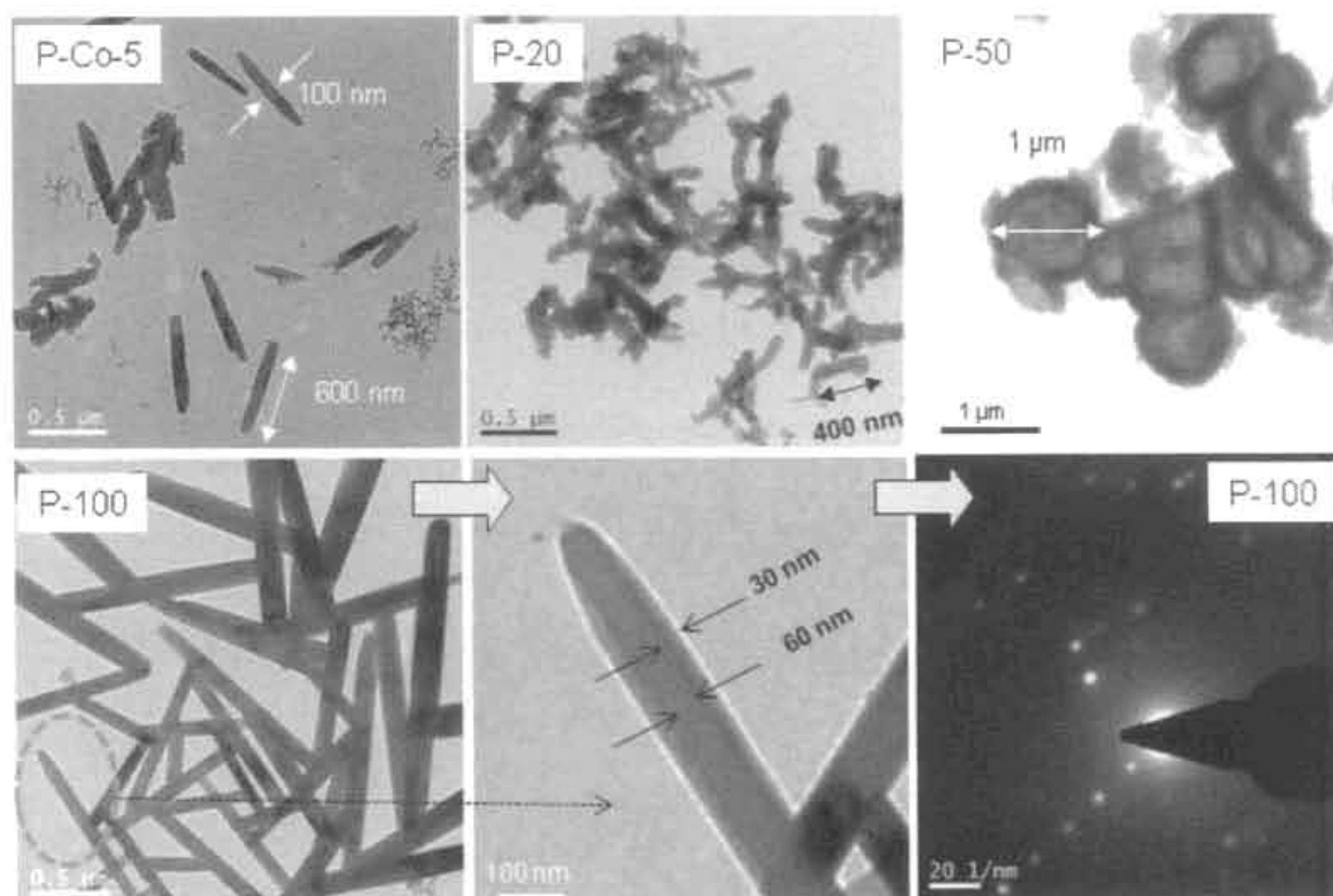


Figure 4.6. TEM image of copolymer nanomaterials.

Table 4.2. Dimensions of the nanomaterials.

Sample	Nano Dimensions		
	Shape	Length (nm)	Width (nm)
PANI	Fiber	4-6 μm	200 \pm 20
P-Co-5	Rod	600 \pm 50	150 \pm 10
P-20	Rod	425 \pm	90 \pm 10
P-50	Hollow spheres	-	920 \pm 100
P-100	Tubes	1600 \pm 300	120 \pm 20

4.3.4. Mechanism of copolymer nanomaterials

In order to study the mechanism of the evolution of nanomaterial transformation, the polymerization mixtures (emulsions) were subjected to dynamic light scattering (DLS, in solution) and electron microscopic analysis. The orange or brown color emulsions showed in the vials (in figure 4.7.) are corresponding to the polymerization mixtures consisting of monomers + surfactant before the chemical oxidation by ammonium persulfate. The size of surfactant + aniline complex was obtained in the range of 3-5 μm [Anilkumar, P. *et al* 2008]. DLS plots of the P-Co-5 and P-20 samples showed mono-modal distribution with average micellar aggregates of ~ 500 nm. The DLS plots of P-50 and P-100 showed bi-modal distributions, with size in the micrometer range. DLS analysis clearly evident that the monomers + dopant existed as sub-micrometer size aggregates in the polymerization mixtures.

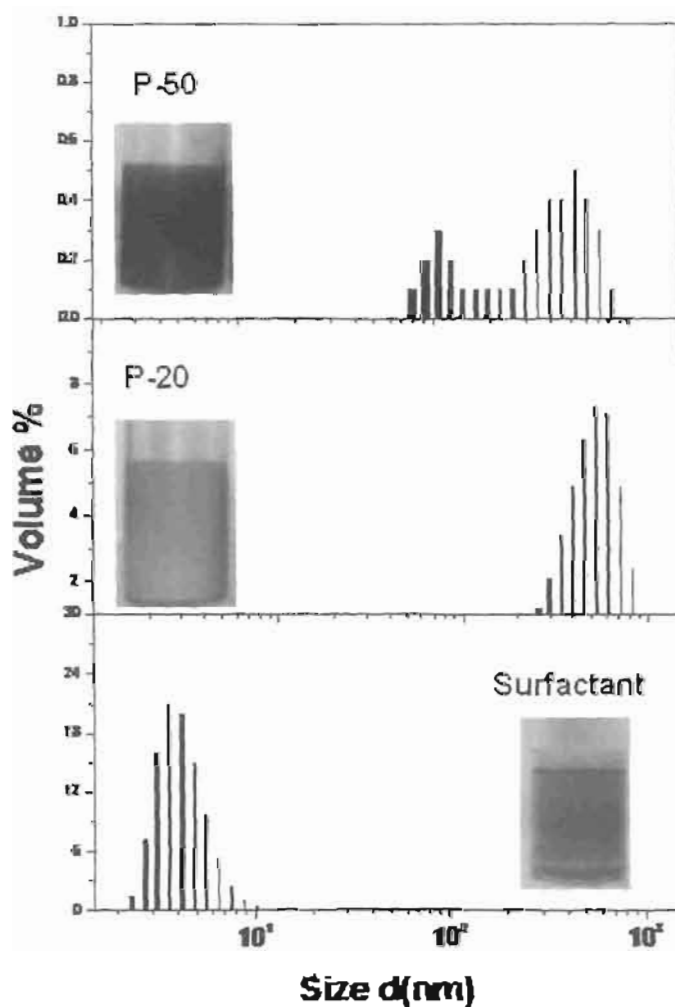


Figure 4.7. DLS histograms of the emulsion templates.

The polymerization mixtures were very stable (for more than a week) which enabled us to trace the shape of the template aggregates by SEM shown in figure 4.8. The polymerization mixtures were drop casted on SEM stud and subjected to slow evaporation. SEM image of the aniline + dopant template showed long fiber like cylindrical type-aggregates which template for polyaniline nanofibers. SEM images of copolymer templates of **P-Co-5** and **P-20** were found short cylindrical flake like aggregates whereas the largely diluted polymerization mixtures **P-50** and **P-100** showed hollow-spherical aggregates. The hollow spherical morphology is typical example for the formation of spherical vesicular template aggregates. The short flake-like templates in **P-Co-5** and **P-20** produced short nano-rods. Interestingly, in largely dilute cases **P-50** and **P-100**, the 3D spherical vesicular aggregates template for hollow spheres and nano-tubes. Thus, the electron microscopic studies confirmed the evolution of nanofiber-to nanorod-to-hollow sphere-to-nanotube is the resultant of the change in the shape of the polymerization templates from cylindrical-to- vesicular aggregates during the dilution process.

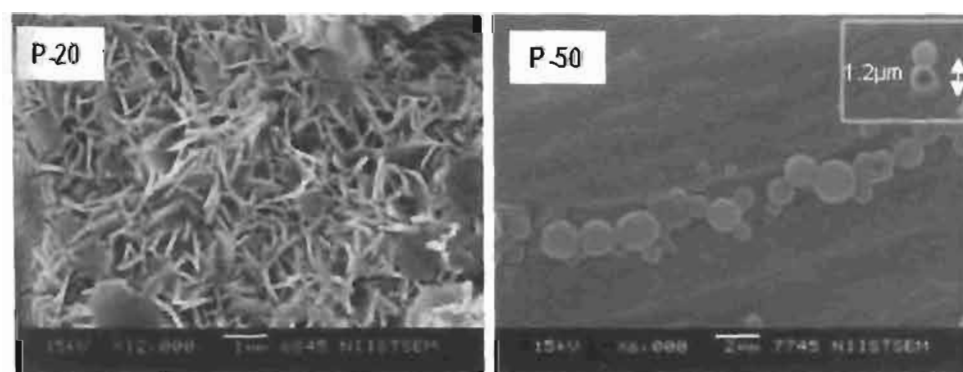


Figure 4.8. SEM images of the emulsion templates.

Based on the above studies, the following mechanism has been proposed for the evolution of nanomaterials morphology (see figure 4.9.). Amphiphilic azobenzene sulphonic acid forms micelles of size 4.3 nm in water. Surfactant micelles in presence of aniline self-assemble as aggregated cylindrical micelles which produce nanofibers (PAN). Aniline monomer effectively neutralizes polar head of the dopant in addition to their inclusion to the aromatic core of the micelles. In presence of the co-monomer

pyrrole in feed (5 mole %). long range order cylindrical aggregates were truncated into short and thin cylindrical aggregates. On subsequent dilution, the cylindrical assemblies were completely transformed to vesicular aggregates which account for the morphological evolution of nanorod-to-hollow sphere-to- nanotube. The various types of interactions of monomers (95 % aniline + 5 % pyrrole) with dopant during the dilution can be explained as follow: (i) aromatic aniline interact with the dopant micelles in water to produce cylindrical aggregates. (ii) the subsequent dilution of cylindrical aggregates with addition of water (10 ml. more) did not change the shape of the aggregates and (iii) with excess dilution (more than 50 ml. of water), the cylindrical aggregates transformed into spherical vesicular aggregates. The transformation of cylindrical to vesicular aggregates had been observed by Davies *et al.* in cetyltrimethylammonium bromide surfactant using aromatic molecules like 5-methylsalicylic acid as transformation agent [Davies, T. S. *et al* 2006]. Recently, Anilkumar *et al.* from our research group also reported such a cylindrical to vesicular transformation in a new amphiphilic 4-(3-dodecyl-8-enylphenoxy) butane sulphonic acid surfactant in dispersion route (water/toluene/aniline complex) [Anilkumar, P. *et al* 2009]. It supports the effect of dilution on the transformation of cylindrical aggregates into vesicular aggregates in the present system. In order to confirm the above hypothesis, the average sizes of the synthesized nanomaterials were compared with that of the polymerization templates based on their SEM and TEM images. The average diameter of a vesicular template aggregate was determined from SEM image (see figure 4.5.) as $1.2 \pm 0.3 \mu\text{m}$. The average diameter of hollow spheres for P-50 sample were obtained as $0.92 \pm 0.2 \mu\text{m}$ and $1.00 \pm 0.1 \mu\text{m}$ based on SEM (see figure 4.5.) and TEM (see figure 4.6.), respectively. The diameter of vesicular template was almost identical to that of the synthesized hollow-sphere which directly evidence for the mechanism. The average length and diameter of the nanotubes were obtained as $1.6 \mu\text{m}$ and 120 nm , respectively with a high aspect ratio of ~ 14 (length/width). If the transformation of hollow sphere to nanotube morphology would have occurred, then one would expect the circumference of hollow sphere ($2\pi r$) should be almost equal to $2L$, where L is the length of the tube (neglecting small contribution from both edges). This can be further easily understood by imagining the squeezing of filled spherical balloon into a long cylindrical one. The average circumference of the hollow sphere

($2\pi r$, $r = 0.5 \mu\text{m}$, from TEM image) was calculated as $3.14 \mu\text{m}$ which was matching well with that of the twice the length of the nanotubes = $3.20 \mu\text{m}$ ($2L$, $L = 1.6 \mu\text{m}$ from TEM image). Hence, it proved that the nanotubes are nothing but the squeezed version of the hollow spheres. It confirmed that the hollow spheres and nanotubes were produced by the chemical oxidation of the vesicular aggregates formed by the dopant + monomers in the dilute polymerization.

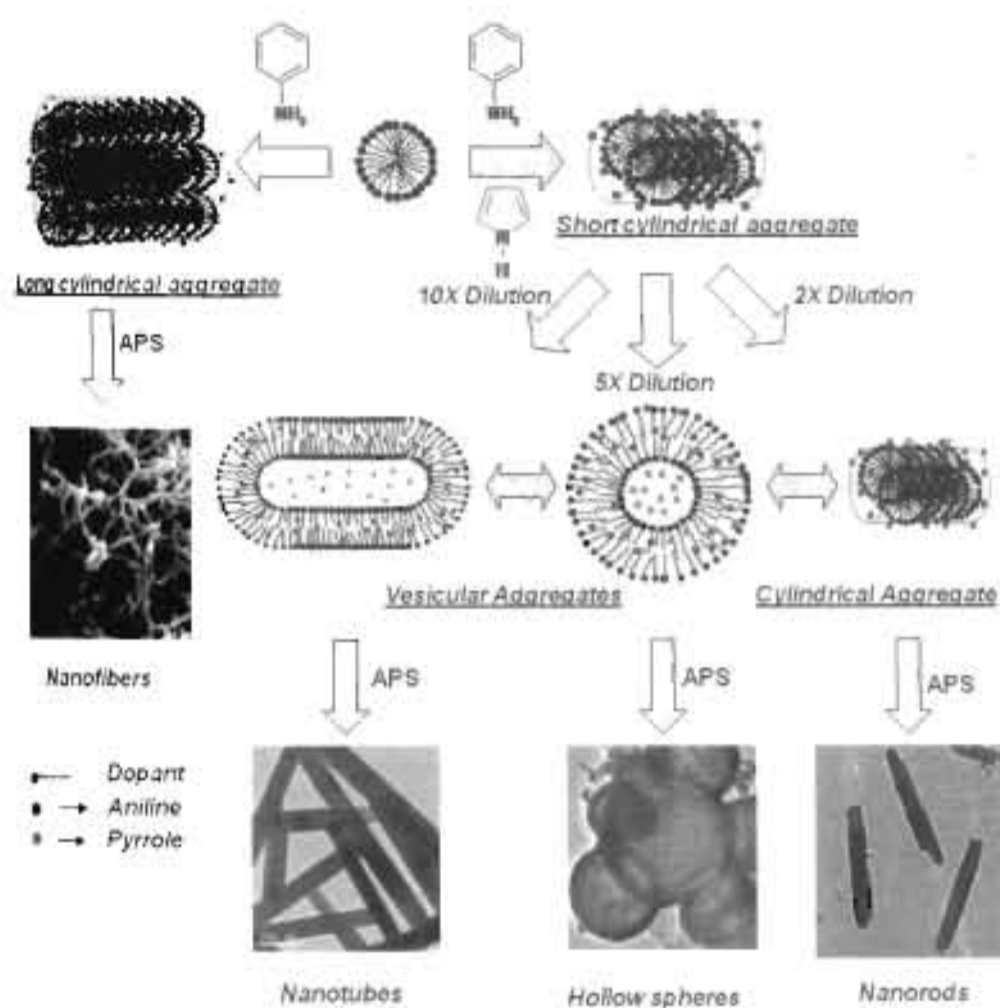


Figure 4.9. Plausible Mechanism of evolution of nanomaterials

4.3.5. Properties of copolymer nanomaterials

Thermal stability of the nano- materials were determined by TGA and thermograms are provided in figure 4.10. The copolymer nano-materials had high thermal stability, and only 10 % weight loss was observed at temperature lower than 280 °C. This indicated that the azo benzenesulphonic acid doped nano-materials were thermally stable as reported for other dopant such as camphorsulphonic acid [Liu, L. *et al* 2005].

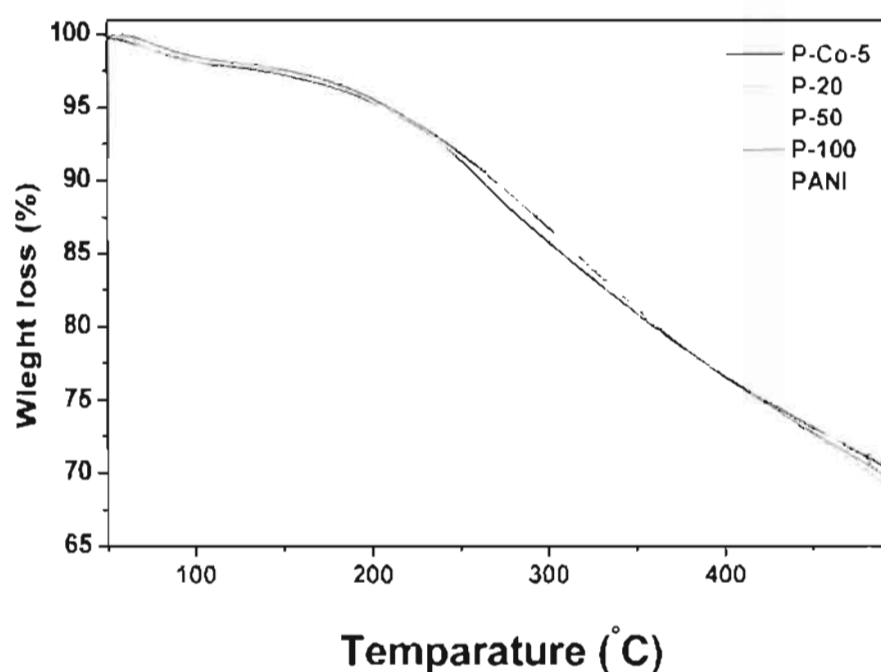


Figure 4.10. TGA of the copolymer nanomaterials.

The amphiphilic nature and long alkyl tail of the renewable resource surfactant enhanced the solubility of the nano- materials in water. The copolymer nano-materials were freely dispersed in water by stirring under ultrasonic at room temperature. The UV-visible spectra of PANI and copolymers were recorded in their doped state and dedoped states were shown in figure 4.11. Polyaniline showed three transitions at 350 nm, 430 nm, and a broad peak at 850 nm with respect to π - π^* transition, polaron to conducting band, valence band to polaron band respectively [Cabala, R. *et al* 2002; Xia, Y *et al* 1995]. The UV-visible spectra of the P-Co-5, P-20, P-50 and P-100 showed similar bands to that of PANI. Polaron band of PANI was highly delocalized

compared to the P-Co-5, P-20, P-50 and P-100. As we employ more and more dilution the charge carrier bands are less delocalized. This result suggests that the pyrrole unit blocked the delocalization in the polymer chain backbone in the copolymers. All the samples were dedoped using 1M aqueous ammonia solution, upon dedoping the polaron band is vanished from 800 nm and quinoid band appears at 680 nm. Dedoped nanomaterials showed peaks at 360 nm and 650 nm similar to conventional emeraldine base (EB) form [Kang, E. T. *et al* 1998].

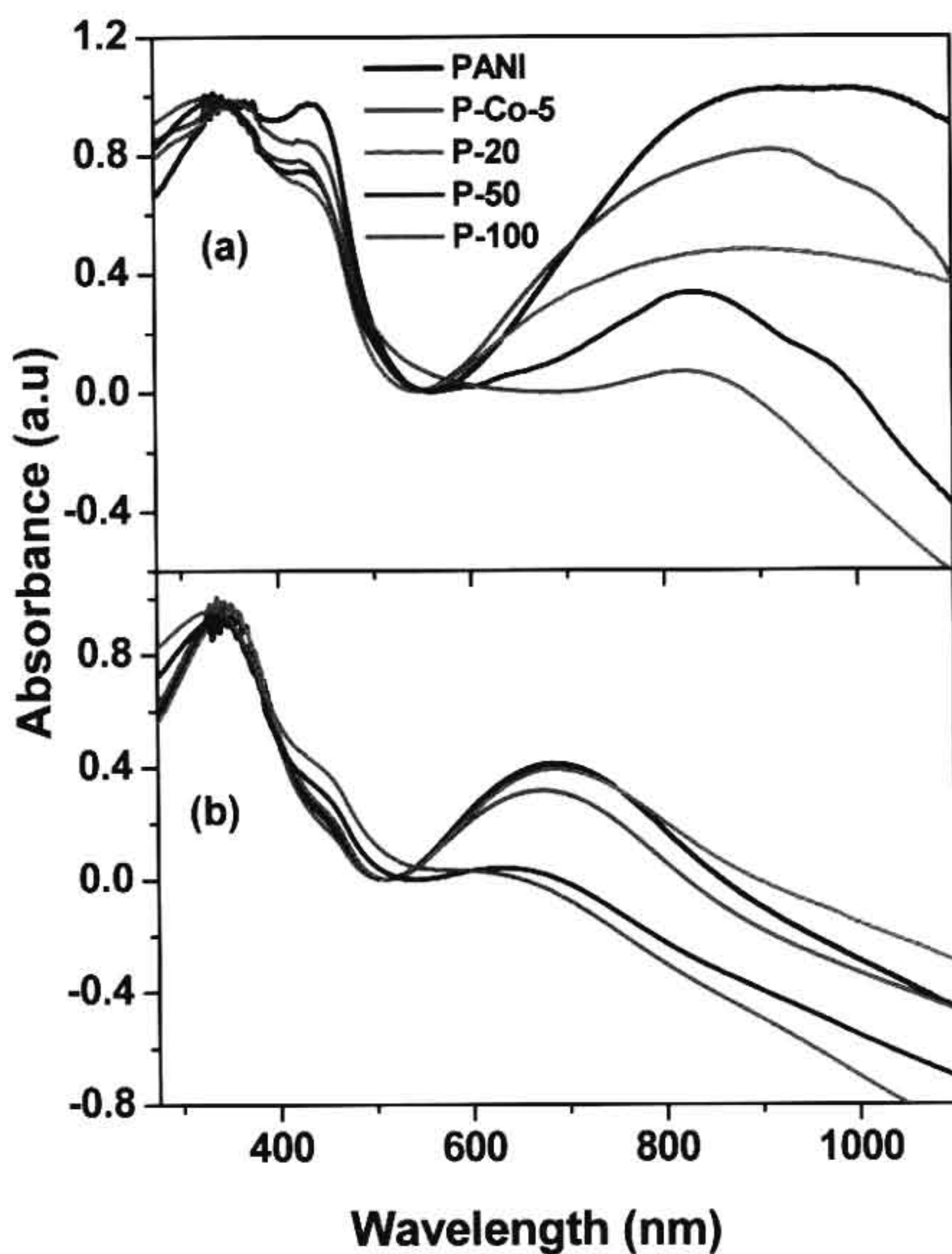


Figure 4.11. UV-visible spectra of the copolymer nanomaterials.

Conductivity of the sample was recorded by four probe conductivity techniques with PID controlled heating oven (see figure 4.12.). All samples PANI, P-

Co-5, P-50 and P-100 were compressed into pellet and subject to I-V measurements. All the samples showed a linear I-V plots (see figure 4.13, and figure 4.14.) and followed the ohm's behaviour [Long, Y. *et al* 2003; Long, Y. *et al* 2003; Long, Y. *et al* 2004]. As expected with increase in the temperature, the resistance decreases. The electrical resistance of the materials was obtained from slope of the I-V plots at 30 °C and their conductivities were reported in table 4.3.



Figure 4.12. Photograph of Keithley Four Probe set up.

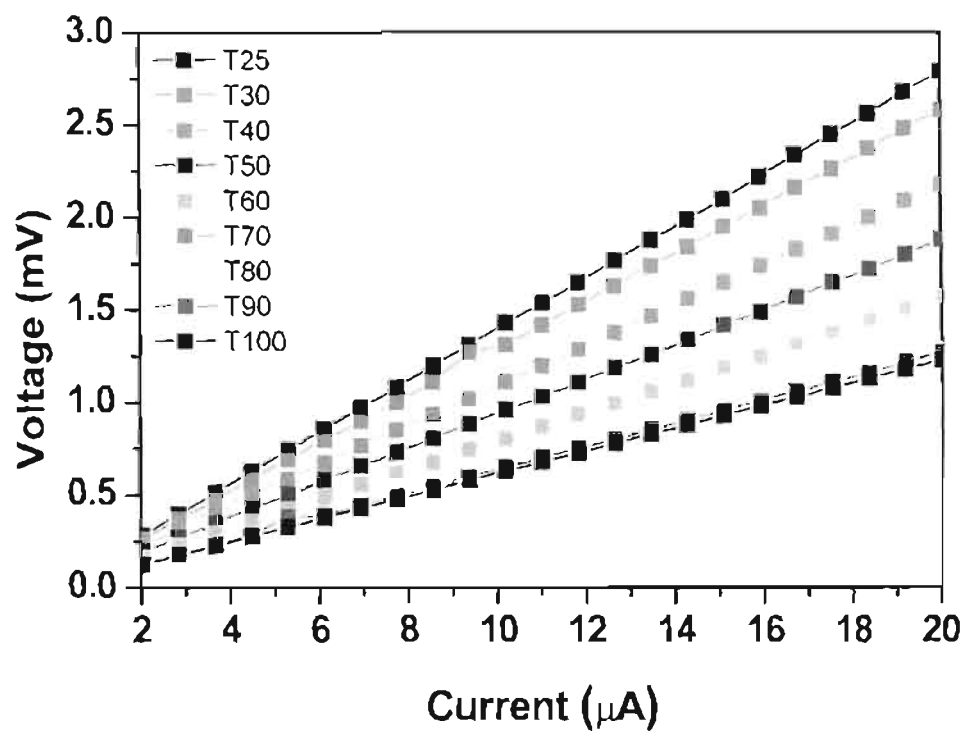


Figure 4.13. I-V plots of PANI at different temperatures.

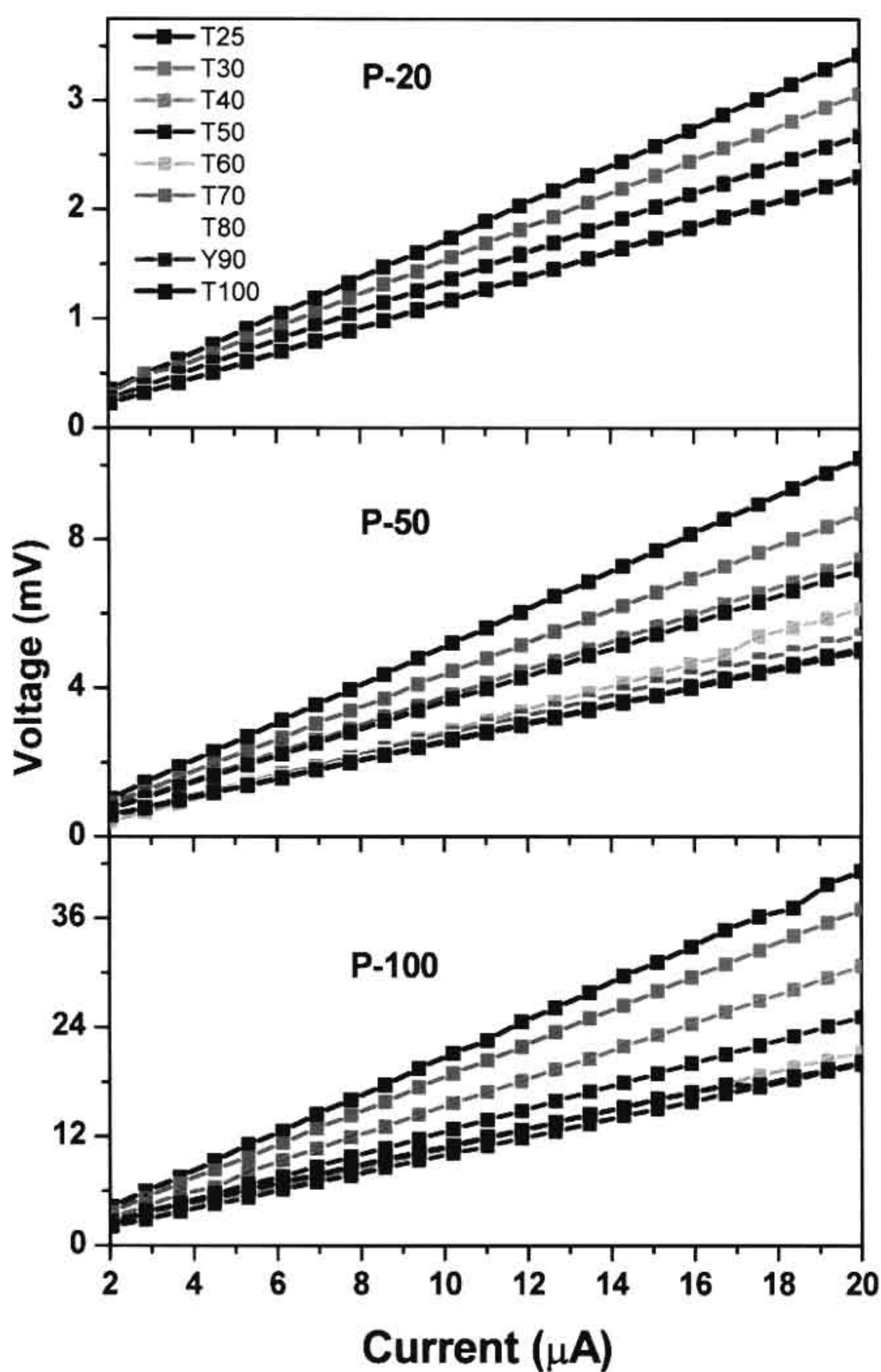


Figure 4.14. *I-V* plots of *P-Co-5*, *P-50*, *P-100* at different temperatures.

The slopes *I-V* plots of the samples increases in the order of nanofiber < nanorod < hollow sphere < nanotube which indicate the increase in the resistance of the samples (see figure 4.15.). The conductivity of the PANI was obtained in the range of 10^{-2} S/cm which was accordance with that of the polyaniline doped with

sulfonic acid derivatives [^aanilkumar, P. *et al* 2006; ^banilkumar, P. *et al* 2007; ^canilkumar, P. *et al* 2007]. The conductivities of nanorod, hollow sphere and nanotubes were found one order lower than that of PANI nanofibers. In order to investigate the effect of temperature on the conductivity of the nanomaterials, they were subjected to variable temperature I-V measurements from 30 to 100 °C. The conductivity of the samples was determined from I-V plots and nanofiber has much higher conductivity than other nano-forms (see figure 4.16a).

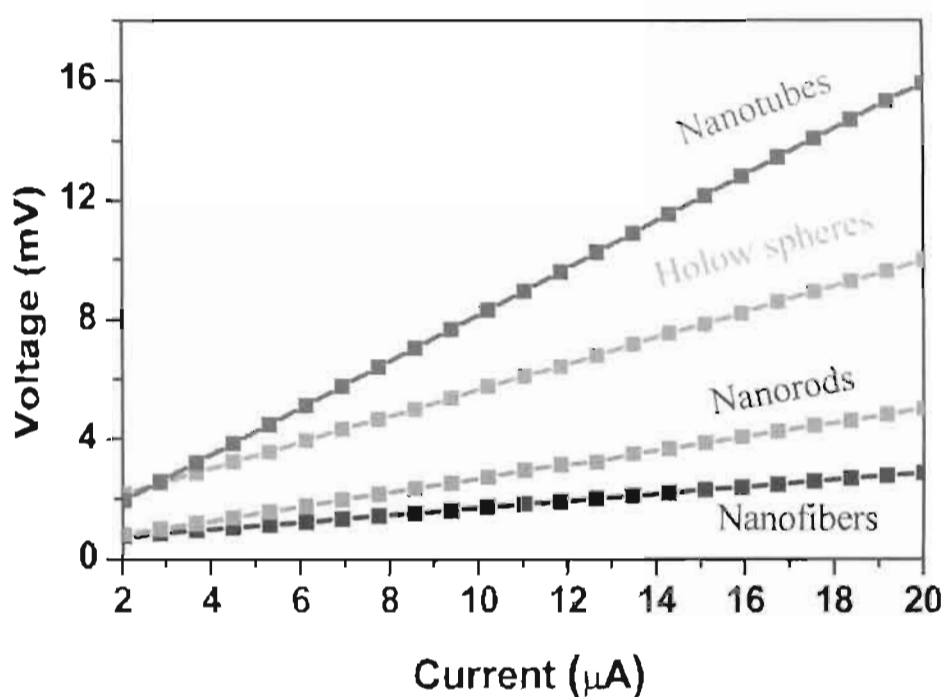


Figure 4.15. I-V plots of copolymer nanomaterials.

All the nanomaterials were synthesized using [monomers]/[dopant] = 100 (100 times lower amount of dopant with respect to monomers), one may argue that these trend may be due to the difference in the doping level in the nanomaterials rather than the difference in their morphology. In order to rule out the difference in the doping level, all the sample pellets were dipped in 1M HCl for 12 h for complete doping. The pellets were washed with water, methanol, dried in vacuum oven and again subjected to variable temperature conductivity measurements (see figure 4.16b). After HCl doping the conductivity of nanofiber, nanorods and hollow spheres did not change much whereas the nanotubes showed a slight increase in values. This detailed analysis

revealed the difference in the conductivity of the samples arose from the difference in the morphology of the nanomaterials and not due to the any other artifact such as incomplete doping, etc.

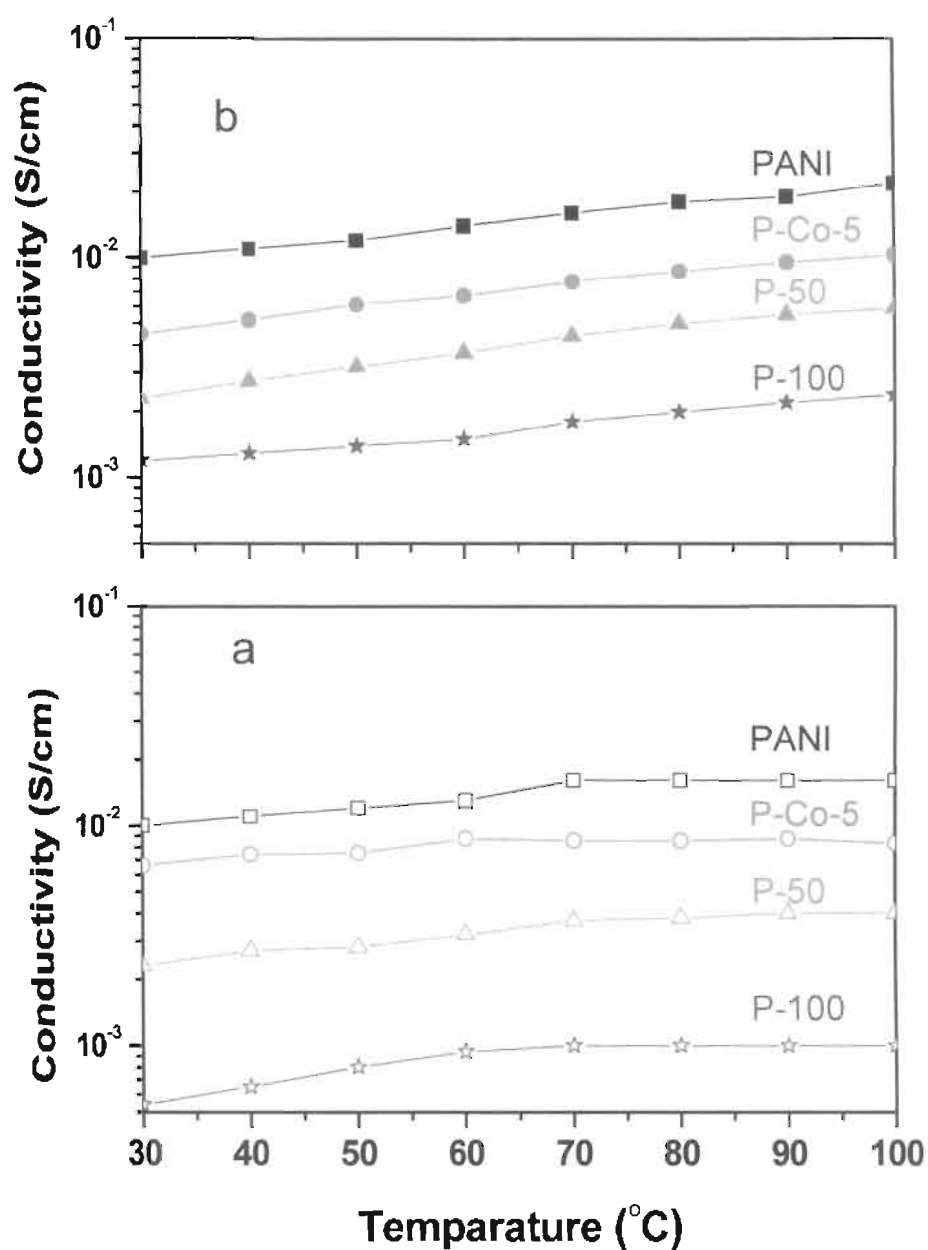


Figure 4.16. Temperature dependant conductivities of the nanomaterials (a) actual (b) HCl treatment.

To study the electronic transport behavior of the material, the resistance ($\ln R$) of the material was plotted over the temperature ($T^{-1/2}$) in the range of 298- 373K (see figure 4.17.). In the insulating regime, the low-temperature resistivity $\rho(T)$ of the conducting polymer followed the exponential temperature dependence of variable

range hopping (VRH) [Long, Y. *et al* 2003; Long, Y. *et al* 2003; Long, Y. *et al* 2003; Mativetsky, J. M. *et al* 2002]

$$\rho(T) = \rho_0 \exp(T_0/T)^m, \dots\dots\dots 2$$

where the exponent $m = 1/2$ for one dimensional (1D) hopping process. T_0 is the Mott characteristic temperature and can be obtained from the slope of $\ln R$ vs $T^{-1/2}$ plot. The plots showed a linear trend and followed VRH model. The T_0 values for nanofiber, nanorods, hollow sphere and nanotubes were obtained as 1.77×10^2 , 1.55×10^2 , 1.75×10^2 and 1.8×10^2 K respectively. These values were in accordance with earlier reports for metallic conductivity of polyaniline [Long, Y. *et al* 2003; Mativetsky, J. M. *et al* 2002]

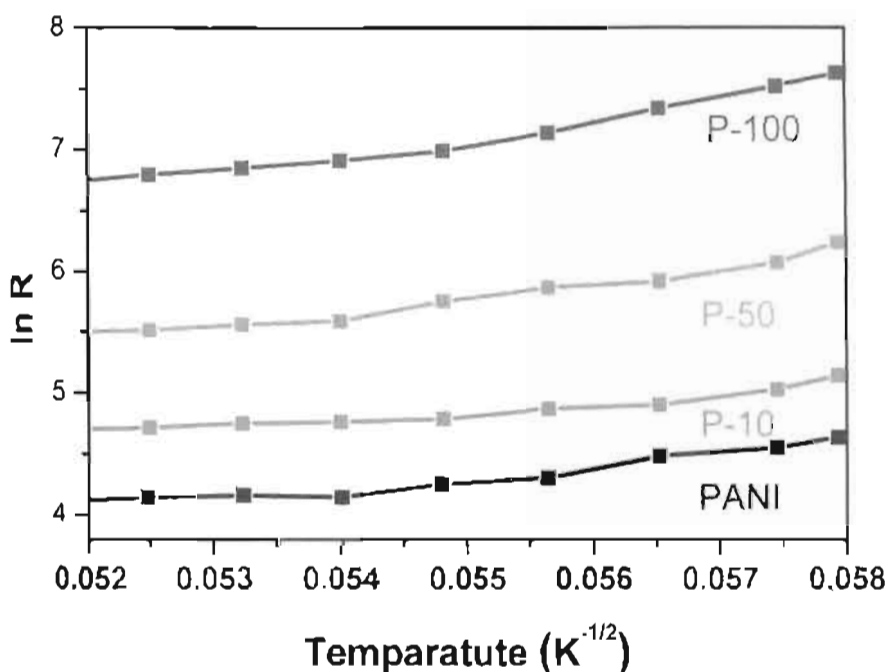


Figure 4.17. Resistance versus temperature plot for nanomaterials.

The comparison of the four probe studies, morphology, solid state ordering and % crystallinity of the samples revealed that the conductivity of the nanomaterials were predominately controlled by the morphology. Since the composition of the all the nano-forms in the present investigation almost identical, one can conclude that the polyaniline nanofibers are better conducting materials than other nanostructures. The empty voids occupied in the middle portion of the hollow sphere (also in nanotube) would restrict the conductivity of the electrons via hopping process. Though, the linear

and thin geometry of nanotubes favoured the compactness in the solid state to form highly crystalline and ordered structures, the presence hollow inner domain behaved as insulating layer for its poor conductivity. In a nut shell, in the present investigation, we have successfully utilized the self-organized molecular templates for the evolution of multiple nanostructures without altering their chemical composition, which enabled us to correlate their conductivities such as fibers, rods, hollow spheres and nanotubes in a single system.

Table 4.3. Wide angle X-ray diffraction and conductivity measurements of copolymers and PANI.

Sample	WXRDa		Crystallinity ^b (%)	σ^c (S/Cm)
	2 θ (Degrees)	d-spacing(A ^o)		
PANI	6.4, 19.4, 25.1	13.8, 4.6, 3.5	15 %	1.2×10^{-2}
P-Co-5	3.3, 25.4	26.7, 3.5	24 %	4.2×10^{-3}
P-20	3.4, 25.3	25.9, 3.5	24 %	2.3×10^{-3}
P-50	3.6, 25.2	24.5, 3.5	24 %	2.1×10^{-3}
P-100	3.6, 6.1	24.5, 14.5	65 %	1.3×10^{-2}

^a wide angle x-ray diffraction analysis carried out at 30 °C. ^b Crystallinity of the samples measured as by deconvolution of the area of amorphous and crystalline domain. ^c electrical conductivity of the samples measured through I-V plots

The polymer nanomaterials were subjected to WXRDa analysis to study the solid state ordering properties see figure 4.18. WXRDa of polyaniline showed three peaks, two at higher angle at $2\theta = 25$ and 19.5 and one at lower angles at $2\theta = 6.75$. The lower angle peak arose from the long range ordering of polyaniline chains via the doping of the surfactant molecules [Jayakannan, M. *et al* 2005; Dufour, B. *et al* 2001; Laska, J. *et al* 2002; Jana, T. *et al* 2000]. The higher angle peaks were assigned to the aromatic chain-chain interaction in the polymers. P-Co-5, P-20 and P-50 showed lower angle peaks at $2\theta = 3.6$ due to the long range ordering from the lamellar arrangement of dopant molecules between the polymer chains [Song, M. K. *et al* 2004; Wernet, W. *et al* 1984] Interestingly in P-100, the lower angle peaks were highly intense and sharp compared to other samples. The percentage crystallinities of

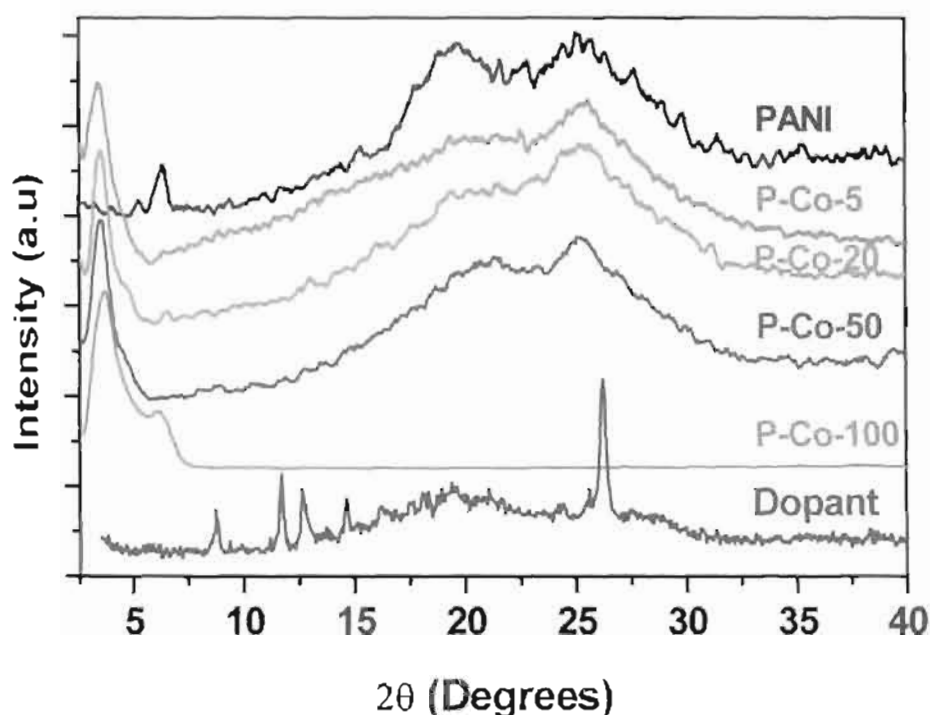


Figure 4.18. WXR D analysis of the copolymers.

the samples were determined from the WXR D patterns by comparing the area of hollow amorphous domain with sharp crystalline peaks (see table 4.3). The WXR D patterns were deconvoluted computationally to calculate the integral intensities of amorphous and crystalline domains. The percent crystallinity of the samples PANI, P-Co-5, P-20 and P-50 were almost identical in the range of 15-24 %. The sample P-100 showed a sharp low angle peak with complete vanishing of the amorphous domain ($2\theta = 15-30$), which resembled the typical nature of highly crystalline sample. The percent crystallinity of P-100 the sample was obtained as more than 60 %. The highly crystalline nature of P-100 was further confirmed by the electron diffraction pattern from the HR-TEM of the nanotubes (see figure 4.6). The electron diffraction patterns showed bright spots with regular periodicity corresponding to lamellar solid state ordering [Jang, J.; 2002]. The reason for the highly crystalline nanotubes may be correlated to the slow kinetics of copolymerization of monomers at largely diluted polymerization samples (see figure 4.18.).

4.4. Conclusion

In conclusion, we have developed unique self-assembled molecular template approach for tracing the morphological evolution of conducting polymers exclusively in polyaniline-co-polypyrrole nanomaterials. The important outcomes of the present chapter are as follows: (i) renewable resource amphiphilic azobenzenesulfonic acid dopant was utilized to study the formation of morphology such as nanofiber, nanorod, hollow-sphere and nanotube in a single system without change in the composition of their chemical constituents. (ii) the dopant micelles in water self-organized with aniline to produce thick emulsion consisting of cylindrical aggregates, which template exclusively for the polyaniline nanofibers. (iii) the self-organization of dopant micelles with aniline : pyrrole (95 : 5 mole %, respectively) produce short cylindrical aggregates and upon chemical oxidation these aggregates produce short nanorods. (iv) the dilution of the emulsion templates with known quantity of water resulted the transformation of cylindrical to vesicular aggregates without phase separation, which template for hollow spheres and nano-tubes. (v) the mechanistic aspects of the dilute polymerization route was studied by dynamic light scattering which support the formation of micrometer sized cylindrical and vesicular aggregates. (vi) the shape of the templates such as cylindrical and vesicular aggregates were confirmed by SEM and HR-TEM. (vii) the size and shape of the template aggregates matched very well with that of the resultant nanomaterials and confirmed the template-assisted polymerization mechanism. (viii) the structure and electronic properties of the nanomaterials were confirmed by NMR, FT-IR and absorption spectroscopy. (ix) WAXRD analysis revealed that the nanotubes produced at large dilution condition was found to possess more than 60 % of crystallinity compared to that of the nanofibers, nanorods and hollow spheres. (x) electron diffraction from the HR-TEM revealed the layer like ordering in the nanotubes. (xi) the variable temperature four probe conductivity measurements revealed that the samples showed typical I-V plots and (xii) the conductivity of the nanofibers were found higher at all the temperatures compared to that of all other nano-forms such as nanorod, hollow sphere and nanotubes. The present investigation enabled us to establish the correlation between the morphology of the conducting polymer nanomaterials with their solid state ordering and conductivity without disturbing either the compositions of the reactants or polymerization procedures.

Chapter-5

Polyaniline Nano-scaffold for Colorimetric Sensing of Biomolecules

5.1. Introduction

Conducting polymers are emerging as important classes of active layers in optoelectronic devices and chemical sensors [McQuade, D. T. *et al* 2000; Li, D *et al* 2009, ^cHuang, J. *et al* 2004; Janata, J. *et al* 2003]. Polyaniline, polypyrrole, polyphenylenevinylene, polythiophene and polyfluorenes were reported for chemical sensing of bio-molecules like DNA, RNA, enzymes, proteins, nucleic acids and so on [^aFeng, F *et al* 2007; Duan, X. *et al* 2010; Jiang, G. *et al* 2009; ^bFeng, F *et al* 2010]. Among all these polymers, polyaniline is unique conjugated polymer due to its good environmental, and chemical stability and possessing excellent reversible non-redox acid/base doping process [Li, D *et al* 2009]. The protonation and de-protonation in the polymer backbone accomplished by both color change as well as solid state conductivity [Li, D *et al* 2009]. Electrochemical assays of polyaniline were explored for detecting bioanalytes like dopamine, glucose (see figure 5.1.), cholesterol, vitamins, and various gases like hydrochloric acid, ammonia, H₂S and hydrogen, etc [Bossi, A *et al* 2000; ^aAli, S. R *et al* 2007; ^bAli, S. R *et al* 2007; ^aShoji, E *et al* 2001; ^bShoji, E *et al* 2001 Jureviciute, I. *et al* 2005; Jiang, Y. *et al* 2007; Korcherginsky, N. *et al* 2007; Gerard, M. *et al* 2002; Andreu, Y. *et al* 2005; Virji, S *et al* 2006]. However, the mechanism of the sensing was more difficult to interpret due to the complex surface morphology and detailed characterization techniques were usually required to confirm the detection pathways [Komsiyaska, L. *et al* 2006; Casella, I. G. *et al* 1997; Zhang, L. *et al*]

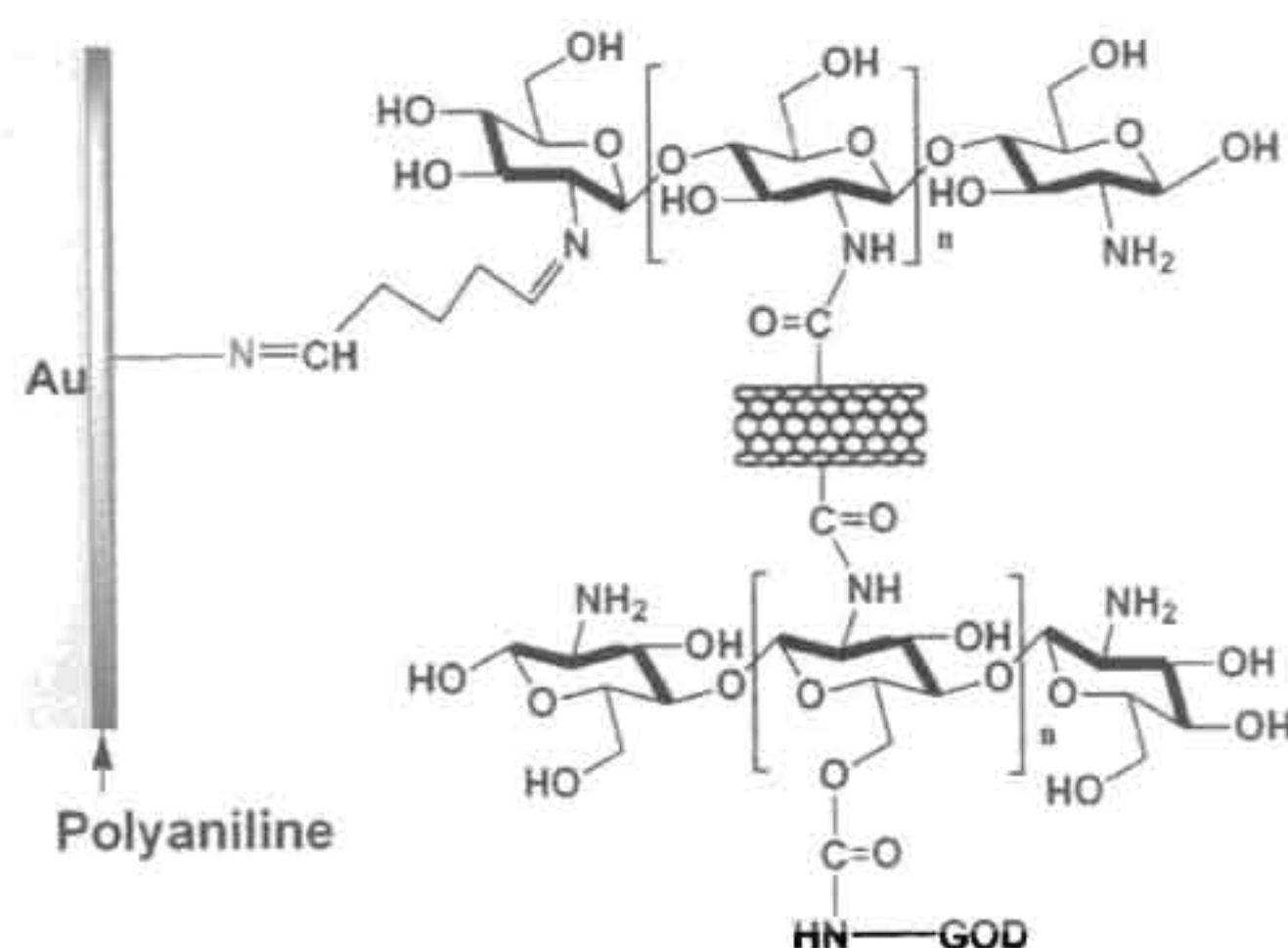
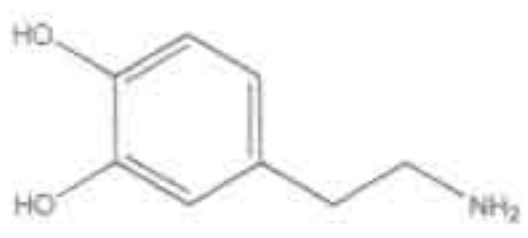
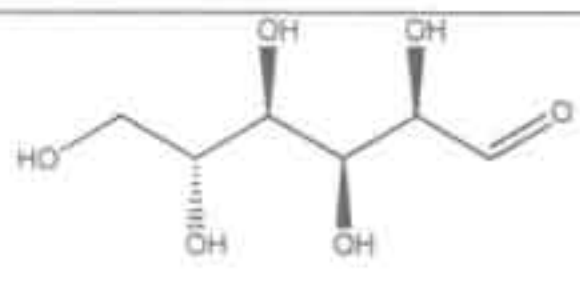
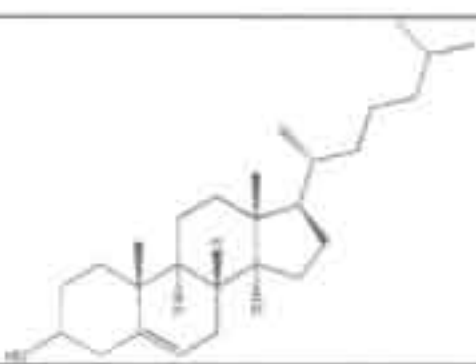
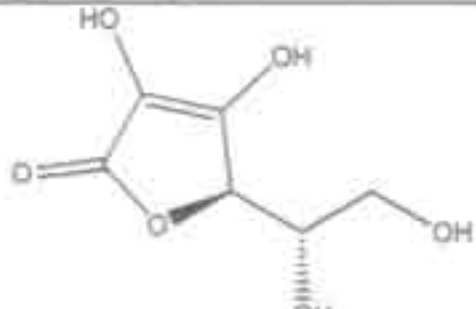


Figure 5.1. Fabrication of modified polyaniline-chitosan- gold electrode for glucose detection [adapted from Wan, D. *et al*]

Some of the analytes detected by polyaniline and corresponding analytical method utilized were shown in table 5.1.

Table 5.1. Type of analyte and method of detection using polyaniline.

Analyte	Structure	Technique	Ref. (et al)
Dopamine		Electrochemical and chemical	^a Ali, S. R 2007
Glucose		Enzymatic and electrochemical	Forzani, E.S 2004 Minkstimiene, A.K 2004 ^b Shoji 2001 Freund, M.S. 2007
Cholesterol		Electrochemical and enzymatic	Suman, S. 2006
Vitamin-C		Electrochemical and chemical	Bossi, A 2000 ^c Anilkumar, P2008
Hydrochloric acid	HCl	Chemical	Virji, S. 2007
Ammonia	NH ₃	Chemical	Li, D. 2009

Poor solubility of polyaniline in water or organic solvents is always being inherent major obstacle in making the assays in device. To overcome the solubility issues, aryl and N-substituted polyaniline derivatives were synthesized via post-polymerization sulfonation of emeraldine base using fuming sulfuric acid or other substitution reactions [Chen, S.-A. *et al* 1995 ; Lin, H. K. *et al* 2000; Malinauskas, A. *et al* 2004; Nguyen, M. T. *et al* 1994; Sivakumar, C *et al* 2001; Freund, M. S. *et al* 2007]. Attempts were also reported for self-doped polymers of N-alkyl sulfonated monomers via electrochemical polymerization [Chen, S.-A. *et al* 1995; Yue, J. *et al* 1991]. These approaches produced either low molecular weight polymers or insoluble

polymers which hampered their complete structural characterization. Nanostructures of polyanilines such as nanofibers, nanospheres and gels were also reported to disperse the nano-objects in water or organic solvents so that films could be prepared for sensor application [McQuade, D. T. *et al* 2000; Li, D. *et al* 2009]. Though the nanostructures showed improved processability, making mechanically stable polyaniline films without losing the morphology or conductivity is still far from the reality. Earlier, we have reported hydroxy substituted polyaniline nanospheres that effectively trace the interaction with ascorbic acid by partly on the effects of hydrogen bonding and doping effects (see figure 5.2.).

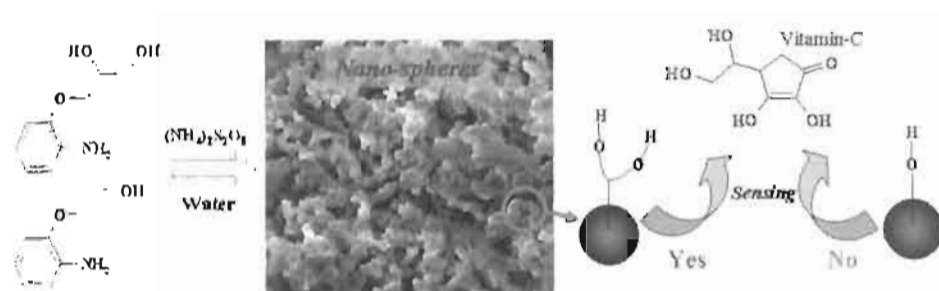


Figure 5.2. Hydroxy substituted polyaniline nanospheres for detection of vitamin-c [Adapted from Anilkumar, P. *et al* 2008]

Chemical or biological sensing via colorimetric naked eye detection is an inexpensive technique and also useful for on-line monitoring in vitro and in vivo studies [Lou, X. *et al* 2010; Miller, S. *et al* 2010; Wei, Y. *et al* 1994]. Polyaniline exists in three major forms: (i) green color emeraldine salt, (ii) blue color emeraldine base and (iii) colorless leucoemeraldine base form (completely reduced states with absorbance in the UV-region less than 320 nm) in solution [Moon, D-K. *et al* 1993; Kurreck, H. *et al* 1984]. The change of the color from blue to colourless is particularly interesting for sensing applications since it matches with detection capabilities of the human-eye. The change of the color from blue (emeraldine base) to colourless form (leucoemeraldine base) is not a straight forward process because it accompanied by both protonation as well as electron transfer. This concept is not explored mainly due to two important reasons: (i) lack of complete solubility of polyaniline materials in water and (ii) mismatching of the redox potential of analytes with polyaniline backbone. Therefore, developing new approaches for making functionalized and water soluble polyaniline derivatives and explore them for colorimetric sensing via

naked eye detection is a challenging problem to be addressed for both fundamental understanding as well as developing new system for sensing of new chemical or biological analytes.

For this purpose, a water soluble N-substituted self-doped polyaniline, poly-N-sulfopropyl-aniline (**PSPA**) was designed and synthesized via oxidative solution polymerization route (see figure 5.3). The polymer was freely soluble in water which enabled its structural characterization by NMR and other spectroscopic techniques. The blue color sodium salt of the polymer (**PSPANa**) was employed as substrate for the detection of cysteine and vitamin-C. Dynamic light scattering and Zeta potential analysis were utilized to trace the molecular interactions and polymer self-assembly in doped and dedoped forms. The polymer aggregates act as nano-reactor site for efficient electron transfer (ET) process and was accompanied with instantaneous sharp change from blue to colorless for naked eye detection of Biomolecules (see figure 5.3.). Both Job's plot and molar ratio methods were employed to study the sensing properties and the binding constants were determined for polymer + analyte using Benesi-Hildebrand equation. The mechanism of the ET process was further confirmed by redox potential analysis by cyclic voltammeter. In a nut shell, in the present investigation, ET was cleverly utilized in a self-doped water soluble polyaniline for colorimetric sensing of biologically important molecules like vitamin-C and cysteine.

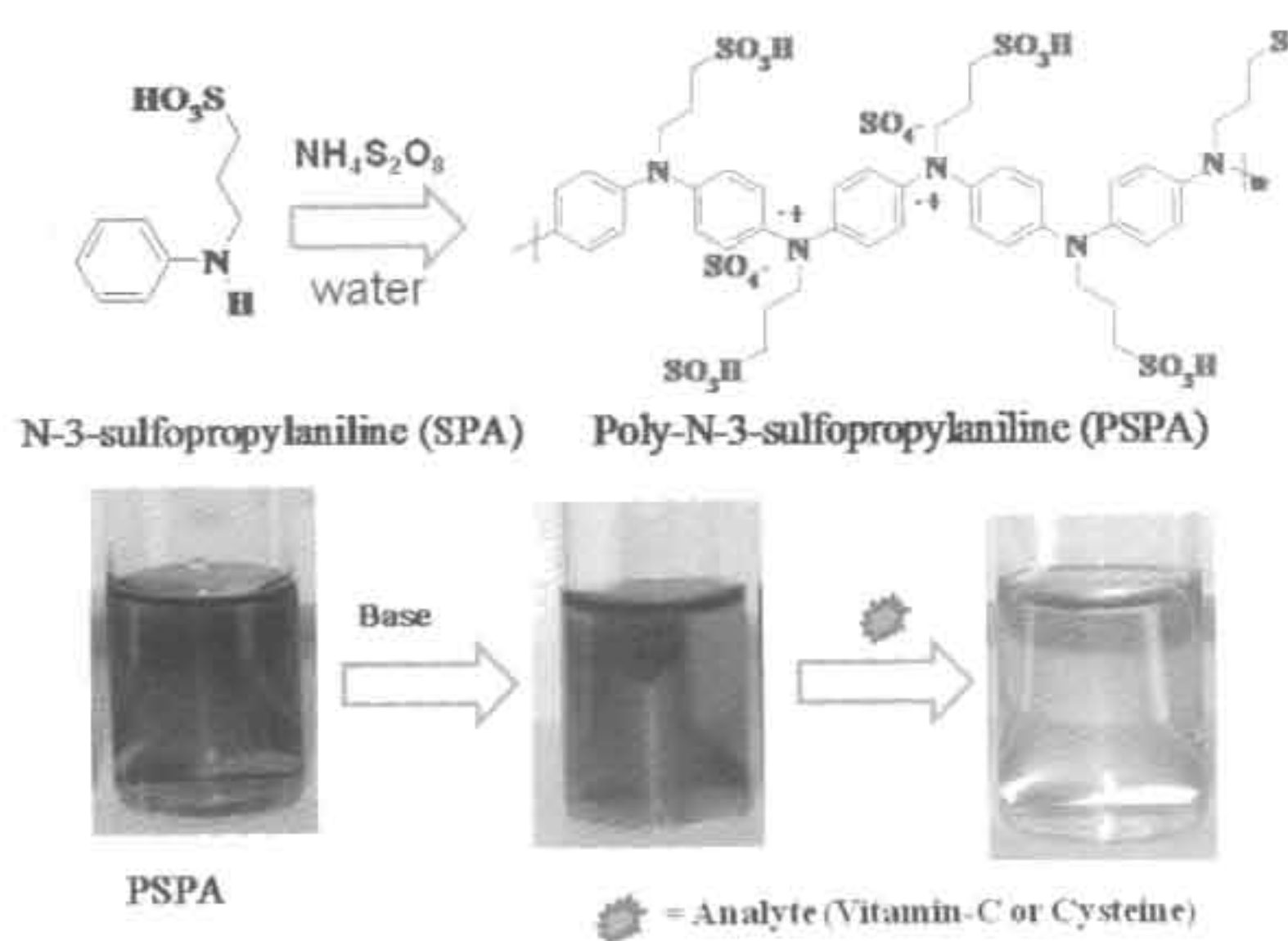


Figure 5.3. Synthesis of self-doped polyaniline and its sensing

5.2. Experimental Procedure

5.2.1. Materials: Aniline, ammonium persulphate (APS), propane sultone were purchased from sigma aldrich. Vitamin-C, sodium hydroxide, sodium carbonate and hydrochloric acid are purchased from merck chemicals (India). All the above chemicals are used without further purification.

5.2.2 General Procedure: NMR spectra of the compounds were recorded using a 500-MHz Bruker NMR spectrophotometer in D₂O containing small amount of tetramethylsilane (TMS) as internal standard. Infrared spectra of the polymers were recorded using Thermo scientific Nicolet 6700 FT-IR Spectrometer in the range of 4000-400 cm⁻¹. The purity of the samples was determined by fast atom bombardment high-resolution mass spectrometry (FAB-HRMS: JOEL JSM 600). The molecular weights of the polymers are determined using Applied Bio Instruments- 4800 Plus MALDI-TOF-TOF. For conductivity measurements, the polymer samples were pressed into a 10 mm diameter pellet and analyzed using a four-probe using Keithley 6221 DC and AC current source and 2181A nanovoltmeter. The resistivities of the sample were measured at five different positions. Temperature dependent measurement of the polymer samples carried out by a PID controlled heating oven. For SEM measurements, polymer samples were subjected to a thin gold coating using a JEOL JFC-1200 fine coater. The probing side was inserted into a JEOL JSM -5600 LV scanning electron microscope for taking photographs. TEM analysis was recorded using a Tecnai 30 G² S-twin 300 KV high resolution transmission electron microscope. For TEM measurements a suspension of self doped material are dispersed in methanol and deposited on a Formvar-coated copper grid drop by drop addition using glass dropper. Wide angle X-ray diffraction (WXRd) patterns of the finely powdered polymer samples were recorded by a Philips analytical Diffractometer using Cu-K α emission. The spectra were recorded in the range of $2\theta = 0- 40$ and analyzed using X'Pert software. The size determination of the polymer solution is carried out by DLS, Nano ZS-90 utilizing 633 nm red laser from Malvern instruments. UV-visible spectra of the polymers were recorded using Evolution 300 UV-Visible thermo-scientific instruments. pH of the samples are measured using pH

1500 pH meter from Eutech instruments and calibrated using buffer solution of pH 4 and 7 and 12. The thermal stability of the polymers was determined using PerkinElmer STA 6000 simultaneous thermal analyzer at a heating rate of 10 °C/min in nitrogen. TGA instrument was calibrated with calcium oxalate monohydrate as standard. The Differential scanning calorimetry of the samples were recorded by DSC Q 20 TA instruments, at a heating rate of 10 °C/min in nitrogen atmosphere and the instrument is calibrated using indium standard. Cyclic voltammetry of the samples measured by epsilon E2 cyclic voltammeter using Ag/AgCl reference electrode, platinum counter electrode and glassy carbon working electrode.

Synthesis of N-3-sulfopropylaniline (SPA): Excess aniline (5.0 mL, 55.0 mmol) was taken in a 100 mL round bottom flask and propane sultone (1.35 g, 11.0 mmol) was added drop wise. The solution was stirred at room temperature for 6 h. The resultant white solid was poured into acetone, filtered and washed with acetone until the filtrate become colorless. The solid was dried under vacuum oven for 12 h at 50 °C. It was further purified by recrystallized from hot methanol. Yield = 8.80 g (95 %). ¹H-NMR (500 MHz, D₂O) δ: 7.46 (m, 3H, Ar-H), 7.36 (d, 2H, Ar-H), 3.47 (t, 2H, NH-CH₂-), 2.9 (t, 2H, CH₂-SO₃H), 2.06 (m, 2H, Aliphatic-H). ¹³C-NMR (125 MHz, D₂O) δ: 134.5, 130.4, 129.9, 122.3, 50.2, 47.7 and 20.9. FT-IR (KBr, cm⁻¹): 1594, 1472, 1168, 1045, 756, 695 and 609. FAB-HRMS (M.W = 215.06): m/z 214.65 (M⁺). Anal. Calcd. for C₉H₁₃NO₃S: C, 50.21; H, 6.09. Found C, 50.31; H, 6.01.

Synthesis of Poly-N-3-sulfopropylaniline (PSPA): N-3-Sulfopropyl-aniline (1.00 g, 4.7 mmol) was dissolved in water (17.0 mL). APS (1.06 g, 4.7 mmol) in water (3.0 mL) was added to monomer solution at 30 °C and the polymerization was allowed for 2 h without disturbance. The green polymer solution was precipitated into acetone, filtered and washed with acetone till the filtrate became colorless. The green powder was dried in a vacuum oven at 60 °C for 6 h. Yield = 0.85 g (85 %). ¹H-NMR (500 MHz, D₂O) δ: 7.46 (m, 3H, Ar-H), 7.37 (d, 2H, Ar-H), 3.48 (t, 2H, NH-CH₂-), 2.9 (t, 2H, CH₂-SO₃H), 2 (t, 2H, Aliphatic-H). FT-IR (KBr, cm⁻¹): 1579, 1493, 1401, 1163, 1045, 807, 736, 598 and 522. UV-visible (water, nm) λ max: 320, 415, 780 and 1040.

Synthesis of Sodium salt of Poly-N-3-sulfopropylaniline (PSPANa): Poly-N-3-sulfo propyl-aniline (1.00 g) was dissolved in water (1.0 mL) and treated with NaOH solution (1.0 mL, 5M). The solution was stirred and the resultant blue colored solution was precipitated from methanol. The blue powder was filtered and dried in vacuum oven 60 °C for 6 h. Yield = 0.95 g (95 %). ¹H-NMR (500 MHz, D₂O) δ: 6.77 (t, 2H, Ar-H), 6.4 (d, 4H, Ar-H), 3.22 (t, 2H, aliphatic), 2.76 (t, 2H, aliphatic), 2.3 (m, 2H, aliphatic). FT-IR (KBr, cm⁻¹): 1620, 1498, 1360, 1168, 1045, 817, 736, 603 and 527. UV-visible (in water, nm) λ_{max}: 300, 630, nm.

5.3. Results and Discussion

5.3.1. Synthesis and Characterization of Poly-N-3-sulfopropylaniline (PSPA)

The monomer N-3-sulfopropyl aniline was synthesized via ring opening of propane sultone with excess aniline and further purified by recrystallization from hot methanol. The monomer was polymerized in water using ammonium persulfate as oxidizing agent and the resultant polymer, poly-N-3-sulfopropyl-aniline (**PSPA**) was isolated as dark green solid (see figure 5.4.). Emeraldine salt (green solid) was reacted with sodium hydroxide or sodium carbonate to produce water soluble deep blue colored polyaniline emeraldine base, poly-N-3-sulfopropyl-aniline sodium salt (**PSPANa**). Interestingly, in the present case, the good solubility of the polymers both in emeraldine salt and base forms in water enabled their structural characterization by ¹H and ¹³C-NMR. ¹H NMR spectra of the monomer and polymers (**PSPA** and **PSPANa**) were recorded in D₂O and shown in figure 5.5. The peaks at 7.46 - 7.36 ppm in the monomer were assigned to aromatic protons and their aliphatic protons appeared at 3.47, 2.9 and 2.06 ppm. The emeraldine salt (**PSPA**) showed two peaks at 7.46 and 7.37 ppm with respect to benzenoid-ring aromatic protons. The three equally intense peaks at 7.15: 7.05: 7.95 with 1:1:1 intensity (J = 50 Hz) were assigned to N-H protons in the self-doped polyaniline [Zhang, J. *et al* 2005; Zhang, J *et al* 2007] Sodium salt of the polymer (**PSPANa**) showed large peaks shift compared to **PSPA**, the peaks corresponding to benzenoid-aromatic peaks were shifted to the up-field region at 7.04 and 6.65 ppm compared to that of its doped polymer. The broad peak appeared at 6.21 - 6.63 ppm was assigned to the aromatic protons of quinoid-rings in

the dedoped form. The disappearance of the N-H protons (at 7.15-7.95 ppm) and the appearance of the quinoid-ring protons in **PSPANa** directly provided evident for completely dedoped structure. ^{13}C -NMR spectra of the monomer, **PSPA** and **PSPANa** in D_2O showed peaks with respect to their number of aromatic and aliphatic carbon atoms (see figure 5.6.). The monomer showed four aromatic carbon atoms at 134.5, 130.4, 129.9, 122.3 and three aliphatic carbons at 50.2, 47.7 and 20.9 ppm with respect to its structure. **PSPA** showed two aromatic carbons in the benzenoid- ring appeared at 130 and 124 ppm (corresponding g and h carbon) and three aliphatic carbons (52, 48 and 22 ppm). The dedoped polymer (**PSPANa**) showed aromatic proton in 130 and 115 ppm and aliphatic protons in 49 and 22 ppm.

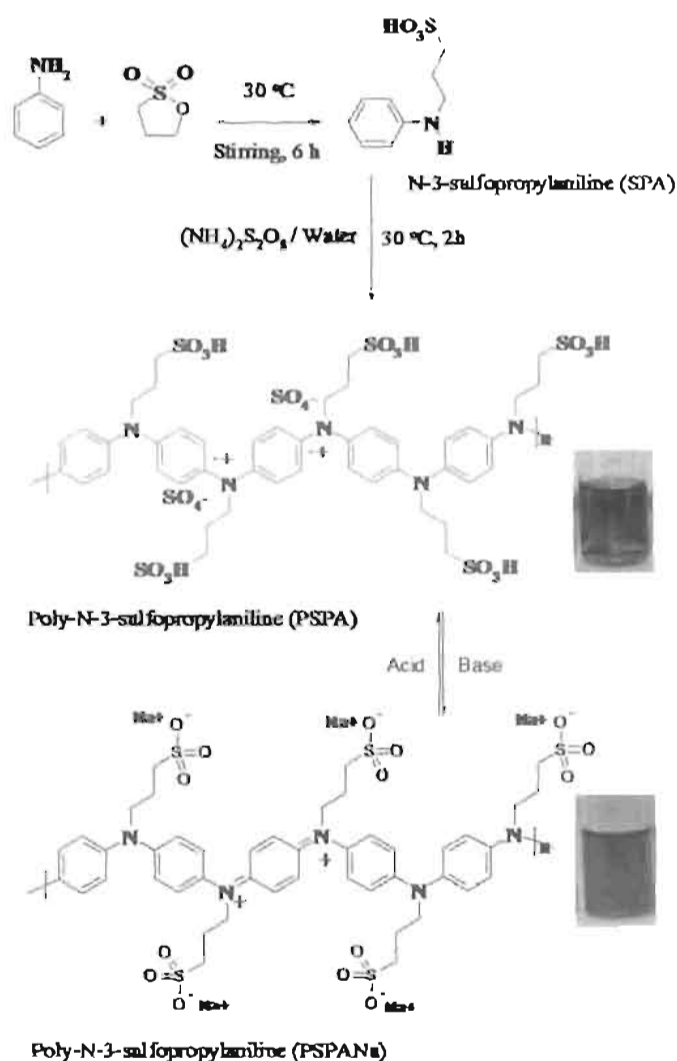


Figure 5.4. Synthesis of the monomer, doped polymer and dedoped polymer.

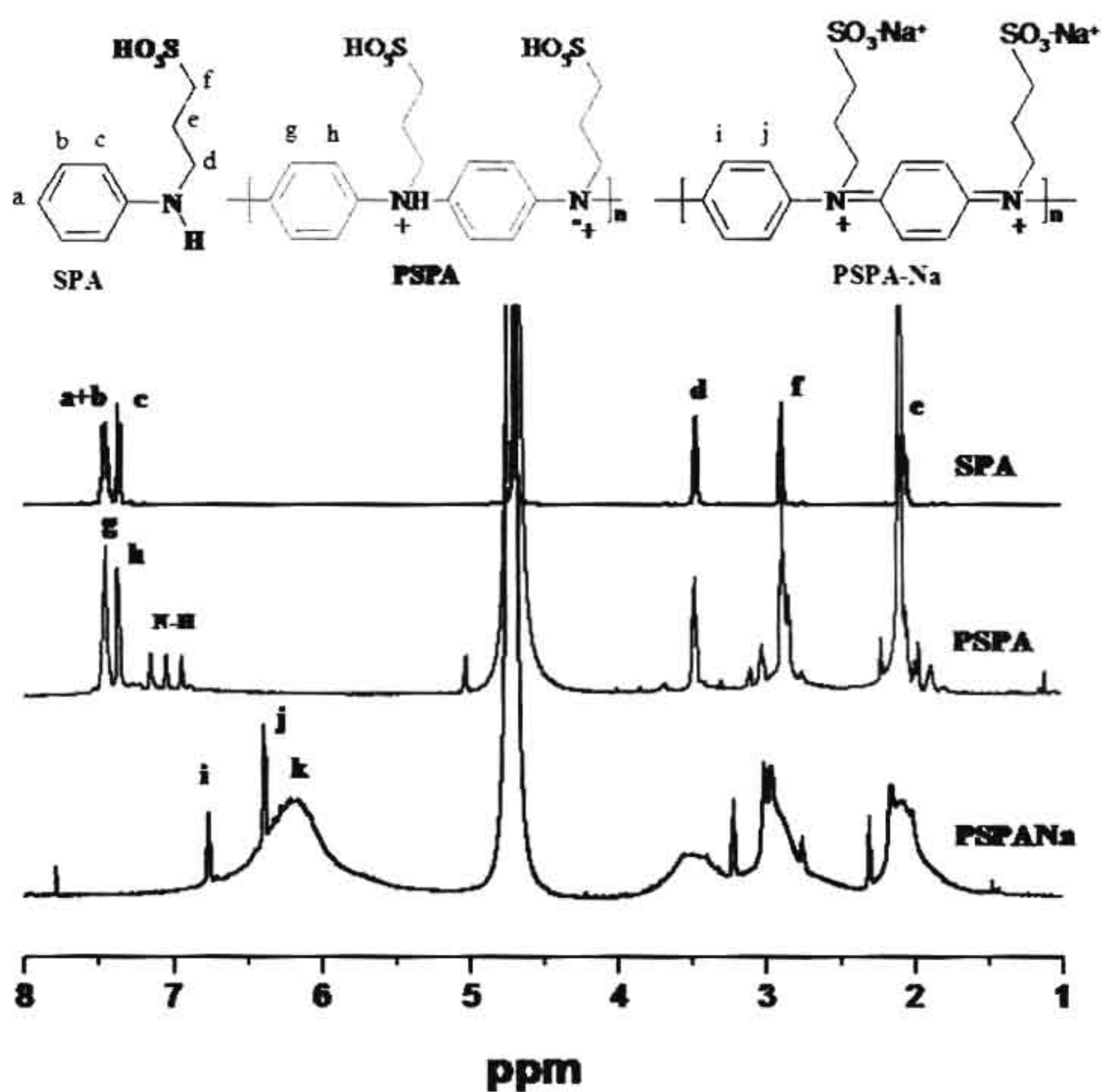


Figure 5.5. ^1H NMR spectra of the monomer (SPA), PSPA and PSPA-Na.

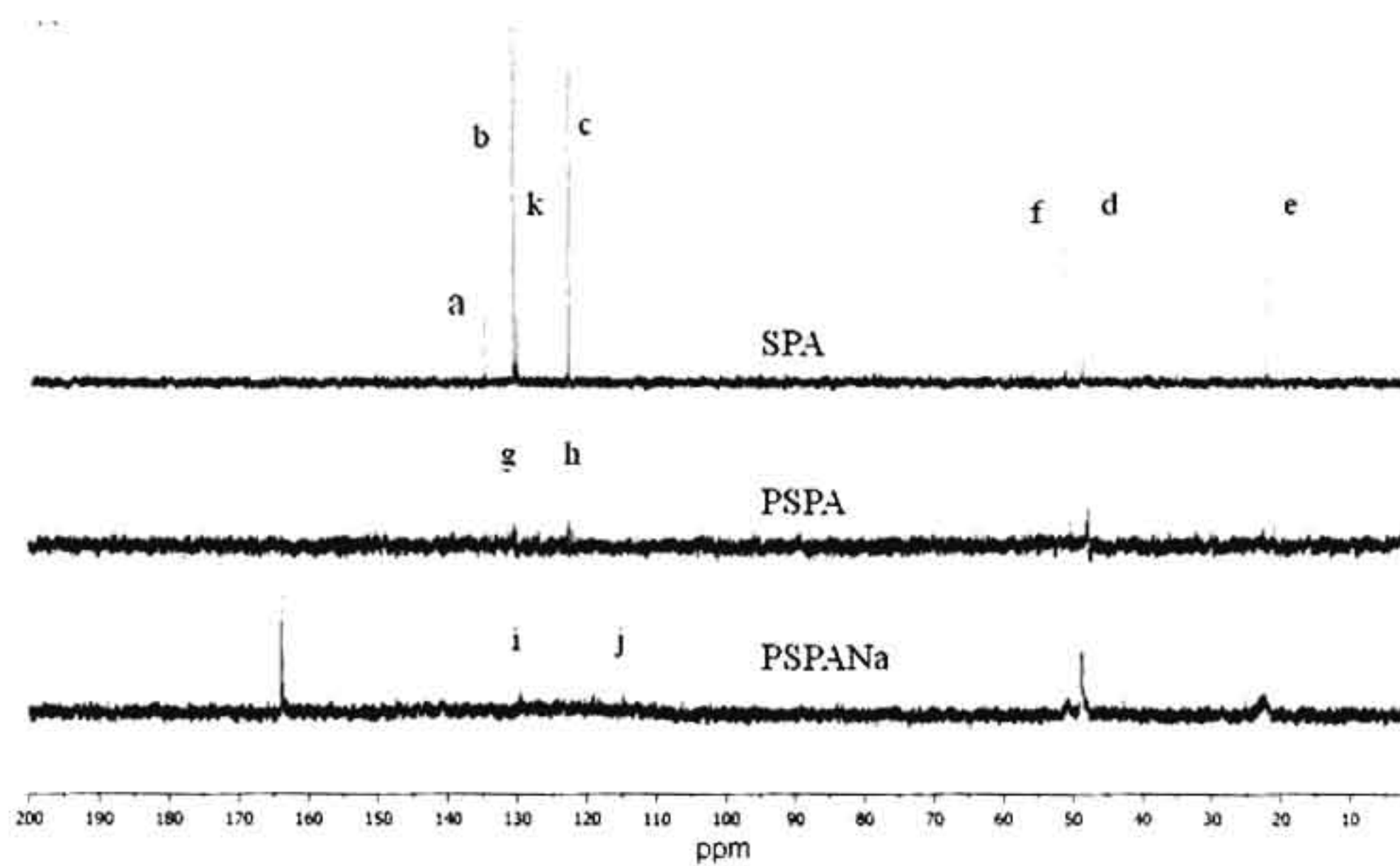


Figure 5.6. ^{13}C NMR spectra of the monomer (SPA), PSPA and PSPA-Na.

FT-IR spectra of the monomer, **PSPA** and **PSPANa** were recorded on KBr pellet and spectra were shown in figure 5.7. The two strong vibrations in the monomer at 1594 and 1472 cm^{-1} were assigned to symmetric (C=C) and anti-symmetric (C=C) stretching vibration [Nabid, M. R. et al 2005; Yuan G-L. et al 2003]. The peaks at 1599 and 1498 in the polymers were assigned to stretching vibration of C=C (quinoid) and C=C (benzenoid), respectively. The peaks at 1350, 1250 and 1041 cm^{-1} were assigned to C-N, O=S=O and C-H vibrations, respectively (Anilkumar et al). The inherent viscosity of the polymer was obtained as 0.18 dL/g in water at 30 °C which indicates the formation of moderate molecular weight polyanilines [Anilkumar, P. et al] 2008.

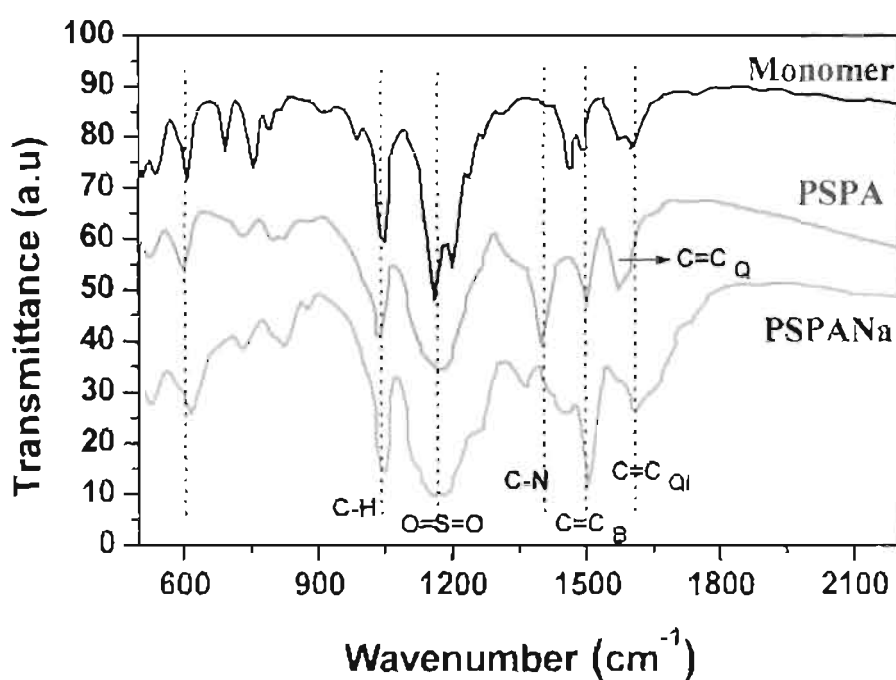


Figure 5.7. FT-IR spectra of the monomer (SPA), PSPA and PSPANa.

The doped polymer was subjected to MALDI-TOF analysis using α -cyano-4-hydroxy-cinnamic acid + trifluoroacetic acid (TFA) matrix (see figure 5.8.). The mass spectrum showed peaks at regular interval of 213 amu corresponding to the repeating units $(P)_n = (C_9H_{11}NO_3S)_n$. Two major peaks were observed at $(P)_n$ and $(P)_n+114$ corresponding to polymer and polymer + TFA. A less intense peak at $(P)_n+18$ also observed with respect to polymer + H_2O . Interestingly all these three peaks appeared exactly at a mass difference 213 amu, which was matching with the

repeating unit and indicated that the polymer contain 10-12 repeating unit in the polymer chains.

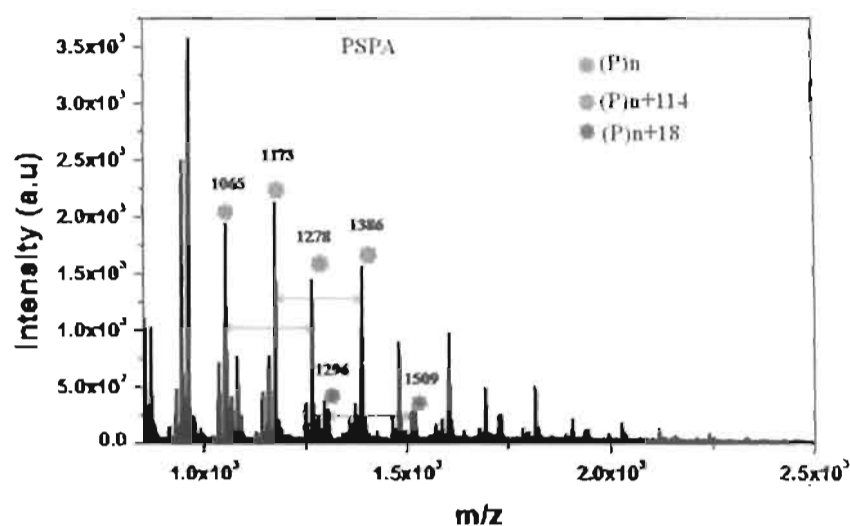


Figure 5.8. MALDI-TOFF spectrum of the PSPA.

5.3.2 Solid state properties of the self doped polymer

The morphology of the PSPA was analyzed by JOEL JSM -5600 LV scanning electron microscope (SEM) and high resolution transmission electron microscope (TEM). The SEM image of PSPA showed flake like structures see figure 5.9. TEM image of the polymer also confirmed the existence of the flake-like morphology. The tendency for the formation of flake-like morphology in the presence system is attributed to the self-doped structure of the polymers. The presences of sulfonic acid groups in the polymer chains induce strong inter-chain interactions for the formation of two dimensional flake-like growth rather than 1D fibrous morphology.

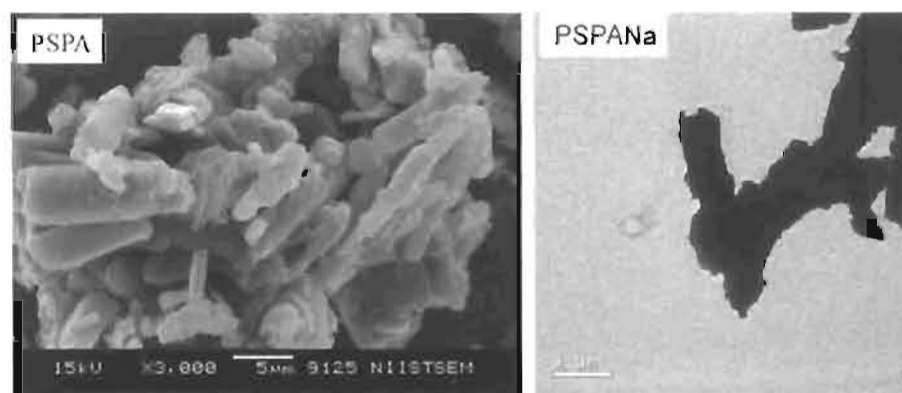


Figure 5.9. SEM and TEM of PSPA.

The **WXR**D of the monomer (**SPA**) and **PSPA** recorded by using powder method were shown in figure 5.10. Polymers samples were shown sharp peaks at $2\theta = 4.1$ degrees ($d\text{-SPACING} = 21.4 \text{ \AA}$) with respect to highly ordered polymer structure. The **PSPA** showed sharp peaks at 2θ values from 17 to 30 with respect inter chain interaction and aromatic $\pi\text{-}\pi$ interaction [Anilkumar, P. et al 2006]. WXR D analysis indicates that the **PSPA** is highly crystalline polymeric material resulting via electrostatic and hydrogen bonding interaction. The thermal transitions of the samples carried out using differential scanning calorimeter (DSC) were shown in figure 5.11. The monomer showed melting transition at $241 \text{ }^\circ\text{C}$ ($\Delta H = 30.7 \text{ J/g}$) and crystallized at $166 \text{ }^\circ\text{C}$ ($\Delta H = 27.1 \text{ J/g}$), respectively. Polymer **PSPA** showed endothermic melting and exothermic cooling peak at $139 \text{ }^\circ\text{C}$ ($\Delta H = 1.11 \text{ J/g}$) and $136 \text{ }^\circ\text{C}$ ($\Delta H = 1.08 \text{ J/g}$). Though, the enthalpy change is relatively small in the polymer compared to the monomer, the self doped polymer possessed tendency for melting or crystallization unlike the normal polyaniline samples. The dedoped polymer **PSPANa** did not show any thermal transition in heating or cooling cycles indicating its amorphous nature of the material in solid state.

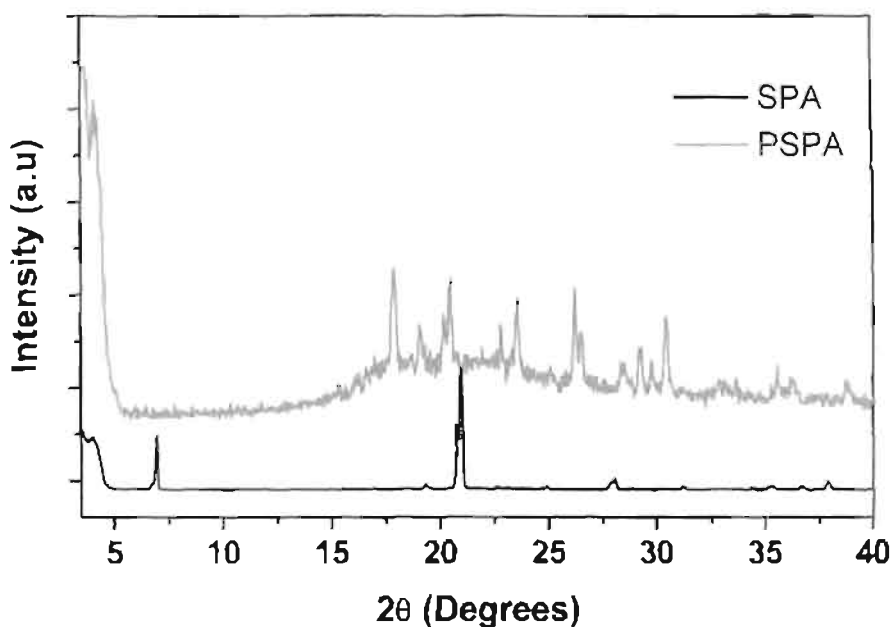


Figure 5.10. WXR D analysis of monomer (**SPA**) and **PSPA** .

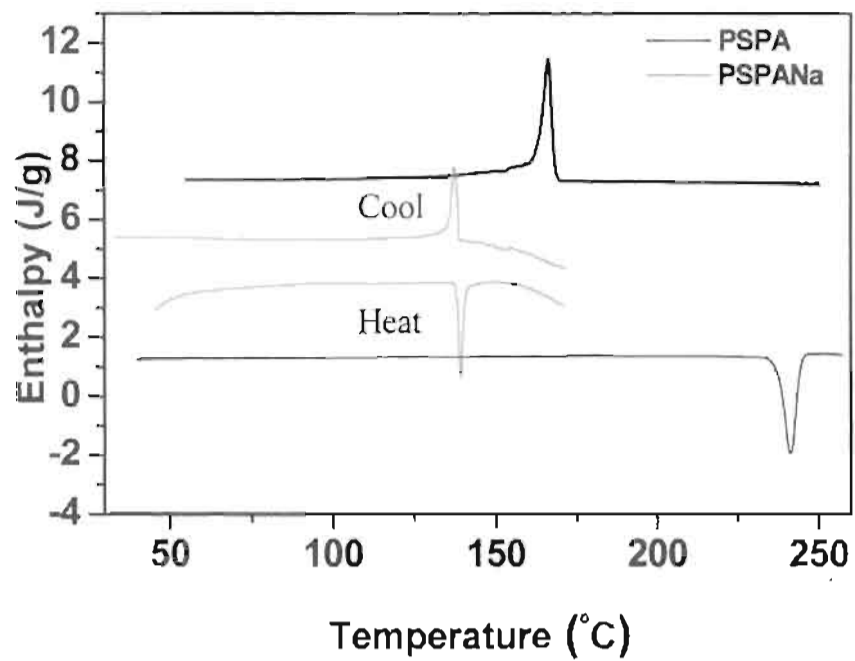


Figure 5.11. DSC thermograms of SPA and PSPA.

The thermal stability of PSPA and PSPANa were recorded by thermogravimetric analyzer under nitrogen flow and it revealed that the polymers were stable up to 370 °C (see figure 5.12.).

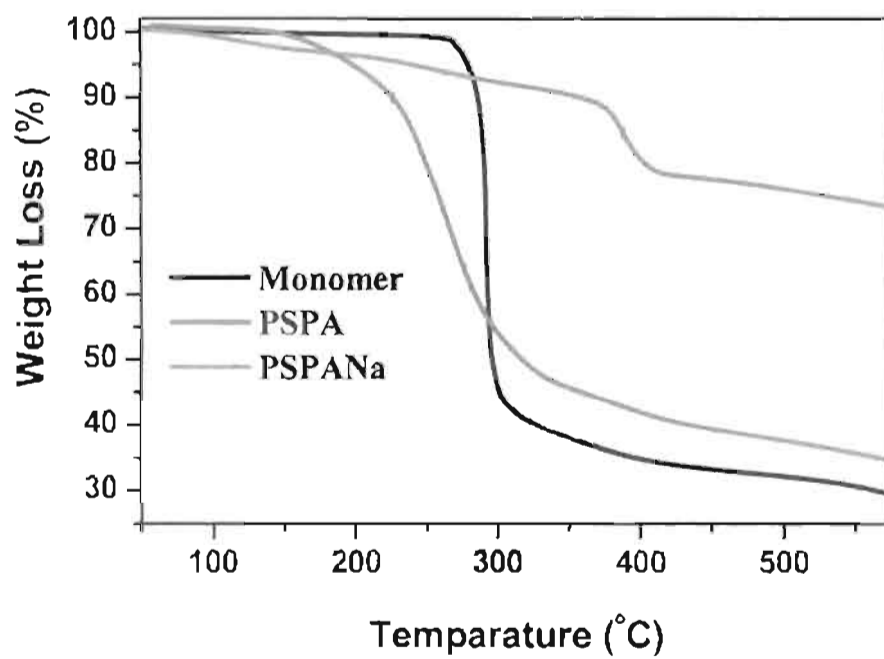


Figure 5.12. TGA analysis of the SPA, PSPA and PSPANa.

I-V plots for the polymers were measured using four probe conductivity meter and the polymers showed a linear increase in voltage with increase in current and followed typical of ohmic behaviour (see figure 5.13.). The conductivity of the doped and dedoped polymer samples were obtained as 1×10^{-3} and 6×10^{-5} S/cm respectively, which are matching with that of the values reported for N-substituted self-doped polyaniline samples [Wei, Y. et al 1994; Moon, D-K. et al 1993]

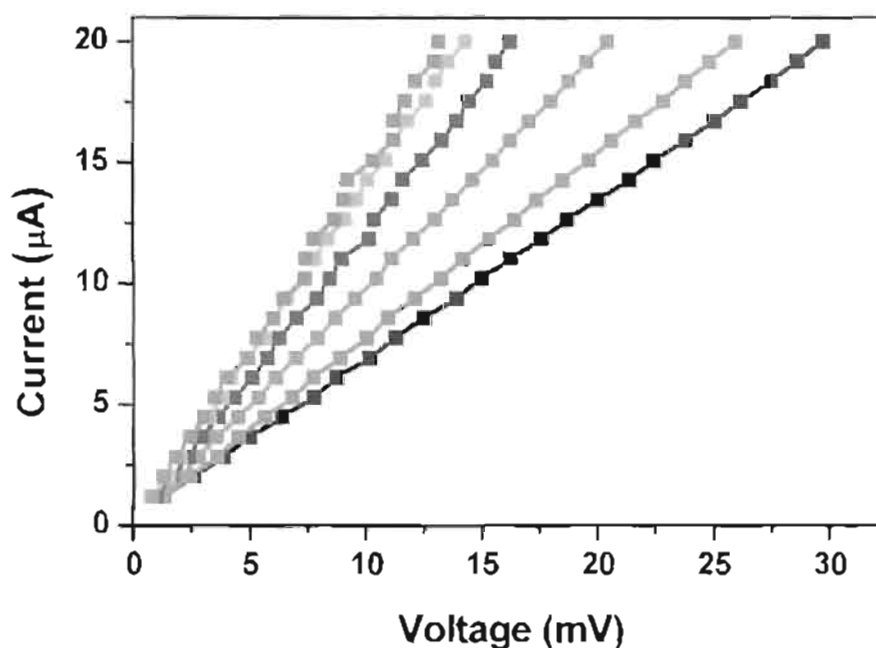


Figure 5.13. I-V plots of the PSPA.

5.3.3. Absorption properties and colorimetric sensing

The polymers both in doped and dedoped forms possessed good solubility in water and their absorption spectra for wider concentrations (from 10^{-3} to 10^{-5} M) were recorded, see figure 5.14. Absorbance spectra of PSPA showed three maxima at 305, 420 and 1040 nm corresponding to π - π^* , polaron- π^* , π -bipolaron electronic transitions, respectively. The sample PSPANa showed two peaks at 300 and 640 nm corresponding to π - π^* and exciton quinoid transitions, respectively [Chen, S-A. et al 1995; Nabid, M. R et al 2005; Yuan G- L. et al 2003]. The concentration dependent absorption spectra of PSPA and PSPANa did not show any change in peak position except the reduction in their intensities. This clearly support that the electronic structures of the self-doped (or dedoped) structures were very stable in water irrespective of their concentration.

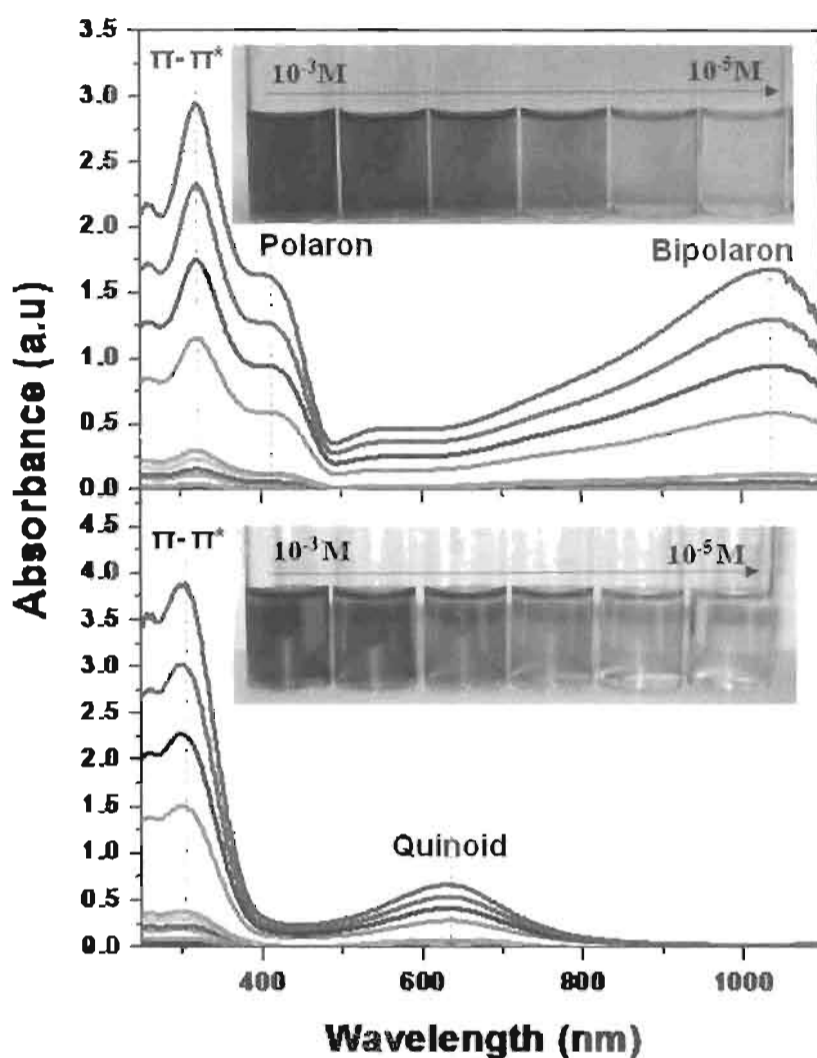


Figure 5.14. Concentration dependent absorption spectra of the *PSPA* and *PSPANa* at 30°C.

The polymer possessed in-built sulfonic acid group in the chain backbone, and therefore, the role of pH on the electronic transitions are very important to be analyzed. For this purpose, the concentration of *PSPA* was fixed as 1×10^{-3} M (pH = 3.2) and different concentration of base NaOH or Na_2CO_3 were added to vary the pH from 3.2 to 12. The absorbance spectra (see figure 5.15) showed that upon increasing the pH, the color of the polymer solutions transformed from the green to deep blue. This confirmed the change in the structure from emeraldine salt to emeraldine base with increase in the pH of the solution. The spectra showed major changes in the four different positions 305, 420, 640 and 1040 nm with respect to variation in the pH. On

increasing the pH from 3.2 to 12.0, the polaron (at 420 nm) and bipolaron (1040 nm) vanishes and a new peak at 640 nm corresponding to quinoid-ring was appeared. The change in the absorbance: $\Delta A = A_0 - A$, where A_0 and A are corresponding to the absorbance at initial and at particular pH (at 420, 640 and 1040 nm) was plotted against the pH of the solution (showed as in-set in the figure 5.15.). All the three ΔA plots showed sharp transition at pH = 8.6 – 9.6 with respected to their transformation in electronic structures from emeraldine base to salt. The pH dependent absorbance studies revealed that the newly synthesized water soluble N-substituted polyaniline provide very sharp change in the color which is very attractive for the colorimetric sensing applications.

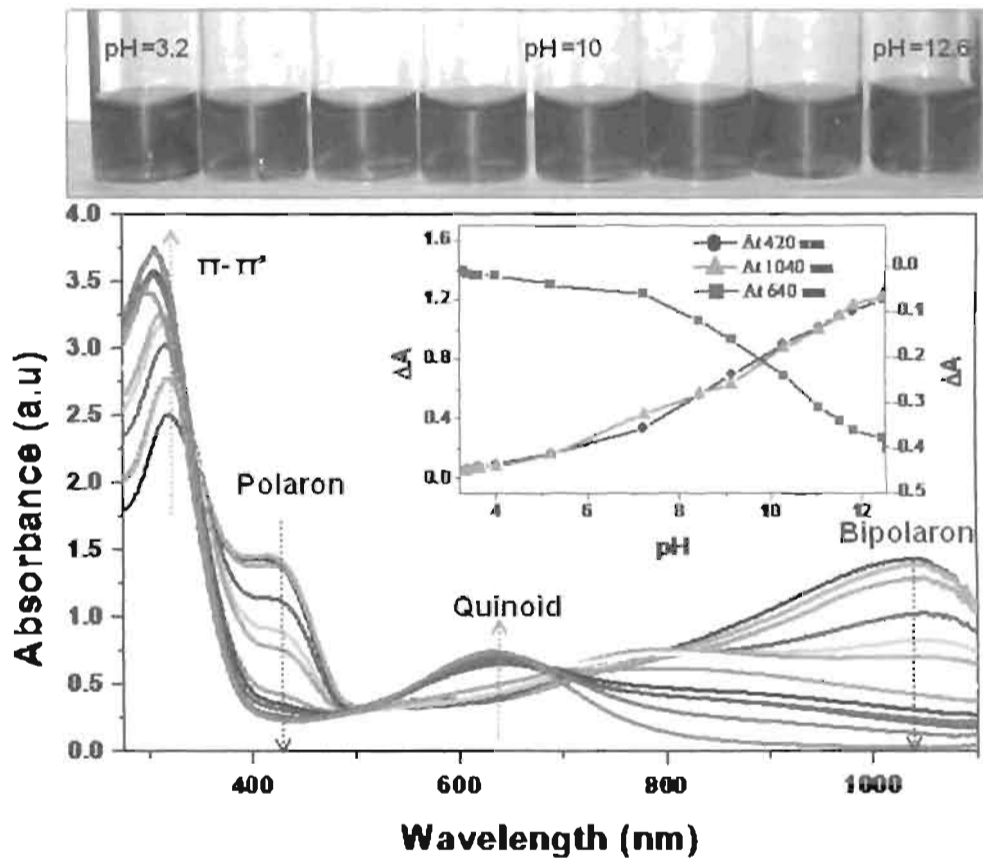


Figure 5.15. Absorption spectra of the PSPA with increase in pH. The photographs are showing the color changes in the solution with increase in pH.

In order to trace the sensing ability of **PSPANa**, it was treated with various acids (dopants) and biomolecules (see figure 5.16). As expected, typical dopants like camphorsulfonic acid (CSA) and HCl, showed color change from blue to green with respect to the transformation of emeraldine base to salt. The biomolecules like folic acid (vitamin B9), glycine and lysine did not show any change due to weak protonation ability of their carboxylic functional groups. Interestingly, vitamin-C (ascorbic acid) and cysteine showed a sharp and unexpected change of color from the blue to colorless.

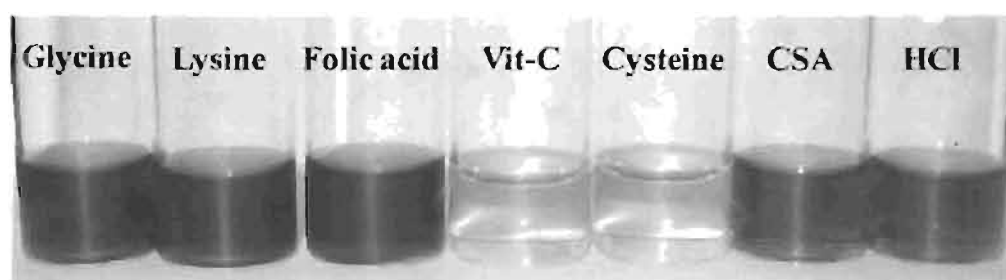


Figure 5.16. Colorimetric sensing of the vitamin-C and Cysteine using **PSPANa** in solution.

Further, a control experiment on PANI-EB (unsubstituted polyaniline) has been carried out by adding vitamin-C and cysteine to provide more insight to the phenomena. PANI-EB (blue color) was produced from PANI (green color) by dedoping with bases like NaOH or sodium carbonate (see figure 5.17). PANI-EB (blue) changes to greenish emeraldine salt after the addition of vitamin-C, on the other hand color was unchanged after cysteine addition. This clearly suggests that the unusual color change from deep blue to colorless by the self-doped polymer structure (**PSPANa**) was unique to the self-doped N-alkyl polyaniline and not for other emeraldine bases.



Figure 5.17. Control experiment with normal **PANI-EB**.

Further, selectivity of cysteine compared to other amino acids for more than 17 numbers were shown in figure 5.18. The studies showed that the self-doped polymer possessed high selectivity only for vitamin-C and cysteine and not for other biomolecules.

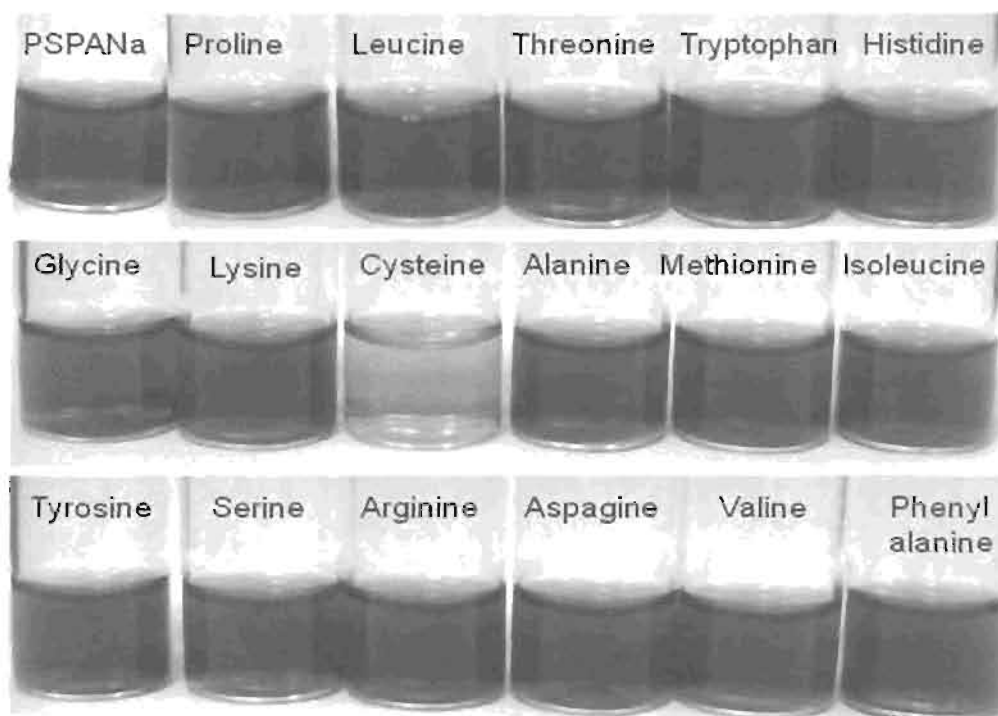


Figure 5.18. Colorimetric sensing of the Cysteine using **PSPANa** in solution.

Colorimetric detection of vitamin-C and cysteine by **PSPANa** were investigated by both Job's plot and molar ratio method. Job's plots for vitamin-C and cysteine are showed in figure 5.19. It is important to mention that sharp color change was noticed for vitamin-C in the sodium salts of polymers of NaOH and Na₂CO₃, however, the sensing for cysteine was found promising for polymer solutions obtained from Na₂CO₃ compared to NaOH. Upon adding vitamin-C (also cysteine), the color change was accompanied by disappearance of the peak at 640 nm (quinoid-ring) with increase in the absorbance at 300-320 nm. The spectral change at 640 nm was plotted against the mole fractions of the constituents and shown in figure 5.19 inset. The

stoichiometry of vitamin-C and cysteine with polymer was found as 3:2 and 4:1, respectively.

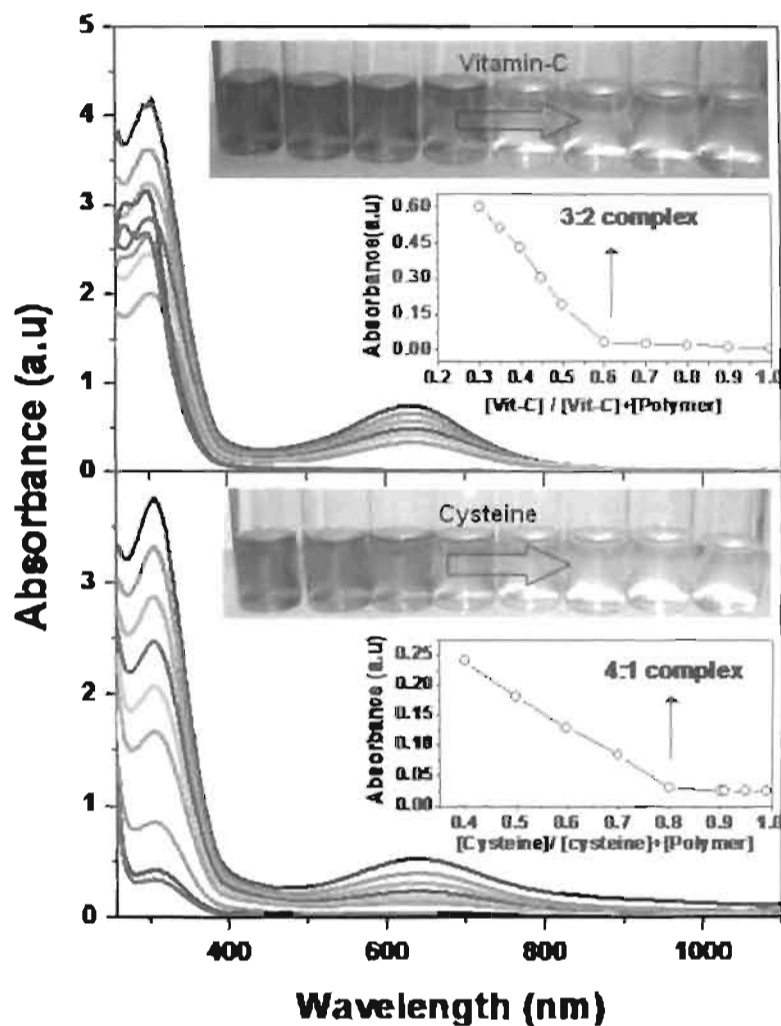


Figure 5.19. Job's Plot method for determining the stoichiometry of polymer + analyte complex via UV-Visible spectra

In order to determine the binding constant, molar ratio method was executed by varying concentration of the analyte (from 1×10^{-4} M to 2×10^{-3} M of vitamin-C and cysteine) with fixed polymer concentration (3×10^{-4} M) (see figure 5.20.). The association constants were calculated using Benesi-Hildebrand equation:

$$1/\Delta A = 1/[R^0]K\Delta\epsilon_{RS}[S^0] + 1/[R^0]K\Delta\epsilon_{RS}$$

Where, ΔA , $[R^0]$, $[S^0]$ and $\Delta\epsilon_{RS}$ are change in absorption, total receptor concentration, total substrate concentration and molar absorptivities of RS ($\Delta\epsilon_{RS} = \epsilon_{RS} - \epsilon_R - \epsilon_S$) [Atoud,

J. L. 1996]. The plot of $1/\Delta A$ versus $1/[\text{vitamin-C}]$ showed straight line plots which suggest that the polymer + analyte followed the Benesi-Hildebrand behaviour. The binding constant (K) were calculated from the intercept/slope of the plots as 2.1×10^3 and $1.5 \times 10^3 \text{ M}^{-1}$ for vitamin-C and cysteine, respectively. The binding constant values for vitamin-C and cysteine in the present case are comparable with that of other sensing substrate molecules like fluorescence [Zou, W. et al 2006].

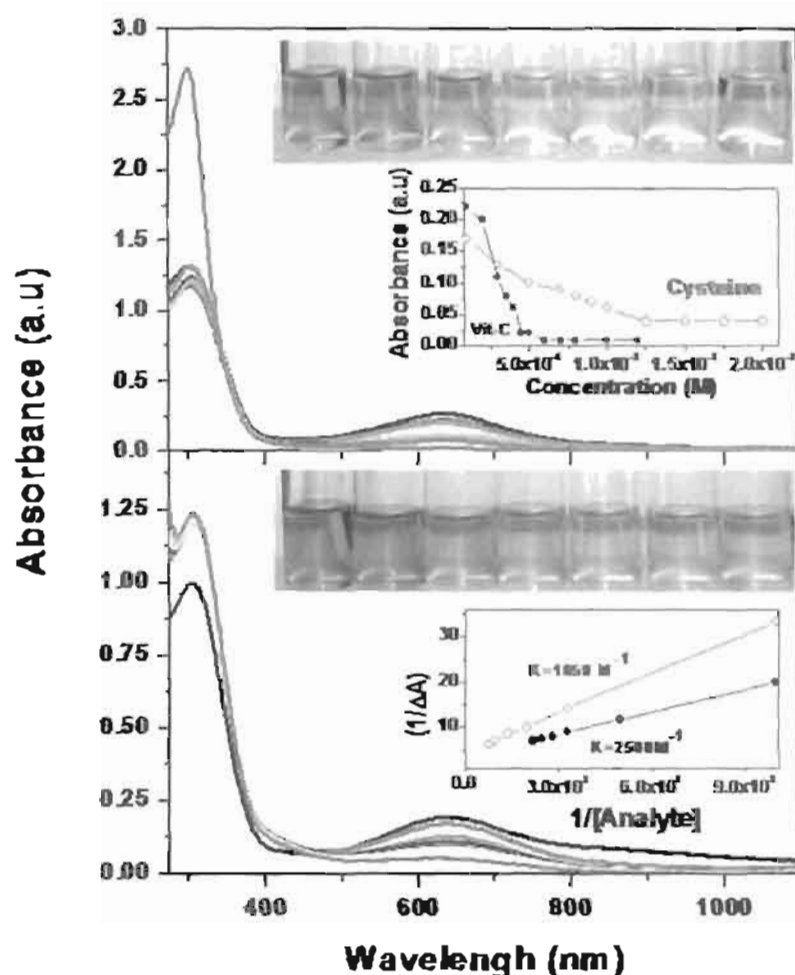


Figure 5.20. Mole ratio method for determining the stability constant for polymer + analyte complex via UV-Visible spectra.

To study the colorimetric sensing ability in solid state form (for practical applications), a simple technique was constructed (see figure 5.21). Thin layer of surgical grade cotton was rolled over plastic stick and dipped into the PSPANa solution to make uniform blue coating. The blue color stick was stable for more than two days without color bleaching. Half-portion of blue stick was dipped to analyte solution of vitamin-C, cysteine, HCl and CSA. The blue color immediately changed

into colorless for vitamin-C and cysteine. On the other hand green color was appeared with respect to emeraldine salt formation for hydrochloric acid and camphor sulfonic acid solution. The detailed calorimetric studies in solution as well as in the solid support (on cotton) revealed that the present water soluble polyaniline possessed unique blue to colorless sensing ability for biomolecules like vitamin-C and cysteine in solution as well as solid state.

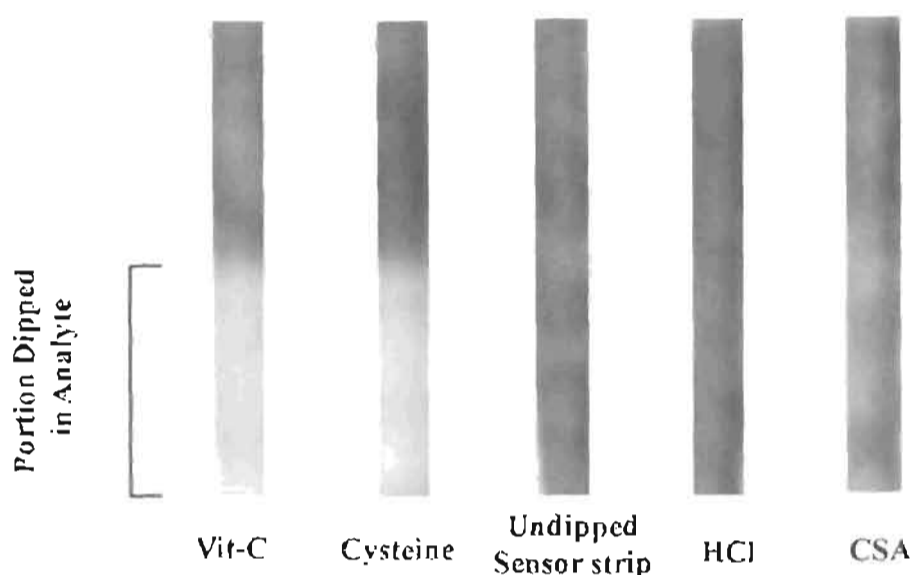


Figure 5.21. Sensing action of analytes in solid supported cotton roll.

5.3.4. Mechanism of colorimetric sensing

The mechanism for the sensing of vitamin-C and cysteine is given in figure 5.22. The chemical structures of N-alkylated polyanilines are different from the normal polyaniline [Kim, E. et al 1995; Lindfors, T. et al 2002; Bergeron, J et al 1990]. The self-doped polyaniline exists as in the emeraldine salt (I) consisting of cation-radicals of p-phenylenediamine. Addition of base, results in the formation of dedoped emeraldine base (II) consisting of di-cations of p-phenylenediimine. The di-cations were stabilized by sulfonate anions attached in the adjacent polymer chains via electrostatic self-assembly [Chen, S. A. et al 1994; Cataldo, F. et al 2002]. Vitamin-C (ascorbic acid) is a dibasic acid for proton transfer to bases and also good reducing agent via donating electrons. In water, it undergoes dissociation to produce dehydroascorbic acid and gives away $2e^-$ and $2H^+$. Cysteine is another important

reducing bio-molecule which undergoes self-oxidation to produce cystine with disulfide linkage and give away $2e^-$ and $2H^+$. Therefore, the reaction of vitamin-C and cysteine with N-alkyl polyaniline backbone is an example of proton induced electron transfer process from the analyte to substrate. The additions of vitamin-C (or cysteine) into polymer induces the following changes: (i) protonation of sodium salts of

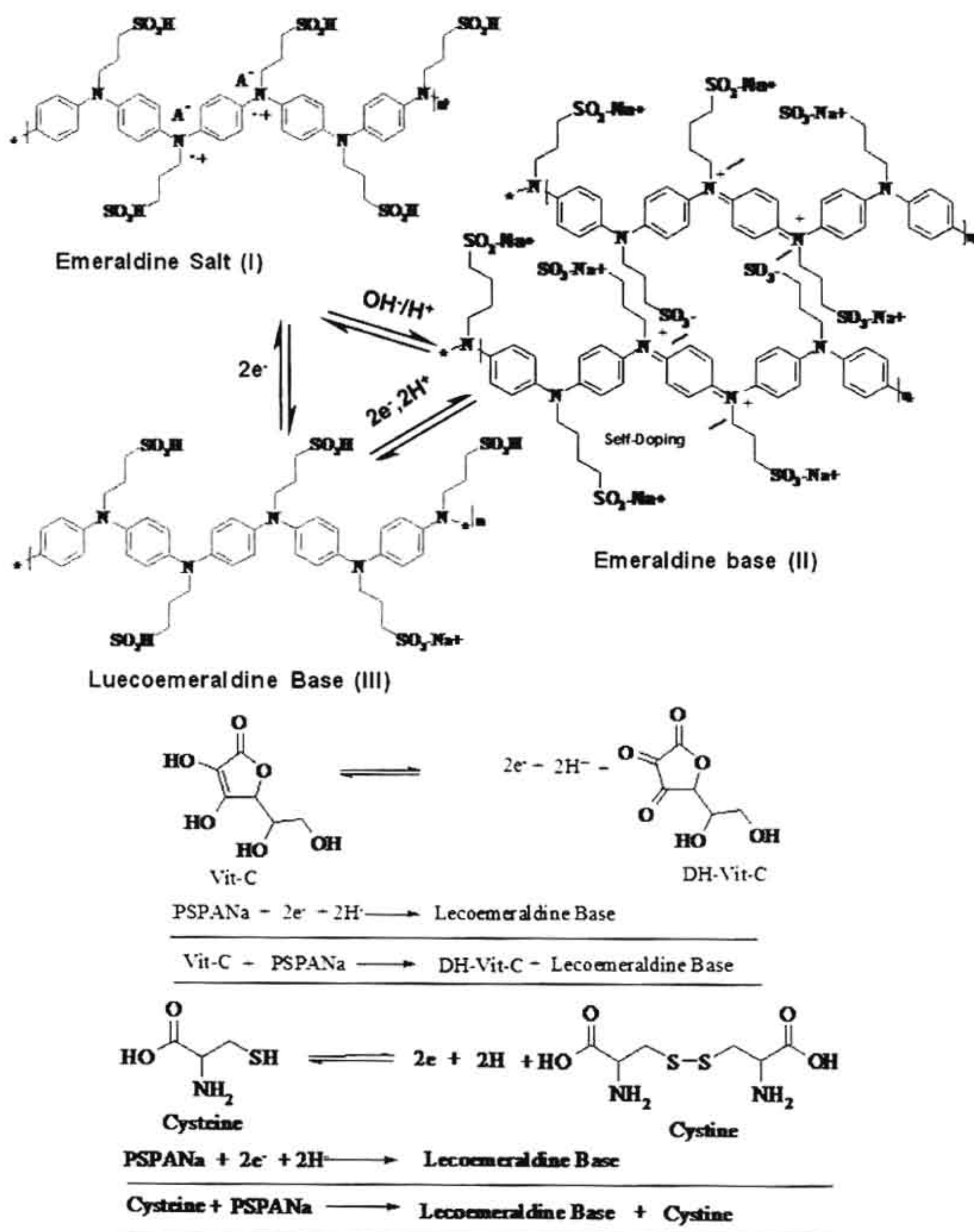


Figure 5.22. Proposed mechanism of colorimetric sensing.

sulfonic acids in the alkyl side chain which further disassociate the electrostatic interaction between SO_3^- and Ph-N^+ cations. (ii) transfer of the two electrons from analyte to the di-cations of p-phenylenediimine units in the polymer and convert the polymer chain into completely reduced form. (i.e leucoemeraldine base). As a net result of the proton coupled electron transfer from vitamin-C (also cysteine) to **PSPANa** (blue color); the color of the polymer solution changes from blue to colorless. Since the kinetics is very fast (observed in the range of $k_{\text{ET}} = 4 \times 10^6 \text{ s}^{-1}$), it accompanies the color change instantaneously for colorimetric detection by naked eye [Young, E.R. et al 2009]. The higher stoichiometry (4:1, in moles) of cysteine could be explained from the mode of chemical reaction it undergoes during sensing process. Two cysteine molecules are oxidized to form one cystine molecule to give 2H^+ and 2e^- . On the other hand, in the case of vitamin-C, each molecule undergoes oxidation to dehydroascorbic acid (DHAA) and 2H^+ and 2e^- . This further reflects in the high detecting ability of vitamin-C and higher association constant compared to that of cysteine.

To understand the electron transfer process, the oxidation and reduction potential of **PSPANa** and its complexes with vitamin-C and cysteine were determined by cyclic voltammetry in water using glassy carbon working electrode (see figure 5.23.). For all samples a C.V. was recorded in the range of +1.2 V to -1.2 V at the scan rate of 50 mV/s and the bases (NaOH and Na_2CO_3 in water) act as electrolytes. The cyclic voltammogram of **PSPANa** showed anodic oxidation peaks at 0.46 mV in the anodic sweep and a reversible reduction peak at -0.21 V in the negative cathodic region [Heras, J. Y. et al 2007; Krishnamoorthy, K. et al 2001]. Under the same sweeping condition, the oxidation potential of vitamin-C and cysteine alone were found as 0.11 V and 0.64 V, respectively. The cyclic voltammograms of the vitamin-C + **PSPANa** and cysteine + **PSPANa** complexes showed complete disappearance of the cathodic peak at -0.21 V. The disappearance of the cathodic peak at -0.21 V upon the addition of analytes (vitamin-C and cysteine) revealed the electron transfer from the analyte to the polymer backbone and supports the mechanism proposed in figure 23. It confirmed that the water soluble self-doped polyaniline is very unique and efficient sensor materials for detecting biomolecules like vitamin-C and cysteine via proton coupled electron transfer process in water

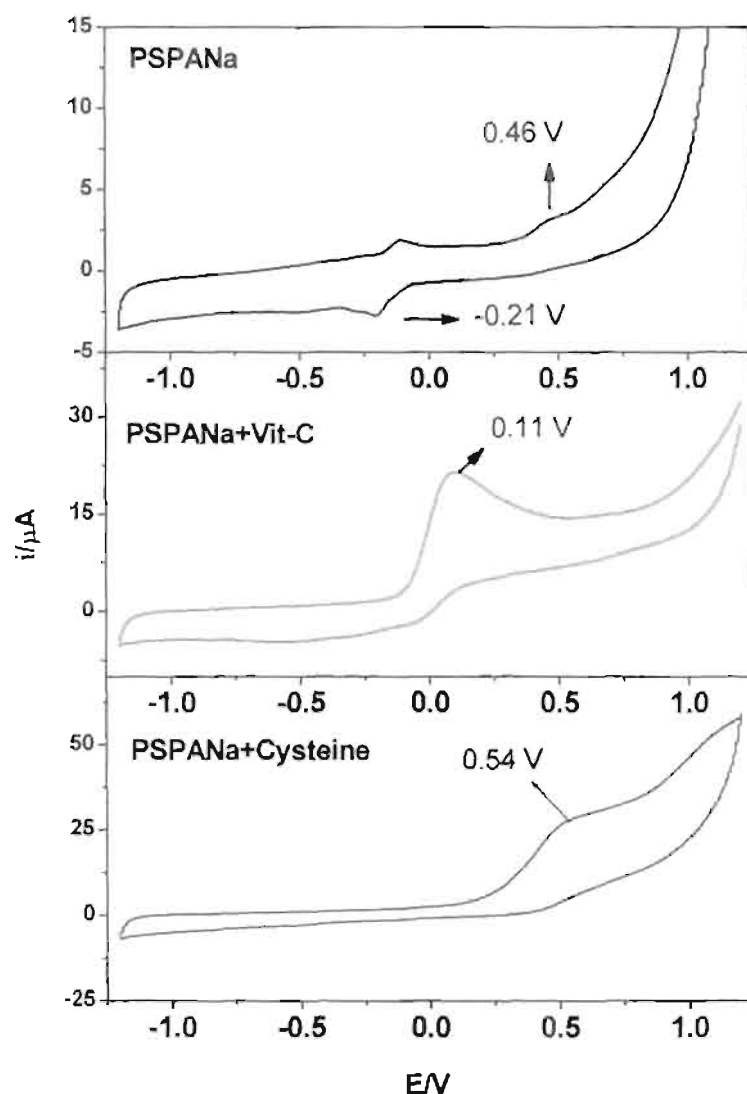


Figure 5.23. Cyclic voltammograms of *PSPANa*, *PSPANa+ Vit-C* and *PSPA +cysteine*.

5.3.5. DLS and Zeta potential studies on the polymer solution

It is very surprising to notice that in the present case, the ET process was efficient between the conducting polymers with analytes (vitamin-c or cysteine) which are not chemically interconnected together. Therefore, it is very important to trace the molecular interactions between vitamin-C (and cysteine) with *PSPANa* to understand the ET process. In order to trace the molecular interactions, the polymer solutions in doped (*PSPA*) and dedoped (*PSPANa*) forms were subjected to dynamic light scattering (DLS) coupled with zeta potential measurements. DLS histograms of

PSPA, PSPANa, PSPANa + vitamin-C and at PSPANa + cysteine are shown in figure 5.24.

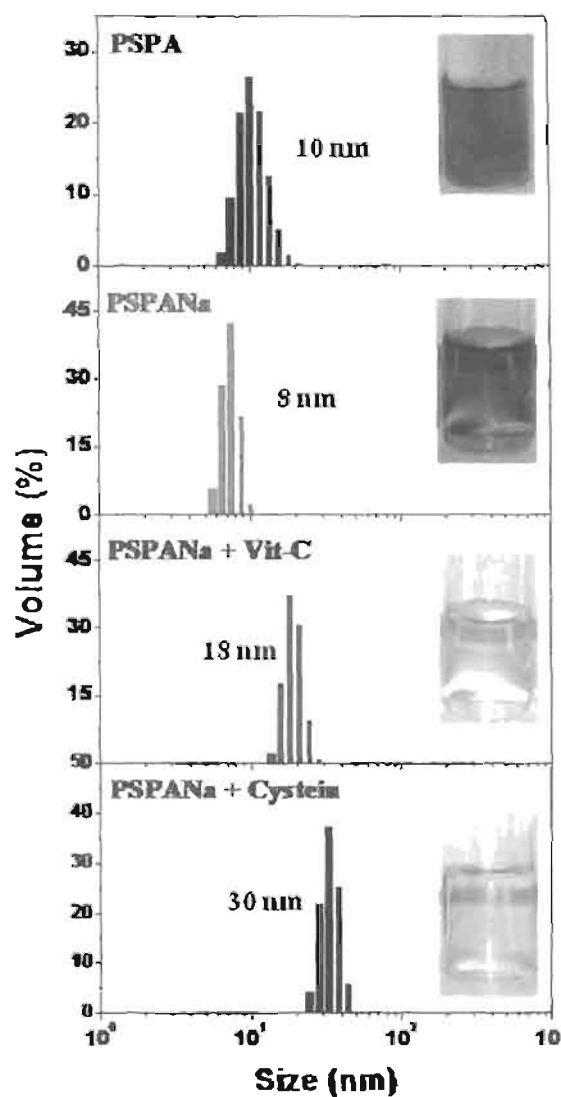


Figure 5.24. DLS histograms of PSPA, PSPANa, PSPA+ Vit-C and SPA+ Cysteine at $4 \times 10^{-4} M$.

The polymer samples in doped and dedoped form showed uniform distribution of aggregates with average sizes of 8 and 10 nm, respectively. It suggests that the self-doped n-alkyl sulfonated polymer self-assembled to produce polymeric nano-micellar aggregates. The polymers possessed typical amphiphilic structure in which the aromatic backbone and alkyl sulfonic acid groups act as hydrophobic and hydrophilic parts. The polymers produce micellar aggregates via core-shell architecture in which

the hydrophilic sulfonic acid part are kept outside facing the aqueous environment and the polyaniline backbone provides hydrophobic core. The schematic model for the polymer nano-aggregates is shown in figure 5.25. Upon dedoping the PSPA with sodium hydroxide, the outer sulfonic acid groups converted into sodium sulfonate and the polyaniline backbone became quinoid, however, the hydrophilicity of the core and outer shell were retained. Therefore, during chemical doping/dedoping process, the polymer chains were retained in the nano-aggregate forms without affecting the hydrophilic/hydrophobic nature of the aggregates.

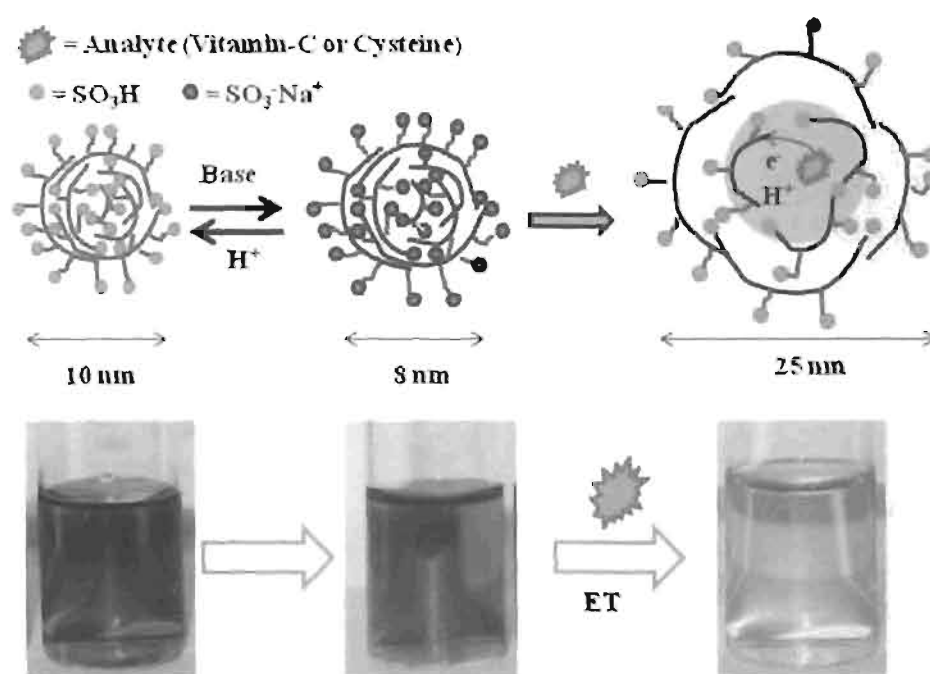


Figure 5.25. Schematic representation of the colorimetric sensing.

Zeta potential measurement is very important tool for understanding the solution dynamic of charged particles or aggregates like the doped and dedoped polymers in the presence case. Electrically charged species tend to move under the influence of an electric field and the electrical potential at the surface of the sphere of radius 'a' and carrying charge q is: $\zeta = q / 4\pi\epsilon a$, where ζ and ϵ are zeta potential and permittivity of the medium in which they are immersed [Evert, D. H. et al 1988]. The effect of concentration on the size of the micellar aggregates and their zeta potential are shown in figure 5.26. The size of the nano-aggregates in PSPANa was less

influenced by concentration variation and the values were found in the range of 10 ± 2 and 8.0 ± 2 nm for both doped and dedoped structures, respectively. The aggregate

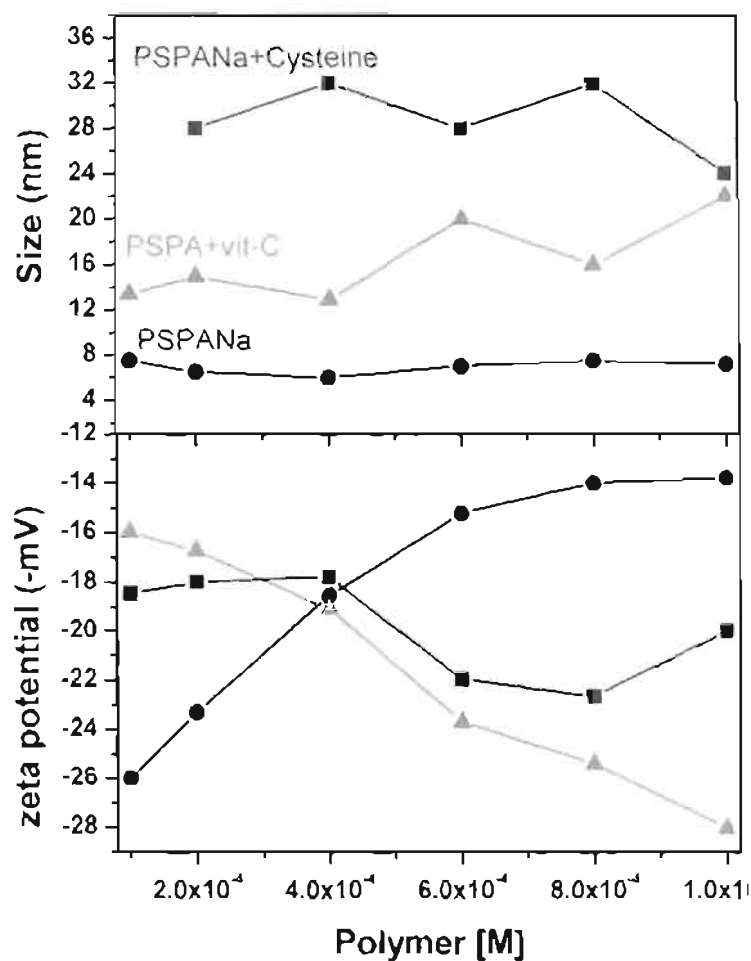


Figure 5.26. Size and Zetapotentials of the PSPANa, PSPANa+Vitamin C and PSPANa+Cysteine at various polymer concentrations for fixed [analyte] = $1 \times 10^{-3} M$.

sizes of the PSPANa + vitamin-C and PSPANa + cysteine complexes were found much higher than that of their homopolymer aggregates. The addition of analytes into the polymer solution increase the sizes of aggregates from 10 to 20 and 30 nm for vitamin-C or cysteine, respectively. The analytes are typical organic molecules and preferentially occupied the hydrophobic cavity provided in the nano-aggregates and these phenomena attributed to the increase in the size of the aggregates. The DLS analysis was also done for stored polymer solution over period of a one week; the polymer did not phase separate and the results were almost reproducible. Zeta potential of the polymer nano-aggregates possessed negative charges, however, their

magnitude vary with the types of the structures. All the three plots in the zeta potential versus concentration showed a non-linear trend with a break points at 4.0×10^{-4} M, which is very close to the critical micellar concentration (CMC) of these nano-aggregates. Since polymer chains possessed long range chain interactions, unlike in the case of small molecule surfactants, it may contain critical association well below the CMC. Nevertheless, the detailed DLS and zeta potential studies confirmed that the additions of vitamin-C or cysteine did not destabilize the polymer nano-aggregate and the aggregates are stable for wider concentration range for the detection process. Thus, electron and proton transfer efficient occurred between the analyte and polyaniline backbone for colorimetric sensing of vitamin-C and cysteine in nano aggregate see.

5.4. Conclusion

In conclusion a water soluble self-doped polyaniline was synthesized and successfully utilized as substrate for detection of biomolecules like vitamin-C and cysteine via electron transfer process. The important outcomes of the present investigation are as follows: (i) N-propylsulfonic acid aniline monomer was synthesized via ring opening of sultone which was further polymerized via chemical oxidative route to produce completely water soluble polyaniline. (ii) the structure of the polymers in doped and dedoped forms were characterized by both ^1H and ^{13}C -NMR and the molecular weights were determined by viscosity and MALDI-TOF techniques. (iii) pH dependent absorbance studies revealed that the newly synthesized water soluble N-substituted polyaniline provide very sharp color change which is very attractive for the colorimetric sensing applications. (iv) various dopants like camphorsulfonic acid (also HCl) showed expected color change from blue to green with respect to the transformation of emeraldine base to its salt. (v) the unusual color change from deep blue to colorless by **PSPANa** was unique to the self-doped N-alkyl polyaniline structure and provides new opportunity for sensing of biomolecules like vitamin-C and cysteine by simple colorimetric techniques. (vi) Job's plots for vitamin-C and cysteine established the stoichiometric composition of vitamin-C and cysteine with polymer as 3:2 and 4:1, respectively. (vii) the binding constants were determined by molar ratio method using Benesi-Hildebrand plots; $K = 2.1 \times 10^3$ and $1.5 \times 10^3 \text{ M}^{-1}$ were obtained for vitamin-C and cysteine, respectively. (ix) the vitamin-C

undergo dissociation to produce 2H^+ and 2e^- which were donated to sulfonate anions and di-cations of p-phenylenediimine backbone via proton coupled with electron transfer process, (x) cysteine undergoes self-oxidation to produce cystine with disulfide linkage and give away 2e^- and 2H^+ which were donated to polyaniline as in the case of Vitamin-C. (xi) cyclic voltammetry studies confirmed the electron transfer from the analyte to polymer with disappearance of the cathodic peak at -0.21 V in the polymers upon the addition of analytes (vitamin-C and cysteine) and (xii) dynamic light scattering with zeta potential measurements confirmed the existence of 8-10 nm aggregates of polymer self-assembly in water. The analytes are typical organic molecules and preferentially occupied in the hydrophobic cavity provided in the nano-aggregates in which the efficient protons coupled electron transfer occurred between the analyte and polyaniline backbone for colorimetric sensing process. In a nut shell, ET process is successfully exploited between the N-substituted polyaniline and analytes for the detection of biomolecules like vitamin-c and cysteine.

Chapter-6

Summary and Conclusions

The thesis entitled “*Self-organization Approach for Conducting Polypyrrole and Their Copolymer Nanomaterials*” describes the self-organization approach developed for polypyrrole and polypyrrole-co-polyaniline nanostructures. Polypyrrole nanospheres were synthesised exclusively by emulsion route and size was controlled by dilution route. Role of oxidising agents like APS and FeCl_3 on morphology of polypyrrole nanospheres were also investigated. A composition dependant emulsion copolymerisation route was carried out to produce morphology transformation from fiber to rods to spheres. Dilution of the fixed composition of the copolymer emulsion was utilised to produce evolution of nanomaterials from nanorods to hollow spheres to nanotubes via oxidative polymerization. The I-V measurements shows that electrical resistance follows the order nanofiber < nanorods < hollow spheres < nanotubes were in accordance with the expected with transport for one dimensional nanomaterial. The nanomaterial were characterised by spectroscopic techniques and mechanism of nanomaterial formation were also discussed. A colorimetric technique was developed for biomolecules like cysteine and vitamin-C utilising the electron transfer (ET) mechanism of the self-doped polyaniline nano-aggregates.

An amphiphilic anionic surfactant 4-[4-hydroxy-2 ((Z)-pentadec-8-enyl) phenylazo]-benzene sulfonic acid, was developed from cardanol and utilized as molecular template for polypyrrole nanomaterials. DLS studies confirmed that the surfactant existed in the form of spherical micelles of 4.8 nm diameter in water. The micellar behaviour of the reaction medium was precisely controlled by varying the composition of [pyrrole]/[surfactant] ratio ranging from 3 to 100. Polypyrrole nanospheres of 150-800 nm were successfully prepared via oxidative polymerization route. The nanosphere formation was unperturbed by the variation of the oxidation agents such as ammonium persulphate (APS) or ferric chloride (FeCl_3). A dilution route polymerisation was carried out on fixed pyrrole: surfactant (1:1/100) ratio by varying the concentration. The size of the polypyrrole nanospheres were systematically controlled from 600 nm to 60 nm diameter. The mechanism of the polypyrrole nanomaterial formation was proposed on the basis DLS and electron microscopic studies on the template and nanomaterials. Larger size spherically aggregated micelles of pyrrole surfactant complex produced at higher concentration was diluted to produce smaller size aggregate micelles at lower concentration.

Surfactant micelles were selective towards aniline and pyrrole to produce cylindrical and spherical micelles respectively. Three structurally different anionic surfactants were developed having same polar head but difference in the hydrophobic tail and utilized for achieving size and shape control in polyaniline, polypyrrole, and their polyaniline-co-polypyrrole random copolymer nanomaterial. All anionic surfactants produce polypyrrole nanospheres, however, they interacted differently with aniline to produce nanofibers of 180 nm in diameter with length up to 3.5 μm . Interestingly, the morphologies of the copolymer nanomaterials underwent transformation from nanofibers to nanospheres via short nano-rod intermediates. Dynamic light scattering technique and electron microscopes were used to study the mechanistic aspects of the template-assisted copolymerization process. Four probe conductivities of the copolymers showed a nonlinear trend and the conductivity passes through minimum at 60–80% of pyrrole in the feed. The unexpected trend in the conductivities of the copolymers was correlated to the difference in the solid state ordering of the copolymer nanomaterials.

An effort has been put to understand the evolution of the different types of nanomaterial morphologies such as nanofiber, nanorod, nanosphere, and nanotube in a single system without changing their chemical composition or polymerization route. Anionic surfactant was self-organized with fixed composition of aniline (95%) and pyrrole (5%) and the resultant white emulsion was diluted with water to induce cylindrical to vesicular aggregate transformation. The chemical oxidation of the cylindrical templates produced nanofibers and nanorods, whereas hollow spheres and nanotubes were produced by vesicular templates. The size and shape of the template aggregates matched very well with that of the synthesized nanomaterials thereby providing direct evidence for the template-assisted evolution of the morphology. NMR, FT-IR and UV-visible spectroscopies were utilized to confirm the structure and electronic properties of the nanomaterials. Wide angle X-ray diffraction and transmission electron microscopy and electron diffraction analysis revealed that the nanotubes possessed three-dimensional lamellar type solid state ordering with high percent crystallinity up to 60%. Variable temperature four-probe conductivity measurements of all samples showed typical $I-V$ plots. The conductivity of the nanofibers was found one order higher than that of nanorod, hollow sphere, and

nanotubes at all temperatures. The present approach enabled to establish the role of various types of nano-morphologies on properties of nanomaterials such as conductivity and solid state ordering without change in their chemical composition.

Self doped polyaniline was developed based on custom designed N-sulfopropyl aniline monomer via chemical oxidative polymerization. Self-doped polymer is completely soluble in water which allowed its structural characterization by ^1H and ^{13}C NMR spectra. Dedoped sodium salt of polymer (PSPANa) was used for the colorimetric sensing of vitamin-C and cysteine. Based on the Job's plot method, the stoichiometry of vitamin-C and cysteine with polymer was determined as 3:2 and 4:1, respectively. Molar ratio method and Benesi-Hildebrand equations were used to determine the association constants: $K = 2.1 \times 10^3$ and $1.5 \times 10^3 \text{ M}^{-1}$ for vitamin-C and cysteine, respectively. The polymers possessed typical amphiphilic structure and zeta potential of the polymer nano-aggregates were found to show negative surface charges in the range of -10 to -30 V. The analytes are typical organic molecules and preferentially occupied the hydrophobic cavity provided in the nano-aggregates for efficient colorimetric sensing in water at biological conditions.

List of Publications

Publications in international Journals

1. **Antony, M. J.;** Jayakannan, M. Molecular Template Approach for Evolution of Conducting Polymer Nanostructures: Tracing the Role of Morphology on Conductivity and Solid State Ordering *J. Phys. Chem. B* **2010**, *114*, 1314-1324.
2. **Antony, M. J.;** Jayakannan, M. Self-Assembled anionic micellar template for polypyrrole, polyaniline, and their random copolymers. *J. Polym. Sci : Part A: Polym. Phys.* **2009**, *47*, 830- 846.
3. **Antony, M. J.;** Jayakannan, M. Amphiphilic Azobenzenesulfonic Acid Anionic Surfactant for Water-Soluble, Ordered, and Luminescent Polypyrrole Nanospheres. *J. Phys. Chem. B* **2007**, *111*, 12772-12780.
4. **Antony, M. J.;** Jayakannan, M. Polyaniline Nano-aggregates for Colorimetric Sensing of Cysteine and Vitamin-C (manuscript communicated for publication)
5. **Antony, M. J.;** Jayakannan, M. Role of Amphiphilic Azobenzene Dopants on the Morphology, Conductivity and Solid State Ordering Polyaniline-Polypyrrole copolymers (manuscript communicated for publication)

Publications in the international conference Proceedings

1. **Antony, M. J.;** Jayakannan, M. Self-assembly approach for evolution of copolymer nanostructures, ICMST-2010, Thiruvananthapuram, India, Oct 29-31-2010
2. **Antony, M. J.;** Jayakannan, M. Molecular template approach for conducting polymer nanomaterial *MACRO 2009*, Chennai, India, Mar 9-11, 2009.
3. **Antony, M. J.;** Jayakannan, M. Functionalized azobenzene surfactant mediated synthesis of polypyrrole nanospheres. *ICAMC-2007*, Thiruvananthapuram, India, Oct. 24-26, 2007.
4. **Antony, M. J.;** Jayakannan, M. Synthesis and size control of polypyrrole nanospheres, *IUMRS-ICAM-2007*, Bangalore, India. Oct 8-13. 2007.

Bibliography and References

- Abbett, K. F.; Teja, A. S.; Kowalik, J.; Tolbert, L. "Preparation of Conducting Composites of Polypyrrole Using Supercritical Carbon Dioxide" *J. Appl. Polym. Sci.* 90 (2003) 1113.
- Acik, M.; Baristiran, C.; Sonmez, G. "Highly surfaced polypyrrole nano-networks and nanofibers" *J. Mater. Sci.* 4 (2006) 4678.
- ^aAli, S. R.; Ma, Y.; Parajuli, R. R.; Balogun, Y.; Lai, W. Y. C.; He, H. "A non-oxidative sensor based on a self-doped polyaniline/carbon nanotube composite for sensitive and selective detection of the neurotransmitter dopamine" *Anal. Chem.* 79 (2007) 2583.
- ^bAli, S. R.; Parajuli, R. R.; Ma, Y.; Balogun, Y.; He, H. "Interference of ascorbic acid in the sensitive detection of dopamine by an nonoxidative approach" *J. Phys. Chem. B.* 111 (2007) 12275.
- An, K. H.; Jeong, S. Y.; Hwang, H. R.; Lee, H. "Enhanced sensitivity of a gas sensor incorporating single-walled carbon nanotube-polypyrrole nanocomposites" *Adv. Mater.* 16 (2004) 1005.
- Andreu, Y.; Marcos, S. D.; Castillo, J. R.; Galban, J. "Sensor film for Vitamin C determination based on absorption properties of polyaniline" *Talanta* 65 (2005) 1045.
- ^aAnilkumar, P.; Jayakannan, M. "New renewable resource amphiphilic molecular design for size-controlled and highly ordered polyaniline" *Langmuir* 22 (2006) 5952.
- ^bAnilkumar, P.; Jayakannan, M. "Flourescent tagged probing agent and structure directing amphiphilic molecular design for polyaniline nanomaterials via self-assembly process" *J. Phys. Chem. C* 111 (2007) 3591.
- ^cAnilkumar, P.; Jayakannan, M. "Single molecular system based selective micellar templates for polyaniline nanomaterials: control of shape, size, solid state ordering and expanded chain to coil like conformation" *Macromolecules*, 40 (2007) 7311.
- ^dAnilkumar, P.; Jayakannan, M. "Divergent nanostructures from identical ingredients: unique amphiphilic micelles template for polyaniline nanofibers, tubes, rods and spheres" *Macromolecules* 41 (2008) 7706.
- ^eAnilkumar, P.; Jayakannan, M. "Hydroxyl-functionalized polyaniline nanospheres :

- tracing the molecular interaction at the nanosurface via vitamin-C sensing” *Langmuir* 24 (2008) 9754.
- ^fAnilkumar, P.; Jayakannan, M. “Self-assembled cylindrical and vesicular templates for polyaniline nanofibers and nanotapes” *J. Phy. Chem. B.* 113 (2009) 11614.
- ^gAnilkumar, P.; Jayakannan, M. “Large-scale synthesis of polyaniline nanofibers based on renewable resource molecular template” *J. Appl. Polym. Sci.* 114 (2009) 3531.
- ^hAnilkumar, P.; Jayakannan, M. “A novel organogel nanotubular template approach for conducting nanomaterials” *J. Phy. Chem. B.*, 114, (2010) 728.
- ⁱAnilkumar, P.; “Self-assembled molecular template for polyaniline nanomaterials” Ph. D Thesis Awarded in Kerala University (2010)
- ^aAntony, M. J.; Jayakannan, M. “Amphiphilic azobenzenesulfonic acid surfactant for water soluble, ordered, and luminescent polypyrrole nanospheres” *J. Phy. Chem. B.* 111 (2007) 12772.
- ^bAntony, M. J.; Jayakannan, M. “Self-assembled anionic micellar template for polypyrrole, polyaniline and their random copolymer nano-materials” *J. Polym. Sci. Part B Polym. Phys.* 47 (2009) 830.
- ^cAntony, M. J.; Jayakannan, M. J. “Molecular template approach for evolution of conducting polymer nanostructures: tracing the role of morphology on conductivity and solid state ordering” *J. Phy. Chem. B.* 114 (2010) 1314.
- Antony, R.; Pillai, C. K. S.; Scariah, K. J. “GPC studies on the cationic polymerization of cardanol initiated by boron trifluoridediethyletherate” *J. Appl. Polym. Sci.* 41 (1990) 1765.
- Argun, A. A.; Cirpan, A.; Reynolds, J. R. “The first truly all polymer electrochromic devices” *Adv Mater* 15 (2003) 1338.
- Atkins, P.; de Paula, J. *Atkin's Physical Chemistry*, (7th Edn), Oxford University Press, (2002) 755.
- Atood, J. L.; Davies, J. E. D.; Macnicol, D. D.; Vogtle, F.; Lehn, J. M.; Suslick, K. S. “Comprehensive supramolecular chemistry” *Pergamon* 8 (1996) 439.
- Atood, J. L.; Steed, J. W. “Organic nanostructures” *Wiley-VCH* (2008)
- Ariga, K.; Kunitake, T. “Supramolecular chemistry fundamentals and applications” *springer* (2006).

- Bay, L.; Mogensen, N.; Skaarup, S.; Sommer-larsen, P.; Jorgenson, M.; West, K.
"Polypyrrole doped with alkyl benzenesulfonate" *Macromolecules* 35
(2002) 9345.
- Berdichevsky, Y.; Lo, Y-H. "Polypyrrole nanowire actuators" *Adv. mater* 18 (2006)
122.
- Bergeron, J.; Chevalier, J-W.; Dao, L. H. "Water-soluble conducting poly(aniline)
Polymer" *J. Chem. Soc. Chem. Commun.* (1990) 180.
- Bidon, G.; Billion, M.; Livache, T.; Mathis, G.; Roget, A.; Torres-Rodriguez, M.
"Conducting polymers as a link between biomolecules and
microelectronics" *Synth. Met.* 102 (1999) 1363.
- Bossi, A.; Piletsky, S. A.; Piletska, E. V.; Righetti, P. G.; Turner, A. P. F. "An assay
for ascorbic acid based on polyaniline-coated microplates" *Anal. Chem.*
72 (2000) 4296.
- Bre´das, J. L.; Themans, B.; Andre, J.M. Chance, R.R.; Silbey, R. "The role of mobile
organic radicals and ions (solitons, polarons and bipolarons) in the
transport properties of doped conjugated polymers" *Synth. Met.* 9 (1984)
265.
- Bre´das, J.L.; Scott, J. C.; Yakushi, K.; Street, G. B. "Polarons and bipolarons in
polypyrrole: Evolution of the band structure and optical spectrum upon
doping" *Phys. Rev. B* 30 (1984) 1023
- Brinke, G. T.; Ikkala, O. "Smart Materials Based on Self-Assembled Hydrogen-
Bonded Comb-Shaped Supramolecules" *The Chemical record* 4 (2004)
219.
- Brydson, J. A. "Plastic materials" *Butterworth heinmann* (1999).
- Bucholz, T.; Sunb, Y.; Loo, Y.L. "Near-monodispersed polyaniline particles through
template synthesis and simultaneous doping with diblock copolymers of
PMA and PAAMPSA" *J. Mater. Chem.* 18 (2008) 5835.
- Cabala, R.; Skarda, J.; Potje-Kamloth, K.; "Spectroscopic investigation of thermal
of doped polypyrrole" *Phys. Chem. Chem. Phys.* 2 (2000) 3283.
- Carswell, A. D. W.; O' Rear, E. A.; Grady, B. P. "Adsorbed templates for the
synthesis of morphologically controlled polyaniline and polypyrrole
nanostructures on flat surface: from spheres to wires to flat films" *J. Am.
Chem. Soc.* 125 (2003) 14793.

- Casella, I. G.; Guascito, M. R. "Electrocatalysis of ascorbic acid on the glassy carbon electrode chemically modified with polyaniline Films" *Electroanalysis* 9 (1997) 1381.
- Cassagnol, C.; Olivier, P.; Richard, A. "Influence of the dopant on the polypyrrole moisture content: effects on conductivity and thermal stability" *J. Apply. Polym. Sci.* 70, (1998) 1567.
- Cataldo, F.; Maltese, P. Synthesis of alkyl and *N*-alkyl-substituted polyanilines: "A study on their spectral properties and thermal stability" *Euro. Polym. J.* 38 (2002), 1791.
- Chandrasekhar, P. Conducting polymers, fundamentals and applications: A practical approach. *Springer* (1999).
- ^aChen, S. A.; Hwang, G-W. "Synthesis of water soluble self acid doped polyaniline" *J. Am. Chem. Soc.* 116 (1994) 7939.
- ^bChen, S-A.; Hwang, G-W.; "Water soluble self acid doped conducting polyaniline: structure and properties" *J. Am. Chem. Soc.*, 117 (1995) 10055.
- Cho, C. H.; Choi, H. J.; Kim, J. W. ; Jhon, M. S.: "Synthesis and electro-rheology of aniline/ pyrrole copolymer" *J. Mater. Sci.* 39, (2004) 1883.
- Cho, S. I.; Kwon, W.; J.; Choi, S. J.; Kim, P.; Park, S.; A.; Kim, J.; Son, S. J.; Xiao, R.; Kim, S. H.; Lee, S. B. "Nanotube-Based Ultrafast Electrochromic Display" *Adv. Mater* 17 (2005) 171.
- ^aChiou, N. R.; Epstein, A. J. "A simple approach to control the growth of the polyaniline nanofibers" *Synth. Met.* 153 (2005) 69.
- ^bChiou, N. R.; Epstein, A. J. " Polyaniline nanofibers prepared in dilute polymerisation" *Adv. Mater.* 17 (2005) 1679.
- Christensen, P.A.; Hamnett, A. "Insitu spectroscopic investigations of the growth, electrochemical cycling, and overoxidation of polypyrrole" *Electrochimica. Acta* 36 (1991) 1263.
- Cosnier, S. "Affinity biosensor based on electropolymerised films" *Electroanalysis* 17 (2005) 1701.
- Davies, T. S.; Ketner, A. M.; Raghavan, S.R. "Self assembly of surfactant vesicles that transforms into viscoelastic worm like micelles upon heating" *J. Am. Chem. Soc.*, 128 (2006) 6669.
- De Armitt, C.; Armes, S. P. "Colloidal dispersions of surfactant stabilized polypyrrole

- particles" *Langmuir* 9 (1993) 652.
- Diaz, A.F., K.K. Kanazawa, and G.P. Gardini. "Electrochemical polymerization of pyrrole" *J. Chem. Soc. Chem. Commun* (1979) 635.
- Duan, X.; Liu, L.; Feng, F.; Wang, S. "Cationic conjugated polymer for optical detection of DNA methylation, lesions, and single nucleotide polymorphism" *Acc. Chem. Res.*, 43 (2010) 260.
- Dufour, B.; Rannou, P.; Fedorko, P.; Djurado, D.; Travers, J. P.; Pron, A. "Effects of plasticizing dopants on spectroscopic properties, supramolecular structure, and electrical transport in metallic polyaniline" *Chem. Mater.* 13 (2001) 4032.
- Evert, D. H. "Basic Principles of Colloid Science" *Royal Society of Chemistry* (1988).
- Fahlman, B. D. "Material chemistry" *Springer* (2007)
- ^aFeng, F.; Tang, Y.; He, F.; Yu, M.; Duan, X.; Wang, S.; Li, Y.; Zhu, D. "Cationic conjugated polymer/DNA complexes for amplified fluorescence assays of nucleases and methyltransferases" *Adv. Mater.* 19 (2007) 3490.
- ^bFeng, F.; Liu, F.; Wang, S. "Fluorescent conjugated polymer-based FRET technique for detection of DNA methylation of cancer cells" *Nature Protocols* 5 (2010) 1255.
- Forster, S.; Plantenberg, T.; "Functional structural hierarchies from self-organizing polymers" *Angew. Chem. Int. Ed.* 41 (2002) 688.
- Forzani, E.S.; Zhang, H.; Nagahara, L. A.; Amlani, I.; Tsui, R.; Tao, N. "A conducting polymer nanojunction sensor for glucose detection" 4 (2004) 1785.
- Franke, D.; Egger, C.C.; Smarsly, B.; Faul, C. F. J.; Tiddy, G. J. T. "Synthesis and phase characterization of a double-tailed pyrrole-containing surfactant: A novel tecton for the production of functional nanostructured materials" *Langmuir* 21 (2005) 2704.
- Freund, M. S.; Deore, B. "Self-Doped Conducting Polymers" *Wiley* (2007).
- Fujii, S.; Aichi, A.; Akamatsu,.; Nawafune, H.; Nakamura, Y. "One-step synthesis of polypyrrole-coated silver nanocomposite particles and their application as a coloured particulate emulsifier" *J. Mater. Chem.* 17 (2007) 3777.
- Fujita, M. "Metal-directed self-assembly of two- and three-dimensional synthetic

- receptors" *Chem. Soc. Rev.* 27 (1998) 417.
- Fusalba, F.; Belanger, D. "Electrical and properties of polyaniline derivatives with liquid crystallinity" *J. Phys. Chem. B.* 103 (1999) 9044.
- Gao, M.; Dai, L.; Wallace, G. G. "Glucose sensors based on glucose-oxidase-containing polypyrrole/aligned carbon nanotube coaxial nanowire electrodes" *Synth. Met.* 137 (2003)1393.
- Gerard, M.; Chaubey, A.; Malhotra, B. D. "Applications of conducting polymers to Biosensors" *Biosens. Bioelectron.* 17 (2002) 345.
- Geetha, S.; Rao, C. R. K. ; Vijayan, M.; Trivedi, D. C. "Biosensing and drug delivery by polypyrrole" *Ana. Chem. Acta* 568 (2006) 119.
- Goddard III, W. A.; Brenner, D. W.; Lyshevski, S. E.; Iafrate, G. J. "Handbook of nanoscience, engineering and technology" Taylor and Francis (2007)
- Goesmann, H; Feldman, C " Nanoparticulate functional materials" *Angew. Chem. Int. Ed.* 49 (2010) 1362.
- Goren, M.; Lennox, R. B. "Nanoscale polypyrrole patterns using block copolymer surface micelles a templates " *Nano Lett.* 1 (2001) 735.
- Goto, H.; Akagi, K. "Synthesis and Properties of Polyaniline Derivatives with Liquid Crystallinity" *Macromolecules.* 35 (2002) 2545.
- Giroto, E. M.; De Paoli, M. A. "Polypyrrole Color Modulation and Electrochromic Contrast Enhancement by Doping with a Dye" *Adv. Mater.* 10 (1998) 790.
- Guimard, N. K.; Gomez, N.; Schmidt, C. E. "Conducting polymers in biomedical engineering" *Prog. Polym. Sci.* 32 (2007) 876
- Hatano, T.; Bae, A. H.; Takeuchi, M.; Fujita, N.; Kaneko, K. ; Ihara, H.; Takafuji, M.; Shinkai, S. "Helical Superstructure of Conductive Polymers as Created by Electrochemical Polymerization by Using Synthetic Lipid Assemblies as a Template" *Angew. Chem. Int. Ed.* 43 (2004) 465.
- Hamley, I. W. "Introduction to soft matter synthetic and biological self assembling of molecules" *Wiley* (2007)
- He, C.; Yang, C.; Li, Y. "Chemical synthesis of Coral like nanowires and nanowire networks of conducting polypyrrole" *Synth. Met.* 139 (2003) 539.
- Heras, J. Y.; Giacobone, A. F. F.; Battaglini, F. Ascorbate amperometric determination using conducting copolymers from aniline and *N*-(3-propane sulfonic acid) aniline *Talanta* 71 (2007) 1684.

- Huang, L.; Wang, Z.; Wang, H.; Cheng, X.; Mitra, A.; Yan, Y. "Polyaniline nanowires by electropolymerization from liquid crystalline phases" *12* (2002) 388.
- ^aHuang, J.; Virji, S.; Weiller, B. H.; Kaner, R. B. "Polyaniline nanofibers: facile synthesis and chemical sensors" *J. Am. Chem. Soc.* 125 (2003) 314.
- ^bHuang, J.; Virji, S.; Weiller, B. H.; Kaner, R. B. "Nanostructured polyaniline sensors" *Chem. Eur. J.* 10 (2004) 1314.
- ^cHuang, J.; Kaner, R. B. Nanofiber formation in the chemical polymerization of aniline: A mechanistic study. *Angew. Chem. Int. Ed.* 43 (2004) 5817.
- Haung, K.; Wan, M.; Long, Y.; Chen, Z.; Wei, Y.; "Multi functional polypyrrole nanofibers via a functional dopant-introduced process" *Synth. Met.* 155 (2005) 495.
- Hulvat, J. F.; Stupp, S.I. "Liquid-crystal templating of conducting polymers" *Angew. Chem. Int. Ed.*, 42 (2003) 778.
- Huck, W. T. S. "Nanoscale assembly chemical techniques" *Springer* (2005).
- Ikegame, M.; Tajima, K.; Aida, T. "Template synthesis of polypyrrole nanofibers insulated within one-dimensional silicate channels: hexagonal versus lamellar for recombination of polarons into bipolarons" *Angew. Chem. Int. Ed.* 42 (2003) 2154.
- Ikkala, O.; ten Brinke, G. *Science*. "Functional Materials Based on Self-Assembly of Polymeric Supramolecules" 295 (2002) 2407.
- Israelachvili, J. N.; Mitchel, D. J.; Ninham, B.W. "Theory of self-assembly of hydrocarbon amphiphiles into micelles and bilayers" *J. Chem. Soc. Faraday Trans. 2.* 72 (1976) 1525.
- ^aJager, E. W. H.; Smela, E.; Inganäs, O. "Microfabricating Conjugated Polymer Actuators" *Science* 290 (2000) 1540.
- ^bJager, E. W. H.; Inganäs, O.; Lundström, I. "Microrobots for micrometer-size objects in aqueous media: potential tools for single-cell manipulation" *Science* 288 (2000) 2335.
- ^cJager, E. W. H.; Inganäs, O.; Lundström, I. "Perpendicular Actuation with Individually Controlled Polymer Microactuators" *Adv. Mater* 13 (2001) 76.
- ^aJana, T.; Nandi, A. K. "Sulfonic Acid-Doped Thermoreversible Polyaniline Gels:

- Morphological, Structural, and Thermodynamical Investigations” *Langmuir* 16 (2000) 3141.
- ^bJana, T. ; Nandi, A. K. “Sulfonic Acid Doped Thermoreversible Polyaniline Gels. 2. Influence of Sulfonic Acid Content on Morphological, Thermodynamical, and Conductivity Properties” *Langmuir*, 17 (2001) 5768.
- ^cJana, T. ; Chatterjee, J. ; Nandi, A. K. “Sulfonic Acid Doped Thermoreversible Polyaniline Gels. 3. Structural Investigations” *Langmuir* 18 (2002) 5720.
- Janata, J.; Josowich, M. “Conducting polymers in electronic chemical sensors” *Nature Materials* 2 (2003) 19.
- ^aJang, J.; Oh, J. H.; Stucky, G. D. “Fabrication of ultrafine conducting polymer and graphite nanoparticles” *Angew. Chem. Int. Ed.* 41 (2002) 4016.
- ^bJang, j.; Oh, J. H. “Novel crystalline supramolecular assemblies of amorphous polypyrrole nanoparticles through surfactant templating” *Chem. Com.* (2002) 2200.
- ^cJang, J.; Yoon, H. “Facile fabrication of polypyrrole nanotubes using reverse microemulsion polymerization” *Chem. Commun.* (2003) 720.
- ^dJang, J.; Oh, J. K. “A facile synthesis of polypyrrole nanotubes using a template-mediated vapor deposition polymerization and the conversion to carbon nanotubes” *Chem. Commun.* (2004) 882.
- ^eJang, J.; Yoon, H.. “Multigram-scale fabrication of monodisperse conducting polymer and magnetic carbon nanoparticles” *Small*, 1 (2005) 1195.
- ^fJang, J.; Yoon, H. “Formation Mechanism of Conducting Polypyrrole Nanotubes in Reverse Micelle Systems” *Langmuir* 21 (2005) 11484.
- ^gJang, J. “Conducting polymer nanomaterials and their applications” *Adv. Polym. Sci* 199 (2006) 189.
- Jayakannan, M.; Annu, S.; Ramalekshmi, S. “Structural effects of dopants and polymerization methodologies on the solid-state ordering and morphology of polyaniline” *J. Polym. Sci., Part B: Polym. Phys.* 43 (2005) 1321.
- Jiang, G.; Susha, A.S.; Lutich, A. A.; Stefani, F. D.; Feldmann, J.; Rogach, A.L. “Cascaded FRET in Conjugated Polymer/Quantum Dot/Dye-Labeled DNA Complexes for DNA Hybridization Detection” *ACS Nano* 3 (2009) 4127.
- Jiang, Y.; Wang, A.; Kan, J. “Selective uricase biosensor based on polyaniline

- synthesized in an ionic liquid" *Sens. Actuators* 124 (2007) 529.
- John, G.; Pillai, C. K. S. "Grafting of bio-monomers I. Cationic graft copolymerisation of cardanol using borontrifluoridediethyletherate onto cellulose" *Polym. Bull.* 22 (1989) 89.
- John, G.; Pillai, C. K. S. "Synthesis and characterization of a self-cross linkable polymer from cardanol: Autooxidation of poly(cardanyl acrylate) to crosslinked film" *J. Polym. Sci., Part A: Polym. Chem.* 31 (1993) 1069.
- John, G.; Masuda, M.; Okada, Y.; Yase, K.; Shimizu, T. "Nanotube Formation from Renewable Resources via Coiled Nanofibers" *Adv. Mater.* 13 (2001) 715.
- John, G.; Jung, J.-H.; Minamikawa, H.; Yoshida, K.; Shimizu, T. "Morphological control of helical solid bilayers in high-axial-ratio nanostructures through binary self-assembly" *Chem. Eur. J.* 8 (2002) 5494.
- John, R.K. and Kumar, D.S. "Structural, electrical, and optical studies of plasma polymerized and iodine-doped polypyrrole" *J Appl Polym Sci* 83 (2002) 1856.
- Jureviciute, I.; Brazdiuviene, K.; Bernotaite, L.; Salkus, B.; Malinauskas, A. "Polyaniline-modified electrode as an amperometric ascobate sensor" *Sens. Actuators. B*, 107 (2005) 716.
- Kang, E. T.; Neoh, K. G.; Tan, K. L. "Polyaniline: A polymer with many interesting intrinsic redox states" *Prog. Polym. Sci.* 23 (1998) 277.
- Kang, T. S.; Lee, S. K.; Joo, J.; Lee, J. Y. "Electrically conducting polypyrrole fibers spun by electrospinning" *Synth. Met.*, 153 (2005) 61.
- Korri-Youssoufi, H.; Garnier, F.; Srivastava, P.; Godillot, P.; Yassar, A. "Toward bioelectronics: specific DNA recognition based on an oligonucleotide functionalized polypyrrole" *J. Am. Chem. Soc* 119 (1997) 7388.
- Kim, E.; Lee, M.; Rhee, S-H. "Liquid crystalline assemblies from self-doped polyanilines" *Synth. Met.* 69 (1995) 101.
- Kim, J. Y.; Kim, J. T.; Song, E. H. ; Min, Y. K.; Hamaguchi, H. O. "Polypyrrole nanostructures self-assembled in magnetic ionic liquid as a template" *Macromolecules*, 41 (2008) 2886.
- N. Kimizuka, T. Kawasaki, K. Hirata and T. Kunitake, *J. Am. Chem. Soc.* 120 (1998) 4094.
- Kim, J. W.; Cho, C. H.; Liu, F. Choi, H. J.; Joo, J. "Physical characteristics of

- aniline/pyrrole copolymer" *Synth. Met.*, 17 (2003) 135.
- Ko, S.; Jang, J. "Controlled amine functionalization on conducting polypyrrole nanotubes as effective transducers for volatile acetic acid" *Biomacromolecules* 8 (2007) 182.
- Korcherginsky, N. M.; Wang, Z. "Polyaniline membrane based potentiometric sensor for ascorbic acid, other redox active species and chloride" *J. Electroanal. Chem.* 611 (2007) 162.
- Komsiyaska, I.; Tsakova, V. "Ascorbic Acid Oxidation at Nonmodified and Copper-Modified Polyaniline and Poly-ortho-methoxyaniline Coated Electrodes" *Electroanalysis*, 18 (2006) 807.
- Kros, A.; Nolte, R. J. M.; Sommerdijk, N. A. J. M. "Conducting polymers with confined dimensions: track etched membranes for amperometric biosensor applications" *Adv Mater* 14 (2002) 1779.
- Krishnamoorthy, K.; Contractor, A. Q.; Kumar, A. "Electrochemical synthesis of fully sulfonated *n*-dopable polyaniline: poly (metanillic acid)" *Chem. Commun.* (2002) 240.
- Kurreck, H.; Boch, M.; Bretz, N.; Elsner, M.; Kraus, H.; Lubitz, W.; Muller, F.; Giessler, J.; Kroneck, P. M. H. "Fluid solution and solid-state electron nuclear double resonance studies of flavin model compounds and flavoenzymes" *J. Am. Chem. Soc.* 106 (1984) 734.
- Laska, J.; Djurado, D.; Lunzy, W. "X-ray study of plasticized polyaniline" *Eur. Polym. J.*, 38 (2002) 947.
- Leclerc, M. "Optical and Electrochemical Transducers Based on Functionalized Conjugated Polymers" *Adv. Mater* 11 (1999) 1491.
- Lee, J-H; Serna, F.; Schmidt, C. E. "Carboxy end capped conductive polypyrrole biomimetic conducting polymer for cell scaffolds and electrodes" *Langmuir* 22 (2006) 9816.
- Lec, J. Y.; Kim, D. Y.; Kim, C. Y. "Synthesis of soluble polypyrrole of the doped state in organic solvents" *Synth. Met.* 74 (1995) 103.
- Lellouche, J. P.; Govindaraji, S.; Joseph, A.; Jang, J.; Lec, K. J. "Polydipyrrole- and polydicarbazole-nanorods as new nanosized supports for DNA hybridization" *Chem. Commun* (2005) 4357.

- Li, D.; Huang, J.; Kaner, R. B. "Polyaniline nanofiber: A unique polymer nanostructure for versatile applications" *Acc. Chem. Res.* 42 (2009) 135.
- Li, G.; and Zhang, Z. "Synthesis of dendritic polyaniline nanofibers in a surfactant gel" *Macromolecules* 37 (2004) 2683
- ^aLi, X. G.; Wang, L. X.; Jin, Y.; Zhu, Z. L.; Yang, Y. L. "Preparation and identification of a soluble copolymer from pyrrole and *o*-toluidine" *J. Appl. Polym. Sci.*, 82 (2001) 510.
- ^bLi, X. G.; Huang, M. R.; Wang, L. W.; Zhu, M. F.; Menner, A.; Springer, J. Synthesis and characterization of pyrrole and *m*-toluidine copolymers *Synth. Met.* 123 (2001) 435.
- ^cLi, X. G.; Huang, M. R.; Zhu, M. F.; Chen, Y. M. "Synthesis and nitrosation of processible copolymers from pyrrole and ethyl aniline" *Polymer* 45 (2004) 385.
- ^dLi, X. G.; Chen, R.F.; Huang, M.R.; Zhu, M. F.; Chen, Q. "Synthesis of a soluble pyrrole copolymer with phenetidine" *J. Polym. Sci., Polym. Chem.* 42 (2004) 2073.
- ^eLi, X. G.; Wei, F.; Huang, M. R.; Xie, Y. B. "Facile synthesis and intrinsic conductivity of novel pyrrole copolymer nanoparticle with inherent self stability" *J. Phys. Chem. B.* 111 (2007) 5829.
- Li, X.; Zhang, X.; Li, H.; "Preparation and characterization of pyrrole-aniline copolymer nanofibrils using the template synthesis method" *J. Appl. Polym. Sci.* 81 (2001) 3002.
- Lim, V.W.L.; Kang, E.T.; Neoh, K.G.; Ma, Z.H.; Tan, K.L.; "Determination of pyrrole-aniline copolymer compositions by X-ray photoelectron spectroscopy" *Appl. Surf. Sci.* 181 (2001) 317.
- Lin, H. K.; Chen, S-A. "Synthesis of New Water-Soluble Self-Doped Polyaniline" *Macromolecules* 33 (2000) 8117.
- Lindman, J.; Kronberg H. "Surfactants and polymers in aqueous solution" John Wiley & sons (1998)
- Lindfors, T.; Ivaska, A. "Potentiometric and UV-vis characterisation of N-substituted polyanilines" *J. Electroanal. Chem.* 535 (2002) 65.
- Liu, J.; Wan, M. "Synthesis, characterization and electrical properties of microtubules

- of polypyrrole synthesized by a template-free method" *J. Mater. Chem.* 11 (2001) 404.
- Liu, L.; Zhao, C.; Zhao, Y.; Jia, N.; Zhuo, Q.; Yan, M.; Jiang, Z. "Characteristics of polypyrrole (PPy) nano-tubules made by templated ac electropolymerization" *Eur. Polym. J.* 41 (2005) 2117.
- *Long, Y.; Chen, Z.; Wang, N.; Ma, Y.; Zhang, Z.; Zhang, L.; Wan, M. "Electrical conductivity of a single conducting polyaniline nanotube" *Appl. Phys. Lett.* 83 (2003) 1863.
- *Long, Y.; Zhang, L.; Ma, Y.; Chen, Z.; Wang, N.; Zhang, Z.; Wan, M. "Electrical conductivity of an individual polyaniline nanotube synthesized by a self-assembly method" *Macromol Rapid Commun.* 24 (2003) 938.
- *Long, Y.; Chen, Z.; Ma, Y.; Zhang, Z.; Jin, A.; Gu, C.; Zhang, L.; Wei, Z.; Wan, M. "Electrical conductivity of hollow polyaniline microspheres synthesized by a self-assembly method" *Appl. Phys. Lett.* 84 (2004) 2205.
- Lou, X.; Zhang, L.; Qin, J.; Zhen, L. "Colorimetric sensing of α -amino acids and its application for the label-free detection of protease" *Langmuir* 26 (2010) 1566.
- Lu, Y.; Shi, G.; Li, C.; Liang, Y. "Thin polypyrrole films prepared by chemical oxidative polymerization" *J. Appl. Polym. Sci.* 70 (1998) 2169.
- Lu, G.; Li, C.; Shi, G. "Polypyrrole micro- and nanowires synthesized by electrochemical polymerization of pyrrole in the aqueous solutions of pyrenesulfonic acid" *Polymer* 47 (2006) 1778.
- MacDiarmid, A. G. Nobel Lecture: "Synthetic metals: A novel role for organic Polymers (Nobel lecture)" *Angew. Chem. Int. Ed.* 40 (2001) 2581.
- MacDiarmid, A.G.; Zhou, Y.; Feng, J. "Oligomers and isomers: new horizons in polyanilines" *Synth. Met.* 100 (1999) 131.
- Malinauskas, A. "Selfdoped polyanilines" *J. Power sources*, 126 (2004) 214.
- Ma, X.; Zhang, X.; Li, Y.; Xu, H.; Li, G.; Wang, M.; Chen, H. "Gas sensing behavior of nano-structured polypyrrole prepared by "carbon nanotubes seeding approach" *J. Nanopart. Res.* 10 (2008) 289.
- Martin, C. R. "Template synthesis of electronically conductive polymer nanostructures" *Science* 266 (1994) 1961.
- Martin, C. R. "Template synthesis of electronically conductive polymer

- nanostructures" *Acc. Chem. Res.* 28 (1995) 61.
- Mativetsky, J. M.; Datars, W. R. "Morphology and electrical properties of template-synthesized polypyrrole nanocylinders" *Physica B* 324 (2002) 191.
- McCarthy, G.P. Armes, S.P. "Synthesis and characterization of carboxylic acid-functionalized polypyrrole-silica microparticles using a 3-substituted pyrrole comonomer" *Langmuir* 13 (1997) 3686.
- Maeda, S.; Corradi, R.; Armes, S. P. "Synthesis and characterization of carboxylic acid-functionalized polypyrrole-silica microparticles using a 3-substituted pyrrole comonomer" *Macromolecules* 28 (1995) 2905.
- McQuade, D. T.; Pullen, A. E.; Swager, T. M. "Conjugated polymer-based chemical sensors" *Chem. Rev.* 100 (2000) 2537.
- Menon, A.R.R., Pillai, C.K.S., Nando, G.B. "Self-adhesion of natural rubber modified with phosphorylated cashew nut shell liquid" 9 (1995) 443.
- Menon, V.P.; Lei, J.; Martin, C. R. "Investigation of molecular and supermolecular structure in template-synthesized polypyrrole tubules and fibrils" *Chem. Mater.* 8 (1996) 2382.
- Miller, S. "Naked eye colorimetric analysis of heparin and its derivatives" *Anal. Chem.* 82 (2010) 1570.
- Minkstimiene, A. K.; Mazeiko, V.; Ramanaviciene, A.; Ramanavicius, A. "Enzymatically synthesized polyaniline layer for extension of linear detection region of amperometric glucose biosensor" *Biosens. and Bioelectronics* 26 (2010) 790.
- Mirkin, C. A. "The beginning of a small revolution" *Small* 1 (2005) 14.
- Moon, D-K.; Ezuka, M.; Maruyama, T, Osakada, Yamamoto. "Kinetic study on chemical oxidation of leucoemeraldine base polyaniline to emeraldine base" *Macromolecules* 26 (1993) 364.
- Mu, S.; Yang, Y. "Spectral Characteristics of polyaniline nanostructures synthesized by using cyclic voltammetry at different scan rates" *J. Phys. Chem. B*, 112 (2008) 11558.
- Murphy, C. A; Jana, N. R. "Controlling the Aspect Ratio of Inorganic Nanorods and Nanowires" *Adv. Mater.* 14 (2002) 80.
- Nabid, M. R.; Entezami, A. A. "Comparative study on the enzymatic polymerization of N-substituted aniline derivatives" *Polym. Adv. Technol.* 16 (2005) 305.

- Nalwa, H. S "Handbook of nanostructured nanomaterials and nanotechnology"
Academic press (2000).
- Nguyen, M. T.; Kasai, P.; Miller, J. L.; Daiz, A.F. "Synthesis and Properties of Novel Water-Soluble Conducting Polyaniline Copolymers" *Macromolecules* 27 (1994) 3625.
- ^aOmastova, M.; Trchova, M.; Kovarova, J.; Stejskal, J. "Synthesis and structural study of polypyrroles prepared in the presence of surfactants" *Synth. Met.* 138 (2003) 447.
- ^bOmastova, M.; Trchova, M.; Pionteck, J.; Prokes, J.; Stejskal, J. "Effect of polymerisation conditions on the properties of polypyrrole prepared in the presence of sodium bis(2-ethyl hexyl) sulfosuccinate" *Synth. Met.* 143 (2004) 153.
- Otero, T. F.; Cortes, M. T. "Artificial muscles with tactile sensitivity" *Adv. mater* 15 (2003) 279.
- Odian, G. "Principles of Polymerization" *John Wiley*, (2004).
- Paul, R.K.; Vijayanathan, V.; Pillai, C.K.S. "Melt/solution processable conducting polyaniline: doping studies with a novel phosphoric acid ester" *Synth Met.* 104 (1999) 189.
- Piepenbrock, M. O. M.; Lloyd, G.O.; Clarck, N.; Steed, J. W. "Metal- and Anion-Binding Supramolecular Gels" *Chem. Rev.* 110 (2010) 1960.
- Pillai, C.K.S., Prasad, V.S., Sudha, J.D., Bera, S.C., Menon, A.R.R. "Polymeric resins from renewable resources. II. Synthesis and characterization of flame-retardant prepolymers from cardanol" *J. Appl. Polym. Sci.* 41 (1990) 2487.
- Ping, Z. "In situ FTIR-attenuated total reflection spectroscopic investigations on the base-acid transitions of polyaniline. Base-acid transition in the emeraldine form of polyaniline" *J. Chem. Soc., Faraday Trans.* 92 (1996) 3063.
- Praveen, V. K.; Babu, S. S.; Vijayakumar, C.; Varghese, R.; Ajayaghosh, A. "Helical supramolecular architectures of self-assembled linear-systems" *Bull. Chem. Soc. Jpn.* 81 (2008) 1196
- Qu, L.; Shi, G.; Chen, F.; Zhang, J. "Electrochemical growth of polypyrrole Microcontainers" *Macromolecules* 36 (2003) 1063.
- Qi, Z.; Pickup, P. G. "Size control of polypyrrole particles" *Chem. Mater.* 9 (1997)

- 2934.
- Ramanathan, K.; Bangar, M. A.; Yun, M.; Chen, W.; Myung, N. V.; Mulchandani, A. "Bioaffinity sensing using biologically functionalized conducting polymer nanowire" *J. Am. Chem. Soc.* 127 (2005) 496.
- Roy, S.; Fortier, J. M.; Nagarajan, R.; Tripathy, S.; Kumar, J.; Samuelson, L. A.; Bruno, F. F. "Biomimetic synthesis of a water soluble conducting molecular complex of polyaniline and lignosulfonate" *Biomacromolecules*, 3 (2002) 937.
- Rao, C.N. R.; Muller, A.; Cheetham, A. K. "The chemistry of materials" *Wiley I'CH* (2004)
- Rekha, N.; Asha, S.K. "Solvent induced self assembly process in cardanol based urethane methacrylate comb polymers" *J. Polym. Sci. Part A: Polym. Chem.* 47 (2009) 2996.
- Sari, M.; Talu, M. "Electrochemical copolymerization of pyrrole and aniline" *Synth. Met.* 94 (1998) 221.
- Santos, M. L.; Magabhaes, G. C. "Utilisation of cashew nut shell liquid from *Anacardium occidentale* as starting material for organic synthesis: A novel route to lasiodiplodin from cardols" *J. Braz. Chem. Soc.* 10 (1999) 13.
- Seal, S. "Functional nanostructures processing, characterization and applications" *Springer* (2008).
- Shen, Y.; Wan, M. "Soluble conductive Soluble conductive polypyrrole synthesized by in situ doping with β -naphthalene sulfonic acid" *J. Polym. Sci. Polym. Chem.* 35 (1997) 3689.
- Shen, Y.; Wan, M. "In situ doping polymerization of pyrrole with sulfonic acid as a dopant" *Synth. Met.* 96 (1998) 127.
- ^aShoji, E.; Freund, M. S. "Poly(aniline boronic acid): a new precursor to substituted poly(anilines)" *Langmuir* 17 (2001) 7183.
- ^bShoji, E.; Freund, M. S. "Potentiometric Sensors Based on the Inductive Effect on the pK_a of Poly(aniline): A Non-enzymatic Glucose Sensor" *J. Am. Chem. Soc.*, 123 (2001) 3383.
- Shimizu, T.; Masuda, M.; Minamikawa, H. "Supramolecular nanotube architectures based on amphiphilic molecules" *Chem. Rev.* 105 (2005) 1401.

- Shirakawa, H. "Synthesis of electrically conducting organic polymers: Halogen derivatives of polyacetylene (CH)_x." *J. Chem. Soc. Chem. Commun.* (1977) 578.
- Skotheim, T. A.; Elsenbaumer, R. L.; Reynolds, J. R. *Handbook of Conducting Polymer* (2nd Ed). (1998).
- Song, M. K.; Kim, Y. T.; Kim, B. S.; Kim, J.; Char, K.; Rhee, H.W. "Synthesis and characterization of soluble polypyrrole doped with alkylbenzene sulfonic acids" *Synth. Met.* 141 (2004) 315.
- Simmons, M.R., P.A. Chaloner, and S.P. Armes. "Synthesis and characterization of colloidal polypyrrole particles using reactive polymeric stabilizers" *Langmuir* 14 (1998) 611.
- Smela, E. "A Microfabricated Movable Electrochromic Pixel Based on Polypyrrole" *Adv. Mater.* 11 (1999) 1343.
- Smela, E. "Conducting polymer actuator for biomedical applications" *Adv Mater* 15 (2003) 481.
- Smith, D. K.; Korgel, B. A. "The Importance of the CTAB Surfactant on the Colloidal Seed-Mediated Synthesis of Gold Nanorods" *Langmuir* 24 (2008) 644.
- Sivakumar, C.; Vasudevan, T.; Gopalan, A. "Chemical oxidative polymerisation and in situ spectrochemical studies of a sulfonated aniline derivative by UV-Visible spectroscopy" *Ind. Eng. Chem. Res.*, 40 (2001) 40.
- Stejskal, J.; Omastova, M.; Fedorova, S.; Prokes, J.; Trchova, M. "Polyaniline and polypyrrole prepared in the presence of surfactants: a comparative conductive studies" *Polymer*, 44 (2003) 1353.
- Stejskal, J.; Trchova, M.; Ananieva, I. R.; Janca, J.; Prokes, J.; Fedorova, S.; Sapurina, I. "Poly(aniline-co-pyrrole) powders, films, and colloids. Thermophoretic mobility of the colloidal particles" *Synth. Met.* 146 (2004) 29.
- Suman, S.; Solanki, P. R.; Pandey, M. K.; Malhotra, B. D. "Cholesterol biosensor based on cholesterol esterase, cholesterol oxidase and peroxidase immobilized onto conducting polyaniline films" *Sens. Actuators* 115 (2006) 534.
- Tian, Y.; Wang, J.; Wang, Z.; Wang, S. Electroreduction of nitrite at an electrode modified with polypyrrole nanowires *Synth. Met* 143 (2004) 309.

- Tian, Y.; Wang, J.; Wang, Z.; Wang, S. Solid-phase extraction and amperometric determination of nitrite with polypyrrole nanowire modified electrodes *Sens Actuators B* 104 (2005) 23.
- Tiitu, M.; Volk, N.; Torkkeli, M.; Serimaa, R.; ten Brinke, G.; Ikkala, O. "Cylindrical Self-Assembly and Flow Alignment of Comb-Shaped Supramolecules of Electrically Conducting Polyaniline" *Macromolecules* 37 (2004) 7364.
- Valkama, S.; Kosunen, H.; Ruokolainen, J.; Haatainen, T.; Torkkeli, M.; Serimaa, R.; Brinke, G. T.; Ikkala, O. "Self-assembled polymeric solid films with temperature-induced large and reversible photonic-bandgap switching" *Nat. Mater* 3 (2004) 872.
- Vemula, P. K.; John, G. "Crops: A green approach toward self assembled soft Materials" *Acc. Chem res.* 41 (2008) 769.
- Virji, S.; Kaner, R. B.; Weiller, B. H. "Hydrogen sensors based on conductivity changes in polyaniline nanofibers" *J. Phys. Chem. B.* 110 (2006) 22266.
- Virji, S.; Kaner, R. B.; Weiller, B. H. "Detection of Toxic Chemicals for Homeland Security Using Polyaniline Nanofibers" *ACS Symposium Series.* 980 (2007)
- Vito, S. D.; Martin, C. R. Towards the colloidal dispersions of template synthesized polypyrrole nanotubes *Chem. Mater.* 10 (1998) 1738.
- Wei, Y.; Hsueh, K. F.; Jang, G. W. "A study of leucoemeraldine and effect of redox reactions on molecular weight of chemically prepared polyaniline" *Macromolecules* 27 (1994) 518.
- Wallace, G. G.; Kane-Maguire, L. A. P. "Manipulating and monitoring biomolecular interactions with conducting electroactive polymers" *Adv. Mater.* 14 (2002) 953.
- Wan, D.; Yuan, S.; Li, G. L.; Neoh, K. G.; Kang, E. T. "Glucose biosensor from covalent immobilization of chitosan coupled carbon nanotubes on polyaniline modified gold electrode" *Macromolecules* 2 (2010) 3083.
- Wang, C.; Guo, Y.; Wang, Z.; Zhang, X. "Superamphiphiles based on charge transfer complex: controllable hierarchical self-Assembly of nanoribbons" *Langmuir* 26 (2010) 14509.
- Wang, J.; Jiang, M. "Towards genelectronics: nucleic acid doped conducting polymers" *Langmuir* 16 (2000) 2269.

- Wang, J.; Musamch, M. Carbon-nanotubes doped polypyrrole glucose biosensor
Anal Chim Acta 539 (2005) 209.
- Wernet, W.; Monkenbusch, M.; Wegner, G. "A new series of conducting polymers with layered structure: Polypyrrole n-alkylsulfates and n-alkylsulfonates"
Macromol.Chem. Rapid Commun. 5 (1984) 157.
- Wei, Y.; Hsueh, K. F.; Jang, G-Y. A Study of Leucoemeraldine and the Effect of Redox Reactions on the Molecular-Weight of Chemically Prepared Polyaniline *Macromolecules* 1994, 27, 518-525.
- Wei, Z.; Zhang, L.; Yu, M.; Yang, Y.; Wan, M.; "Self-assembling sub-micrometer sized tube junctions and dendrites of conducting polymer" *Adv. Mater* 15 (2005) 1382.
- Wei, Z.X., Z.M. Zhang, and M.X. Wan. "Formation mechanism of self-assembled polyaniline micro-nanotubes" *Langmuir* 18 (2002) 917.
- Whitesides, G. M.; Mathias, J. P.; Soto, C. T. "Molecular self assembly and nanochemistry: A chemical strategy for the synthesis of nanostructures"
Science, 254 (1991) 1312.
- Wu, A.; Kolla, H.; Manohar, S. K. "Chemical synthesis of highly conducting polypyrrole nanofiber film" *Macromolecules* 38 (2005) 7873.
- Xia, Y.; Wiesinger, J. M.; MacDiarmid, A. G.; Epstein, A.J. "Camphor sulfonic acid doped polyaniline emeraldine salt: Conformations in different solvents studied by an ultra violet/visible/ near-infrared spectroscopic method"
Chem. Mater. 7 (1995) 443.
- Xia, Y.; Rogers, J. A.; Paul, K. E.; Whitesides, G. M. "Unconventional Methods for Fabricating and Patterning Nanostructures" *Chem. Rev.* 99 (1999) 1823.
- Yoon, H.; Chang, M.; Jang, J. "Sensing behavior of polypyrrole nanotubes prepared in reverse microemulsions: effects of transducer size and transduction mechanism" *J. Phys. Chem. B* 110 (2006) 14074.
- Yoo, S. I.; Sohn, B.; Zin, W. C.; Jung, J. C. "Localised synthesis of polypyrrole in the nanopattern of monolayer films of diblock copolymer micelles" *Langmuir* 20 (2004) 10734.
- Young, E.R.; Rosenthal, J.; Hodgkiss, J. M.; Nocera, D. G. "A Comparative PCET

- Study of a Donor-Acceptor Pair Linked by Ionized and Non-ionized Asymmetric Hydrogen-Bonded Interfaces" *J. Am. Chem. Soc.* 131 (2009) 7678.
- Yuan G-L.; Kuramoto, N. "Synthesis and Chiroptical Properties of Optically Active Poly(*N*-alkylanilines) Doped and Intertwined with Dextran Sulfate in Aqueous Solution" *Macromolecules* 36 (2003) 7939.
- Yuc, J.; Wang, Z. H.; Kromack, K. R.; Epstein, A. J.; Macdiarmid, A.G. "Effect of Sulfonic acid group on polyaniline backbone" *J. Am. Chem. Soc.* 113 (1991) 2665.
- Yuj, H.; Guo, Y.; Koyama, K.; Sawada, T.; John, G.; Yang, B.; Masuda, M.; Shimizu, T. "Local Environment and Property of Water inside the Hollow Cylinder of a Lipid Nanotube" *Langmuir* 21 (2005) 721.
- Zang, J.; Ming Li, C. M.; Bao, S.J.; Cui, X, Bao, Q.; Sun, C. Q. "Template-free electrochemical synthesis of superhydrophilic polypyrrole nanofiber network" *Macromolecules* 41 (2008) 7053.
- Zhang, J.; Shan, D.; Mu, S. "Syntheses and characterizations of aniline/butylthioaniline copolymers: Comparisons of copolymers prepared by the new concurrent reduction and substitution route and the conventional oxidative copolymerization method" *J. Polym. Sci Part A: Polym Chem* 43 (2005) 1767.
- Zhang, J.; Shan, D.; Mu, S. "A promising copolymer of aniline and *m*-aminophenol: Chemical preparation, novel electric properties and characterization" *Polymer* 48 (2007) 1269.
- Zhang, J.; Wan, M. "Chiral polyaniline nanotubes synthesized via self assembly process" *Thin Solid Films*, 447 (2005) 24.
- Zhang, L. "Electrochemical synthesis of self-doped polyaniline and its use to the electro-oxidation of ascorbic acid" *J. solid. State. Electrochem.* 11 (2007) 365.
- ^aZhang, X.; Manohar, S. K. "Narrow pore-diameter polypyrrole nanotubes" *J. Am. Chem. Soc.* 127 (2005) 14156.
- ^bZhang, X.; Zhang, J.; Song, W.; Liu, Z. "Controllable synthesis of conducting polypyrrole nanostructures" *Phys. Chem. B* 110 (2006) 1158.
- ^cZhang, X.; Kolla, H. S.; Wang, X.; Raja, K.; Manohar, S. K. "Fibrillar Growth in

- Polyaniline” *Adv. Funct. Mater* 16 (2006) 1145.
- ^DZhang, X.; Manohar, S. K. “Polyaniline nanofiber: chemical synthesis using surfactants” *Chem. Commun.* (2004) 2360.
- ^aZhang, X.; Wang, C. “Supramolecular amphiphiles” advance article *Chem. Soc. Rev* (2010).
- Zhong, W.; Liu, S.; Chen, X.; Wang, Y.; Yang, W. “High-yield synthesis of superhydrophilic polypyrrole nanowire networks” *Macromolecules* 39 (2006) 3224.
- ^aZhou, C.; Han, J.; Song, G.; Guo, R. ‘Fabrication of Poly(aniline-co-pyrrole) Hollow Nanospheres with Triton X-100 Micelles as Templates’ *J. Polym. Sci. Polym. Chem.* 46 (2008) 3563.
- ^bZhou, C.; Han, J.; Guo, R. “Dilute anionic surfactant solution route to polyaniline rectangular sub-microtubes as a novel nanostructure” *J. Phys. Chem. B.* 112 (2008) 5014.
- Zheng, W.; Angelopoulos, M.; Epstein, A. J.; MacDiarmid, A. G. “Concentration dependence of aggregation of polyaniline in NMP solution and resulting cast films” *Macromolecules* 30 (1997) 7634.
- Zhong, W.; Liu, S.; Chen, X.; Wang, Y.; Yang, W. “High yeild synthesis of superhydrophilic polypyrrole nanowire networks” *Macromolecules* 39 (2006) 3224.
- Zou, W.; Yue, P.; Lin, L.; He, M.; Zhou, Z.; Lonial, S.; Khuri, F, R.; Wang, B.; Sun, S-Y. “Vitamin C Inactivates the Proteasome Inhibitor PS-341 in Human Cancer Cells” *Clin. Cancer. Res.* 12 (2006) 273.